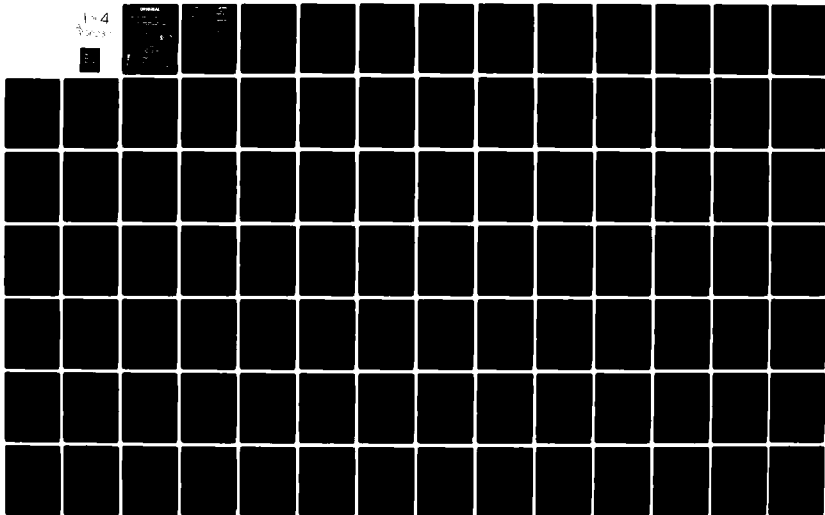


AD-A106 237

NORTHEASTERN UNIV BOSTON MASS DEPT OF BIOPHYSICS AN--ETC F/G 6/18  
BIOLOGICAL EFFECTS OF LASER RADIATION. VOLUME IV. OPTICAL SECON--ETC(U)  
OCT 78 W P HANSEN, S FINE DA-49-193-MD-2436  
NL

UNCLASSIFIED

1-4  
Pages



**ORIGINAL**

①

**LEVEL III**

VOL 3 - A105236

**BIOLOGICAL EFFECTS OF LASER RADIATION**

**Final Scientific Report - Volume IV  
Optical Second Harmonic Generation in Biological  
Tissues)**

AD A106237

**W. Peter Hansen  
Samuel Fine**

**DTIC  
ELECT  
OCT 28 1981  
A**

**Submitted October 17, 1978  
(1 July 1968 to 30 September 1971)**

**Supported By  
U.S. ARMY MEDICAL RESEARCH AND DEVELOPMENT COMMAND  
Fort Detrick, Frederick, Maryland 21701**

**Contact No. DA-49-198-MD8436**

**Department of Biophysics and Biomedical Engineering  
Northwestern University  
Boston, Massachusetts 02115**

**Approved For Public Release,  
Distribution Unlimited**

**81 10 27 286**

**DTIC FILED**

REPORT DOCUMENTATION PAGE		READ INSTRUCTIONS BEFORE COMPLETING FORM	
1. REPORT NUMBER	2. GOVT ACCESSION NO. <b>AD-A106</b>	3. RECIPIENT'S CATALOG NUMBER <b>239 (9) (C. t.)</b>	
4. TITLE (and Subtitle) <b>BIOLOGICAL EFFECTS OF LASER RADIATION, Volume IV (Optical Second Harmonic Generation in Biological Tissues)</b>		5. TYPE OF REPORT & DATES COVERED <b>Final 1 July 1963 - 30 September 1971</b>	6. AUTHORING ORG. REPORT NUMBER
7. AUTHOR(s) <b>W. Peter/Hansen Samuel/Fine</b>		8. CONTRACT OR GRANT NUMBER(s) <b>DA-49-193-MD2436</b>	9. PERFORMING ORG. REPORT NUMBER <b>61102A/38161102B805</b>
10. PERFORMING ORGANIZATION NAME AND ADDRESS <b>Department of Biophysics and Biomedical Engineering Northeastern University, Boston, MA 02115</b>		11. SECURITY CLASS. (of this report) <b>Unclassified</b>	
11. CONTROLLING OFFICE NAME AND ADDRESS <b>US Army Medical Research and Development Command Fort Detrick Frederick, MD 21701</b>		12. REPORT DATE <b>October 17, 1978</b>	13. NUMBER OF PAGES <b>347 pages</b>
12. MONITORING AGENCY NAME & ADDRESS (if different from Controlling Office)		14. SECURITY CLASS. (of this report) <b>Unclassified</b>	
15. DISTRIBUTION STATEMENT (of this Report)  <b>Approved for Public Release; Distribution Unlimited</b>			
16. DISTRIBUTION STATEMENT (of the abstract entered in Block 20, if different from Report)			
17. SUPPLEMENTARY NOTES			
18. KEY WORDS (Continue on reverse side if necessary and identify by block number) <b>Optical Second Harmonic Generation in Tissue; Second Harmonic Generation in Collagen; Glutathione SHG; Mechanisms; Conversion Efficiency; Significance of order</b>			
19. ABSTRACT (Continue on reverse side if necessary and identify by block number) <b>Radiation which appeared to be due to optical second-harmonic generation (SHG) at 347 nm. was observed from cornea, tendon, sclera, and skin on 694 nm. Q-switched ruby laser irradiation. A possible source of this second-harmonic generation was tissue collagen; because of high tissue content and relatively high order. SHG was also observed from glutathione, but not from the lens; and from frog skeletal muscle. Studies were consequently conducted on purified collagen fibers; SHG was observed from a commercial preparation. Collagen order is reduced near 60°C. A large reduction in conversion efficiency at 347 nm. was</b>			

20 (continued)

observed when cornea and tendon were heated above the collagen phase transformation temperature. Therefore, the collagen component of tissue may be the principal site for the SHG. Experiments on normal corneas showed the 347 nm. scattering pattern to more closely resemble coherent second-harmonic generation from a crystalline material than it did incoherent second-harmonic generation from an amorphous material. Corneal models for SHG were developed. The observed conversion efficiency of the normal cornea was in much better agreement with that calculated for coherent than for incoherent conversion. The reduction in conversion efficiency for corneas treated above the collagen phase transformation temperature was explained as a reduction in coherent second-harmonic generation in corneal stroma lamellae due to a decrease in collagen fibril order.

Accession For	
NTIS GR&I	<input checked="" type="checkbox"/>
DTIC TAB	<input type="checkbox"/>
Unannounced	
Justification	
P. _____	
Distribution/	
Availability Codes	
Distribution/	
Availability Codes	
DIA	
A	

The findings in this report are not to be construed as an official Department of the Army position unless so designated by other authorized documents.

BIOLOGICAL EFFECTS OF LASER RADIATION  
Final Scientific Report - Volume IV  
(Optical Second Harmonic Generation in Biological Tissues)

W. Peter Hansen  
Samuel Fine

Submitted October 17, 1978

(1 July 1963 to 30 September 1971)

Supported By

US ARMY MEDICAL RESEARCH AND DEVELOPMENT COMMAND  
Fort Detrick, Frederick, MD 21701

Contract No. DA-49-193-MD2436

Department of Biophysics and Biomedical Engineering  
Northeastern University  
Boston, MA 02115

Approved For Public Release;  
Distribution Unlimited

### **Note on Content**

**This volume contains essentially the material presented by W. Peter Hansen to the Department of Electrical Engineering at Northeastern University for a Doctor of Philosophy degree in June 1974.**

**This volume was reviewed as a thesis by three readers. These are Professor Martin Schetzen, Department of Electrical Engineering; Professor Richard Murphy, Department of Mechanical Engineering; and Professor Welville Nowak, Department of Mechanical Engineering.**

**The thesis was supervised by the principal investigator.**

**In conducting the research described in this report, the investigator(s) adhered to the "Guide for Laboratory Animal Facilities and Care," as promulgated by the Committee on the Guide for Laboratory Animal Resources, National Academy of Sciences-National Research Council.**

## Abstract

The specific concern of this volume is the generation of optical second-harmonic radiation in biological tissue at an ultraviolet wavelength of 347 nm on irradiation with a Q-switched ruby laser at a visible wavelength of 694 nm.

Radiation which appeared to be due to optical second-harmonic generation was observed from cornea, tendon, sclera, and skin. It was surmised that the possible source of the second-harmonic generation in these tissues was the collagen component, since it is present in high concentration and appears to have a relatively high degree of order. Second-harmonic generation was also observed from a crystalline preparation of glutathione, but not from the lens for which it is a constituent. Frog skeletal muscle also produced second-harmonic radiation.

Since second-harmonic generation was observed in collagenous tissue, studies were carried out on purified collagen fibers. Second-harmonic generation was observed from a commercial preparation of collagen.

There is a phase transformation for collagen in tissue near 60°C where the collagen molecules unwind into three random coil chains. The order within the collagen component of the tissue is thereby reduced. A large reduction in the second-harmonic conversion efficiency at 347 nm was observed when cornea and tendon were heated above the collagen phase transformation temperature. These results were a further indication that the collagen component of tissue may be the principal site for optical second-harmonic generation at 347 nm.

There is a predicted difference in the scattering patterns for second-harmonic radiation from crystalline (ordered) and amorphous (disordered) media. Experiments carried out on normal corneas showed the 347 nm scattering pattern to more closely resemble coherent second-harmonic generation from a crystalline material than it did incoherent second-harmonic generation from an amorphous material.

Models were developed to predict the efficiency of second-harmonic generation in the normal cornea. The observed conversion efficiency of the normal cornea was in much better agreement with the calculated coherent conversion efficiency than it was with the calculated incoherent conversion efficiency. The reduction in conversion efficiency for corneas treated above the collagen phase transformation temperature was explained in the models as a reduction in coherent second-harmonic generation in the lamellae of the corneal stroma due to a decrease in the order of the collagen fibrils.

### Support Acknowledgement

These studies were supported in part by a research contract, project number DA-49-193-MD-2436 from the Medical Research and Development Command, United States Army, and by research grants GB-30320 and GK-40575 from the National Science Foundation, and NASA grant NGR22-011-007. This support, which made these studies possible and permitted completion of this volume, is gratefully acknowledged.

### Technical Acknowledgements

We wish to thank the many individuals who have been of assistance during this research.

The readers gave considerable time, assistance and encouragement. We are particularly grateful to Professor Martin Schetzen who devoted an unusual amount of time. He offered valuable guidance in the development of the analytical models and in the interpretation of the experimental results of the research. Professor Richard Murphy and Professor Welville Nowak offered helpful suggestions regarding specific technical aspects of these studies.

We greatly appreciate the assistance and information given by Professor Donald MacKeen, Dr. John Swanson, Dr. Joel Cohen, and Mr. Donald Rust. We also wish to acknowledge the help given by Dr. Bert Litwin, Professor Helen Lambert, Professor Richard Grojean, Professor Ioannis Yannas, Professor Frederick Bowman, and Mr. Eugene Joyce.

## TABLE OF CONTENTS

	Page <i>i</i>
Note on Content	<i>i</i>
Abstract	<i>ii</i>
Support Acknowledgement	<i>iv</i>
Technical Acknowledgements	<i>v</i>
Table of Contents	<i>vi</i>
Chapter 1 Background and Scope of Research	1
Chapter 2 Outline of Optical Second-Harmonic Generation	15
2.1 Linear electric dipole moments	17
2.2 Nonlinear electronic dipole moments	19
2.3 Scalar dipole moments	21
2.4 Model for scalar polarizabilities	22
2.5 Second-harmonic generation by multimode lasers	31
2.6 Second-harmonic generation in a material medium	34
2.7 Coherent second-harmonic generation in a non-dispersive medium	35
2.8 Incoherent second-harmonic generation in non-crystalline media	44
2.9 Sample calculations for water	49
2.9a Calculation of incoherent second-harmonic conversion efficiency - Comparison with experiments by Terhune et al	50
2.9b Calculations related to coherent second-harmonic generation	63
2.10 Summary	68
Chapter 3 A Brief Description of the Constituents and Characteristics of Certain Vertebrate Connective Tissues	71
3.1 Collagen and collagen-related molecular constituents of connective tissue	71

3.2	A brief description of the cornea and sclera	77
3.3	A brief description of tendon	80
3.4	A brief description of skin	81
<b>Chapter 4</b>	<b>Experimental Identification of Optical Second-Harmonic Generation in Biological Tissue</b>	<b>84</b>
4.1	Methods and materials	86
4.2	Results	95
4.2a	Peak emission wavelength	95
4.2b	Square-law dependence	98
4.2c	Bandwidth of emission at 347 nm	100
4.2d	Ancillary results concerning sample damage	101
4.3	Discussion	103
4.3a	Peak emission wavelength	103
4.3b	Square-law relationship	107
4.3c	Bandwidth of emission at 347 nm	110
4.3d	Sample damage and broadband emission	113
4.4	Summary and Conclusions	115
	Appendix A	118
	Figures	120
<b>Chapter 5</b>	<b>Second-Harmonic Generation from Collagen</b>	<b>153</b>
5.1	Methods and materials	153
5.2	Results	154
5.2a	Sample transmission	154
5.2b	Sample emission	155
5.3	Discussion	157
5.4	Amorphous collagen	160

5.5	Summary and conclusions	162
	Appendix A	163
	Figures	166
Chapter 6	Angular Distribution of Second-Harmonic Radiation from the Rabbit Cornea	172
6.1	Methods and materials	173
6.2	Results	178
6.3	Discussion	181
6.4	Summary and conclusions	189
	Figures	191
Chapter 7	Effects of Collagen Phase Transformation on Second- Harmonic Generation	199
7.1	Methods and materials	202
7.1a	Outline of methods and materials	202
7.1b	Details of methods and materials	204
7.2	Results	206
7.2a	Brief summary of results	206
7.2b	Results from tendons	207
7.2c	Results from corneas	214
7.2d	Ancillary results	216
7.3	Discussion	217
7.4	Summary and conclusions	253
	Appendix A	257
	Appendix B	269
	Appendix C	275
	Appendix D	281
References		309-320

## CHAPTER 1

### BACKGROUND AND SCOPE OF RESEARCH

Research concerning the interaction of laser radiation with biological systems has been in progress for about 12 years at a number of laboratories throughout the world. Symposia proceedings and reviews of progress in this area include those published by Litwin and Earle (1965); Fine, Klein, and Scott (1964); Fine and Klein (1965, 1966, 1969a, 1969b, 1970); Goldman (1967); Goldman and Rockwell (1971); Fine, Bushor, and Cox (1968); Wolbarscht (1971); and Ready (1971, Chapter 7).

There have been a number of publications of basic biophysical interest as a result of this research. These include: the production of free radicals in tissue (Derr, Klein, and Fine, 1965; Stratton, Pathak, and Fine, 1965); two-photon fluorescence in biomolecules (Rounds, Olson, and Johnson, 1966); laser beat-frequency spectroscopy of biomolecules (Dubin, Lunacek, and Benedek, 1967); alteration of genetic material (Berns, Rounds, and Olson, 1969); cellular microsurgery (Saks, 1971); studies of focal hepatic injury and repair (Fine et al, 1968); reversible depigmentation associated with melanogenesis in rodent skin (Klein et al, 1965); and interaction of middle infrared CO<sub>2</sub> laser radiation with the cornea (Fine et al, 1967).

A number of analytical models have been developed for the analysis of tissue temperature elevation and thermal injury due to the interaction

of laser radiation with tissues. Publications in this area include thermal models for injury to the retina (Georcats et al, 1965; Nam et al, 1966; Hansen, Feigen and Fine, 1967; Hansen and Fine, 1968; Hayes and Welbarht, 1968; Hansen and Fine, 1968b; Clarke, Georcats and Nam, 1969; Vassiliadas, 1971); injury to the cornea (Peppers et al, 1969); injury to the skin (Fine et al, 1965; Fine et al, 1966); injury to hepatic tissue (Fine et al, 1968); and injury to single cells (Barnes et al, 1966). Analyses of laser induced temperature elevation in tissues have been given in conjunction with models for the measurement of the thermal conductivity of biomaterials (Hansen et al, 1973; Hansen et al, 1973b).

Psychophysical studies have been carried out with regard to lasers. These include studies on the visibility of infrared radiation (Vasilenko, Chebotaev and Trietskii, 1965); the effects of pulsed laser radiation on discriminative avoidance behavior (Taylor and Ebers, 1966); studies of thermal sensation with the CO<sub>2</sub> laser (Campbell and Fine, 1970); and an interpretation of visible laser speckle patterns (Baldwin, 1968).

There has been considerable interest in laser interaction with biological systems at ultraviolet wavelengths (Fine and Klein, 1969b). Cataracts have been produced in rabbit eyes on laser irradiation at 325nm in the middle ultraviolet (MacKoen, Fine and Fine, 1973). In this latter paper, the production of cataracts was considered as probably the result of a photochemical rather than a photothermal

mechanism.

The specific concern of this thesis is the generation of optical second-harmonic radiation in biological tissue at an ultraviolet wavelength of 347nm. Optical second-harmonic generation was first observed by P. A. Franken and his co-workers in 1961 (Franken et al, 1961). In their experiments, high intensity ruby laser radiation was passed through crystalline quartz and the small second-harmonic frequency component in the transmitted light spectrum was detected by a photographic prism spectrograph. Following these initial studies, Maker and his co-workers developed coherent phase matching techniques in crystalline media (Maker et al, 1962) which led to commercial crystalline frequency doubling units with 20% second-harmonic conversion efficiency. Members of this same research group later reported observation of weak incoherent optical second-harmonic generation in amorphous media such as water, and fused quartz (Terhune, Maker and Savage, 1965). Reviews of optical second-harmonic generation research in physical systems have been published by Franken and Ward (1963); Bloembergen (1965); Minck, Terhune and Wang (1966); Pershan (1966); Yariv (1968); Yariv (1971); Baldwin (1969); and Akhmanov and Khokhlov (1972).

The possibility of optical second-harmonic generation in biological systems was first suggested by Fine at the First Annual Conference on The Biologic Effects of Laser Radiation in 1964 (Fine, 1965, s-47).

4

He indicated that it was important to consider the conversion of laser radiation at a given wavelength to other wavelengths in tissue. He referred to thermal radiation, from the highly luminous plume, and to the fact that it was not yet known whether second-harmonic generation might occur in the skin. In the proceedings of this same conference, a paper by Zaret considered the possibility of harmonic generation in the melanin granules of the retinal pigment epithelium on ruby laser irradiation (Zaret, 1965, s-64). Zaret indicated that second-harmonic radiation at ultraviolet wavelengths might be hazardous to retinal tissue. In 1965, Reickhoff and Peticolas reported observation of second-harmonic generation upon ruby laser irradiation of powdered crystalline amino acid preparations (Reickhoff and Peticolas, 1965). Some of these crystalline preparations yielded second-harmonic conversion efficiencies that were comparable to those observed with powdered preparations of inorganic crystals with known high conversion efficiency, such as potassium dihydrogen phosphate.

In 1965 Vasilenko and his co-workers reported studies in which human subjects observed radiation from a pulsed Ne-H<sub>2</sub> laser at wavelengths of 950nm, 1100nm, and 1180nm (Vasilenko, Chebotaev and Troitskii, 1965). Radiation at 950nm was seen as red light. The other laser wavelengths are nominally invisible; however, color matching showed the color sensation in these studies to be extremely close to the color of the second-harmonic of each wavelength. The observed colors were in the yellow-green and orange regions of the spectrum. These authors

concluded that, "Consideration of this data leads to the rather firm conclusion that the light seen by the eye in observing infrared emission corresponds to the harmonic of the given radiation. The present experiment may be useful in elucidating the non-linear properties of the eye." They were probably thinking of optical second-harmonic generation.

It was of interest to us to verify these observations by objective measurements of the radiation emission from tissues, including the eye, on laser irradiation in the near infrared. However, a laser with the necessary characteristics was not available to us at the time of initiation of this research. Because of our interest in second-harmonic generation at ultraviolet wavelengths, and since a Q-switched ruby laser was available, these studies were undertaken at Northeastern University in 1970 using a ruby laser at 694nm. The results of the initial experimental investigations in tissue were reported by Fine and Hansen in 1971 (Fine and Hansen, 1971), and are also contained in this thesis. This thesis is a direct outgrowth of these initial studies.

Our initial studies were conducted on a crystalline preparation of glutathione, on the lens, cornea, vitreous, tendon, sclera, retinal-choroidal tissue, melanin granules, frog skeletal muscle, and on whole blood. Radiation which appeared to be second-harmonic (347nm) was observed from glutathione, but not from the lens of which it is a constituent. Such radiation was also observed from cornea, sclera,

skin and tendon. "Order" is required for efficient second-harmonic generation. It was surmised that the possible source of the second-harmonic generation in these latter tissues was the collagen component, since it is present in high concentration and appears to have a relatively high degree of order. In addition, second-harmonic generation was observed from muscle, which also appears to be a highly ordered tissue. However, muscle does not contain significant amounts of collagen.

Since second-harmonic generation was observed in collagenous tissue, studies were carried out on purified collagen. Second-harmonic generation was observed from a commercial preparation of purified collagen obtained from Sigma Chemical Company but not from fibers prepared by another method.

There is a phase transition temperature for tissue collagen near 60°C where the collagen molecules unwind into three random coil chains. This, therefore, reduces the order within the collagen component of the tissue (Flory, 1956). Consequently, second-harmonic conversion efficiency experiments were performed in two collagenous tissues (cornea and tendon) that had undergone heating to temperatures below and above 60°C. When these tissues were heated above the collagen phase transformation temperature, a large reduction in second-harmonic conversion efficiency at 347nm was observed. These results were a further indication that the collagen component of tissue may be the principal site for

optical second-harmonic generation on ruby laser irradiation.

There is a predicted difference in the scattering patterns for second-harmonic radiation from crystalline (ordered) and amorphous (disordered) media (Barsohn, Pao and Frisch, 1966). Experiments were carried out on normal corneas which showed the 347nm scattering pattern to more closely resemble coherent second-harmonic generation from a crystalline material than it did incoherent second-harmonic generation from an amorphous material. In addition, the scattering studies also indicate that the normal cornea possesses a certain degree of order.

Models were developed to predict the efficiency of second-harmonic generation in the normal cornea. The observed conversion efficiency of the normal cornea was in much better agreement with a calculated coherent second-harmonic conversion efficiency than it was with a calculated incoherent second-harmonic conversion efficiency for the normal cornea. The conversion efficiency of the cornea decreased by a large amount after heating through the collagen phase transformation temperature. This is explained in the models as a reduction in coherent second-harmonic generation in the collagen fibrils of the cornea due to a decrease of the order in the fibrils.

The studies are set forth in the following order in this thesis. A review of the literature on optical second-harmonic generation and models for coherent and incoherent optical second-harmonic generation from crystalline and amorphous media respectively are given in Chapter 2.

A brief description of collagen and collagenous tissue is given in Chapter 3. The initial experimental studies showing narrow band 347nm emission from tissue on irradiation at 694nm with a Q-switched ruby laser are included in Chapter 4. Contained in this chapter is substantiation of the thesis that the observed 347nm emission is second-harmonic radiation. In Chapter 5, the experiments on purified collagen are discussed. Two forms of purified collagen were used. Second-harmonic generation was observed in collagen fibers obtained from Sigma Chemical Company; second-harmonic generation was not observed from collagen fibers prepared by another method. This difference is discussed on the basis of a difference between these two preparations with regard to the relative orientation of the collagen molecules.

The observed 347nm scattering pattern from a normal cornea is presented in Chapter 6. The results are compared with predicted second-harmonic scattering patterns from crystalline and amorphous media. The observed pattern more closely resembled the predicted pattern for coherent second-harmonic generation from a crystalline medium than it did the predicted pattern for incoherent second-harmonic generation from an amorphous medium. Scattering patterns for corneas heated above 60°C could not be obtained because the 347nm emission intensity was too low.

The results of experiments concerning heated corneas and tendons are contained in Chapter 7. An order of magnitude reduction in the

second-harmonic conversion efficiency was observed in these tissues following heating to temperatures above 60°C. A model for second-harmonic generation in the collagen fibrils of the cornea is presented. In this model, the peptide bonds of the collagen molecules are considered to be the source of second-harmonic radiation. The measured conversion efficiency from normal cornea is in reasonable agreement with this model when the collagenous component of the cornea is considered to be highly ordered. The measured conversion efficiency of corneas that had been heated through the collagen phase transformation was several orders of magnitude above the level predicted on the basis that all of the collagen was converted to a random coil form and the thermally transformed cornea was amorphous. The difference between the observed and predicted conversion efficiency of the heated corneas was considered to be due to the possibility that heating of the corneas above 60°C did not transform all of the collagen to an amorphous random-coil phase. The remaining degree of order following heating may account for the observed conversion efficiency being higher than expected in thermally altered corneas. The results of the studies in Chapter 7 were not inconsistent with the results obtained from the models used for analysis.

It has been shown in this thesis that the cornea produces second-harmonic radiation at a wavelength of 347nm on irradiation with a ruby laser at 694nm. The cornea may produce second-harmonic radiation when

irradiated in the near infrared (e.g. with neodymium or erbium lasers). It is possible that the threshold for visibility of a second-harmonic lies below the threshold for injury to the eye at the fundamental wavelength. Consequently, harmonic generation in ocular tissue may be of significance to vision (Fine and Hansen, 1971).

Although second-harmonic radiation was observed from crystalline glutathione, it was not observed from the rabbit lens for which glutathione is a constituent. Further studies in this regard are required, particularly since the lens appears to possess considerable order.

Other significant aspects of optical second-harmonic generation studies in tissue have been discussed in part in the publication by Fine and Hansen (1971). As stated by the authors, "Harmonic generation as made available with lasers may offer an additional tool for characterization of biologically significant molecules, tissue components, and structure, as well as kinetic biological processes both in vivo and in vitro. In particular, these latter dynamic studies may be feasible because of the great number of wavelengths, high pulse repetition frequencies, and short pulse durations currently available from reliable laser systems.

Separation, purification, or synthesis of macromolecules may result in structural changes in the molecules or in the aggregation patterns of the molecules. Identification of those changes that are associated with the above procedures can be difficult, time-consuming,

or require a larger sample amount than can be conveniently spared. This is especially true if the changes are minor. In some cases, harmonic generation in macromolecular samples may be altered during separation, purification, or synthesis. This alteration may be indicative of a change in structure not otherwise readily detectable. Consequently, harmonic generation at various wavelengths should be considered as a technique for rapid and possibly nondestructive testing of certain aspects relating to molecules and their aggregation patterns, both on a laboratory and production basis" (Fine and Hansen, 1971).

Two of the many possible aggregation patterns of collagen are discussed in Chapter 5 of this thesis. In this chapter, experimental evidence is given that these two collagen forms have significantly different second-harmonic conversion efficiencies. Consequently, a distinction might indeed be made between aggregation patterns based on second-harmonic generation studies.

The possibility and significance of optical second-harmonic generation in the skin and eye at ultraviolet wavelengths has been previously considered (Fine, 1965, p. s-47; Zaret, 1965, p. s-64; Fine and Klein, 1969b). The results of this thesis indicate that ultraviolet second-harmonic generation is produced at deep layers of the cornea and skin when a visible wavelength ruby laser is used. It is still unclear whether the second-harmonic generation observed is due to lack of molecular inversion symmetry or lack of inversion

symmetry in structural units at the intramolecular level, and to what extent tissue order is important.

Some studies were carried out to provide a basis for the resolution of these questions. Cornea and tendon were heated above the collagen phase transformation temperature. Above this temperature, collagen is believed to be transformed from an ordered to a random coil configuration, as evidenced by tissue contraction, decreased birefringence, increased mechanical compliance, and altered optical transmission. Consequently, we believe there is a decrease in order above this temperature. It was observed that the second-harmonic conversion efficiency decreased when these tissues were heated above this phase transformation temperature. We believe that these results indicate that tissue order may be an important factor in second-harmonic conversion efficiency. Further studies are required to resolve the questions stated above. However, the experimental studies do indicate that changes in the second-harmonic conversion efficiency may be a sensitive indicator of structural changes which may not otherwise be readily detectable.

Although the collagen fibers of tendon are well-aligned, they are of varying diameter. In addition, normal tendon is quite opaque. In the sclera and skin, the fibers do not appear to be as well-aligned as they are in cornea; the fibers are of varying diameter; and these tissues are not as transparent or as homogeneous as the cornea. For

these reasons further work will be required to develop adequate models for these tissues with respect to second-harmonic generation.

When heated slowly in water beyond the collagen phase transformation temperature and allowed to mechanically creep under light loading, the tendon becomes transparent at both 694nm and 347nm. Consequently, with further investigation it might be possible to develop second-harmonic generation models for tendon in this condition. Measurement of collagen concentration would have to be carried out in order to develop these models. It may be necessary to find a material with refractive index that matches that of collagen that could be used to impregnate the normal tendon. This may improve the transparency of this tissue and allow comparisons of theory and experiment. Skin and sclera, because of their inherent irregularity, will be probably the most difficult to model and compare with experiment with regard to second-harmonic generation.

The peptide bond in collagen was considered to be the possible source of second-harmonic generation. Further work is required to determine the validity of this hypothesis. Studies on amino acids and on synthetic peptides may provide information in this regard. For example, crystalline glycine has been shown to produce relatively insignificant levels of second-harmonic radiation in comparison to that produced by other crystalline amino acids (Reickhoff and Peticolas, 1965). Studies on polyglycine may assist in evaluating the hypothesis.

Although such studies were considered, time precluded carrying out this work. These studies were carried out at a single fundamental wavelength of 694nm. This may not have produced the maximum possible conversion efficiency in collagenous tissue. The use of a tunable laser to determine the wavelength dependence of the conversion efficiency may yield information regarding the identity of the second-harmonic oscillators.

In addition, the reason for the increased transparency of tendon, when heated above the collagen phase transformation temperature, may not be understood, and consequently warrants further study.

## CHAPTER 2

## OUTLINE OF OPTICAL SECOND-HARMONIC GENERATION

There is an extensive literature in the physical sciences describing experimental and theoretical aspects of optical second-harmonic generation in solids, liquids and gases. Review articles have been written by Franken and Ward (Franken and Ward, 1961), Pershan (Pershan, 1966), Bloembergen (Bloembergen, 1965), and Minck et al (Minck et al, 1966).

Most experimental studies have been carried out with carefully prepared systems of molecules with relatively well-understood optical characteristics. As a result, the companion analytical models that have been reported for these systems have contained substantial physical and mathematical detail. For example, it is common to find analyses that include the effects of material birefringence on nonlinear wave propagation in solids (Bloembergen, 1965, p. 84). There are also models of second-harmonic generation in liquids that include the statistical effects of intermolecular orientation (Bersohn et al, 1966).

Compared to physical systems, the optical characteristics of biological tissues are poorly understood. Because of the complexity of biological tissue, the analysis of optical second-harmonic generation in tissue must proceed along simple lines.

The purpose of the present chapter is to first review some of the analytical methods of nonlinear optics that have appeared in

the physical science literature. These methods will then be used to obtain estimates of the parameters that are needed to compute the second-harmonic generation efficiency of materials. These methods are not exact, and at best will yield order of magnitude agreement with experimental data for physical systems (Bloembergen, 1965, Chap. 5; Yariv, 1968, pp. 344-348; Garrett and Robinson, 1966). In later chapters these methods will be used to estimate the approximate second-harmonic conversion efficiency of biological tissues.

We shall first review some of the classical physical principles concerning optical second-harmonic generation. The discussion will begin with a review of both linear and nonlinear induced dipole moments in matter. We shall then present the solutions to the differential equation for the anharmonic oscillator (Bloembergen, 1965, Eq. 1-9; Garrett and Robinson, 1966, Eq. 2; Pershan, 1966, Eq. 3.3). These anharmonic oscillator solutions provide estimates of the harmonic content of the induced dipole moment oscillations. However, the arrangement of the dipoles within the medium determines the harmonic content of the electromagnetic radiation. The second-harmonic content of the radiation will be estimated for two limiting cases of matter - crystalline matter and amorphous matter. The second-harmonic conversion efficiency can be significantly greater in crystalline matter than it is in amorphous matter.

Equations will be written in Gaussian cgs units since much of

the literature has been written in these units. A list of important conversion factors to MKS units is given in Appendix A.

## 2.1 Linear electric dipole moments

When an isolated pair of equal and opposite point charges with fixed charge magnitudes are separated by a fixed distance  $x$ , the charge configuration is said to be a static electric dipole. The static dipole moment  $\vec{\mu}$  is a vector with magnitude  $qx$  that is directed from the negative to the positive charge. If a charge distribution is allowed to vary in such a way that  $\vec{\mu}(t)$  is a periodic function, then the charge distribution is said to be an oscillating electric dipole.

An applied electric field that varies sinusoidally in time will induce periodically varying dipole moments in the molecules of a material medium. The major mechanism responsible for induced dipole moments at frequencies corresponding to visible and ultraviolet radiation is called electronic polarization. Physically, electronic polarization can be viewed as the forced motion of a bound electron cloud around a massive stationary positive charge (Siegman, 1971, p. 68). At lower frequencies (i.e. infrared, microwave, and radio frequencies) the massive positive charge centers can also move appreciably during a period of the applied electric field oscillation. Large oscillating low frequency dipole moments can be induced in polar molecules when the low frequency applied electric field produces

rotational motion of the molecule as a whole, or when vibrational motion of the molecular nuclei with respect to the center of mass of the molecule is produced (Kittel, 1965, p. 164). We shall not be concerned with these lower frequency polarization mechanisms. The magnetic dipole interactions at optical frequencies will also be neglected (Baldwin, 1969, p. 19).

A linear, or first-order, electric dipole moment is defined as one that is directly proportional to the local electric field that acts on the dipole. The first order dipole moment is a vector. A vector component will be denoted by the subscript  $p$ . Therefore, the time varying  $p^{\text{th}}$  component of the first-order dipole moment will be denoted by  $\mu_{p,1}(t)$ . The local electric field is also a vector. We shall denote its components by the subscript  $q$ . Since we shall be considering harmonic fields later on, it is convenient to denote the fundamental field by an additional subscript "1". Therefore,  $E_{loc,q,1}(t)$  is the  $q^{\text{th}}$  vector component of the local fundamental electric field. We shall also write this field in terms of its complex amplitude as  $E_{loc,q,1}(t) = \text{Re} \{ \hat{E}_{loc,q,1} e^{j\omega t} \}$  where the symbol " $\hat{\phantom{x}}$ " denotes the complex amplitude of a time-varying quantity. We then define  $\mu_{p,1}(t)$  by:

$$\mu_{p,1}(t) = \text{Re} \left\{ \sum_{q=1}^3 \alpha_{pq} \hat{E}_{loc,q,1} e^{j\omega t} \right\} \quad (1)$$

In Eq. (1), the  $\alpha_{pq}$  are complex components of the first-order

polarizability tensor ( $\alpha_{pq}$ ) (Bersohn et al, 1966, p. 3184).

## 2.2 Nonlinear electronic dipole moments

When the local electric field strengths are high and the electron cloud displacements are large, Eq. (1) is not sufficient to predict the total induced dipole moment. More generally, higher order terms in  $E_{loc,q,1}(t)$  are required to predict the total dipole moment. Let  $\mu_p(t)$  be the  $p^{\text{th}}$  component of the total electric dipole moment, then when the electron cloud displacement is large,  $\mu_p(t)$  is expressed as follows

$$\mu_p(t) = \mu_{p,1}(t) + \mu_{p,2}(t) + \mu_{p,3}(t) + \dots \quad (2)$$

In Eq. (2),  $\mu_{p,1}(t)$  is proportional to the local field,  $\mu_{p,2}(t)$  is proportional to the local field squared and so on. We have already defined  $\mu_{p,1}(t)$  in Eq. (1). The next two dipole moments  $\mu_{p,2}$  and  $\mu_{p,3}$  are defined in Eqs. (2a) and (2b).

$$\mu_{p,2}(t) = \text{Re} \left\{ \sum_{q=1}^3 \sum_{r=1}^3 \beta_{pqr} \hat{E}_{loc,q,1} \hat{E}_{loc,r,1} e^{2j\omega t} \right\} \quad (2a)$$

$$\mu_{p,3}(t) = \text{Re} \left\{ \sum_{q=1}^3 \sum_{r=1}^3 \sum_{s=1}^3 \gamma_{pqrs} \hat{E}_{loc,q,1} \hat{E}_{loc,r,1} \hat{E}_{loc,s,1} e^{3j\omega t} \right\} \quad (2b)$$

(Bersohn et al, 1966, Eq. 1). In Eqs. (2a) and (2b) the  $\beta_{pqr}$  are

complex components of the second-order polarizability tensor and the  $\gamma_{pqrs}$  are complex components of the third-order polarizability tensor. Higher order polarizability tensors are defined in a similar way. Each term in Eq. (2) is often referred to as a dipole moment. The first term is the  $p^{\text{th}}$  component of the first-order dipole moment, the second term is the  $p^{\text{th}}$  component of the second-order dipole moment, and so on.

Successively higher order dipole moments become small very rapidly. Bloembergen has estimated that even with the very high fields of  $10^{10}$  Watts/cm<sup>2</sup> in the focus of a Q-switched laser, and for intra-atomic electric fields that are typically of the order of  $3 \times 10^8$  volts/cm each dipole moment in Eq. (3) is approximately a thousand times smaller than the preceding moment (Bloembergen, 1965, p. 8).

The tensor polarizabilities of Eqs. (1), (2a), and (2b) are physical properties of the molecule and therefore their symmetry properties are dependent upon the symmetry properties of the structure of the molecule (Nye, 1957, p. 20). When this principle is applied to the tensors ( $\alpha_{pq}$ ), ( $\beta_{pqr}$ ), ( $\gamma_{pqrs}$ ), etc. it is found that the even order polarizabilities (e.g.  $\beta_{pqr}$ ) vanish for molecules that are symmetric under inversion (Bersohn et al, 1966, p. 3185). Relations among the components of the polarizability tensors can be obtained from considerations of other symmetry properties of the molecular structure. Thermodynamic arguments have also been proposed to derive symmetry properties of the

second-order tensor polarizability (Franken & Ward, 1962, p. 27).

### 2.3 Scalar dipole moments

In the early nonlinear optics literature, emphasis was often placed on estimating the magnitude of the induced nonlinear molecular dipole moment without concern for its direction (Franken & Ward, 1961). For the biological molecules with which we will be concerned in this thesis, there is not enough available information to treat the polarizabilities as tensors; therefore we shall also be mainly concerned with predicting the approximate magnitude rather than the direction of the induced nonlinear dipole moments. In an early review, Franken and Ward (Franken & Ward, 1962, p. 23) used a scalar version of Eq. (2) which we shall write as:

$$\mu(t) = \text{Re} \{ \alpha \hat{E}_{loc,1} e^{j\omega t} + \beta \hat{E}_{loc,1}^2 e^{2j\omega t} + \gamma \hat{E}_{loc,1}^3 e^{3j\omega t} + \dots \} \quad (3)$$

In Eq. (3),  $E_{loc,1}$  is the complex amplitude of the local fundamental field at frequency  $\omega$  and  $\alpha$ ,  $\beta$  and  $\gamma$  are complex coefficients. While Eq. (3) is a scalar equation, it still reflects an important anisotropic property of a nonlinear dipole. That is, the coefficient  $\beta$  and all other even order term coefficients vanish if  $\mu$  simply changes sign when  $\hat{E}_{loc}$  changes sign (i.e. if the graph of  $\mu$  vs.  $\hat{E}_{loc}$  is anti-symmetric about the origin). Note that:

$$\beta = \frac{1}{2} \left( \frac{d^2 \hat{\mu}}{dE_{loc}^2} \right)_{E_{loc}=0} \quad (4)$$

and that  $(d^2 \hat{\mu}/dE_{loc}^2)_{E_{loc}=0}$  vanishes for such graphs. This is the one-dimensional equivalent to the rule that  $(\beta_{ijk})$  vanishes in centrosymmetric molecules.

In future discussions we shall call  $\mu_1(t) = \text{Re} \{ \alpha \hat{E}_{loc,1} e^{j\omega t} \}$  the first-order scalar dipole moment,  $\mu_2(t) = \text{Re} \{ \beta \hat{E}_{loc,1}^2 e^{2j\omega t} \}$  the second-order scalar dipole moment and so on. The dipole moments can then be written as  $\mu_1(t) = \text{Re} \{ \hat{\mu}_1 e^{j\omega t} \}$  and  $\mu_2(t) = \text{Re} \{ \hat{\mu}_2 e^{j\omega t} \}$  where  $\hat{\mu}_1$  and  $\hat{\mu}_2$  are the complex amplitudes of the first- and second-order dipole moments respectively. Combining these expressions establishes relationships between the complex field amplitudes and the complex dipole moment amplitudes. These are:  $\hat{\mu}_1 = \alpha \hat{E}_{loc,1}$  and  $\hat{\mu}_2 = \beta \hat{E}_{loc,1}^2$ .

In the next section, models will be presented for calculating the complex scalar polarizabilities  $\alpha$  and  $\beta$ .

#### 2.4 Model for scalar polarizabilities

There are two approaches to calculating polarizabilities. One is quantum mechanical and the other is an older classical approach (Bloembergen, 1965). In the classical approach, the dipole is modeled in terms of an oscillator. Calculations of second-harmonic generation using classical scalar models have yielded results that

agree with experiment (Yariv, 1968, Section 21.3).

A complete review of the classical oscillator model will not be given. In presenting expressions for  $\alpha$  and  $\beta$  we shall mainly follow the development by Bloembergen (Bloembergen, 1965).

In the classical picture, each oscillator is considered to be an electron that moves under a restoring force, a small damping force, and a force produced by an applied electric field (Ditchburn, 1963, p. 563). We shall only consider the case of electrons that are bound to local sites in atoms or molecules. We shall not consider semiconductors or metals. The damping force and the restoring force can be computed approximately from molecular theory (Ditchburn, 1963, p. 564). When restoring force calculations are required in this dissertation, we will assume that the electron is a spherical, uniform, negative charge cloud surrounding a stationary positive point charge. The cloud will have a total negative charge equal to the electronic charge,  $e$ , and a mass equal to the electronic mass,  $m$ . The positive point charge will also have a charge magnitude of  $e$ .

If the electron cloud is displaced by a small amount from its equilibrium position and then allowed to move freely, it will execute an oscillatory motion. For small damping the frequency of this oscillation is  $\omega_0 = (K/m)^{1/2}$  where  $K$  is the linear restoring force constant (Ditchburn, 1963, p. 564). The displacement is assumed to be small since the restoring force is assumed to be linear only for

small displacements.

If the electron cloud displacement,  $x$ , is large, then the anharmonicity of the restoring force must be accounted for. The one-dimensional anharmonic oscillator equation is (Bloembergen, 1965, p. 5, Eq. 1.9)

$$m\ddot{x} + m\Gamma\dot{x} + m\omega_0^2 x + m\Omega x^2 = -fe \operatorname{Re} \{ \hat{E}_{loc,1} e^{j\omega t} \} \quad (5)$$

In Eq. (5)  $m\Gamma\dot{x}$  represents a damping force proportional to velocity. The natural (resonant) frequency of the oscillator is  $\omega_0$ . The linear restoring force is  $m\omega_0^2 x$  and the anharmonic restoring force is  $m\Omega x^2$ . The resonant frequency  $\omega_0$  is taken to be the frequency of an observed spectral line (Bloembergen, 1965, p. 8). We shall use simple atomic and molecular models to estimate the constant  $\Omega$  in the expression for the anharmonic restoring force.

The right hand side of Eq. (5) differs from Bloembergen's (Eq. 1.9) in two respects. The first is that we are considering a single monochromatic driving frequency,  $\omega$ , whereas Bloembergen considers the case of two monochromatic driving frequencies. Bloembergen does this to discuss optical mixing as well as second-harmonic generation. The second difference is that we have included an oscillator strength,  $f$ . The oscillator strength must be determined by experiment (Ditchburn, 1963, p. 688). Experimental values of  $f$  are usually less than unity and are often much less than unity

(Ditchburn, 1963, p. 711). This means that a local field,  $\text{Re} \{E_{loc,1} e^{j\omega t}\}$ , generally produces a smaller oscillation amplitude than would be expected from classical considerations alone.

Series solutions have been obtained for Eq. (5) (Bloembergen, 1965, p. 6). The general form of the solution is:

$$x(t) = \text{Re} \{ \hat{x}_0 + \hat{x}_1 e^{j\omega t} + \hat{x}_2 e^{2j\omega t} \} \quad (6)$$

The d.c. term,  $\hat{x}_0$ , is manifested as a small constant polarization and is called optical rectification. This term will not be considered further. The complex amplitudes,  $\hat{x}_1$  and  $\hat{x}_2$  of the fundamental and second-harmonic terms are (Bloembergen, 1965, Eqs. 1.10, 1.11):

$$\hat{x}_1 = \frac{fe}{m} \frac{\hat{E}_{loc,1}}{D(\omega)} \quad (7)$$

$$\hat{x}_2 = \frac{f^2 e^2 \Omega}{m^2} \frac{\hat{E}_{loc,1}^2}{D^2(\omega) D(2\omega)} \quad (8)$$

where:

$$D(\omega) = \omega_0^2 - \omega^2 - j\Gamma\omega \quad (9)$$

$$D(2\omega) = \omega_0^2 - 4\omega^2 - 2j\Gamma\omega \quad (10)$$

$$(\omega_0^2 - \omega^2) \gg \Gamma\omega \quad (11)$$

$$(\omega_0^2 - 4\omega^2) \gg 2\Gamma\omega \quad (12)$$

Under these conditions  $D(\omega)$  and  $D(2\omega)$  can be approximated by the real variables:

$$D(\omega) = \omega_0^2 - \omega^2 \quad (13)$$

$$D(2\omega) = \omega_0^2 - 4\omega^2 \quad (14)$$

In the instances that we will consider, the fundamental frequency,  $\omega$ , and the second-harmonic frequency,  $2\omega$ , are remote from the frequencies,  $\omega_0$ , of narrow spectral lines. Therefore, the approximate equations (13) and (14) will be used.

The polarizabilities  $\alpha$  and  $\beta$  can now be estimated. There are two expressions for the first order dipole moment  $\mu_1$ :

$$\mu_1 = e\hat{x}_1 \quad (15)$$

$$\mu_1 = \alpha\hat{E}_{loc,1} \quad (16)$$

Combining these yields:

$$\alpha = e\hat{x}_1/\hat{E}_{loc,1} \quad (17)$$

Using Eq. (7) for  $x_1$ , one then obtains:

$$\alpha = \frac{fe^2}{m} \frac{1}{D(\omega)} \quad (18)$$

Similarly, there are two expressions for the second-order dipole moment  $\mu_2$ :

$$\mu_2 = e\hat{x}_2 \quad (19)$$

$$\mu_2 = \beta \hat{E}_{loc,1}^2 \quad (20)$$

Combining these yields:

$$\beta = e\hat{x}_2 / \hat{E}_{loc,1}^2 \quad (21)$$

Using Eq. (8) for  $x_2$  one then obtains:

$$\beta = \frac{f^2 e^3 \Omega}{m^2} \frac{1}{D^2(\omega) D(2\omega)} \quad (22)$$

The constant  $\Omega$  in Eq. (22) will now be estimated. Bloembergen has suggested that the nonlinear restoring force,  $m\Omega x^2$ , is of the same order as the linear restoring force,  $m\omega_0^2 x$ , when the oscillator displacement,  $x$ , is of the order of the radius,  $a_0$ , of the equilibrium orbital of the electron (Bloembergen, 1965, p. 7). Using this

criterion, the following approximation for  $\Omega$  is obtained:

$$\Omega = \omega_0^2/a_0 \quad (23)$$

The frequency of an electronic spectral line is related to the dimensions of the atomic or molecular structural unit. In some cases mathematical expressions for this relationship have been derived (Setlow and Pollard, 1962, pp. 223-225). A simple classical atomic model will be used to derive a relationship between  $\omega_0$  and  $a_0$  in Eq. (23).

Recall that each classical oscillator is assumed to be an electron that is bound to an atom or molecule. One simple model considers the electron to be a uniform spherical negative charge cloud with radius  $a_0$ , charge  $-e$ , and mass  $m$  (Siegman, 1971, p. 68). In this simple model the cloud surrounds a single (nuclear) point charge  $+e$ . When the cloud is displaced by an amount  $x$  from its equilibrium position, it feels a linear restoring force  $Kx$  when  $x \leq a_0$ , and a nonlinear Coulomb restoring force  $e^2/x^2$  when  $x \geq a_0$ . Since both equations are valid when  $x = a_0$ , we can equate them and obtain the following relation:

$$K = e^2/a_0^3 \quad (24)$$

The resonant frequency of the classical electron oscillator is

$\omega_0 = (K/m)^{1/2}$ . Combining this with Eq. (24) yields:

$$a_0 = \left( \frac{e^2}{\omega_0^2 m} \right)^{1/3} \quad (25)$$

Equation (25) is a classical result that shows an inverse relationship between atomic size and resonant frequency. Quantum-mechanical models of large complicated molecular structures also show an inverse relationship between molecular size and the frequency of the lowest energy spectral lines of the structure (Setlow and Pollard, 1962, p. 225). Equation (25), however, may not be the correct specific inverse relationship for complicated molecules.

Combining Eq. (23) and Eq. (25) yields the following expression for  $\Omega$ :

$$\Omega = \left( \frac{\omega_0^8 m}{e^2} \right)^{1/3} \quad (26)$$

When Eq. (26) is used for  $\Omega$ , the expression for  $\beta$  becomes:

$$\beta = \frac{f^2 e^3}{m^2} \left( \frac{\omega_0^8 m}{e^2} \right)^{1/3} \frac{1}{D^2(\omega) D(2\omega)} \quad (27)$$

Equation (27) has been derived for the case where there is a single spectral line at frequency  $\omega_0$ . Kielich has treated the case where there is more than one spectral line for each atom (Kielich, 1964). His results are similar to those obtained for

linear dipoles (Ditchburn, 1963, p. 565) in that each spectral line at frequency  $\omega_{oi}$  makes a separate contribution  $\hat{\mu}_{2i}$  to the total second-order dipole moment for the atom,  $\hat{\mu}_2$  (Kielich, 1964, p. 5a):

$$\hat{\mu}_2 = \sum_{i=1}^{N'} \hat{\mu}_{2i} \quad (28)$$

In Eq. (28) the sum is taken over  $N'$  spectral lines. The  $\hat{\mu}_{2i}$  are given by:

$$\hat{\mu}_{2i} = \beta_i \hat{E}_{loc,1}^2 \quad (29)$$

Combining Eqs. (28) and (29):

$$\hat{\mu}_2 = \hat{E}_{loc,1}^2 \sum_{i=1}^{N'} \beta_i \quad (30)$$

where

$$\beta_i = \frac{f_i^2 e^3}{m^2} \left( \frac{\omega_{oi}^8}{e^2} \right)^{1/3} \frac{1}{D_i^2(\omega) D_i(2\omega)} \quad (31)$$

and

$$D_i(\omega) = \omega_{oi}^2 - \omega^2 - j\Gamma_i \omega \quad (32)$$

$$D_1(2) = \frac{2}{\omega_1} - 4^2 - 2j\Gamma_1 \quad (33)$$

In the instances that we will consider, the fundamental frequency,  $\omega$ , and the second-harmonic frequency,  $2\omega$ , are remote from the frequencies,  $\omega_{0i}$ , of narrow spectral lines. Therefore, the approximations used in Eqs. (13) and (14) can again be employed.

We shall define the second-order polarizability of the atom for the case of  $N'$  spectral lines to be:

$$\beta = \sum_{i=1}^{N'} \beta_i \quad (34)$$

In summary, the methods used in this section allow values of the polarizabilities  $\alpha$  and  $\beta$  (Eqs. (18) and (31)) to be estimated for simple electron cloud resonances such as those for "hydrogen-like" atoms. It has been shown that when a classical electron oscillator is bound by an anharmonic restoring force, the cloud oscillates in a periodic motion with a fundamental frequency equal to the frequency of the applied electric field. The motion of the oscillator also contains higher harmonics for which the second-harmonic motion has been calculated.

## 2.5 Second-harmonic generation by multi-mode lasers

Consider the second order dipole moment  $\mu_2(t)$ . If the local electric field varies sinusoidally at a frequency  $\omega$  then the first

term in Eq. (2) gives rise to dipole radiation at frequency  $\omega$  and the second term gives rise to a d.c. field and dipole radiation at frequency  $2\omega$ . The d.c. field gives rise to a bias field in the medium which we shall neglect. The  $2\omega$  radiation is the source of second-harmonic generation with which we shall be concerned.

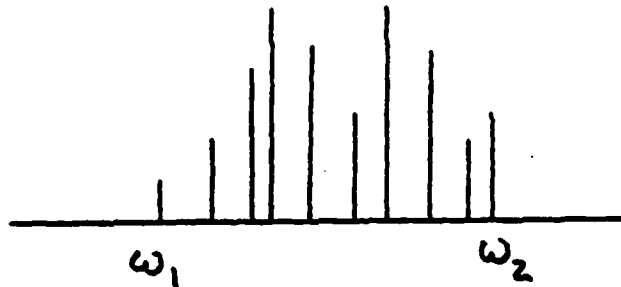
If the local electric field contains two discrete frequencies  $\omega_1$  and  $\omega_2$ , i.e.  $E_{loc,1}(t) = E_a \cos \omega_1 t + E_b \cos \omega_2 t$ , then the second order term in Eq. (2), being proportional to the square of the local field, gives rise to sum and difference frequencies. It can be shown with simple trigonometric manipulation that the frequencies and relative amplitudes of the sinusoidal components of  $\mu_2(t)$  are as follows.

Frequency	Relative Amplitude of Sinusoidal Component
zero	$\frac{1}{2} (E_a^2 + E_b^2)$
$2\omega_1$	$\frac{1}{2} E_a^2$
$2\omega_2$	$\frac{1}{2} E_b^2$
$\omega_1 + \omega_2$	$E_a E_b$
$\omega_1 - \omega_2$	$E_a E_b$

If the local field contains many discrete frequencies rather than

just two frequencies, then as a consequence of the second order nonlinearity in  $\mu(t)$  there will be a large number of harmonic, sum, and difference frequency combinations.

The short-term output spectrum of a laser can be modeled as containing many discrete frequencies. These essentially monochromatic frequencies,  $\omega_n$ , cover a narrow spectral range between  $\omega_1$  and  $\omega_2$  as shown below.



Each discrete frequency in the sketch corresponds to an active laser mode emitting an essentially monochromatic wave at frequency  $\omega_n$ . If a laser with this kind of output spectrum is used to drive a dipole with nonlinearities described by  $\beta E^2$ , then the second-harmonic of each  $\omega_n$  as well as a large number of sum and difference frequency components will appear in the nonlinear part of the scattered light spectrum of the molecule. The second-harmonic and sum frequencies will lie between  $2\omega_1$  and  $2\omega_2$ . The difference frequency spectrum lies at much lower frequencies such as at microwave

frequencies.

Ruby lasers have a recognizable transverse mode structure when operated near threshold. However, in high peak power operation, such as is employed in nonlinear optical studies, recognizable transverse modes are not exhibited (Ready, 1971, p. 15). The mode structure of millisecond pulse ruby lasers changes during the pulse. It is not clear to what extent the mode structure of Q-switched ruby lasers changes during a typical 20 nsec pulse (Ready, 1971, p. 16). It is difficult to resolve the narrow band short term spectrum of a Q-switched laser pulse and its associated second-harmonic and sum-frequency pulse. Because of this practical difficulty, all of the narrow band radiation between  $2\omega_1$  and  $2\omega_2$  is often referred to simply as second-harmonic radiation.

#### 2.6 Second-harmonic generation in a material medium

There are two limiting cases of second-harmonic generation in material media that will be useful to consider. In the first case, the molecules of the medium are assumed to be in perfect mutual alignment and arranged in a regular lattice with a lattice spacing much smaller than an optical wavelength. This situation has been analyzed in detail by a number of authors since it can be used to represent crystalline media from which relatively intense collimated beams of second-harmonic radiation have been obtained (Bloembergen, 1965). We shall call this the case of coherent second-harmonic

generation in a crystalline medium.

In the second case to be considered, the molecules of the medium are assumed to be random in position and orientation. This situation has also been analyzed by a number of authors since it can be used to represent gaseous, liquid and amorphous solid media (Kielich, 1963; Terhune et al, 1965; Bersohn et al, 1966). Weak wide angle scattered second-harmonic radiation has been observed from liquids and amorphous solids and used in the analysis of molecular structure (Terhune et al, 1965). We shall call this the case of incoherent second-harmonic generation in a non-crystalline medium.

In our analysis of both of these limiting cases, we shall neglect problems of reflection and refraction at the boundaries of the medium. We shall also assume the medium to be non-dissipative.

## 2.7 Coherent second-harmonic generation in a non-dissipative crystalline medium

Armstrong et al (Armstrong et al, 1962) have provided a detailed analysis of second-harmonic generation in what we have called a crystalline medium. They have shown that the macroscopic polarization of the medium at the second-harmonic frequency is the source for a second-harmonic wave in the medium. Consider a single position in the medium. At this position let  $P_2(t) = \text{Re} \{ \hat{P}_2 e^{2j\omega t} \}$  be the scalar second-harmonic macroscopic polarization. Let  $E_1(t) =$

Let  $\hat{E}_1 e^{j\omega t}$  be the total scalar macroscopic field in the medium at this same position. The complex amplitudes  $\hat{P}_2$  and  $\hat{E}_1$  are related by the following equation (Bloembergen, 1965, Eq. 1-13; Armstrong et al, 1962, Eq. 3-17):

$$\hat{P}_2 = \chi_2 \hat{E}_1^2 \quad (35)$$

The quantity  $\chi_2$  is called the complex scalar second-order nonlinear dielectric susceptibility of the medium. In some cubic or amorphous media,  $\chi_2$  is related to  $\beta$  (See Eq. (3) ) by a simple expression (Bloembergen, 1965, Eq. 3.18)

$$\chi_2 = L^2(\omega) L(2\omega) N_v \beta \quad (36)$$

where  $N_v$  is the number of molecules per cubic centimeter and the function  $L$  is the Lorentz factor which is a conversion factor that is needed because  $\beta$  is defined in terms of local fields and  $\chi_2$  is defined in terms of macroscopic fields. When written in terms of refractive indices, (Bloembergen uses dielectric constants rather than refractive indices) the Lorentz factors are (Bloembergen, 1965, Eq. 3.18):

$$L(\omega) = (n_1^2 + 2)/3 \quad (37)$$

$$L(2\omega) = (n_2^2 + 2)/3 \quad (37)$$

The refractive indices at the fundamental and second-harmonic frequencies are  $n_1$  and  $n_2$  respectively. In the above equations, the refractive index is a real number and  $\beta$  is complex.

Bloembergen has pointed out that Eqs. (36) and (37) apply in crystals only when the valence electrons are localized around a lattice point with cubic symmetry. He suggests that CuCl, which is cubic and lacks inversion symmetry, may be described by these equations. For symmetries other than cubic, the local field correction factors will be more complicated and are difficult to determine. Bloembergen has stated that since these correction factors are not small they are a significant source of error in analytical estimates of  $\chi_2$  (Bloembergen, 1965, pp. 69-70).

Let the total field at the fundamental frequency in a homogeneous isotropic medium be plane waves of the form:

$$E_1(z, t) = \text{Re} \{ \hat{E}_1 e^{j(\omega t - k_1 z)} \} \quad (38)$$

In this equation,  $\hat{E}_1$  is constant,  $\omega$  is the fundamental frequency, and  $k_1$  is the fundamental wave number which is assumed to be real. We have taken  $E_1$  to be constant and  $k_1$  to be real because we shall assume that there is a negligible fraction of the fundamental wave energy converted to energy in higher harmonic fields and because

we shall assume that the medium is lossless. The second-harmonic polarization is taken to be of the form:

$$P_2(z, t) = \text{Re} \left\{ \hat{P}_2 e^{j(2\omega t - 2k_1 z)} \right\} \quad (39)$$

In Eq. (39),  $\hat{P}_2$  is constant. This follows from Eq. (35) and the assumption that  $\hat{E}_1$  is constant in Eq. (38) (Minck et al, 1966, Eq. 7, p. 1359 and discussion following Eq. 17, p. 1359). The second-harmonic field is assumed to have a slightly more general form than the fundamental field. That is:

$$E_2(z, t) = \text{Re} \left\{ \hat{E}_2(z) e^{j(2\omega t - k_2 z)} \right\} \quad (40)$$

In Eq. (40), the complex amplitude  $\hat{E}_2(z)$  is taken to be a function of  $z$  since the fractional change in the second-harmonic field energy as a function of  $z$  is significant. This should be compared to the constant complex amplitude of the fundamental field in Eq. (38). Also, in Eq. (40),  $k_2$  is a real wavenumber. This is based on the assumption that the medium is lossless at the second-harmonic frequency.

The complex differential equation for the second-harmonic plane wave amplitude is (Minck et al, 1966, Eq. 17):

$$\frac{d\hat{E}_2(z)}{dz} = -j \frac{2\pi k_2}{n_2} \chi_2 \hat{E}_1^2 e^{j(2k_1 - k_2)z} \quad (41)$$

Equation (41) can be derived from Maxwell's equations together with Eqs. (35), (38), (39), and (40). This equation has been derived in cgs units; however it can be shown to agree with an equation derived by Minck et al (Minck et al, 1966, Eq. 17) in MKS units through the conversion factors given in Appendix A to this chapter.

Let the medium be an isotropic infinite slab with boundaries at  $z = -\frac{L}{2}$  and  $z = +\frac{L}{2}$ . Let  $\hat{E}_2 = 0$  at  $z = -L/2$ . The amplitude of the second-harmonic wave at  $z = L/2$  is then given by the following solution to Eq. (41) (Minck et al, 1966, Eq. 18):

$$\hat{E}_2(L/2) = - \left( \frac{4\pi j k_2 \chi_2 \hat{E}_1^2}{n_2} \right) \left( \frac{\sin \Delta k L/2}{\Delta k} \right) \quad (42)$$

In Eq. (42),  $\Delta k = 2k_1 - k_2$ . We shall continue to neglect reflections at the slab boundaries. Therefore, we shall let  $\hat{E}_1$  and  $\hat{E}_2(L/2)$  in Eq. (42) also stand for the electric fields just outside the output face of the slab in air.

Equation (42) can also be written in terms of the time-averaged power per unit area of the fundamental and second-harmonic fields at the output face of the slab in air. These are  $S_1$  and  $S_2$  respectively (Jackson, 1962, Eq. 7.67):

$$S_1 = \frac{c^2 k_{1a}}{8\pi\omega} \hat{E}_1 \hat{E}_1^* \quad (43)$$

$$S_2 = \frac{c^2 k_{2a}}{16\pi\omega} \hat{E}_2(L/2) \hat{E}_2^*(L/2) \quad (44)$$

where  $k_{1a}$  and  $k_{2a}$  are the fundamental and second-harmonic wave numbers in air and  $c$  is the speed of light in vacuum. Since  $n_1$  and  $n_2$  are both close to unity in air, we can write  $k_{1a} = k_{2a}$  and:

$$S_1 = \frac{c}{8\pi} \hat{E}_1 \hat{E}_1^* \quad (45)$$

$$S_2 = \frac{c}{8\pi} \hat{E}_2(L/2) \hat{E}_2^*(L/2) \quad (46)$$

Using Eqs. (45) and (46) in Eq. (42) and  $k_{1a} = \omega/c$  yields:

$$\frac{S_2}{S_1} = S_1 \left( \frac{64\pi^3 k_2^2 \chi_2^2}{c n_2^4} \right) \left( \frac{\sin^2 \Delta k L/2}{\Delta k^2} \right) \quad (47)$$

If the fundamental and second-harmonic fields are confined to beams of cross sectional areas  $A_1$  and  $A_2$  respectively, then Eq. (47) can be written in the form:

$$\frac{W_2}{W_1} = W_1 \left( \frac{64\pi^3 k_2^2 \chi_2^2 A_2}{A_1^2 c n_2^4} \right) \left( \frac{\sin^2 \Delta k L/2}{\Delta k^2} \right) \quad (47a)$$

where  $W_1$  and  $W_2$  are the fundamental and second-harmonic beam powers respectively.  $W_2/W_1$  is the second-harmonic power conversion efficiency. If the fundamental and second-harmonic powers are

interpreted as peak pulse powers, then the second-harmonic energy conversion efficiency is given by  $\tau_2 W_2 / \tau_1 W_1$  where  $\tau_1$  and  $\tau_2$  are the fundamental and second-harmonic pulse durations.

From Eq. (47a) it can be seen that the coherent second-harmonic conversion efficiency is a periodic function of the slab thickness  $L$ . The second-harmonic intensity first reaches a maximum when:

$$|\Delta k|L/2 = \pi/2 \quad (48)$$

Using the fact that  $k_1 = n_1\omega/c$  and  $k_2 = 2n_2\omega/c$  one obtains for this value of  $L$ , which is called  $L_{\text{coh}}$  (Minck et al, 1966, p. 1360):

$$L_{\text{coh}} = \lambda_1/4|n_1 - n_2| \quad (49)$$

where  $\lambda_1$  is the fundamental wavelength in vacuum. The thickness defined by Eq. (49) is called the coherence length,  $L_{\text{coh}}$ , of the medium. From Eq. (49), the coherence length is infinite when the medium is non-dispersive, i.e., when  $n_1 = n_2$ . When  $\lambda_1$  is the ruby laser wavelength (700nm) it is found that quartz exhibits a value of  $|n_1 - n_2|$  of the order of  $2 \times 10^{-2}$  (Pressley, 1971, p. 517). In this case  $L_{\text{coh}}$  is about ten ruby laser wavelengths.

The periodic growth and decay of the second-harmonic field can be understood by noting that solutions of Eq. (41) are not freely propagating waves. The travelling second-harmonic wave is

produced by a polarization distribution that has been created by the fundamental travelling wave. (That is, the fundamental travelling wave  $E_1$  produces a polarization  $P_2$  in the medium that in turn produces the travelling second-harmonic waves  $E_2$  that are found from the solution of the differential equation (41) ). The fundamental waves propagate at a different speed than the second-harmonic waves in a dispersive medium. Hence, the second-harmonic field produced at a point in the medium will not necessarily interfere constructively with second-harmonic waves that have been produced at other points in the medium. Constructive or destructive interference at a point depends upon how far that point is from  $z = -L/2$  and the difference between the wave velocities at  $\omega$  and  $2\omega$  in the medium.

If the slab is cut to a thickness that is an integral multiple of a coherence length, then the second-harmonic conversion efficiency of the slab will be a relative maximum. Periodic changes in the travelling wave conversion efficiency have been observed by rotating thin quartz slabs so as to vary the optical path length of light in the crystal (Maker et al, 1962). When the slab thickness has been "adjusted" to yield a relative maximum of conversion efficiency, the actual value of the conversion efficiency is proportional to  $(\Delta k)^{-2}$  (see Eq. (48) ). Since  $\Delta k = \frac{4\pi}{\lambda_1} (n_1 - n_2)$  the actual conversion efficiency, at maximum, is proportional to  $(n_1 - n_2)^{-2}$ .

In many materials that have been investigated for second-harmonic

generation with ruby lasers  $|n_1 - n_2|$  is a small number ( $|n_1 - n_2| \approx 10^{-2}$  for quartz and KDP) (Pressley, 1971, Table 18-4). In later chapters, the theory of second-harmonic generation in crystalline media will be applied to biological tissue (cornea and tendon) where values of  $|n_1 - n_2|$  are not generally available. In its fresh state, tissue contains significant amounts of water. When the fundamental is at the ruby laser wavelength, the factor  $n_1 - n_2 = 0.018$  for water is also small (ICT, Vol. 7, p. 13). Therefore, the factor  $(n_1 - n_2)^{-2}$  can be an important source of error in the biological calculations. A further source of error is, of course, not knowing the extent to which biological tissue can be considered crystalline.

Complete constructive interference occurs for  $n_1 = n_2$  (or  $\Delta k = 0$ ) which is called the "index-matched condition". Index matching can be achieved for extraordinary waves at  $\omega$  and ordinary waves at  $2\omega$  in certain directions in birefringent crystals where the birefringence,  $|n_o - n_e|$ , exceeds the dispersion  $|n_1 - n_2|$  ( $n_o =$  ordinary ray refractive index,  $n_e =$  extraordinary ray refractive index) (Franken & Ward, 1963, p. 29). In these crystals the conversion efficiency can become high (20% for crystals outside the laser cavity) (Yariv, 1968, p. 351). We have not attempted, in our experimental work, to obtain an index matched condition in biological tissue.

## 2.8 Incoherent second-harmonic generation in non-crystalline media

Terhune, Maker and Savage (Terhune et al, 1965) have observed second-harmonic generation from liquids and amorphous solids composed of molecules that lack inversion symmetry. Their experiments have also been reviewed by Minck et al (Minck et al, 1966, p. 1371). In these experiments, second-harmonic radiation did not appear as a beam but appeared rather as weak multi-directional scattered radiation analogous to the Rayleigh scattering that occurs in linear media. In quantum mechanical terms, the process can be thought of as two photons being simultaneously absorbed from the laser field and a third photon of twice the energy being released via spontaneous emission (Minck et al, 1966, p. 1371). From a classical standpoint, the second-harmonic polarization on each is randomly oriented and each molecule acts as a separate independent source of second-harmonic radiation (Minck et al, 1966, p. 1371). In this incoherent second-harmonic generation the net second-harmonic energy per laser pulse is assumed to be the sum of the energies at the second-harmonic frequency radiated by each separate molecule or molecular cluster (Kielich, 1964, p. 56). In Terhune's experiments, the total second-harmonic energy was a very small fraction of the laser input energy. Conversion efficiencies only of the order of  $10^{-13}$  were obtained even when a high peak power, Q-switched ruby laser beam was focused within the sample medium (Terhune et al, 1965, p. 681).

We shall now develop a simplified scalar model for incoherent second-harmonic generation in non-dissipative amorphous media. In Appendix A of Chapter 5 of this thesis it is shown that when independent nonlinear noncentrosymmetric molecules are randomly oriented in an amorphous medium, the instantaneous second-harmonic polarization induced on each molecule by a coherent fundamental driving field is also independently randomly oriented (Minck et al., 1966, p. 1371; Chapter 5, Appendix A of this thesis). The phase of the second-harmonic radiation reaching a distant observer from a given molecule is affected by the relative position of the molecule and by the orientation of the induced second-harmonic dipole moment. These orientational effects can be seen through the following scalar example drawn from Appendix A of Chapter 5. Let  $\hat{E}_{loc}$  and the easy direction of polarization of a one dimensional noncentrosymmetric molecule be aligned. To second order, the induced dipole moment is given by  $\hat{\mu} = \alpha \hat{E}_{loc} + \beta \hat{E}_{loc}^2$ . Now rotate the easy direction of polarization by  $180^\circ$ . Then the induced dipole moment is  $\hat{\mu} = \alpha \hat{E}_{loc} - \beta \hat{E}_{loc}^2$ . This molecular rotation produces a  $180^\circ$  phase change in the second-harmonic radiation from the molecular dipole. Now consider a collection of closely spaced oscillators. Let there be as many oscillators oriented in a given direction as there are oriented in the exact opposite direction. There can be no coherent constructive interference for second-harmonic waves radiated by this collection since for every oscillator radiating at  $2\omega$  with phase  $\phi$  there is

another oscillator radiating at  $2\omega$  with phase  $\phi + \pi$  which leads to destructive interference of coherent waves.

Now we shall consider the possibility of incoherent second-harmonic generation by a collection of independent, randomly oriented oscillators. We shall assume that in three dimensions the random orientation of independent molecules produces a uniform probability distribution for an independent random variable  $\phi_n$  where  $\phi_n$  is the phase angle of the second-harmonic radiation that reaches a distant observer from the  $n^{\text{th}}$  molecule of the medium. The range of phase angles will be from  $\phi_n = 0$  to  $\phi_n = 2\pi$ . We shall also assume that the amplitude of the second-harmonic wave that reaches the observer from the  $n^{\text{th}}$  molecule is affected by the distance between the molecule and the observer but is not affected by the orientation of the molecule. This last assumption is consistent with our scalar approach. The effects of molecular orientation on the amplitude of the observed second-harmonic wave can be taken into account with a tensor approach.

Consider a group of  $N$  independent randomly oriented molecules under the conditions described above. Let the intermolecular spacing  $R_{nm}$  be much less than the distance  $R_{no}$  from a molecule to the observer.

The second harmonic field amplitude  $E_2$  at the observer position is then proportional to the sum  $\sigma = \sum_{n=1}^N e^{j\phi_n}$ . The time-averaged second-

harmonic power at the observer position is proportional to

$$\sigma\sigma^* = \sum_{n=1}^N e^{j\phi_n} \sum_{m=1}^N e^{-j\phi_m}. \text{ When averaged with respect to the uniformly}$$

distributed independent random variable  $\phi$ , one obtains the well-known result that  $\overline{\cos^2 \phi} = \frac{1}{2}$  (Sommerfeld, 1964, pp. 192-193). Therefore, under the conditions of this scalar model, the time-averaged incoherent second-harmonic power from a non-dissipative amorphous medium is the sum of the time-averaged second-harmonic powers radiated by the individual non-centrosymmetric molecules of the medium.

The time averaged second-harmonic power,  $W_{21}$ , from an individual dipole with oscillation frequency  $2\omega$  and dipole moment amplitude  $|\mu_2|$  is (Jackson, 1962, p. 272)

$$W_{21} = \frac{16\omega^4}{3c^3} |\mu_2|^2 \quad (50)$$

where  $|\mu_2|^2 = \hat{\mu}_2 \hat{\mu}_2^*$ . The dipole moment scalar amplitude  $|\mu_2|$  will be different for different orientations of the molecule with respect to the local field,  $E_{loc}$ . In the present scalar treatment these differences will be neglected. Therefore, we shall assume

$$|\hat{\mu}_2| = \beta E_{loc,1}^2 \quad (51)$$

With this substitution, Eq. (50) becomes:

$$W_{21} = \frac{16\omega^4}{3c^3} \beta^2 E_{loc,1}^4 \quad (52)$$

The total second-harmonic power,  $W_2$ , from  $N$  molecules is:

$$W_2 = \frac{16\omega^4}{3c^3} \beta^2 \hat{E}_{loc,1}^4 N \quad (53)$$

The Lorentz factors given by Eq. (37) for certain cubic crystalline media have also been employed by Armstrong et al in their analysis of second-order nonlinear polarization in isotropic media (Armstrong et al, 1962, p. 1925). Bloembergen has cautioned that these factors may be used only when the ions or molecular groups of the medium are well localized (Bloembergen, 1965, p. 68). Therefore, under these conditions, the relationship between  $\hat{E}_{loc,1}^2$  and the applied (macroscopic) field quantity  $\hat{E}_1^2$  is:

$$\hat{E}_{loc,1}^2 = L^2(\omega) L^2(2\omega) \hat{E}_1^2 \quad (54)$$

With this relation, Eq. (53) becomes

$$W_2 = \frac{16\omega^4}{3c^3} \beta^2 L^4(\omega) L^2(2\omega) \hat{E}_1^4 N \quad (55)$$

Equation (45) can be used to relate  $\hat{E}$  in Eq. (55) to the laser power per unit area  $S_1$ :

$$\hat{E}_1^4 = \frac{64\pi^2 S_1^2}{c^2} \quad (56)$$

If the laser intensity is uniform over a beam with area  $A_1$ , then  $S_1 = W_1/A_1$  where  $W_1$  is the laser power. With these substitutions made in Eq. (55), the incoherent second-harmonic power conversion efficiency  $W_2/W_1$  becomes:

$$\frac{W_2}{W_1} = \frac{1024\pi^2 \omega^4 \beta^2 L^4(\omega) L^2(2\omega) N W_1}{3c^5 A_1^2} \quad (57)$$

As described previously, the energy conversion efficiency under pulsed conditions is  $C_{ie} \tau_2 W_2/\tau_1 W_1$ .

There are no coherence length considerations in our model of a non-crystalline medium. In this type of medium, Eq. (57) predicts that the conversion efficiency increases linearly with the number of irradiated molecules  $N$  which if the beam cross sectional area is held constant, would mean a linear increase of second-harmonic power with increasing thickness of the nonlinear medium. This should be contrasted with the periodic change with increasing slab thickness of the conversion efficiency in a crystalline medium. No experimental test of this result has been found in the literature. Such verification is important since there are a number of assumptions used in the development of the theory.

## 2.9 Sample calculations for water

A theoretical estimate of the incoherent second-harmonic conversion efficiency of (amorphous) liquid water will be made from

the scalar model presented above. The result will be compared with experimental second-harmonic generation data reported for water by Terhune et al (Terhune et al, 1965).

A theoretical value of  $\chi_2$  will also be obtained for a hypothetical case. The hypothetical case that will be considered is that of a cubic crystal with the water molecule oscillators localized at the cubic lattice points. The value of  $\chi_2$  for this hypothetical crystal will be compared with the tensor components of  $\chi_{ijk}$  that have been measured in KDF (Minck, 1966, p. 1361). Water was chosen for these calculations because oscillator strength data is available. Other materials for which experimental conversion efficiency data has been reported (e.g. quartz, carbon tetrachloride, acetonitrile (Terhune et al, 1965) ) could not be used to test the scalar model due to a lack of oscillator strength data. It will be demonstrated that the oscillator strength is a sensitive parameter in calculations of both incoherent and coherent conversion efficiencies. The crystalline water example is given to demonstrate the scalar model for crystalline media; it is not meant to be a realistic practical example.

## 2.9a Calculation of incoherent second-harmonic conversion efficiency of liquid water - Comparison with experiments by Terhune et al.

### 1. Ultraviolet spectrum of water

A one-dimensional dipole oscillator is assigned to each

electronic dipole absorption band of the molecule being modeled. The second-order dipole moment of the molecule  $\mu_2$  is taken to be the sum of the second-order dipole moments of the oscillators assigned to the molecule. In water, the electronic dipole absorption bands are in the vacuum ultraviolet region of the electromagnetic spectrum (Herzberg, 1966, p. 489; Watanabe and Zelikoff, 1953). The following description of these bands is based on low pressure water vapor spectra obtained by Watanabe and Zelikoff (Watanabe and Zelikoff, 1953; Herzberg, 1966, pp. 489-493). The lowest frequency band is centered at approximately 165nm and is quite broad (145nm - 186nm). The oscillator strength for this band is 0.041 (Watanabe and Zelikoff, 1953, p. 754). The next higher frequency absorption appears as a progression of diffuse bands superimposed upon a broad band. The short wavelength limit of the underlying broad band is at approximately 115nm and the long wavelength limit is at approximately 145nm. The center of the underlying broad band is at about 130nm. The oscillator strength of the underlying broad band is approximately 0.05 (Watanabe and Zelikoff, 1953, p. 755). The diffuse bands extend to shorter wavelengths. Another series of bands is evident in the range 105nm to 115nm. Oscillator strength data for the diffuse bands and the short wavelength series of bands was not given by Watanabe and Zelikoff.

In our calculations for liquid water at 20°C and 1atm pressure we shall only consider the 130nm band and the 165nm band. We shall

assume that the oscillator strength and band locations are the same for water vapor and liquid water. The oscillator strength is a measure of the coupling between an oscillating dipole moment and the radiation field (Siegmán, 1971, pp. 82-83). The oscillator-field coupling may be different for low pressure water vapor and liquid water. Therefore, the assumption of an invariant oscillator strength may be incorrect. Insufficient information could be located to incorporate a change in oscillator strength in our calculations. An increase in the strength of the local field, which constitutes one change in the coupling between the oscillator and the macroscopic field is included in our calculations via the Lorentz factors for liquid water.

#### ii. Calculation of $\beta$

The incoherent second-harmonic power conversion efficiency is given by Eq. (57).

$$\frac{W_2}{W_1} = \frac{1024\pi^2 \omega^4 \beta^2 L^4(\omega) L^2(2\omega) N W_1}{3c^5 A_1^2} \quad (57)$$

The scalar polarizability  $\beta$  is calculated from Eqs. (31) and (34). The factors  $D_1(\omega)$  and  $D_1(2\omega)$  in Eq. (31) are complex numbers. The following table compares the real and imaginary parts of these factors. The comparison is based on a 20nm linewidth for both the 130nm and 165nm lines (Watanabe and Zelikoff, 1953, Fig. 1, p. 754).

The entries in the third column show the imaginary part to be less than 10% of the real part of each of the  $D_1$  factors. We therefore retained only the real part as an approximation to the  $D_1$  factors when computing  $\beta$ . The result for  $\beta$  is  $2.97 \times 10^{-32} \text{ cm}^{9/2} \text{ erg}^{-1/2}$ .

Spectral Line	$D_1$ Factor	$\text{Re}\{D_1\} + j \text{Im}\{D_1\}$	$(\text{Im}\{D_1\}/\text{Re}\{D_1\})\%$
165nm	$D_1(\omega)$	$(1.31-0.73)\times 10^{32} - j3.75\times 10^{30}$	3%
165nm	$D_1(2\omega)$	$(1.31-0.29)\times 10^{32} - j7.50\times 10^{30}$	7%
130nm	$D_1(\omega)$	$(2.10-0.07)\times 10^{32} - j6.06\times 10^{30}$	3%
130nm	$D_1(2\omega)$	$(2.10-0.29)\times 10^{32} - j1.21\times 10^{31}$	7%

#### iii. Calculation of Lorentz factors

For the ruby laser with a wavelength of 694nm, the refractive indices  $n_1$  and  $n_2$  are (ICT, Vol. 7, p. 13):

$$n_1 = 1.33$$

$$n_2 = 1.34$$

Using Eq. (37), the Lorentz factors are:

$$L(\omega) = 1.26$$

$$L(2\omega) = 1.27$$

iv. Calculation of laser power

Terhune et al report that a 1MW ruby laser was used (Terhune et al, 1965, p. 681). However, when referring to experimental spectra of second-harmonic generation they list the laser power as  $\frac{1}{2}$  MW for water (Terhune et al, 1965, Fig. 2). We shall use the  $\frac{1}{2}$  MW value, or  $5 \times 10^{12}$  erg/sec in Eq. (57).

v. Calculation of the dimensions of the focus of a laser beam

Two additional difficulties arise in this part of the calculations. These are both related to the fact that Terhune et al used a focused laser beam rather than a collimated beam in their experimental studies (Terhune et al, 1965, p. 681). First, it is very difficult to accurately estimate the cross sectional area of a focused ruby laser beam. With low order mode gas lasers these estimates can be made more accurately. Second, Eq. (57) is based on homogeneous plane wave illumination by the laser. It is not known whether homogeneous plane waves exist anywhere within a focused ruby laser beam. With gas lasers, where a high degree of coherence can exist, and with high f-number (f-number  $\gg 1$ ) aberration free lenses, theory predicts that a plane wave region exists

around the lens focus (Kleinman, 1962, p. 1772; Bloembergen, 1965, p. 122). In order to continue these calculations we shall present two limiting values of the laser beam cross sectional area  $A_1$  at the lens focus and assume the existence of a homogeneous plane wave region at the lens focus. Concentrating on the focal region is consistent with the report by Terhune et al that second-harmonic generation was observed only in the focal region of the lens (Terhune et al, 1965, p. 681).

The dimensions of the focal region in which Terhune et al observed second-harmonic generation are not known. For the purposes of the present calculations, we shall approximate the high intensity region of the focused laser beam by a cylinder and assume that the only significant second-harmonic generation occurs within the cylinder. The radius  $r$  of the minimum focal spot size obtainable with a single-mode laser beam with a divergence half-angle  $\theta$  and an aberration-free lens of focal length  $F$  is commonly estimated by  $r = F\theta$  (Ready, 1971, p. 19). If the laser operates in  $N_m$  transverse modes, the focal spot size increases by a factor of  $\sqrt{N_m}$  (Ready, 1971, p. 19). If the lens is not perfect and if the mode structure is very complicated (e.g. with ruby lasers), then the focal spot size is yet larger (Ready, 1971, pp. 22-23). Ready has performed studies with non-Q-switched multimode ruby lasers, and found that the minimum spot diameter produced with a simple lens is of the order of 300 microns (Ready, 1971, Fig. 1.8 and p. 23).

Ready's studies also include an examination of the length of the focal region produced by a simple lens and a multimode non-Q-switched ruby laser. From his data it appears that there is a maximum range of about 1mm in which the focal spot diameter is approximately constant (Ready, 1971, Fig. 1.8).

Based on Ready's studies, the cylindrical region that we would use to approximate the focus of a non-Q-switched ruby laser in air would have a maximum length of  $L_f = 1\text{mm}$  and a minimum cross-sectional area of  $A_1 = 7 \times 10^{-4} \text{ cm}^2$ . The method used by Ready was based on the size of holes punched in thin aluminum films, which may not yield a true measure of the dimensions of the focal region (Ready, 1971, Fig. 1.8).

There are a number of errors that can occur if we use Ready's results to estimate the size of the focal region in the studies of second-harmonic generation by Terhune et al. First, Ready's laser was non-Q-switched while Terhune's was Q-switched. These lasers may be focused differently since the mode structure may be different. Second, Ready's focus was produced in air and in the presence of metallic vapors, while Terhune's focus was produced in water. The optical properties of these media are different. Third, the results that we have quoted from Ready apply to only one laser pulse energy. Ready has also shown that  $L_f$  decreased by about a factor of 2 and  $A_1$  increased by about a factor of 1.7 when the laser energy was

raised from 0.7 Joules to 1.2 Joules (Ready, 1971, Fig. 1.8). The energy from Terhune's laser was only approximately 0.05 Joules, based on 1/2 Megawatt peak power and a 100μsec pulse duration (Terhune et al, 1965, Figs. 1 and 2). Therefore  $A_1$  may have been smaller than  $7 \times 10^{-4} \text{ cm}^2$  and  $L_f$  may have been longer than 1mm in Terhune's experiments due to his lower laser energy. This, of course, assumes that energy and not peak power is the determining factor. Fourth, Terhune et al used a lens with about a 10cm focal length while Ready presented most of his results for a 2.5cm focal length lens. These differences should affect the dimensions of the focal region.

The dimensions of the focal region enter Eq. (57) via the factor  $N/A_1^2$  where  $N$  is the number of molecules that radiate at the second harmonic frequency. To determine  $N$ , both the length and cross-sectional area of the focal region must be known. The above factor can also be written as  $N_v L_f/A_1$  where  $N_v$  is the number of molecules per unit volume that radiate at the second-harmonic frequency. Since  $N_v$  can be estimated independently from chemical data the dimensions of the focal region actually enter Eq. (57) via the factor  $L_f/A_1$ . Using  $L_f = 0.1\text{cm}$  and  $A_1 = 7 \times 10^{-4} \text{ cm}^2$  yields  $L_f/A_1 = 1.42 \times 10^2 \text{ cm}^{-1}$ . Based on parts of the above list of errors we shall now estimate the possible numerical peak error introduced by using this value of  $L_f/A_1$  in the analysis of the studies by Terhune et al.

First, the effect of focusing the laser beam in water rather than in air will be considered on the basis of a change of wavelength. We can only estimate this effect by using the equations for an ideal focus (Kleinman, 1962, p. 1772). Using these equations it can be shown that the factor  $L_f/A_1$  is reduced by  $1/n$  where  $n$  is the refractive index of water ( $n \approx 1.3$ ).

Second, by using a linear extrapolation from the pulse energies used by Ready to those used by Terhune et al, the cylinder length  $L_f$  can be shown to increase from 1mm to 1.7mm and  $A_1$  can be shown to decrease from  $7 \times 10^{-4} \text{ cm}^2$  to  $0.8 \times 10^{-4} \text{ cm}^2$ . This amounts to a factor of 15 increase in the ratio  $L_f/A_1$  over the value of  $1.42 \times 10^{-4} \text{ cm}^2$  taken directly from Ready's studies.

Third, we shall again employ the equations for an ideal focus to estimate the effect of the lens focal length differences in the studies by Ready and Terhune et al. Both  $L_f$  and  $A_f$  are proportional to the focal length  $F$  (Kleinman, 1962, p. 1772). Therefore, to a first approximation there is no error introduced by lens focal length differences insofar as  $L_f/A_1$  is concerned.

Combining these computed factors, we see that the assumption that  $L_f/A_1 = 1.42 \times 10^2 \text{ cm}^{-1}$  in the second-harmonic experiments by Terhune et al may be a factor of 11 too large.

It is useful to also compute the ratio  $L_f/A_1$  for a perfectly coherent beam and an aberration-free simple lens from the equations

given by Kleinman (Kleinman, 1962, p. 1772). For the ruby laser wavelength ( $\lambda = 694\text{nm}$ ) and a focus in water ( $n = 1.3$ ) this ratio is  $L_f/A_1 = 4.8 \times 10^4 \text{ cm}^2$ . This is a factor of 338 times larger than the value of  $L_f/A_1$  estimated from practical laser data.

The above calculations have been carried out to show that there can be very large errors in the estimate of the dimensions of the focal region of a laser. These errors produce an uncertainty in the factor  $L_f/A_1$  in Eq. (57) of as much as two orders of magnitude.

vi. Calculation of  $N_v$

The number density of dipoles  $N_v$  is:

$$N_v = \frac{\rho N_o}{\text{M.W.}} \quad (58)$$

where  $\rho = 1\text{gm/cm}^3$  for  $\text{H}_2\text{O}$ ,  $N_o = 6.02 \times 10^{23}$  molecules/gm mole and  $\text{M.W.} = 18$  (molecular weight of water). Thus  $N_v = 3.34 \times 10^{22} \text{ cm}^{-3}$  for liquid water at  $20^\circ\text{C}$  and  $1\text{atm}$ . Also  $N/A_1$  is  $9.45 \times 10^{-24} \text{ cm}^{-4}$  when  $L_f/A_1 = 1.42 \times 10^{+2}$  is used in  $N/A_1^2 = N_v L_f/A_1$ .

vii. Final result for incoherent conversion efficiency of water

Based on the above parameter values, the predicted incoherent power conversion efficiency for water, under the experimental conditions used by Terhune et al, is:

$$\frac{W_2}{W_1} = 1.29 \times 10^{-12}$$

The above number is the ratio of the total power radiated at  $2\omega$  to the total power incident at  $\omega$ . If the laser pulse duration is  $\tau_1$  and the second-harmonic pulse duration is  $\tau_2$  then the energy conversion efficiency is:

$$\frac{\tau_2}{\tau_1} \frac{W_2}{W_1} \tag{59}$$

It is shown in Chapter 3 of this dissertation that  $\tau_2/\tau_1 = 0.707$  for Gaussian-shaped laser pulses. Therefore, if the laser pulse is assumed to be Gaussian in the experiments by Terhune et al, then the incoherent energy conversion efficiency is

$$C_{ie} = 9.1 \times 10^{-13}$$

Terhune et al have reported that about  $10^{-13}$  of the incident laser energy emerged as scattered radiation near twice the laser frequency (Terhune et al, 1965, p. 681). Our theoretical estimate given above is approximately an order of magnitude larger than their reported experimental energy conversion efficiency.

Oscillator strengths for low pressure water vapor were used to obtain our theoretical value of the second-harmonic energy con-

version efficiency in liquid water. It has been previously mentioned that the oscillator strengths for liquid water may differ from those for water vapor. The oscillator strength appears as  $f^4$  in the calculation of the energy conversion efficiency. Therefore, an uncertainty in  $f$  can be an important source of error in our calculations. A factor of 0.56 lower oscillator strength for the liquid water absorption bands would reduce the calculated energy conversion efficiency by about one order of magnitude.

Another important source of error in our model is introduced by neglecting the effects of oscillator orientation. In our totally scalar approach we have assumed that the induced dipole moment of a molecule is independent of the orientation of the molecule with respect to the electric field of the laser. By assuming a random distribution of molecular orientations and using tensor polarizabilities, the calculated energy conversion efficiency should be lower than that obtained from the scalar model.

Finally, we have shown that large errors are introduced by the uncertainty in the factor  $L_f/A_1$  in Eq. (57). This uncertainty stems from difficulties associated with modeling the focal region of a Q-switched ruby laser.

viii. Synopsis of calculations of incoherent conversion efficiency of other amorphous materials.

Meaningful calculations of the conversion efficiency of the other

non-crystalline materials studied by Terhune et al (carbon tetrachloride, acetonitrile, fused quartz) were not possible. Oscillator strength data could not be located for these materials. In the case of  $\text{CCl}_4$ , for example, the strongest absorption band occurs at 130nm (Zobel and Duncan, 1955, p. 2612). There is a water vapor absorption band at this wavelength as well (Watanabe and Zelikoff, 1953, p. 755). Using just the 130nm band and the same approach employed for water we have computed the energy conversion efficiency of  $\text{CCl}_4$ . The parameter values used in this computation are listed below.

- a)  $\beta = 6.24 \times 10^{-30} \text{ cm}^{9/2} \text{ erg}^{-1/2}$  for  $f = 1$ , and assuming imaginary part of D factors negligible
- b)  $\beta = 1.56 \times 10^{-32} \text{ cm}^{9/2} \text{ erg}^{-1/2}$  for  $f = 0.05$  (same  $f$  as for  $\text{H}_2\text{O}$  band at 130nm), and assuming imaginary part of D factors negligible
- c)  $n_1 = 1.45$   
 $n_2 = 1.50$  } (AIP, pp. 6-18)
- $L(\omega) = 1.37$
- $L(2\omega) = 1.42$
- $L^4(\omega) L(2\omega)^2 = 7.1$
- d)  $W_1 = 5 \times 10^{12} \text{ erg/sec}$  (same as  $\text{H}_2\text{O}$ )
- e)  $L_2/A_1 = 142$  (same as  $\text{H}_2\text{O}$ )

f)  $\rho = 1.59 \text{ gm/cm}^3$  (AIP, pp. 2-147)

M.W. = 154

$N_v = 6.23 \times 10^{21}/\text{cm}^3$

g)  $\tau_2/\tau_1 = 0.707.$

$6.5 \times 10^{-9}$  for  $f = 1$

Energy conversion efficiency =

$4.1 \times 10^{-14}$  for  $f = 0.05$

The above oscillator strengths represent a very strong oscillator ( $f = 1$ ) and an oscillator with strength equal to that of water at 130nm ( $f = 0.05$ ). The wide range of conversion efficiency values brackets the conversion efficiency of about  $10^{-13}$  reported by Terhune et al (Terhune et al, 1965, p. 681). To obtain agreement with their value, an oscillator strength of 0.1 is required. This may be a reasonable value of  $f$ ; however, we have no a priori basis upon which to assume this value.

#### 2.9b Calculations related to coherent second-harmonic generation

The calculation of coherent second-harmonic conversion efficiencies requires computation of  $\chi_2^2$  which itself depends upon  $\beta^2$  (Eq. (36)). Therefore, the factor  $f^4$  also enters in the analysis of crystalline media. In addition, the dispersion of the index of refraction between  $\omega$  and  $2\omega$  is a sensitive parameter in the calculations of coherent conversion efficiency.

Consider the extension of the calculations on water to the

following hypothetical case. Let the water molecule oscillators be localized at the sites of a cubic crystalline lattice. The nonlinear susceptibility  $\chi_2$  is then (Eq. (36) ):

$$\chi_2 = L^2(\omega) L(2\omega) N_v \beta$$

Using the values of  $N_v, n(2\omega), n(\omega)$  and  $\beta$  for liquid water yields  $\chi_2 = 2 \times 10^{-9} \text{ cm}^{3/2} \text{ erg}^{-1/2}$ . Compare this result to the components of  $\beta_{pqr}$  for KDP, which range from  $6 \times 10^{-9} \text{ cm}^{3/2} \text{ erg}^{-1/2}$  to  $5.2 \times 10^{-9} \text{ cm}^{3/2} \text{ erg}^{-1/2}$  (Minck, 1966, p. 1361). The higher values of nonlinear susceptibility in KDP may be related to the higher index of refraction which produces higher local fields in KDP than occur in liquid water (Minck, 1966, p. 1361).

The hypothetical water "crystal" would have a considerably higher second-harmonic conversion efficiency than liquid water. The difference between the coherent conversion efficiency of a real crystalline material and the incoherent conversion efficiency of a real non-crystalline material can be demonstrated with quartz. Terhune et al have found the incoherent conversion efficiency of non-crystalline (fused) quartz to be  $\sim 10^{-13}$  using a focused 1MW peak-power ruby laser (Terhune et al, 1965, p. 681). Franken et al obtained a value of about  $10^{-8}$  for the conversion efficiency of crystalline quartz using a focused 3kW peak-power ruby laser (Franken et al, 1961; Pershan, 1966, p. 123). The coherent conversion

efficiency is five orders of magnitude greater than the incoherent conversion efficiency even though the laser power was lower in the experiments with crystalline quartz.

With certain assumptions, the ratio of these experimental conversion efficiencies can be predicted from the scalar model presented in this chapter. First, it will be assumed that in the experiments by Franken et al the coherent conversion efficiency was approximately a maximum (i.e.  $\sin^2 \frac{\Delta k L}{2} = 1$  in Eq. (47a)). Second, it will be assumed that second-harmonic generation occurred only in the focal region of the lenses used by Terhune et al (fused quartz study) and Franken et al (crystalline quartz study). Furthermore, the focal region for both the fused and crystalline quartz studies will be approximated by a cylinder that is 0.1cm long and 0.03cm in diameter as was done in the analysis of liquid water carried out above. This assumption can be a serious source of error.

The maximum coherent energy conversion efficiency  $C_{cem}$  is (Eq. (47a)):

$$C_{cem} = \frac{64\pi^3 \tau_2 \chi_2^2 W_1}{\tau_1 n_2^4 A_1 c(n_1 - n_2)^2}$$

Assume that  $\chi_2$  and  $\beta$  are related by the approximate expression (see Eq. (36))

$$\chi_2 = L^2(\omega) L(2\omega) N_v \beta$$

As indicated before, this expression may only be suitable for cubic or noncrystalline media where the electron clouds are well localized. Crystalline quartz is not cubic, therefore using this expression may introduce a source of error.

Let the incoherent energy conversion efficiency be given by Eqs. (57) and (59) with  $N/A_1^2$  replaced by  $N_v L_f/A_1$ .

The ratio of the maximum coherent energy conversion efficiency  $C_{cem}$  to the incoherent energy conversion efficiency  $C_{ie}$  is then

$$\frac{C_{cem}}{C_{ie}} = (0.6) \left( \frac{\tau_2 W_{lc}}{\tau_1 W_{li}} \right) \left( \frac{N_v c^4}{L_f n_2^2 (n_1 - n_2)^2 \omega^4} \right) \quad (61)$$

where

$W_{lc}$  = Laser power in coherent conversion experiments

$W_{li}$  = Laser power in incoherent conversion experiments

The values of the parameters used in Eq. (61) are

$$\tau_2/\tau_1 = 0.707$$

$N_v = 3 \times 10^{22} \text{ cm}^{-3}$  for both crystalline and fused quartz (CRC, p. B-218).

$$n_2 = 1.47 \text{ (AIP, p. 6-31)}$$

$$(n_1 - n_2)^2 = 4 \times 10^{-4} \text{ (AIP, p. 6-31)}$$

$$L_f = 0.1 \text{ cm}$$

$$C_{ie} = 10^{-13} \text{ (Terhune et al, 1965)}$$

$$W_{li} = 10^6 \text{ watts (Terhune et al, 1965)}$$

$$W_{lc} = 3 \times 10^3 \text{ watts [Based on 3J pulse (Franken et al, 1961) and 1msec pulse duration. Pulse duration not given by Franken et al. Value assumed is typical of non-Q-switched lasers]}$$

$$\omega = 2.72 \times 10^{15} \text{ rad/sec (ruby laser)}$$

Using these values with Eq. (61) one obtains  $C_{cem} = 4.5 \times 10^{-10}$  for the predicted value of the maximum coherent energy conversion efficiency of crystalline quartz.

Franken et al reported that on the order of  $10^{11}$  second-harmonic photons were produced by each ruby laser pulse of  $\sim 3\text{J}$  energy at 694.3nm (Franken et al, 1961, p. 119). A 3J laser pulse at 694nm contains  $1.05 \times 10^{19}$  photons. The ratio of photons at  $2\omega$  to photons at  $\omega$  is therefore  $9.5 \times 10^{-9}$ . The ratio of the total energy at  $2\omega$  to the total energy at  $\omega$  is twice the photon ratio or  $1.9 \times 10^{-8}$ . Therefore, the coherent energy conversion efficiency observed in the experiments by Franken et al is a factor of 42 larger

than the maximum coherent energy conversion efficiency predicted by the scalar model.

The assumption that the coherent conversion efficiency was at a maximum in the experiments by Franken et al is questionable. Experiments have been reported where the conversion efficiency of crystalline quartz was explored for crystal thicknesses that were equal to a coherence length (Eq. (49) ) (Maker et al, 1962). Insufficient information was given in these latter studies to enable a comparison with prediction by the scalar model. The assumption that  $A_1$  was the same in both studies may be the major source of error in these calculations.

Equation (61) shows that if quartz is transformed from a crystalline to an amorphous phase while the laser power and focusing parameters are held constant, then a five order of magnitude decrease in the energy conversion efficiency will occur. This suggests second-harmonic generation measurements as being sensitive indicators of certain crystalline to amorphous material transformations. An application of this to biomaterials will be reported in Chapter 6 of this dissertation.

#### 2.10 Summary

We have reviewed some of the general principles of optical second-harmonic generation. Approximate scalar models for the

second-order polarizability and susceptibility, and the second-harmonic conversion efficiency of ordered (crystalline) and amorphous (non-crystalline) media were given. These models were shown to yield numerical predictions that were within an order of magnitude of experimental measurements of the conversion efficiency of water (unordered medium) and crystalline quartz (ordered medium). In later chapters these models will be employed in an analysis of second-harmonic generation by biological tissue.

## APPENDIX A

The following table is presented to allow the reader to convert the Gaussian cgs symbols used in this dissertation to their MKS form. To use the table, replace the Gaussian symbol by the corresponding MKS symbol. A more complete conversion table that includes the defining equations can be found in Scott, 1959, Table A.7A.

<u>Quantity</u>	<u>Gaussian cgs</u>	<u>MKS</u>
Dielectric permittivity	$\epsilon$ (dimensionless)	$\epsilon$ (coul <sup>2</sup> /n - m <sup>2</sup> )
Free space dielectric permittivity	$\epsilon = 1$	$\epsilon_0 = 8.854 \times 10^{-12} \text{sec}^2 \text{coul}^2 / \text{kg}$
Dielectric Constant		$K = \epsilon / \epsilon_0$
Electric field	$E$ (statvolt/cm)	$E$ (volt/m)
Polarization	$P$ (statcoul/cm <sup>2</sup> )	$P$ (coul/m <sup>2</sup> )
First order scalar susceptibility	$\chi_1 = \frac{\epsilon - 1}{4\pi}$	$\chi_1 = \epsilon - 1$
Second order scalar susceptibility	$\chi_2$ (cm <sup>3/2</sup> erg <sup>-1/2</sup> )	$\frac{\chi_2}{4\pi\sqrt{4\pi} \epsilon_0}$ (m - volt <sup>-1</sup> )
Refractive index	$n = \sqrt{\epsilon}$	$n = \sqrt{\epsilon / \epsilon_0}$

### CHAPTER 3

#### A BRIEF DESCRIPTION OF THE CONSTITUENTS AND CHARACTERISTICS OF CERTAIN VERTEBRATE CONNECTIVE TISSUES

Most of the biological tissues studied in this research (cornea, sclera, tendon, dermis) belong to the class of connective tissues. These are tissues whose function is generally structurally supportive, however, in the case of the cornea, the optical roles of light transmission and focusing as well as the supportive role are important. Connective tissue contains cells (fibroblasts and histiocytes are present), extracellular fibers imbedded in a ground substance, and tissue fluid in spaces (Bloom and Fawcett, 1968). The extracellular fibers are either elastic (extensible) or collagenous (inextensible). In the case of tendon, cornea, and sclera, there is a preponderance of collagenous fibers. In general, there is a greater volume of extracellular material than there is of cellular material in connective tissue.

#### 3.1 Collagen and collagen-related molecular constituents of connective tissue.

Collagen is a natural protein polymer that forms a fibrous component of skin, tendon, cornea, and sclera. It is primarily responsible for the limited extensibility of these tissues. The thermo-mechanical properties of collagen fibers have been shown to change during the life of rats (Verzar, 1963; Kohn, 1971). For this reason collagen has been of interest in specifying biological age

rather than calendar age in gerontological studies (Verzar, 1963).

Collagen is widely used as a weakly antigenic material for sutures and bandages (Van Winkle, 1954), and has been investigated for use in a variety of surgical procedures (L'Esperance, 1965). In industry, leather production is based upon cross-linking of collagen-rich animal corium; glue manufacturing is based on gelatin which is the thermal degradation product of collagen; and in meat processing, relatively insoluble collagen is converted to gelatin which is digestible. From this list it is clear that collagen is a material of wide-ranging importance and it is not surprising that a vast literature on collagen has been developed.

The optical properties of collagen form a part of this literature. For example, birefringence and optical rotation studies of collagen have contributed information regarding collagen molecular structure (Doty, 1959). The spatial distribution of collagen in the cornea is thought to be the determining factor in the transparency of this tissue (Langham, 1969). To the best of our knowledge, the non-linear optical properties of collagen have not been previously investigated.

When connective tissue is examined with the light microscope, collagen normally appears as fiber bundles. At very high magnifications, faint longitudinal striations are discernable within individual fibers of the bundles (Bloom and Fawcett, 1968). With the polarizing microscope, all fibers show form birefringence (Bloom and Fawcett, 1968). The striations and form birefringence suggest the existence of

structural elements of much smaller diameter than the fiber with long axes along the axis of the fiber. With the electron microscope, these smaller structural elements are found to be non-branching fibrils of indefinite length that range in diameter from approximately 10nm to 250nm depending upon the tissue of origin (Bloom and Fawcett, 1968; Gross, 1961; Schmitt et al, 1942).

Early low angle x-ray diffraction studies as well as electron microscopic studies have been reviewed by Bear (Bear, 1952). These studies showed that native collagen fibrils possess a basic repeating structure with approximately 640A (64nm) period along the fibril axis. In the x-ray studies, this periodicity was manifested by a low angle, horizontal, diffraction pattern at 640A while in the electron microscopic studies, characteristic cross bands with 640A period were found to traverse the diameter of each fibril. With phosphotungstic acid stains, asymmetric sub-bands (intraproduct pattern) were resolved (Bear, 1952). According to Gross (Gross, 1961), it was, at first, thought that the 640A period band in native collagen fibrils was formed when collagen molecules aggregated side-by-side and end-to-end in exact register.

The hypothesis that the collagen molecule is approximately 640A long was seriously questioned when it was found that dissolved collagen fibrils could, under the right conditions, be precipitated to form not only fibrils with the "native" 640A periodicity but also to form fibrils of various lengths with 2800A periodicity, 210A periodicity,

or no periodicity at all (Wood, 1970). The careful viscosity, light scattering, flow birefringence and sedimentation studies of Bodtker and Doty (Doty, 1959) using highly monodisperse solutions of ichthyocol collagen showed the collagen molecule to be an extremely asymmetrical rodlet approximately 3000A long, 13A in diameter, and having a molecular weight of about 330,000. Studies on other soluble collagens such as that from rat tail tendon, rat skin, codfish skin, cod swim bladder, and calf skin, have yielded molecular dimensions and molecular weights in close agreement with those quoted above (Wood, 1970). The various periodic aggregation patterns of collagen have been successfully interpreted by assuming a basic molecular unit of these dimensions. For example, native collagen fibrils are thought to be formed by an end-to-end aggregation of collagen molecules to form protofibrils with a stagger of about one-fourth the length of a molecule between adjacent protofibrils. This model pictures the collagen fibril as a highly ordered aggregate of collagen molecules.

In the cornea, it has been found that in addition to there being a high level of order among collagen molecules inside the collagen fibrils (intrafibrillar order), there is also a discernable order among the fibrils themselves (interfibrillar order). By "order among the fibrils", it is meant that in local regions of the cornea the fibril diameters are approximately equal, the fibril long axis directions are approximately the same, and the fibrils are separated by approximately equal distances without touching one another (Maurice,

1969a). The diameters and spacing of the collagen fibrils of other connective tissues, such as the skin and sclera (white tunic of the eyeball), may not be as regular as in the cornea (Maurice, 1969b; Benedek, 1971).

Some authors believe that the interfibrillar order in the cornea is dependent upon certain large molecules (macromolecules) that exist in an apparently amorphous material (ground substance) that fills the spaces between the fibrils (Mathews, 1969; Dische, 1970; Maurice and Riley, 1970). These macromolecules are carbohydrate-amino acid complexes and can be placed into two categories according to whether their properties are mostly sugar-like (glycosaminoglycans) or mostly protein-like (glycoproteins). Two general types of models have been proposed for the ordering action of the above ground substance macromolecules upon the collagen fibrils of the cornea. In the first type of model, spring-like carbohydrate side chains are pictured as being attached to the collagen fibrils. These side chains hold the fibrils apart from one another in a loose lattice of parallel fibrils with approximately equal spacing. In the second type of model, a ground substance glycoprotein is pictured as forming a covalently bound coating around the collagen fibrils. The observed regular separation between the fibrils may be controlled by the thickness of the coating. This coating may also regulate the diameter to which a collagen fibril can grow. The coating is not visible with the electron microscope; only the fibrils themselves are seen.

Water may also play a role in the structure and order of collagen fibrils. Elden (Elden, 1968) has reviewed research on the adsorption, or binding, of water by collagen fibers in vitro and has compared experimental results to several models for water adsorption from gas and liquid water phases. There is appreciable binding of water multilayers to the fibers from the water gas phase at low vapor pressure. At higher vapor pressures, water eventually condenses in hypothetical capillary spaces in the fibrils and in larger fibers. This water is also classified as being bound.

Elden has also reviewed significant early x-ray diffraction studies of wetted and dry tendons performed by Bolduan and Bear (Elden, 1968; Bolduan and Bear, 1949). These studies showed decreased contrast in the x-ray scattering pattern of dry tendon fibers compared to moist tendon fibers. Smearing of the scattering pattern along the axis of dry fibers indicated decreased order along this axis. Thus the band and interband regularity of the collagen fibril, and therefore the intrafibrillar order, is apparently affected by the presence of water. In reviewing the work of Rougive and Bear in kangaroo tail tendon, Elden reports that at low relative humidity, water may form a monolayer around collagen molecules within the fibril which somehow increases the basic longitudinal period of the fibril from 600A to 640A. When the relative humidity is increased, an apparent slight lateral separation between fibrils occurs. Additional lateral separation and a further increase in the basic axial period

to 690A occurs at very high relative humidity.

In contrast with the tendon studies reviewed by Elden, Maurice (Maurice and Riley, 1970a) has provided evidence that no significant quantity of water exists in corneal collagen fibrils.

We have seen that the collagen fibrils of connective tissue are aggregates of collagen molecules with a high level of orientational and positional regularity existing among these molecules. In the cornea, there is also a noticeable regularity of fibril position. We have indicated that carbohydrate-amino acid molecular complexes and some water may be bound to the collagen fibril. On this basis, there may then be a degree of orientational and positional order among these collagen-related molecules that is produced by their interaction with the collagen fibrils. As was indicated in Chapter 2, orientational and positional order is important for efficient optical second-harmonic generation. Therefore, collagen, water, and the carbohydrate-amino acid complexes may all contribute to the optical second-harmonic conversion efficiency of connective tissue. Connective tissue, by virtue of its relative molecular regularity, should not be likened to a liquid but may, as in the case of the cornea, behave more like a crystalline medium insofar as second-harmonic generation is concerned.

### 3.2 A brief description of the cornea and sclera

The outline presented in this section generally follows a more

detailed critical review by Maurice (Maurice, 1969). The mechanical functions of the cornea and sclera are to provide a protective coat for the eye, to provide a constant volume outer chamber for the ocular fluids which exert an outward hydrostatic pressure, and to provide (in the case of the sclera) a smooth lubricated bearing surface for the rotational motion of the eye. In the normal eye, the cornea is highly transparent to visible radiation and, as a result of its curvature and refractive index, is the major refracting component of the eye (the lens provides a correction for optimal imaging onto the retina). In the normal eye, the sclera is white and opaque as a result of intense, visible light scattering.

The diameter of the cornea in mature rabbits is about 1cm. The normal thickness of the rabbit cornea is approximately 0.4mm at the center with the thickness of the corneal periphery being approximately 0.6mm. When the cornea is excised and exposed to air, it gradually loses water, its thickness decreases slightly, it becomes less flexible, and its surface becomes irregular, however its transparency remains high. When a freshly excised cornea is placed in aqueous solution, it absorbs water, its thickness increases markedly, it becomes more rigid, its surface remains regular, and it clouds and becomes relatively opaque.

The thickness of the rabbit sclera is approximately the same as the corneal periphery. When excised and exposed to air, the sclera becomes thinner, and less flexible. The sclera is markedly more

transparent when dry, but the surface becomes irregular. There is only a slight swelling and hydration of the sclera when placed in aqueous solution.

Classical descriptions of the structure of the cornea subdivide this tissue into five parallel internal layers. Beginning with the outermost layer, these are called epithelium, Bowman's zone, stroma, Descemet's membrane, and endothelium. The epithelium is bathed by the tear layer.

In both the rabbit and man, the outermost layer (epithelium) is five to six cells deep.

In man, Bowman's layer is approximately the first  $12\mu$  of tissue subjacent to (on the deep side of) the epithelium. In rabbits there is a similar layer which is only  $1-2\mu$  thick.

The collagen fibrils of the stroma are approximately  $19\text{nm}$  in diameter in anterior regions and progressively increase to approximately  $34\text{nm}$  in posterior regions. In any given region, the statistical distribution of fibril diameters is quite narrow. Schwarz and Keyserlingk have reported that in a particular normal human stromal region where the mean fibril diameter was approximately  $20\text{nm}$ , a decided majority of the fibril diameters were between  $14\text{nm}$  and  $26\text{nm}$  (Schwarz and Keyserlingk, 1967). Hart and Farrell give an approximate value of  $50\text{nm}$  for the center-to-center spacing of collagen fibrils (Hart and Farrell, 1969). The low amplitude, short range fluctuations

about the average fibril diameter and average inter-fibrillar spacing have been suggested to be an important factor in corneal transparency (Benedek, 1971; Hart and Farrell, 1969).

The corneal stroma contains a small number of modified fibroblasts and polymorphonuclear leucocytes (Bloom and Fawcett, 1968).

Maurice (Maurice, 1969c) gives a value of  $5\mu$  to  $10\mu$  for the thickness of Descemet's membrane. Jakus (Jakus, 1956) has reported varying degrees of apparent organization for different species in electronmicrographs of Descemet's membrane. Chemical analysis for hydroxyproline indicates that collagen is also present in this region (Maurice, 1969d).

Maurice (Maurice, 1969d) has reviewed studies which show that collagen is responsible for 75% of the dry weight of the sclera. The collagen fibrils of the sclera show more interweaving than corneal fibrils. Also, scleral fibril diameters are larger than corneal fibrils in addition to having a broader statistical spread of diameters which range from approximately 30nm to a maximum value of about 250nm (Schwarz, 1957).

### 3.3 A brief description of tendon

In general, tendons function as virtually inextensible links between muscle and other tissues, as for example between muscle and bone. These tendons transmit forces from the muscle to the other

tissue. Electron micrographs of rat tail tendon by Vanamee and Porter (Vanamee and Porter, 1957) show collagen fibrils with diameters ranging from approximately 80nm to 160nm and with the usual cross-band period of about 640A. Schwarz (Schwarz, 1957) has found that the fibril diameters in this tendon range from 30nm to 190nm. In this tendon, fibrils are closely packed in parallel arrays to form fiber bundles whose axes are along the direction of maximum tensile stress. The fiber bundle diameters are of the order of magnitude of 10 $\mu$  (Bloom and Fawcett, 1968). Between the fiber bundles is a thin layer of connective tissue and cells.

#### 3.4 A brief description of skin

The general functions of skin include mechanical protection, protection from dehydration, heat transfer and temperature regulation, sensation, and energy storage in the form of subcutaneous adipose tissue. There are two principal layers of the skin, the outer cellular layer (epidermis) and the underlying inner layer containing collagen fibers (dermis). Beneath the second layer is a third layer (subcutaneous tissue) that contains collagen fibers as well as fat.

Although the dermis contains a number of elements such as cells and blood vessels, its major constituents are extracellular fibers such as collagen and elastin. Of these, collagen is the major component by weight (75% of the dry weight of human skin) and an important component by volume (18% - 30% of the volume) (Bloom and Fawcett, 1968).

Schwarz (Schwarz, 1957) reports a fibril diameter range of 20nm - 90nm for the human adult dermis. Tregear reports a range of 60nm - 140 nm for the same tissue (Tregear, 1966; Braun-Falco and Rupec, 1964; Gross and Schmitt, 1948). These fibrils become part of a hierarchy of larger fiber units similar to the case in tendon. According to Tregear, the diameter of dermal fibers is  $1\mu$  -  $20\mu$ , and throughout a given fiber, the fibril diameters are "remarkably constant". He notes that, within a fiber, the space between fibrils is less than or about equal to a fibril diameter and that the fibril directions are approximately parallel within a fiber (Tregear, 1966). Unlike the cornea, the collagen fibers of skin are not all parallel, some surround hair follicles and others lie at various angles to the surface. In general, a large fraction of the fibers appear to lie parallel to the surface forming a feltwork mesh.

The following table is a summary of the approximate sizes of the various structural units of collagen fibers in several different connective tissues.

	Cornea	Tendon	Skin
Collagen molecule	$13\text{\AA} \times 3000\text{\AA}$	$13\text{\AA} \times 3000\text{\AA}$	$13\text{\AA} \times 3000\text{\AA}$
Collagen fibril diameter	15nm - 30nm	80nm - 160nm	50nm - 150nm
Collagen fiber* cross-sectional dimensions	$2\mu \times 200\mu$	$10\mu$ diameter	$1\mu - 20\mu$ diameter

\*In the cornea these units are called lamellae, in the tendon they are

generally called fiber bundles, and in the skin they are generally called fibers.

AD-A106 237

NORTHEASTERN UNIV BOSTON MASS DEPT OF BIOPHYSICS AN--ETC F/G 6/18  
BIOLOGICAL EFFECTS OF LASER RADIATION, VOLUME IV. OPTICAL SECON--ETC(U)  
OCT 78 W P HANSEN, S FINE DA-49-193-MD-2436

UNCLASSIFIED

NL

2 - 4

1 - 1

1 - 1

1 - 1

1 - 1

1 - 1

1 - 1

1 - 1

1 - 1

1 - 1

1 - 1

1 - 1

1 - 1

1 - 1

1 - 1

1 - 1

1 - 1

1 - 1

1 - 1

1 - 1

1 - 1

1 - 1

1 - 1

1 - 1

1 - 1

1 - 1

1 - 1

1 - 1

1 - 1

1 - 1

1 - 1

1 - 1

1 - 1

1 - 1

1 - 1

1 - 1

1 - 1

1 - 1

1 - 1

1 - 1

1 - 1

1 - 1

1 - 1

1 - 1

1 - 1

1 - 1

1 - 1

1 - 1

1 - 1

## CHAPTER 4

EXPERIMENTAL IDENTIFICATION OF OPTICAL  
SECOND-HARMONIC GENERATION IN BIOLOGICAL TISSUE

The experiments reported in this chapter were carried out to determine whether optical second-harmonic generation occurs in biological tissue. A summary of the material presented in this chapter has been published (Fino and Hansen, 1971). The choices of tissue for study were based in part upon the characteristics of transparency and microscopic structural regularity. Transparency at the fundamental wavelength and the second-harmonic wavelength was desirable in order that the tissue would not be damaged by the laser and in order that second-harmonic radiation could escape the tissue and be detected. A Q-switched ruby laser was available for these studies, which meant that the transparency requirements had to be met at a fundamental wavelength of 694nm and a second-harmonic wavelength of 347nm. Structural tissue regularity was sought in order to improve the second-harmonic conversion efficiency. Separate studies relating to the effect of order in collagen and collagenous tissue are reported in chapters 5 and 6.

The cornea is highly transparent at both 694nm and 347nm. A major region, the stroma, appears to be well-ordered. Tendon is also well-ordered and is relatively transparent when dry. The skin, which is less ordered and less transparent was also studied since it is a superficial, collagenous tissue and, in humans, might be

exposed to laser radiation. Second-harmonic generation in the eye may have implications for vision (Vesilouhe et al, 1963; Zaret, 1965). Second-harmonic generation in the skin may be important (Finn, 1965). Second-harmonic generation by visible lasers could result in calls deep in the skin being exposed to a higher intensity of ultraviolet radiation than occurs under normal conditions (Finn and Klein, 1966b). In conjunction with these tissues, comparative studies were carried out on the sclera, which like the cornea, tendon and skin, contains collagen. Preliminary studies were carried out on muscle since it is another well-ordered tissue.

Other preliminary studies were carried out on hair and nails since these are superficial tissues with possibly sufficient order to yield detectable second-harmonic radiation. These last tissues were easily damaged, therefore, the laser power could not be raised to a level where the second-harmonic signal exceeded our system noise level. Similar difficulties were encountered with retinal melanocomas. These studies were terminated. Dog retina was also investigated for second-harmonic generation. This is a well-ordered transparent tissue and is the site of maximum irradiance in the eye. No second-harmonic generation was detected with these tissues. The degeneration of the retina that occurs after death may have reduced the order in this tissue and therefore prevented our detecting second-harmonic generation.

#### 4.1 Methods and materials

##### 4.1a General outline

A general outline of our methods and materials is presented in this section. Details of the topics presented here are found in Section 4.1b.

A block diagram of the experimental apparatus is shown in Figure 4.1. The Korad KIQ laser supplied an adjustable duration (20nsec - 100nsec) pulse of radiation at a wavelength of 694nm. Glass beam splitters were used to extract a small amount of this radiation for monitoring by a fast Korad KDI silicon photodiode. The photodiode output was fed to one channel of a 50MHz, Fairchild 777 dual-beam oscilloscope where the laser pulse width and pulse height were monitored visually and photographically.

The main beam from the laser was passed through optical filters to remove light from the laser pumping lamps. The beam was focused by lens A (positive lens). The tissue samples to be irradiated were mounted on glass microscope slides and placed just beyond the focal point of lens A where the beam diameter was  $\sim 0.2$ cm. In this way, a controlled high concentration of radiant power was achieved at the sample without operating the laser at high peak powers that would degrade its performance. Radiant emission (scattered light) from the sample was collected in an  $8^\circ$  half angle forward cone by lens B (positive lens). Lens B then imaged the sample at the entrance slit of a Bausch and Lomb Model 33-86-01 grating monochromator. By using

two different gratings, the monochromator could scan from 300nm to 800nm at various wavelength resolutions. Near 347nm, the center wavelength of the monochromator pass band could be read to  $\pm 0.2$ nm accuracy. Theoretically, the smallest achievable band pass of the monochromator is approximately 0.2nm. In practice, the band pass was larger.

A glass tank containing a copper sulfate solution was placed between lens B and the monochromator to absorb radiation at 694nm and transmit radiation between 300nm and 600nm. At approximately one quarter saturated concentration at room temperature, attenuation of the 694nm radiation by the copper sulfate filter was such that second-order spectra and scattered light at 694nm were below detectable levels. ( $\text{CuSO}_4$  filters are mentioned by Franken and Ward (1963)).

The RCA 1P28 (S-5 response) photomultiplier output was displayed on the second channel of the dual beam oscilloscope where pulse widths and pulse heights were monitored visually and photographically. A correction for the slightly nonlinear photomultiplier response was used.

Samples were irradiated while fresh or, in the case of turbid samples, after drying in a vacuum dessicator.

Sample emission spectra were obtained by firing the laser several times at a given laser pulse height and pulse duration for each monochromator wavelength setting. The average pulse height and standard deviation were then plotted versus wavelength.

A detailed description of the experimental methods is given below.

#### 4.1b Details of methods and materials

The ruby laser was a commercial (Korad Corporation) Q-switched oscillator using a Pockels cell shutter. The shutter system was specially designed by the manufacturer to permit selection of laser pulse durations between 20 and 100 nanoseconds (nsec). In practice, pulses from 60nsec to 100nsec were used. Sufficiently fast rise-time oscilloscopes with sufficiently bright traces were not available for pulses shorter than 60nsec. The pulse duration was selected by a circuit that delayed the shutter opening with respect to the beginning of the flash-lamp current pulse. Progressively longer pulses at lower amplitude were obtained by increasing the delay beyond the time of the maximum value of the population inversion. The laser energy was selected by charging the flash-lamp capacitor to a given voltage.

The laser pulse duration (at the half peak power points) showed no detectable variation from shot to shot for a given shutter delay selection. The laser pulse height showed an rms deviation from the mean of 8% at a given flash-lamp capacitor setting. The laser pulse height could be reset to within an estimated peak error range of  $\pm 20\%$  once the flash-lamp capacitor voltage dial setting had been changed.

Laser energies above 0.1 Joule were measured with a Korad KJ-3

liquid calorimeter. A more sensitive TMC ballistic thermopile was used for pulse energies of the order of 0.1 Joule or less. The slow rise-time output of these devices was preamplified by a Hewlett-Packard Model 419A DC microvoltmeter with 300mV zero suppression, and the amplified signal was displayed on a Speedomax II chart recorder. Corrections for thermal drift and detector cooling rate between pulses were made on the chart paper. Zero suppression was needed to reset the chart to zero when a temperature build-up occurred in the thermopile.

Only an estimate could be made of the beam diameter at the sample position. This estimate was based on geometrical optics and the assumption that laser action occurred uniformly over the entire laser rod cross-section. This is a good assumption when using the spiral flasulamp pumping system of the K-1Q oscillator well above laser threshold. This assumption is questionable at near-threshold output energies, where an intense lasing filament covering only the inner one-fourth of the rod diameter often may exist. The laser was operated considerably above the threshold in these studies. Exposed Polaroid film was placed at the sample position and the diameter of the burned or ablated emulsion was measured as an approximate check of the calculated beam diameter. The diameter of the ablated zone was in close agreement with the calculated target beam diameter, based on the assumption of uniform laser action over the rod face.

The copper sulfate solution was held in a tank made from ordinary window glass with a 1.75 inch light path through the liquid. The copper sulfate concentration was increased until no second-order laser spectrum or scattered light was detected by the photomultiplier when the monochromator was scanned from 300nm to approximately 650nm with no sample in place.

When samples were in place and pulses were observed with the monochromator set near 347nm, checks were employed to be sure that 694nm radiation was not, for some unforeseen reason, being detected by the photomultiplier. The check that was consistently employed was to cover the monochromator entrance slit with a Corning CS2-58 (red pass, UV blocking) filter and repeat the laser firing with nothing else changed. If the pulse was again present, then laser radiation at 694nm was possibly reaching the photomultiplier on both trials. If this occurred, the copper sulfate concentration was increased. Emission spectra were obtained once it was certain that the observed pulse on the photomultiplier channel was not due to 694nm radiation.

The flash-lamp capacitor voltage setting was held constant while obtaining tissue emission spectra. A group of 10 wavelength settings between 344nm and 350nm was chosen for observation. The laser was first fired once at each setting in this group. The laser was then fired several more times at settings where the signal was high. The wavelength setting was changed between each of these

observations. The settings were chosen in a different order for each run through the group of high signal settings so that slow changes in the tissue would affect the data evenly. One observation was generally made at each wavelength setting in the low intensity wings of the spectra. The average and standard deviation of the emission pulse heights was then plotted versus wavelength setting.

A vernier was added to the wavelength scale of the monochromator to assist in determining the wavelength at which the peak of the emission line occurred. The unit together with the vernier was calibrated for wavelength using a low pressure mercury discharge lamp. The mercury lines at 365.10nm and 334.14 nm (Am. Inst. Physics Handbook, 1957) were used for this purpose. Repeated approaches from alternate sides of the calibration line maxima gave average values of 362.9nm and 332.9nm on the wavelength dial of the monochromator with a standard deviation of 0.2nm in both cases. It was assumed that the wavelength dial systematic error was a linear function of the wavelength dial setting. The slope of the resulting error correction line was small. For four significant figure wavelength data, it was sufficient to use a constant correction of +1.6nm for settings between 343nm and 348nm. This region is where most of the sample emission spectra were obtained.

The bandpass of the Bausch and Lomb monochromator with narrowest useful slits was estimated to be 0.2nm. A narrower bandpass would have been helpful in examining the emission line-width near 347nm

(see Section 4.3c).

The normalized response of the monochromator with the 1P28 photomultiplier is shown in Figure 4.2a. This was obtained at various wavelengths by placing the monochromator in and out of a spectrophotometer beam that had been brought out into the room to illuminate the photomultiplier. The spectrophotometric transmission of the copper sulfate filter is shown in Figure 4.2b. The curve shown in Figure 4.2c is the product of the measured transmission spectra of lens B and lens C (Fig. 4.1). Figure 4.2d is the product of the curves in Figures 4.2a, b and c which has been renormalized to unity at 400nm. The overall relative system response (Fig. 4.2d) is highest in the visible. The response is low at 347nm. The response at 694nm is about  $10^8$  times lower than the response at 347nm (extrapolate curve 4.2d). This provided sufficient rejection of laser radiation that might reach the detector when the monochromator was set to 347nm.

The discontinuity in the curves of Figures 4.2a and 4.2c was produced by the change of gratings that was required to span the wavelength range indicated. The light source used to determine the monochromator-photomultiplier response was too weak to obtain reliable data for  $\lambda < 340\text{nm}$ . (A different spectrophotometer with a higher intensity lamp was used to obtain the  $\text{CuSO}_4$  transmission.) The dotted line in Figure 4.2a is an extrapolation.

Our spectrophotometric measurements showed that only 14% of the

radiation at 347nm was transmitted by the combination of lenses B and C. Approximately 30% of the attenuation by these lenses was due to reflection at the curved lens surfaces. Quartz lenses were not available. With quartz, the transmission of these lenses would have been improved by a factor of about 5.

Tissue samples were mounted on glass microscope slides and irradiated while fresh as well as after air or vacuum drying at room temperature. Sample transmission was monitored at 694nm and 347nm with a Beckman Model B single-beam spectrophotometer while the samples were fresh and after drying. Ten corneas, ten tendons, five skin samples, and four scleras were investigated for second-harmonic generation.

An interfering signal (termed pick-up in this report), consisting of a damped oscillation at about 10MHz, was observed on both oscilloscope traces. Analysis of the Pockels cell pulsing circuit indicated that the Pockels cell crystal may have acted as a source of electromagnetic radiation near 10MHz. The crystal was RC coupled to a 20 foot RG8-U (50 ohm) coaxial cable. The other end of the cable was connected to a thyatron switch through a nominal 50 ohm series resistor. The Pockels cell was "opened" by discharging the line through the thyatron. Assume that the crystal end of the coaxial cable is open. If  $R_L$  is exactly equal to the characteristic impedance of the cable,  $Z_0$ , then the cable voltage at the crystal end should fall from the initial voltage,  $V_0$ , to zero after one cable

transit time (30nsec). If  $R_L < Z_0$ , then the cable voltage will be a damped square wave oscillation with a period equal to 4 cable transit times (120nsec). If  $R_L > Z_0$ , then the cable voltage will decay in a "staircase" manner where the steps are 4 cable transit times long. In the case where  $R_L < Z_0$ , the (open) Pockels cell crystal end of the cable would radiate a damped signal at a fundamental frequency of  $1/120\text{nsec}$  or 8.3MHz. This corresponds very closely to the  $\sim 10\text{MHz}$  damped oscillation picked up by our detection equipment. Shielding the Pockels cell housing with aluminum foil reduced the 10MHz pick-up significantly. Moving the detection equipment away from the Pockels cell and shortening the detector leads also reduced the pick-up. Even after these measures were taken, the pick-up current amplitude at the oscilloscope was approximately 0.2ma. The photomultiplier output current had to be on the order of 2ma to achieve about a 10:1 signal to noise ratio. At these high currents the photomultiplier power response was nonlinear. Had we adjusted the series resistor at the thyatron there may have been a reduction in the amplitude of the cable oscillation. This might have allowed us to use the photomultiplier in a lower current range where it was possibly linear.

The 1P28 photomultiplier was calibrated for linearity as a function of input peak power at 694nm. The previously mentioned calorimeters were used in the manufacturer's suggested linear range to show that the KD-1 photodiode was linear at 694nm. The photodiode and 1P28 photomultiplier were then compared at 694nm. It was

found that, in the range of output pulse heights used in these studies (0.5mA - 5mA), the 1P28 photomultiplier peak output voltage was proportional to  $(P_1')^{0.85}$  where  $P_1'$  is the relative radiant input peak power (Figs. 4.4a and 4.4b). This relationship was assumed to also hold for radiant inputs at 347nm and was used as a systematic error correction of the observed photomultiplier output.

The ability of the system to show second-harmonic emission spectra was checked by obtaining isolated emission maxima at 347nm from KDP (potassium dihydrogen phosphate) powders and aspartic acid powders that have been reported to yield second-harmonic radiation (Reickhoff and Peticolas, 1965). No emission was observed at 347nm from glycine crystalline powders. Glycine crystallizes in a centrosymmetric form and has been shown to yield very low second-harmonic radiation levels (Reickhoff and Peticolas, 1965).

## 4.2 Results

### 4.2a Peak emission wavelength

Emission spectra for cornea, sclera, skin, and tendon were obtained point-by-point in the vicinity of 347nm using a variety of monochromator slit widths. A number of these spectra are shown in Figures 4.5 through 4.12. The data in these figures has been corrected for the photomultiplier nonlinear responsivity. The system response as a function of wavelength was considered constant over the bandwidth of the input signal.

All of these spectra show an emission peak near 347nm which is the

approximate second-harmonic wavelength of the ruby laser. The low resolution, wide range spectrum in Figure 4.5 also shows a small peak at 694nm which is a residual signal that passed through the  $\text{CuSO}_4$  filter from the laser itself. The small peak at 694nm corresponds to radiation that, at the laser, is  $\sim 10^{10}$  times more intense than the radiation at 347nm from the tissue. There are no evident peaks between 347nm and 694nm despite the fact that over a good portion of this range the system response was high (Fig. 4.2d).

In the case of opaque tissues (tendon, sclera, and skin), the collected sample emission at 347nm was small but detectable while the samples were fresh. When these samples were dried in air or vacuum, spectrophotometric transmission at 347nm and 694nm improved markedly, as measured with the Beckman Model B unit. For these dried tissues, sample emission at 347nm became easily measurable. Corneal samples remained quite transparent whether fresh or dry. No marked change in corneal emission intensity occurred after drying.

Emission at 347nm vanished when (a) the sample was removed, (b) the glass microscope slide sample mount was irradiated alone, (c) when a CS2-58 red pass, ultraviolet blocking filter was placed over the monochromator entrance slit.

A free-hand smooth curve was drawn through the emission data for each tissue and the peak of the curve was estimated. The wavelengths corresponding to the peaks of these smooth curves are shown in Table 4.1. The average of the entries in this table is  $\bar{\lambda}_p = 347.1\text{nm}$

with a standard deviation of 0.2nm. We will show in Section 4.4 that this value of  $\bar{\lambda}_p$  is within one standard deviation of the expected peak for second-harmonic generation.

TABLE 4.1

<u>Tissue</u>	<u><math>\lambda_p</math> (nm)</u>
Dog cornea (fresh)	347.1
Rabbit cornea (fresh)	346.7
Rabbit skin (whole, dry)	347.4
Rabbit skin (without superficial layers, dry)	347.1
Dog cornea (dry)	347.1
Rabbit tendon (dry)	347.3
Dog cornea (dry)	346.8
Average ( $\bar{\lambda}_p$ )	347.1nm
Standard deviation ( $\sigma_p$ )	0.2nm

The centroid of the distribution of spectral data points was determined. The wavelength value of the centroid,  $\lambda_c$ , was obtained from:

$$\lambda_c = \frac{\sum P'_{21} \lambda_1}{\sum P'_{21}}$$

where  $P_{21}^i$  is the relative peak power and  $\lambda_i$  is the wavelength setting for the  $i^{\text{th}}$  data point. The results of these centroid measurements are shown in Table 4.2. The average of these entries is  $\bar{\lambda}_c = 347.2\text{nm}$  with a standard deviation of 0.1nm.

The agreement between  $\bar{\lambda}_p$  and  $\bar{\lambda}_c$  is an indication that the spectral curves are symmetric about their peak.

TABLE 4.2

<u>Tissue</u>	<u><math>\lambda_c</math> (nm)</u>
Dog cornea (fresh)	347.1
Rabbit cornea (fresh)	347.1
Rabbit skin (whole)	347.3
Rabbit skin (without superficial layers, dry)	347.3
Dog cornea (dry)	347.1
Rabbit tendon (dry)	347.3
Dog cornea (dry)	347.0
Average ( $\bar{\lambda}_c$ )	347.2nm
Standard deviation ( $\sigma_c$ )	0.1nm

#### 4.2b Square-law dependence

Two measurements were performed to investigate the functional dependence of the radiant intensity from the sample at 347nm upon the input intensity to the sample at 694nm. The first measurement

involved fitting a regression line to a log-log plot of peak power at 347nm versus peak power at 694nm. The second measurement involved monitoring the shape of the radiant pulse at 347nm as a function of time.

Simultaneous measurements were made of the relative peak power  $P'_2$  reaching the photomultiplier near 347nm and the relative laser peak power  $P'_1$  reaching a rabbit cornea sample near 694nm (Fig. 4.1). The results of these measurements are shown on a plot of  $\log P'_2$  versus  $\log P'_1$  in Figure 4.13. In this plot, the individual values of  $P'_2$  are corrected for the nonlinearity of the photomultiplier (Methods and materials, and Fig. 4.4b). Each data point represents a single laser shot.

A regression line was obtained for the data in Figure 4.13 (Parratt, 1961). The average percentage deviation of the data points from the regression line was computed from:

$$c = \frac{100}{N} \sum_{n=1}^{n=N} \frac{|P'_2(n) - P'_2(\text{st. line})|}{P'_2(\text{st. line})}$$

The value of  $c$  is 20%. The slope of the regression line is 2.0 over the range of data shown. This slope is in agreement with experimental results on second-harmonic generation that have been reviewed by Pershan (Pershan, 1966).

If the instantaneous relative power  $P'_2(t)$  near 347nm and the instantaneous relative power  $P'_1(t)$  near 694nm are related by a

square-law,  $P_2'(t) = A (P_1'(t))^2$ , then the pulse at 347nm should be temporally narrower than the pulse at 694nm (except in the special case of rectangular pulses). Oscilloscope measurements of the 347nm pulse width ranged from 65% to 75% of the width of the associated laser pulses at 694nm. (The pulse full-width at half-maximum, FWHM, was used for these comparisons.) The uncertainty in the per-cent difference between the 694nm and 347nm pulse widths was a result of difficulties in reading the time scale on the oscilloscope photographs. A pair of pulses is shown in Figure 4.14 for which a rabbit cornea was used. There is some asymmetry in the 347nm pulse that is probably related to the photomultiplier system. The asymmetry was not present when more efficient KDP powders were monitored with the less sensitive KD-1 photodiode. The asymmetry was again present when these powders were monitored with the photomultiplier. Pulse narrowing was still observed when the 347nm and 694nm pulses were fed to interchanged oscilloscope channels.

It will be shown in Section 4.3b that pulse narrowing by 30% is consistent with second-harmonic generation.

#### 4.2c Bandwidth of emission at 347nm

The bandwidth of the 347nm emission from the tissues shown in Figures 3.5 - 3.12 was monitored as the monochromator slits were progressively narrowed. The results of these measurements are shown connected by line A in Figure 4.15 (data enclosed by circles).

For comparison, two other curves (B and C) are also shown in

Figure 4.15. Curve B (straight line) shows the theoretical monochromator band pass for perfectly aligned slits and grating according to the manufacturer's specifications. Curve C shows the measured bandwidth of a Hg-Cd Osram lamp spectral line near 350nm as a function of the entrance slit width (data enclosed by triangles). According to the manufacturer, the actual bandwidth of the Hg-Cd line is  $\sim 0.19\text{nm}$ .

Curves A and C diverge from the theoretical bandpass curve, B, for slit widths less than  $\sim 2\text{mm}$ . These results will be discussed in Section 4.3c.

#### 4.2d Ancillary results concerning sample damage

When the laser peak power at the tissue sample (cornea, sclera, skin, tendon) was raised above  $\sim 20\text{MW}/\text{cm}^2$  there was a sudden increase in the measured radiant emission from the sample at both visible and ultraviolet wavelengths. Accompanying this increase were these changes: the observed sample emission covered a band from  $\sim 300\text{nm}$  to  $\sim 700\text{nm}$  rather than a narrow band of less than  $1\text{nm}$  near  $347\text{nm}$ ; the temporal peak of the sample emission pulse occurred near the end of the laser pulse rather than coinciding with the peak of the laser pulse; either an audible "crack" accompanied the laser pulse or the sample was visibly damaged or both of these effects occurred. A new mechanism of radiant emission, related to sample damage, was apparently present at laser powers above  $20\text{MW}/\text{cm}^2$ . While second-harmonic generation may have still occurred at these higher laser powers, it could not be clearly identified, due to the high intensity of the broad-band emission.

The broad band emission apparently covered the entire sensitive range of our short wavelength (ultraviolet) monitoring system which was from 300nm (glass and photomultiplier cut-off) to 400nm (grating cut-off). Repeatability was poor; however, the radiant emission levels appeared to be about the same at each wavelength over this range. The broad band emission was not systematically monitored with the second grating that spanned the range from 400nm to 800nm. However, spot checks showed that the broad band emission extended well into the visible range. A spectral emission peak at 347nm could not be discerned.

Figure 4.16 is a sketch of the laser pulse (curve A) and two types of broad band emission pulses (curves B and C) that were drawn from oscilloscope photographs and transferred to the same time scale. The peaks of the three pulses have been normalized to be equal. Curves B and C were obtained with a 450nm long wavelength cutoff filter replacing the monochromator (Fig. 4.1). A rabbit cornea was used for curve B and a rabbit lens was used for curve C.

Several temporal features of broad band emission pulses are illustrated by these curves. First, the temporal peak of the broad band emission pulses occurred after the peak of the laser pulse. Second, when measured at half-maximum, the broad-band emission pulses were temporally narrower than the laser pulse. Third, in some cases a long, delayed decay of the broad-band emission pulse extended beyond the laser pulse duration (curve C). This decay "tail"

was not always visible on oscilloscope photographs (curve B, Fig. 4.16). This was due to the fact that the peak of the pulse was usually at least 10 times higher than the tail. If the peak could be seen, the tail was generally below the least count of the oscilloscope scale. When the oscilloscope gain was increased, the tail usually became discernable but the peak was off scale. The rabbit lens was an exception (curve C, Fig. 4.16). For this (easily damaged) material, both the peak and the tail of the broad band emission pulses were observable. Definitive, narrow band radiation at 347nm was never observed from the rabbit lens.

### 4.3 Discussion

#### 4.3a Peak emission wavelength

We have estimated the peak emission wavelength of the ultraviolet radiation from tissue to be  $\lambda_p = 347.1\text{nm}$  with a standard deviation of 0.2nm. To determine whether this estimate agrees with the peak second-harmonic wavelength for ruby laser excitation we must first establish the peak emission wavelength of our ruby laser. From this we will derive the expected second-harmonic peak wavelength in air.

The peak emission wavelength for a single ruby laser pulse is a function of the laser rod temperature,  $T$ , that exists just before firing the laser. Abella and Cummins (Abella and Cummins, 1961) have shown that the mean peak emission wavelength for long pulse (1msec pulse duration) ruby lasers increases by 0.0065nm for each centigrade

degree increment in initial rod temperature over the range 25°C to 80°C. A linear extrapolation of their data to 20°C yields the following equation for peak laser wavelength as a function of temperature near 20°C:

$$\lambda_1(T) = 694.325 + 0.0065 (T - 20) \quad (1)$$

In Equation (1),  $\lambda_1(T)$  is the peak laser emission wavelength in nm and T is the initial rod temperature in centigrade degrees. We will assume the validity of this equation for Q-switched lasers as well as long pulse lasers.

The peak emission wavelength for ultraviolet emission from tissue was obtained from a series of laser pulses. Therefore, the stability of the peak laser emission wavelength from pulse to pulse is an important factor in determining the second-harmonic peak emission wavelength. This stability is a function of the difference in initial laser rod temperature from one pulse to the next.

The peak emission wavelength can steadily increase from shot-to-shot if the laser rod is not given sufficient time to cool between flash-lamp pulses. The KIQ oscillator system was equipped with a circulating water cooling system to provide cooling of the rod between pulses. Under actual operating conditions, 300 seconds were allowed between laser firings. This can be shown to have been sufficient time to allow the rod to cool to the temperature of the

circulating water (21°C) within the limits of the temperature regulator ( $\pm 1^\circ\text{C}$  by manufacturer's specifications) (Appendix A).

The only temperature effect on the peak laser emission wavelength is probably that due to temperature fluctuations in the cooling system which are less than  $\pm 1^\circ\text{C}$ . Therefore, we can specify  $\lambda_1(T)$  from Equation (1) at  $T = 21^\circ\text{C} \pm 1^\circ\text{C}$  as

$$\lambda_1 = 694.331 \pm 0.0065\text{nm}$$

We need only five significant figures for the value of  $\lambda_1$  in order to calculate the second-harmonic wavelength,  $\lambda_2$ , to one more significant figure than was obtained experimentally. Rod temperature fluctuations of  $\pm 1^\circ\text{C}$  do not produce any uncertainty in the value of  $\lambda_1$  to five significant figures.

In finding the second-harmonic wavelength  $\lambda_2$  corresponding to the above value of  $\lambda_1$ , the effects of the dispersion of air between 694nm and 347nm should be considered. The fundamental frequency  $\nu_1$  and the second-harmonic frequency  $\nu_2$  are related by:

$$\nu_2 = 2\nu_1$$

This expression can be rewritten in terms of the (measurable) fundamental wavelength in air,  $\lambda_{1a}$ , and the second-harmonic wavelength in air,  $\lambda_{2a}$  as follows:

$$\frac{C}{n_{2a} \lambda_{2a}} = \frac{2C}{n_{1a} \lambda_{1a}}$$

where  $C$  is the speed of light in vacuum and  $n_{1a}$ ,  $n_{2a}$  are the refractive indices of dry air at STP at  $\nu_1$  and  $\nu_2$  respectively. Solving the above equation for  $\lambda_{2a}$  yields

$$\lambda_{2a} = \frac{n_{1a} \lambda_{1a}}{2 n_{2a}} \quad (2)$$

For the ruby laser and its second-harmonic the ratio  $n_{1a}/n_{2a}$  is 0.99998 (Handbook of Chemistry and Physics, 1965a). This correction is very small and does not affect the value of  $\lambda_2$  in air when written to five significant figures.

From the above considerations, we conclude that our peak ruby laser wavelength,  $\lambda_1$ , should be written as:

$$\lambda_1 = 694.33\text{nm}$$

and that the second-harmonic wavelength,  $\lambda_2$ , is given by  $\lambda_1/2$  or:

$$\lambda_2 = 347.16\text{nm}$$

This is our theoretical estimate of the second-harmonic wavelength of the K1Q ruby laser. This value is in close agreement with our experimentally observed peak emission wavelength from tissue of  $\lambda_p = 347.1$  with a standard deviation of 0.2nm.

We have shown that the peak wavelength of the isolated ultraviolet emission line from tissue is in close agreement with the calculated peak second-harmonic wavelength of the K1Q ruby laser. This is taken to be evidence that optical second-harmonic generation in tissue is responsible for the observed ultraviolet emission.

#### 4.3b Square-law relationship

In Section 4.2b, the equation:

$$\log P'_2 = A + 2.0 \log P'_1 \quad (3)$$

where  $P'_2$  is the relative peak power near 347nm and  $P'_1$  is the relative laser peak power at 694nm, was shown to fit the experimental data (Fig. 4.13). By differentiating Equation (3), it can be seen that a fractional variation in the laser peak power  $\Delta P'_1/P'_1$  should produce a fractional variation in the 347nm peak power equal to  $2\Delta P'_1/P'_1$ . If  $P'_1$  and  $P'_2$  are random variables in Equation (3), then the per-cent standard deviations in these quantities are related by  $\sigma'_2 = 2\sigma'_1$  (Meyer, 1965). This last equation is not consistent with our experimental data. In studies on cornea, sclera, tendon and skin it was determined that  $\sigma'_2 = 35\%$  when  $\sigma'_1 = 10\%$ . Similar results have been cited by Pershan in reviewing experimental studies of optical second-harmonic generation in non-biological media (Pershan, 1966). Pershan has concluded that "on the average", a square-law relation is observed between  $P'_1$  and  $P'_2$ , but there are considerable fluctuations

from the average behavior. As an example, Ducuing and Bloembergen (Ducuing and Bloembergen, 1964) have observed  $\sigma_2' = 40\%$  when  $\sigma_1'$  was approximately 4%.

Ducuing and Bloembergen (Ducuing and Bloembergen, 1964) have explained these inconsistencies by including the effects of random phase fluctuations in the laser field when computing the second-harmonic intensity. It should be noted that they refer to the sum-frequencies as well as the second-harmonic frequencies within the 347nm line as "second-harmonic" frequencies (we have also adopted this viewpoint). According to their analysis, large fluctuations in the second-harmonic peak power are due to fluctuations in the intensity of the sum-frequency radiation within this line. A given sum-frequency mode,  $\nu_s$ , can be fed by a number of pairs of laser modes that, due to the less than perfect coherence of the laser, vary randomly in relative phase during a laser pulse. A given mode pair may interfere constructively at one time and destructively at another time. This will cause a large variation in the intensity of certain sum-frequency modes even though the individual amplitudes of these modes may be constant. In our experiments, the second-harmonic pulse heights (peak powers) were compared from pulse to pulse under conditions where the laser pulse height was approximately the same from pulse to pulse (10%). The relatively large fluctuations in second-harmonic pulse height that we observed (35%) may have been caused by the random interference of certain sum-frequency modes near the time of the pulse peak. According to Ducuing and Bloembergen's

model these large second-harmonic power fluctuations would not be observed with a monochromatic laser but probably should be observed with the system used in our studies.

From the above discussion, it is apparent that with our methods it would be difficult to obtain a least-squares empirical equation of the form of Equation (3) with a low standard deviation in the slope. The fact that our regression line slope of 2.0 (Fig. 4.13) agrees with the slope of 2 that is associated with second-harmonic generation (Pershan, 1966) is evidence in support of second-harmonic generation as the mechanism responsible for emission at 347nm from the tissues investigated.

Evidence for a square-law relation between  $P_2'(t)$  and  $P_1'(t)$  was also obtained by comparing the laser pulse width and the 347nm emission pulse width. Both pulses appeared to be nearly Gaussian functions on the oscilloscope photographs. Let:

$$P_1'(t) = P_1' \exp [-t^2/T_1^2] \quad (4)$$

If  $P_2'(t) = A (P_1'(t))^2$ , then:

$$P_2'(t) = A (P_1')^2 \exp [-2t^2/T_1^2] \quad (5)$$

From Equations (4) and (5) it can be seen that the width at any percent of maximum of the  $P_2'$  Gaussian pulse is  $1/\sqrt{2}$  or 71% of the width

of the  $P_1'$  pulse at the same per-cent of maximum. Our experimental measurements were carried out at 50% maximum where it was shown that the  $P_2'$  pulse was 65% to 75% of the width of the  $P_1'$  pulse (Fig. 4.14). It was estimated that the  $P_1'$  pulse width could be read to about 5% accuracy and the  $P_2'$  pulse width could be read to about 7% accuracy. Our experimental pulse width measurements are within the expected experimental error of the theoretical pulse width estimates which are based on a square-law relationship and Gaussian pulses.

#### 4.3c Bandwidth of emission at 347nm

Using the smallest practical entrance slit width (0.15nm entrance slit), our monochromator yielded a bandwidth measurement of  $\sim 0.8$ nm for Hg-Cd lamp lines near 350nm (Curve C, Fig. 4.15). Under ideal conditions of perfect slit and grating alignment, as well as optimum focusing the monochromator band pass should be 0.2nm with an 0.1mm entrance slit (Curve B, Fig. 4.15). Therefore, under ideal conditions, with a monochromatic band pass of 0.2nm, our unit should have yielded a measurement of approximately 0.4nm for the Hg-Cd lines, since the actual bandwidth of these lines is  $\sim 0.2$ nm. The divergence of curve C from curve B indicates a systematic error of alignment or focusing in the monochromator. There was no provision by the manufacturer to correct such errors.

Curve C does not necessarily represent the smallest bandwidths that can be practically obtained at each slit width. A source with less than  $\sim 0.2$ nm actual spectral bandwidth may produce a measured

bandwidth curve below curve C. However, such a curve should still lie above curve B.

The measured bandwidth curve for 347nm emission from cornea, sclera, tendon and skin (curve A) lies below curve C and above curve B. Since curve C was generated by measurements on  $\sim 0.2$ nm bandwidth radiation near 347nm, curve A is associated with emission with a bandwidth that is less than 0.2nm.

The expected bandwidth of second-harmonic emission is 50 times smaller than the useful resolution of our monochromator when perfectly aligned. The expected bandwidth for second-harmonic pulses is determined by the bandwidth of the laser pulse. The manufacturer of the K1Q laser system has specified a wavelength bandwidth of  $\Delta\lambda_1 = 0.01$ nm for the laser pulse. The wavelength bandwidth of the second-harmonic pulse,  $\Delta\lambda_2$ , should be smaller than  $\Delta\lambda_1$ . This can be shown as follows. The second-harmonic pulse is compressed in time by a factor  $b$  relative to the laser pulse. The frequency bandwidth of the second-harmonic pulse,  $\Delta\omega_2$ , is therefore  $b$  times greater than the frequency bandwidth of the laser pulse,  $\Delta\omega_1$ .

$$\Delta\omega_2 = b\Delta\omega_1$$

When the wavelength bandwidth  $\Delta\lambda$  is much smaller than the peak wavelength  $\lambda$  we can use the following difference approximations that are obtained from the equation  $\omega = 2\pi c/\lambda$ :

$$|\Delta\omega_2| = 2c \frac{\Delta\lambda_2}{\lambda_2^2} \quad (6)$$

$$|\Delta\omega_1| = 2c \frac{\Delta\lambda_1}{\lambda_1^2} \quad (7)$$

Combining Equations (6) and (7):

$$\Delta\lambda_2 = \frac{b\lambda_2^2}{\lambda_1^2} \Delta\lambda_1 \quad (8)$$

We have shown previously that  $\lambda_2 = \frac{\lambda_1}{2}$  is an excellent approximation because of the low dispersion of air. Equation (8) can therefore be written as:

$$\Delta\lambda_2 = \frac{b}{4} \Delta\lambda_1$$

If  $b < 4$ , then  $\Delta\lambda_2 < \Delta\lambda_1$ . For Gaussian pulses we showed that  $b = \sqrt{2}$ . For these pulses, therefore,  $\Delta\lambda_2 = 0.35 \Delta\lambda_1$ , or  $\Delta\lambda_2 = 0.0035\text{nm}$  which could not be resolved by our instrumentation.

If the second-harmonic spectrum is obtained by reading emission at a single wavelength for each laser pulse and then plotting the data for a number of laser pulses, then temperature differences in the laser rod from pulse to pulse could broaden the second-harmonic spectrum. This broadening was calculated as negligible in our system. The laser rod temperature fluctuations were approximately  $\pm 1^\circ\text{C}$  which could cause a shift of  $\pm 0.0065\text{nm}$  in the laser peak emission wavelength.

This small shift is much smaller than our system resolution.

#### 4.3d Sample damage and broad band emission

It has been shown that pulses of second-harmonic radiation were temporally narrower than the laser pulse. However, another form of radiant emission was also found to yield a temporally arrowed pulse. This emission was found to accompany sample damage and was also found to cover a much broader wavelength range than second-harmonic radiation. The broad band emission pulse peak occurred near the end of the laser pulse whereas the second-harmonic pulse peak coincided with the temporal peak of the laser pulse. The relative placement of these pulse peaks was not always easy to determine, therefore a wavelength scan with the monochromator was considered to be a necessary step in order to distinguish between these two kinds of emission.

With physical and biological targets, obvious sample damage is often accompanied by the creation of a highly luminous "plume" that expands away from the irradiated surface, while the surface itself may or may not be luminous (Fine et al, 1965; Ready, 1971). The composition of these plumes is variable and depends on the surface and the laser peak power level. Within its luminous volume, the plume may contain ablated macroscopic material particles; the vapor phase of the sample constituents; ionized atoms and molecules; and, with Q-switched lasers, the plume can become a plasma (Ready, 1971). Radiation from laser plumes has been observed with emission extending from the UV into the visible spectrum (Ready, 1971). Therefore, our

observation of broadband radiation in the ultraviolet and visible range may have been due to the creation of a luminous plume from the damaged sample.

The temporal behavior of plume emission has been investigated photographically by Ready (Ready, 1971). In his studies, a 45nsec pulse Q-switched ruby laser was used to irradiate a carbon target in air while the interaction was photographed at various times after the start of the laser pulse. A bright plume rapidly appeared somewhat after the peak of the laser pulse. The volume of the luminous plume reached a maximum well after the end of the laser pulse, then the luminosity and the volume decreased slowly until the plume had essentially vanished nearly 1 $\mu$ sec after the beginning of the laser pulse.

The rapid rise in intensity of broad band radiation that we have observed after the peak of the laser pulse (Fig. 4.16) is in agreement with emission from a luminous plume according to Ready's results. We do not have an explanation for the initial rapid decay in broad band intensity that occurs near the end of the laser pulse. The rapid expansion of laser plumes could, however, be a factor in our measurements that yields this decay. That is to say, Q-switched laser plumes have been reported to show a strongly anisotropic expansion away from the target surface (Ready, 1971). The expansion velocity of the luminous front increases by an order of magnitude in the period of time between the peak and before the end of the laser pulse. This acceleration is sharply curtailed at the end of

the laser pulse (Ready, 1963). If this occurred in our studies, then much of the luminous plume volume could have expanded beyond the range of optimum focusing by lens A (Fig. 4.1) and, therefore, rapidly lowered the collected broad band intensity while the plume itself may have been actually increasing in intensity. After the laser pulse, the plume does not grow rapidly, and remains relatively stationary in space (Ready, 1971). This could then lead to the "decay tail" in broad band intensity that we have observed.

The broad band emission that we have observed from damaged tissue samples may therefore have been produced by a luminous plume that has been found to generally accompany Q-switched laser induced damage of physical and biological materials. In our studies, this emission pulse accompanying sample damage was temporally narrowed relative to the laser pulse for reasons given above. However, in contrast with second-harmonic generation pulses, this pulse occurred at the end of the laser pulse and exhibited a "tail". This temporal delay for broad band emission would be expected because of the time necessary for plume generation.

#### 4.4 Summary and conclusions

Fresh and dried dog and rabbit cornea, dried rabbit Achilles tendon, dried rabbit skin, and dried rabbit skin with the superficial layers removed were irradiated by a Q-switched ruby laser at 694nm. Emission spectra were obtained for these collagenous tissues over the range 300nm - 700nm. When the samples were not visibly damaged

by the laser, an isolated, narrow emission line was found near 347nm.

Analysis of the spectral curves showed that the peak emission wavelength for these tissues was 347.1nm with a standard deviation of 0.2nm. The peak emission wavelength expected for second-harmonic generation is 347.16nm.

The relative peak power at 347nm was shown to increase as  $(P_1')^{2.0}$  where  $P_1'$  is the relative peak power at 694nm. This square-law is expected for second-harmonic generation. The 347nm temporal pulse width was 25% to 35% less than the 694nm laser pulse width. Both the laser and second-harmonic pulses appeared to be roughly Gaussian functions. With a Gaussian laser pulse, a second-harmonic pulse should be Gaussian and 29% narrower than the laser pulse due to the square-law relation.

The emission bandwidth at 347nm could not be resolved by our instrumentation. We have shown the emission bandwidth to be less than 0.2nm. The expected emission bandwidth for second-harmonic generation is about 2 orders of magnitude smaller than 0.2nm. Higher resolution equipment is needed for wavelength bandwidth measurements of the observed emission.

Our measurements of peak emission wavelength, peak power dependence, and temporal pulse width are in agreement with optical second-harmonic generation being the mechanism for the observed emission near 347nm.

In addition to the collagenous (connective) tissues, muscle,

hair, nails, and melanosomes were irradiated. Second-harmonic generation was found in muscle in a preliminary study but not in the other tissues. Thus, collagenous tissue and possibly muscle possess the requisite material characteristics for optical second-harmonic generation. The collagen component of connective tissue may be the principal site for the observed harmonic generation.

## APPENDIX A

Approximately 400cal were dissipated in the laser flash lamp at each firing. If all this energy is assumed to appear as heat in the laser rod then, with no heat conduction during the flash lamp pulse, the temperature rise in the rod is given by

$$T = Q/\rho VC \quad (A1)$$

In Equation (A1),  $Q = 400\text{cal}$ ,  $\rho = 3.98\text{gm/cm}$  (Adolf Meller Company, Synthetic Sapphire Properties),  $V = 7.85\text{cm}^3$  (the volume of a 1cm diameter 10cm long rod),  $C = 0.18\text{cal/gm}^\circ\text{C}$  (Abella and Cummins, 1961). With these values  $T = 70^\circ\text{C}$ . After 300sec, with cooling only occurring through the sides and with the rod surface temperature held at the cooling water temperature of  $21^\circ\text{C}$ , the spatial average temperature of the rod is given by (Carslaw and Jaeger, 1959):

$$T(^{\circ}\text{C}) = 21 + (280) \sum_{n=1}^{\infty} \frac{1}{\alpha_n^2} e^{-K\alpha_n^2 t} \quad (A2)$$

In Equation (A2), the  $\alpha_n$  are positive roots of  $J_0(\alpha_n a) = 0$ ,  $a$  is the rod radius,  $K$  is the thermal diffusivity of the rod ( $0.125\text{cm}^2/\text{sec}$  (Adolf Meller Company, Synthetic Sapphire Properties)); and  $t = 300\text{sec}$ . Only the first term of Equation (A2) is significant. In this case  $\alpha_n = 4.8\text{cm}^{-1}$  and

$$T(^{\circ}\text{C}) = 21 + 12e^{-868} \quad (\text{A3})$$

Equation (A3) shows that it can be assumed that there are no cumulative heating effects in the rod due to repeated flash lamp firings.

Fig. 4.1

Overall schematic of experimental apparatus.

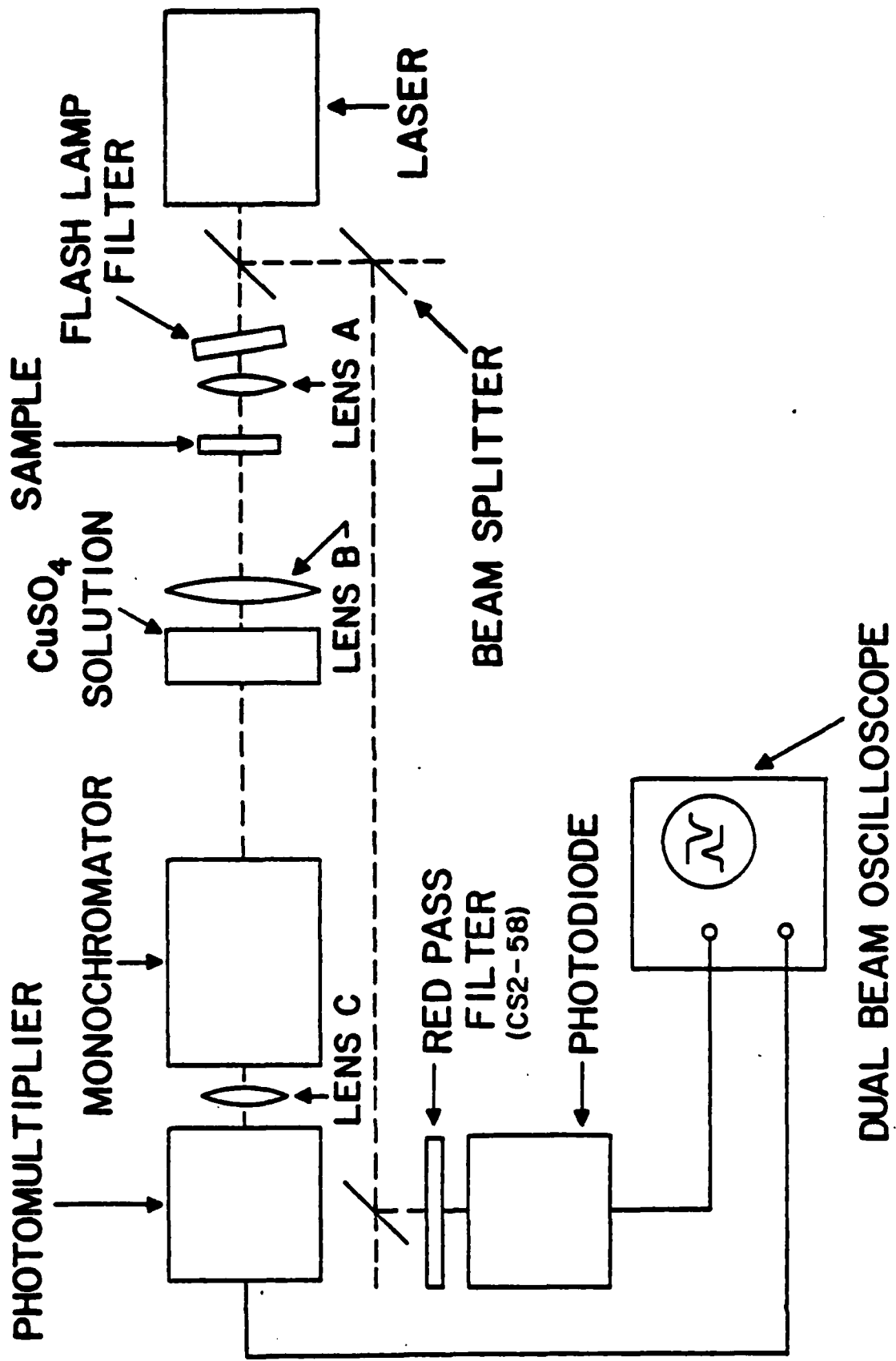


Fig. 4.2a

Normalized response of monochromator and photomultiplier

Fig. 4.2b

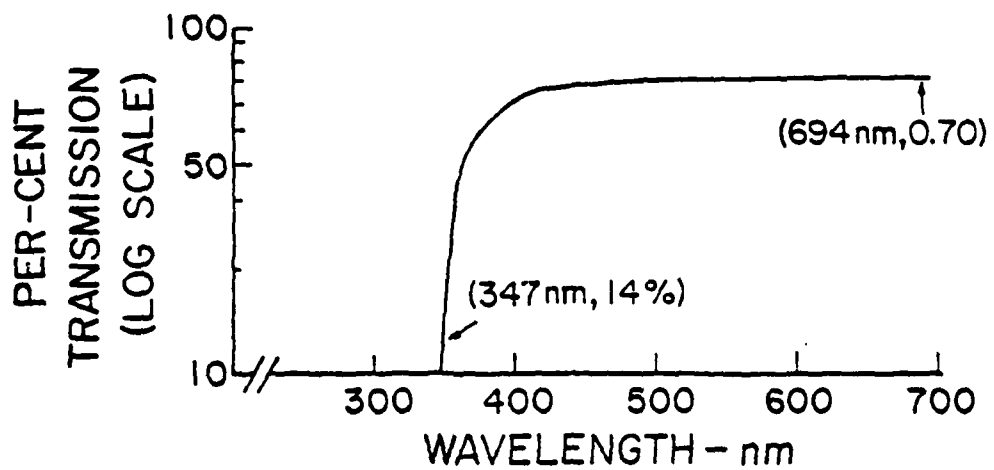
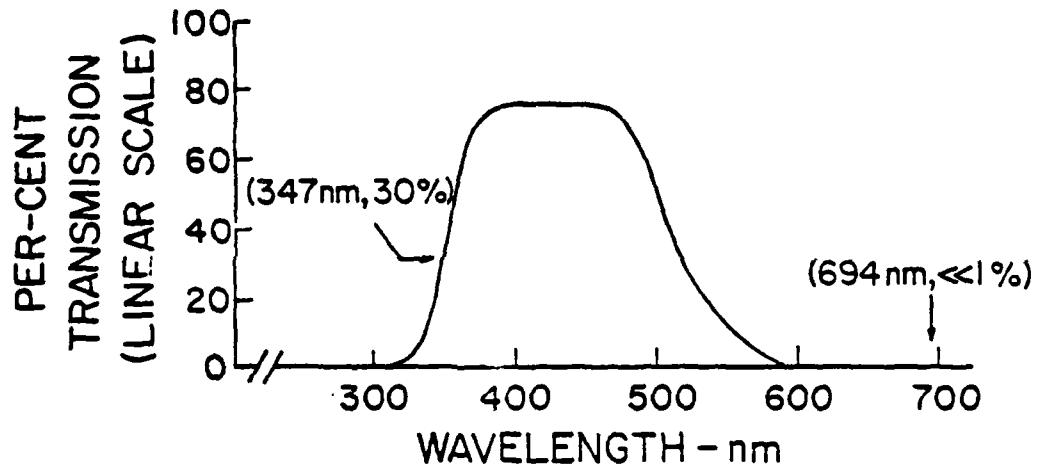
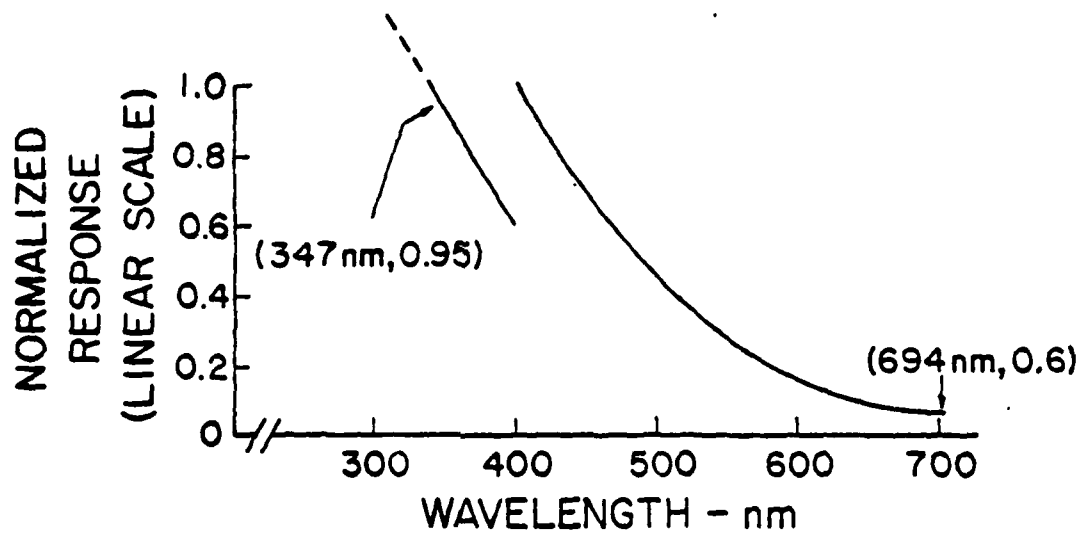
Transmission of copper sulfate filter

Fig. 4.2c

Combined transmission of lens B and lens C.  
These lenses are shown in Fig. 4.1.

Fig. 4.2d

Product of curves 4.2a, b and c.  
Renormalized to unity at 400nm.



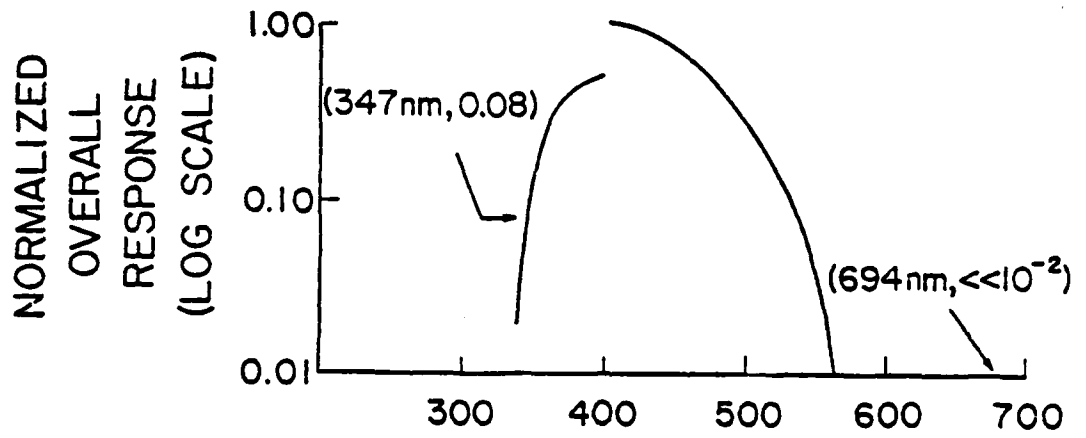


Fig. 4.4a

Peak current from 1P28 photomultiplier  
versus peak current from KD1 photodiode.

Straight line was fitted by eye.

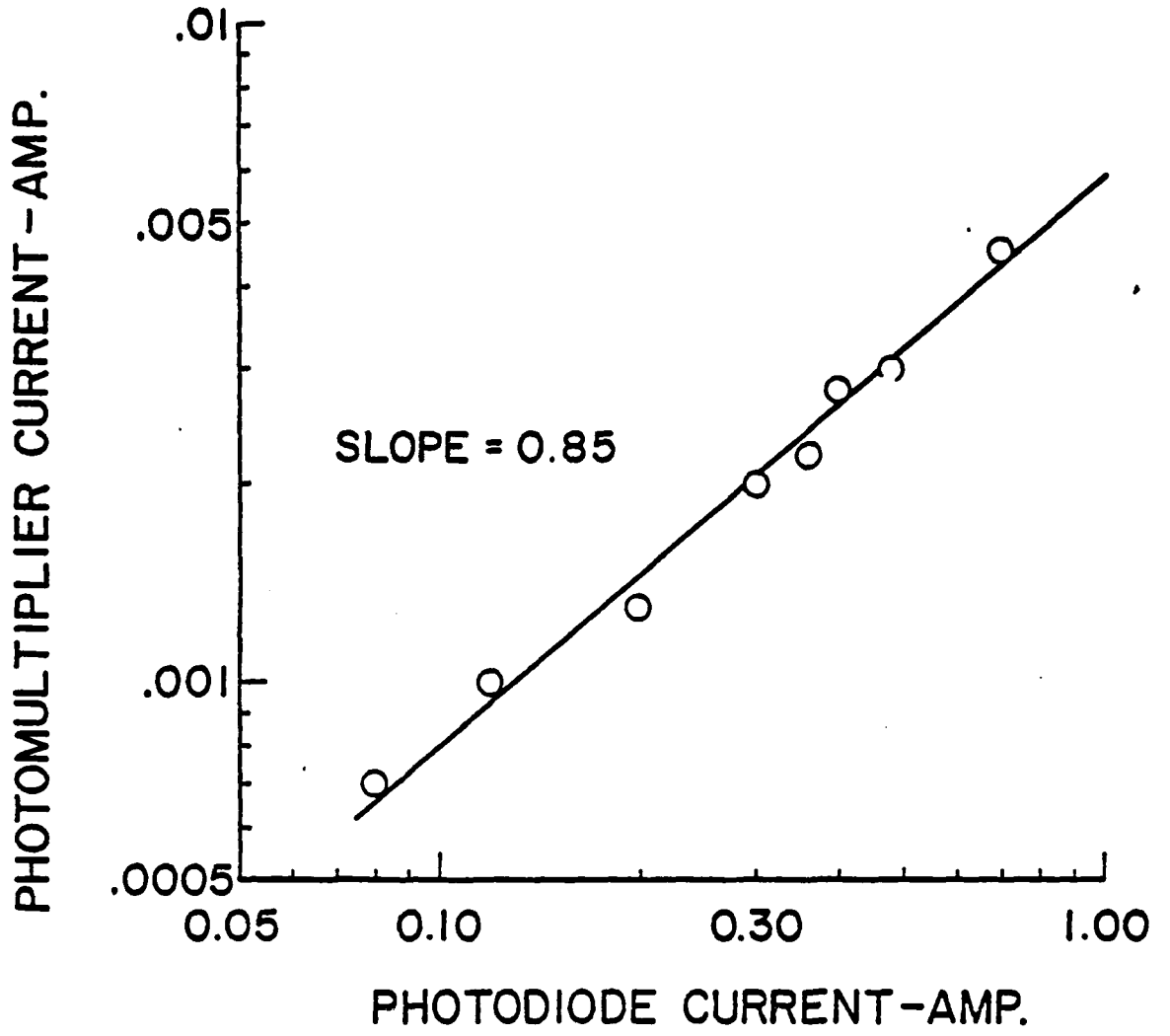


Fig. 4.4b

Curve A is a reproduction of the curve shown in Fig. 4.4a but with linear coordinates. Curve B is a straight line drawn through the origin and approximately tangent to curve A near the origin. Curve B is an approximation to the response of an ideal linear photomultiplier with the same low current sensitivity as the 1P28.

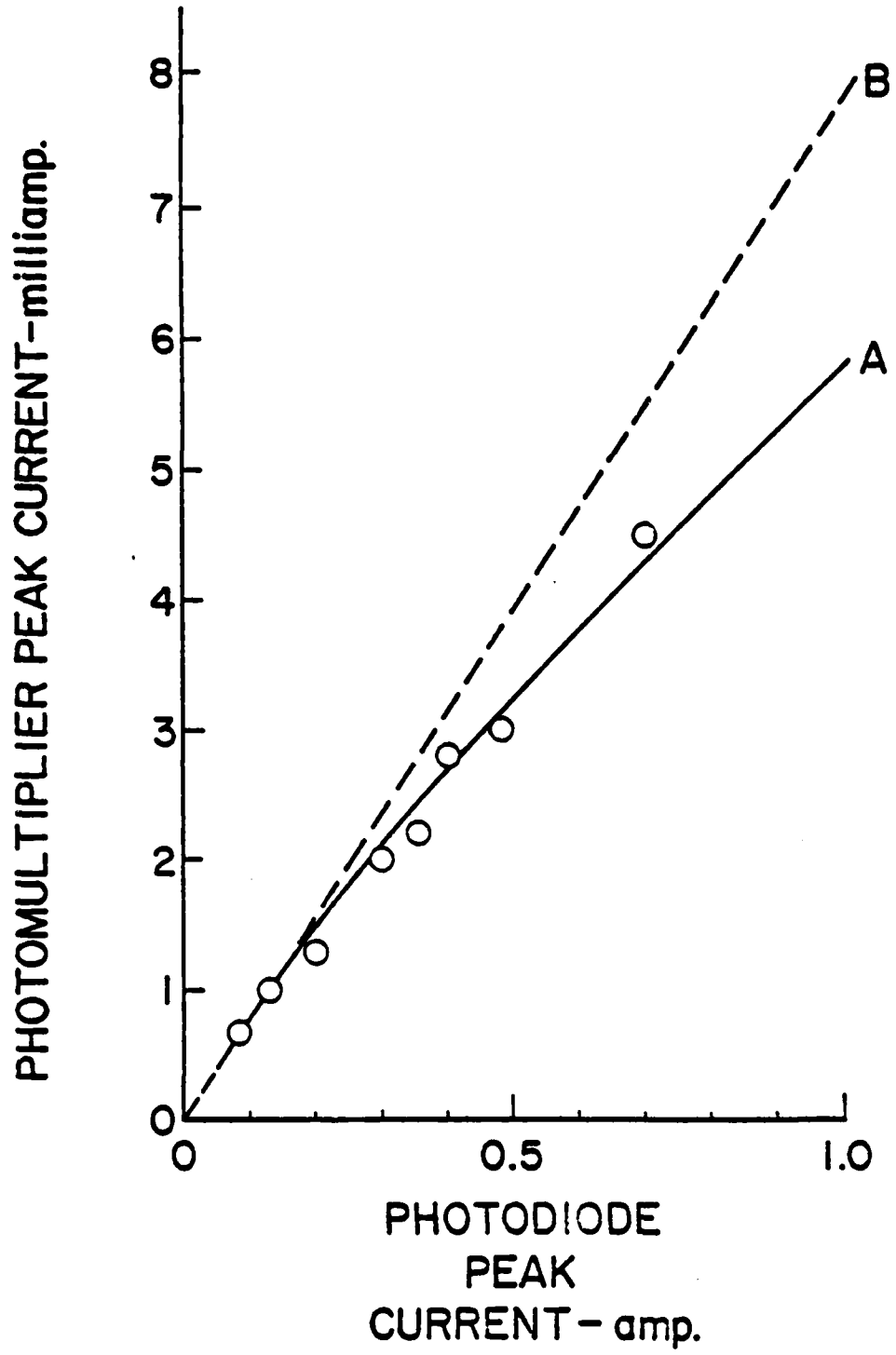
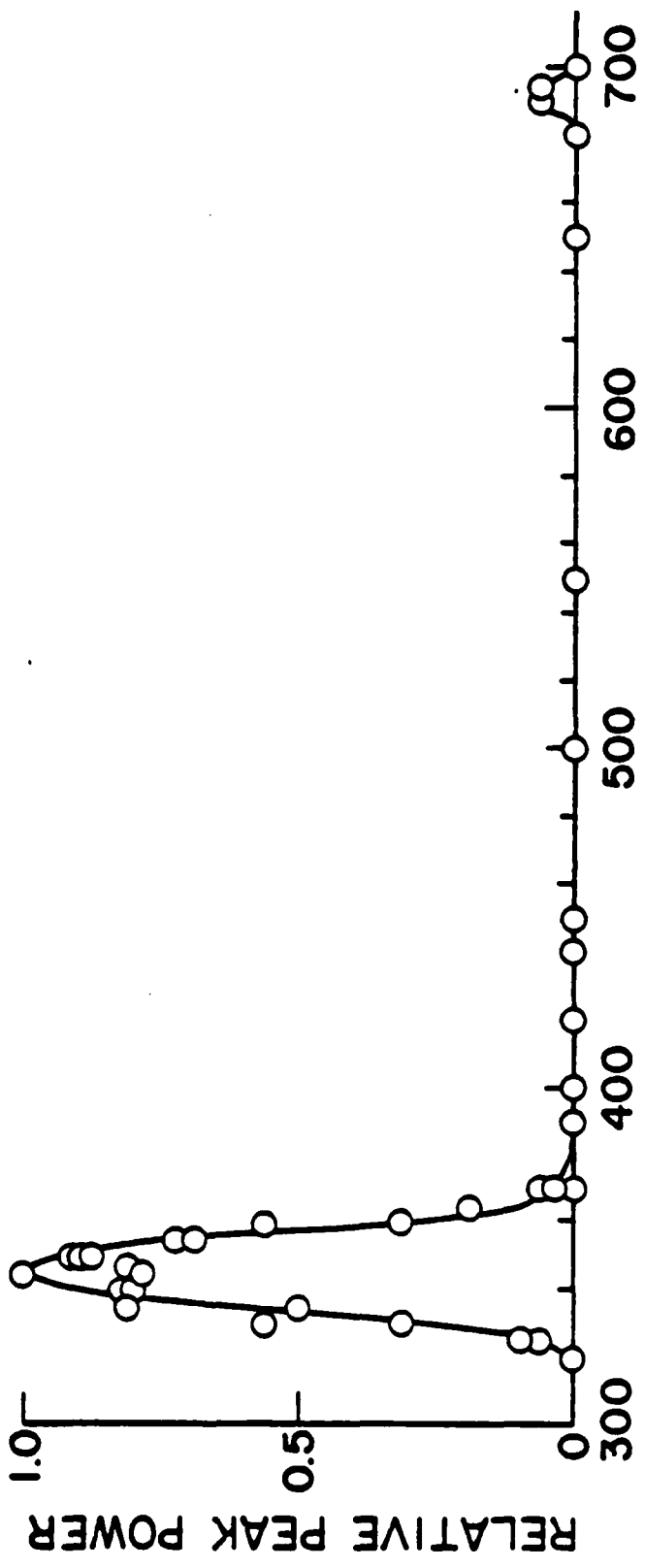


Fig. 4.5

Low resolution spectrum showing 347nm emission from dried dog cornea. Despite the high relative response of the system between 400 and 500nm, no emission is observed in this region. A small signal is seen at 694nm which is the highly attenuated residual response to the laser pulse. The emission intensity at 347nm is actually  $\sim 10^{-10}$  that at 694nm. Monochromator entrance slit width = 15mm. Each data point represents one reading. The solid line was drawn free-hand through the data points.



WAVELENGTH -- nm

DRY DOG CORNEA

Fig. 4.6

Fresh dog cornea emission spectrum.

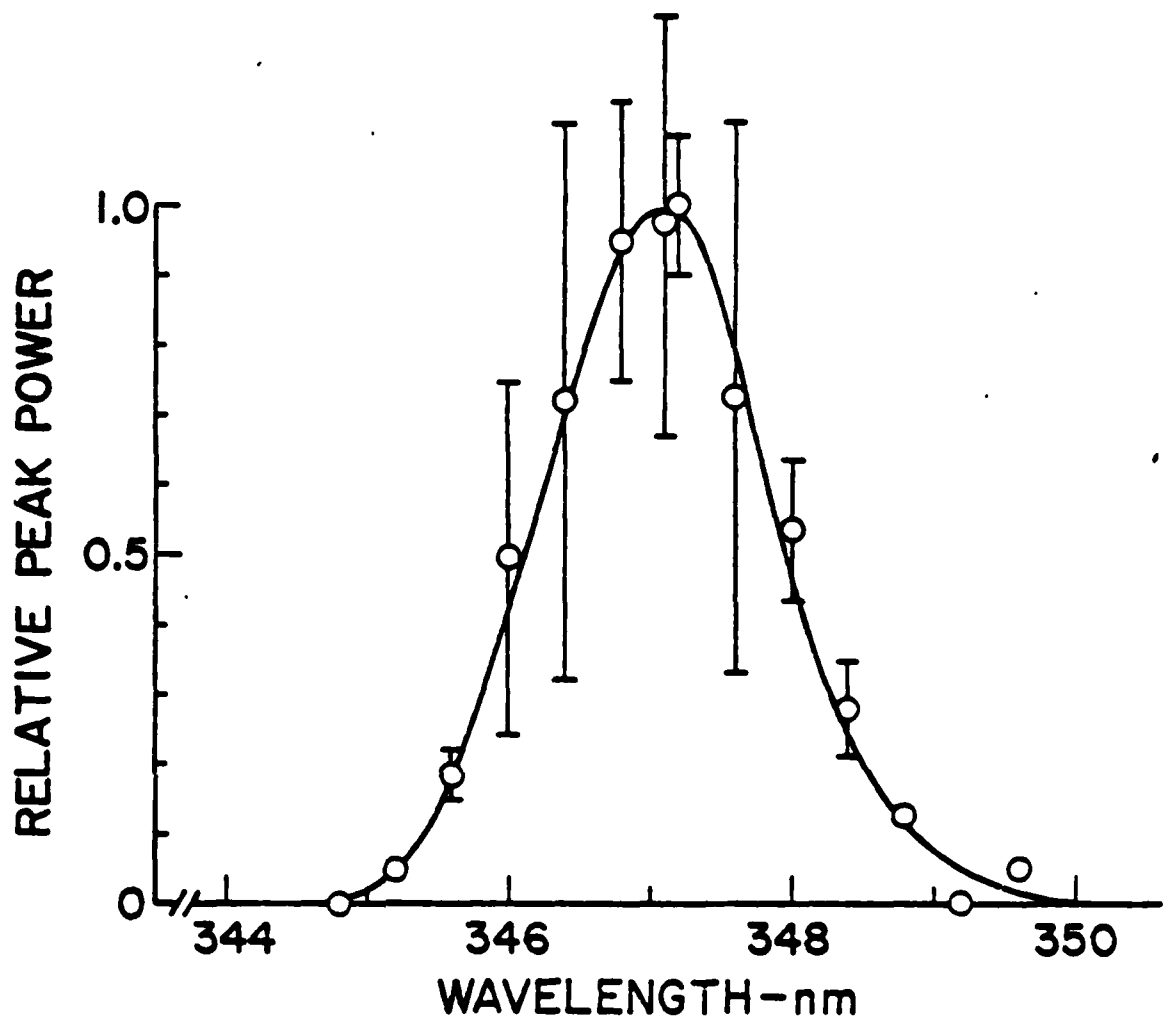
1mm entrance slit width.

$\lambda_p = 347.1\text{nm}$

$\lambda_c = 347.1\text{nm}$

FWHM = 1.9nm

For Figs. 4.6 - 4.12 data points with error bars represent the average and standard deviation of pulse heights obtained at a given monochromator wavelength setting. Data points without error bars represent a single reading of pulse height.



FRESH DOG CORNEA

Fig. 4.7

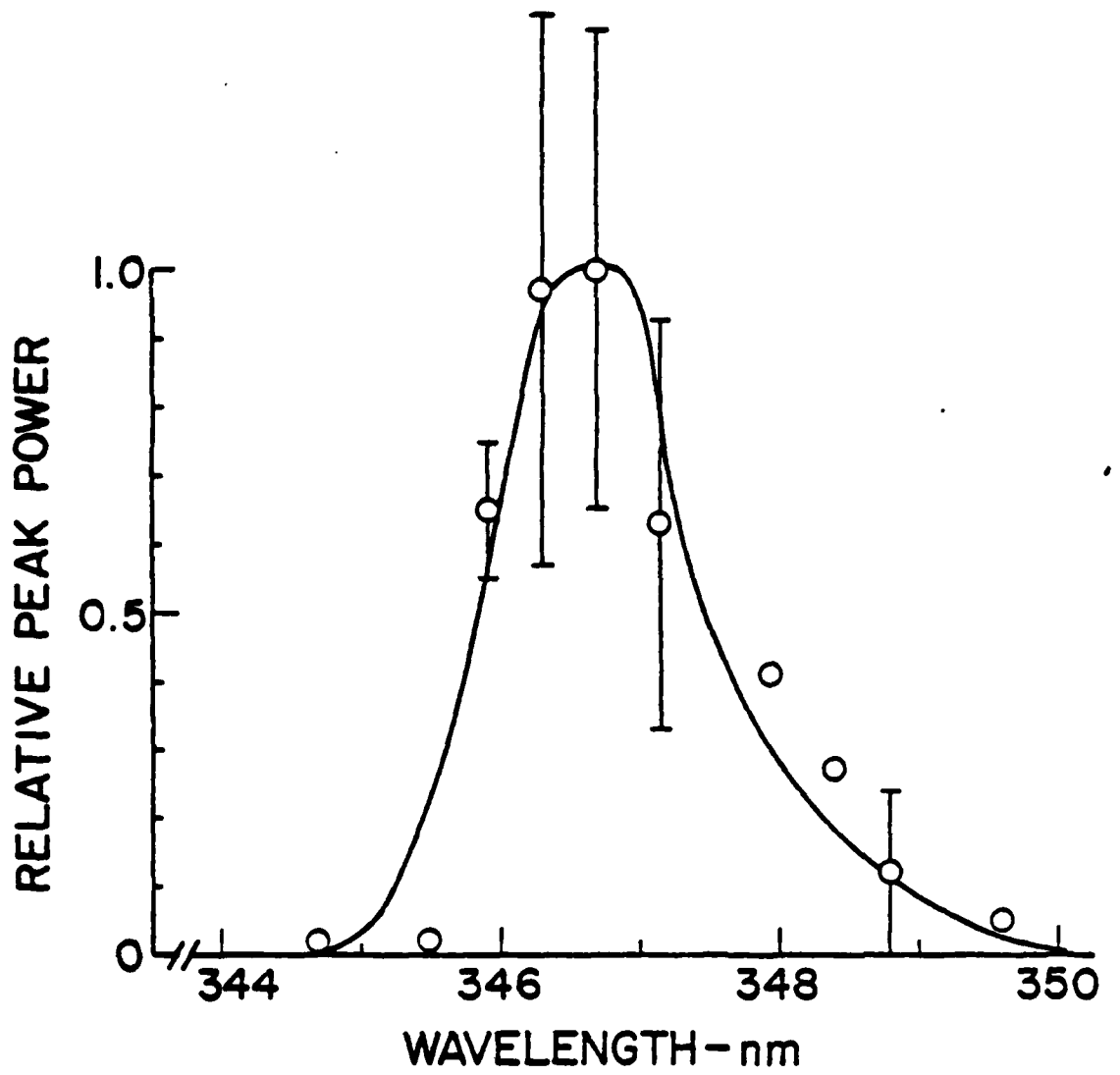
Fresh rabbit cornea emission spectrum

1mm entrance slit width

$\lambda_p = 346.7\text{nm}$

$\lambda_c = 347.1\text{nm}$

FWHM = 1.7nm



FRESH RABBIT CORNEA

Fig. 4.8

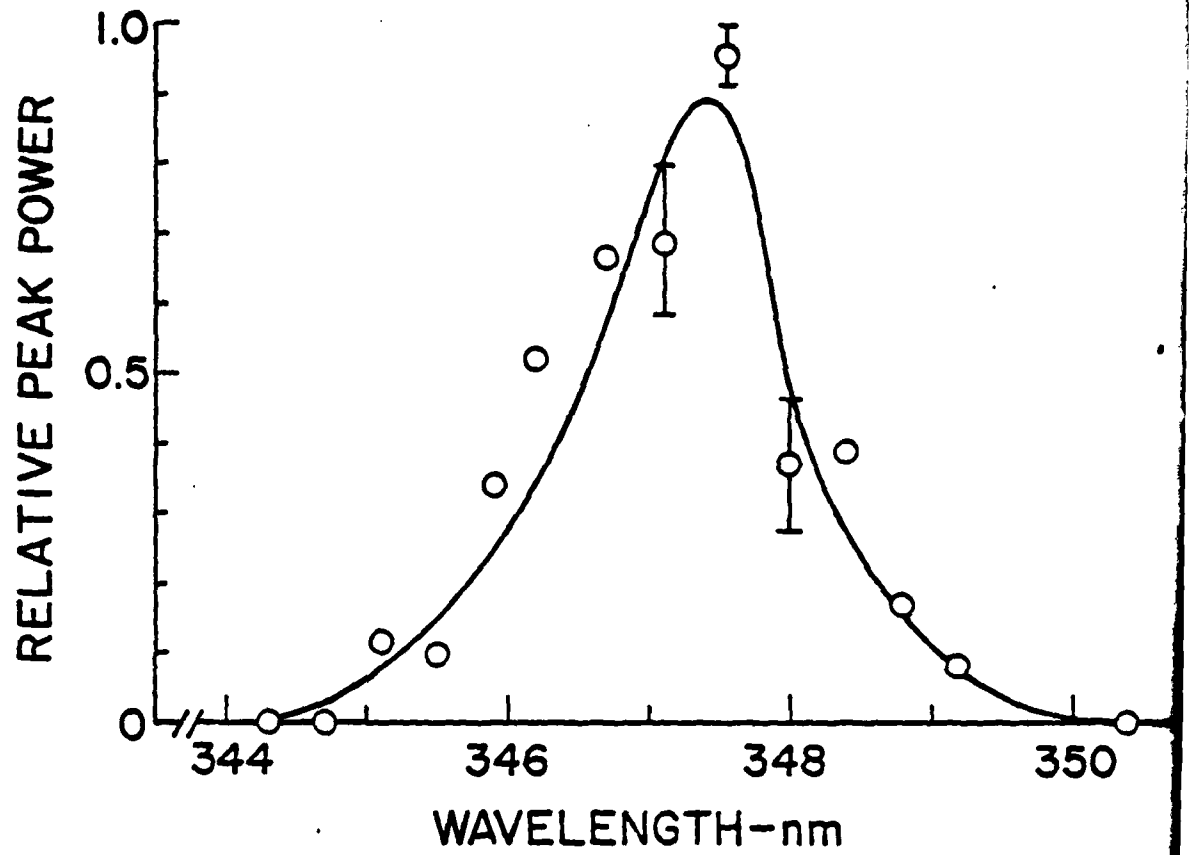
Dried abdominal skin from albino rabbit

1mm entrance slit width

$\lambda_p = 347.4\text{nm}$

$\lambda_c = 347.3\text{nm}$

FWHM = 1.4nm



DRIED ABDOMINAL SKIN  
(ALBINO RABBIT)

Fig. 4.9

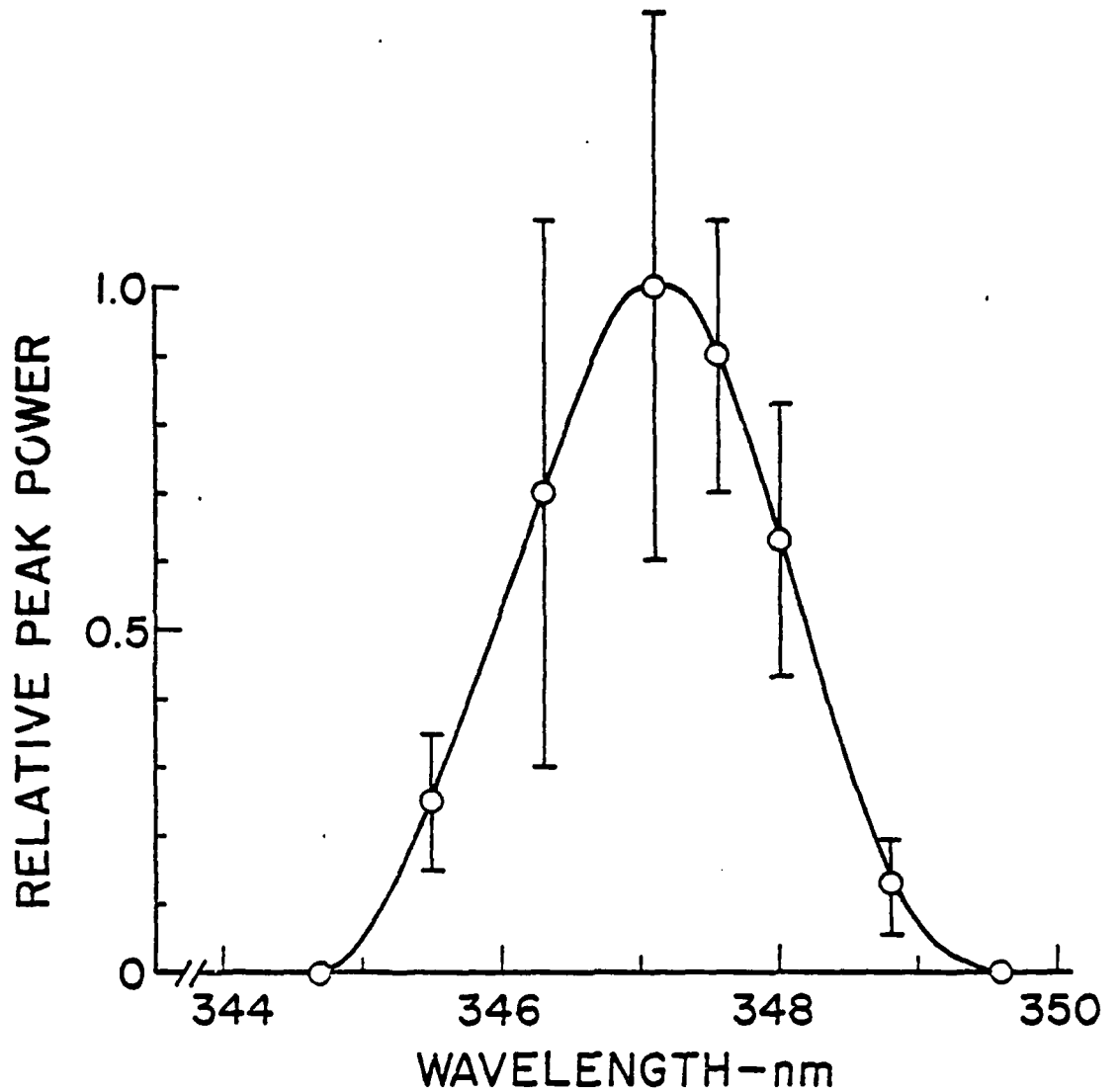
Dried abdominal skin from albino rabbit. In this case the superficial skin layers were removed leaving the fatty sub-epidermal tissue to be irradiated.

Imm entrance slit width

$$\lambda_p = 347.1\text{nm}$$

$$\lambda_c = 347.3\text{nm}$$

$$\text{FWHM} = 2.2\text{nm}$$



DRIED ABDOMINAL SKIN  
(ALBINO RABBIT)

Fig. 4.10

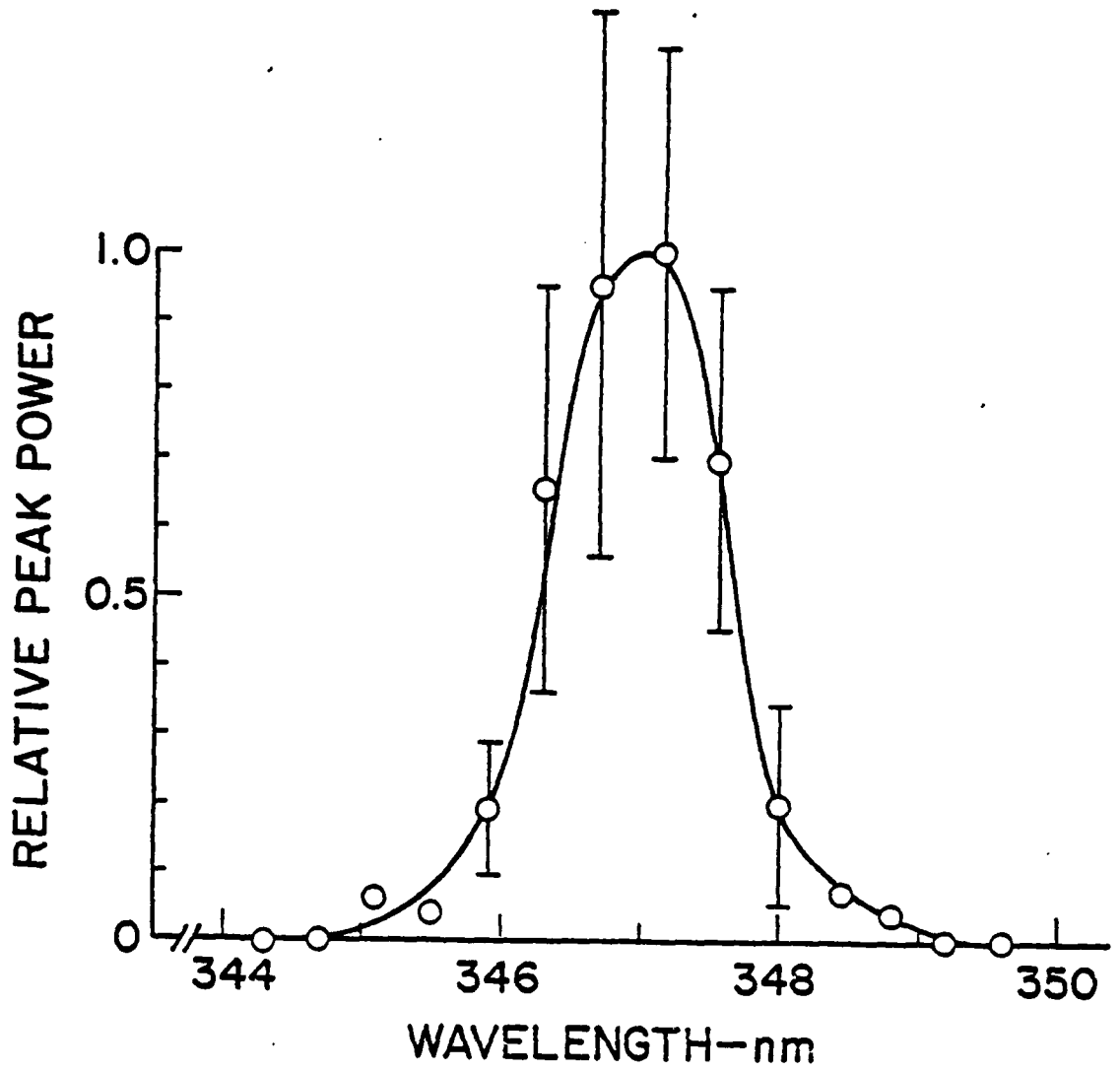
Dried dog cornea

0.5mm entrance slit width

$\lambda_p = 347.1\text{nm}$

$\lambda_c =$

FWHM = 1.4nm



DRIED CORNEA  
(DOG)

Fig. 4.11

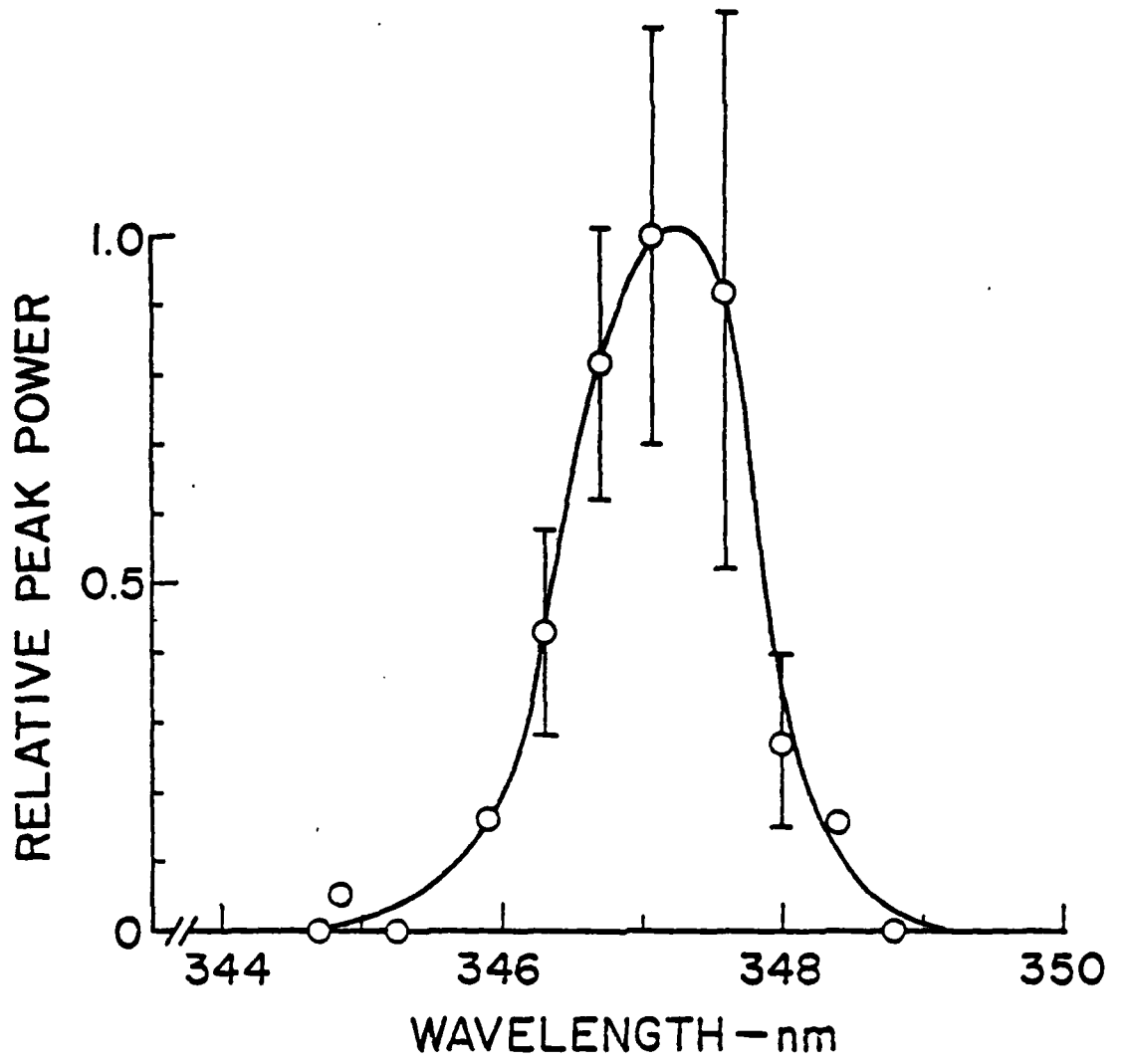
Dried rabbit Achilles tendon

0.5mm entrance slit width

$\lambda_p = 347.3\text{nm}$

$\lambda_c = 347.3\text{nm}$

FWHM = 1.5nm



ACHILLES TENDON  
(RABBIT)

Fig. 4.12

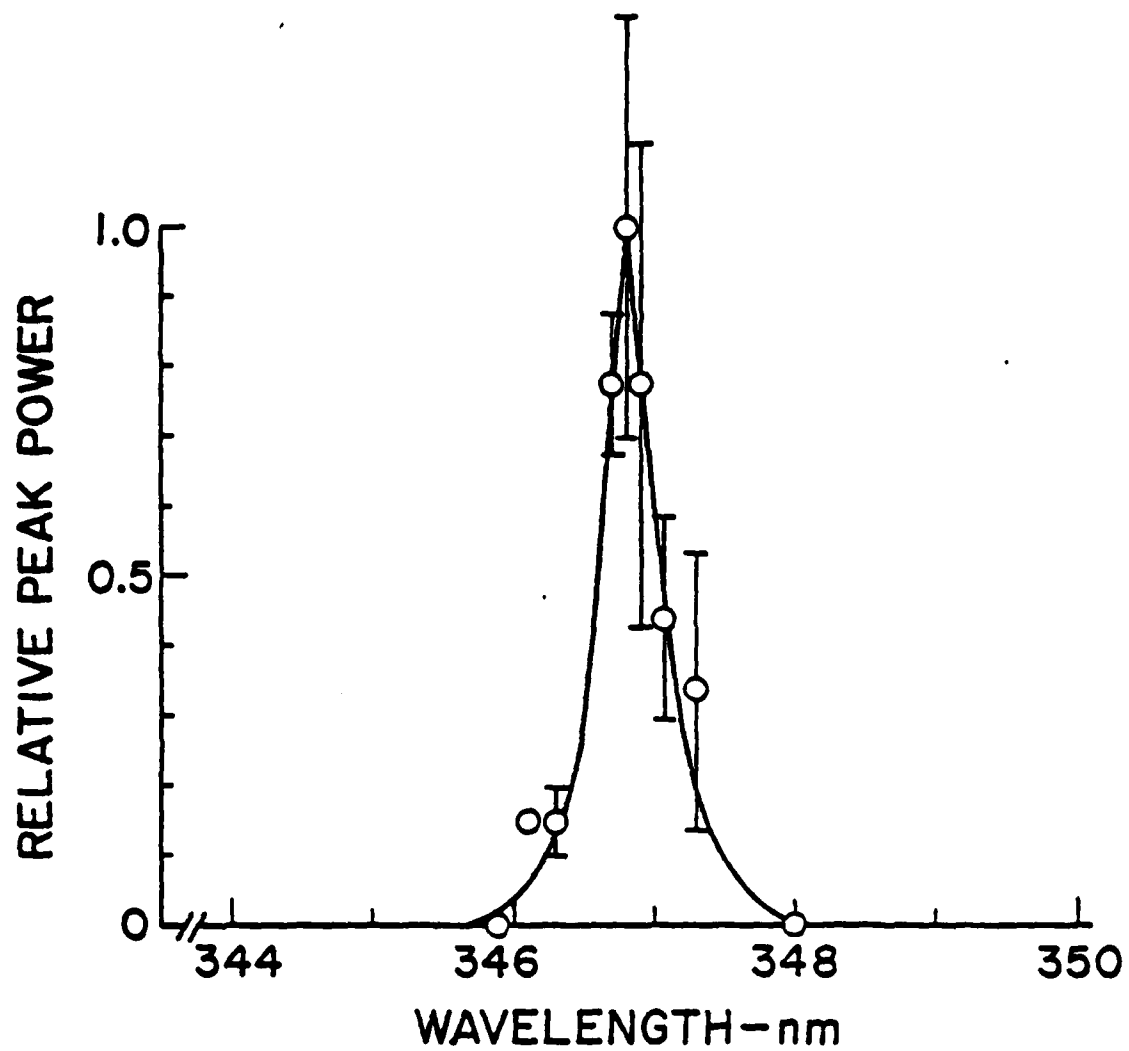
Dried dog cornea

0.15mm entrance slit

$\lambda_p = 346.8\text{nm}$

$\lambda_c = 347.0\text{nm}$

FWHM = 0.5nm



DRIED CORNEA  
(DOG)

Fig. 4.13

$P_2'$  is the relative peak power emitted by rabbit cornea at 347nm.  $P_1'$  is the relative laser peak power at 694nm. Straight line is a least squares fit. Slope of line is 2.0.

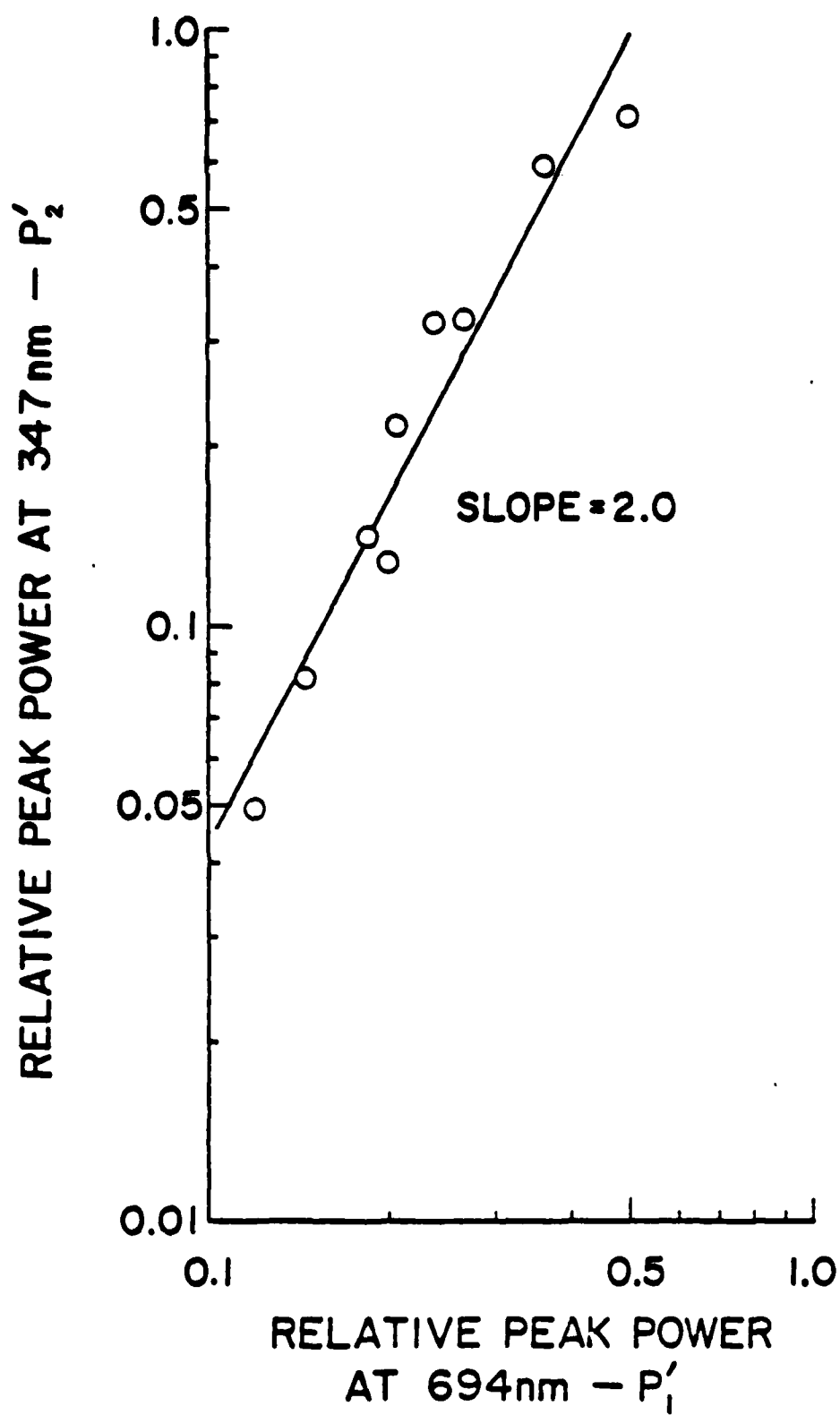


Fig. 4.14

Laser pulse at 694nm and sample emission pulse from rabbit cornea at 347nm. Pulses have been normalized to equal amplitude. There is no discernable delay between pulse peaks. The 347nm pulse full width at half maximum (FWHM) is 35% less than the laser pulse FWHM.

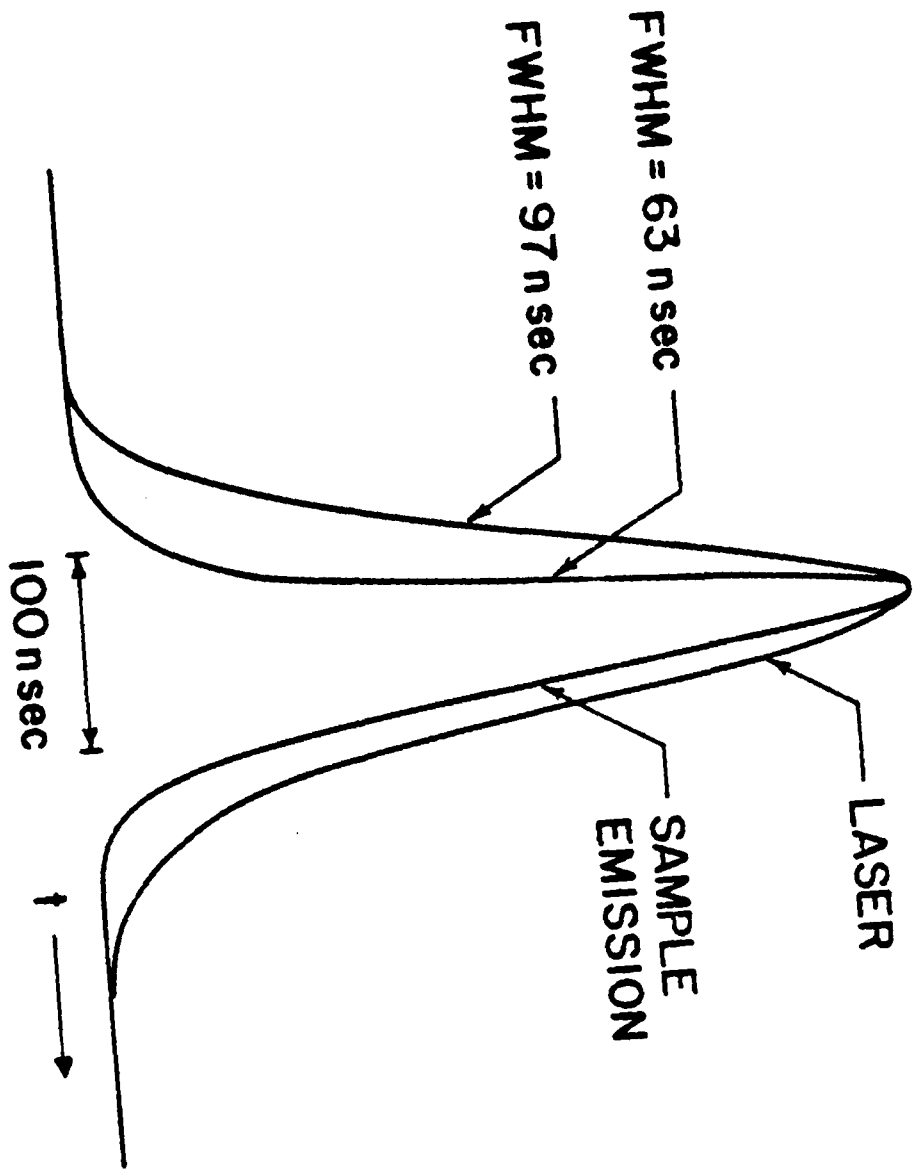


Fig. 4.15

Curve A is the FWHM of the emission spectra in Figs. 4.4 through 4.12 versus monochromator entrance slit width. Curve B is the manufacturer's theoretical bandwidth of the monochromator versus entrance slit width. Curve C is the FWHM of a Cd line near 347nm as measured by the monochromator. The Cd line FWHM was 0.19nm according to the manufacturer of the standard lamp that was used for curve C.

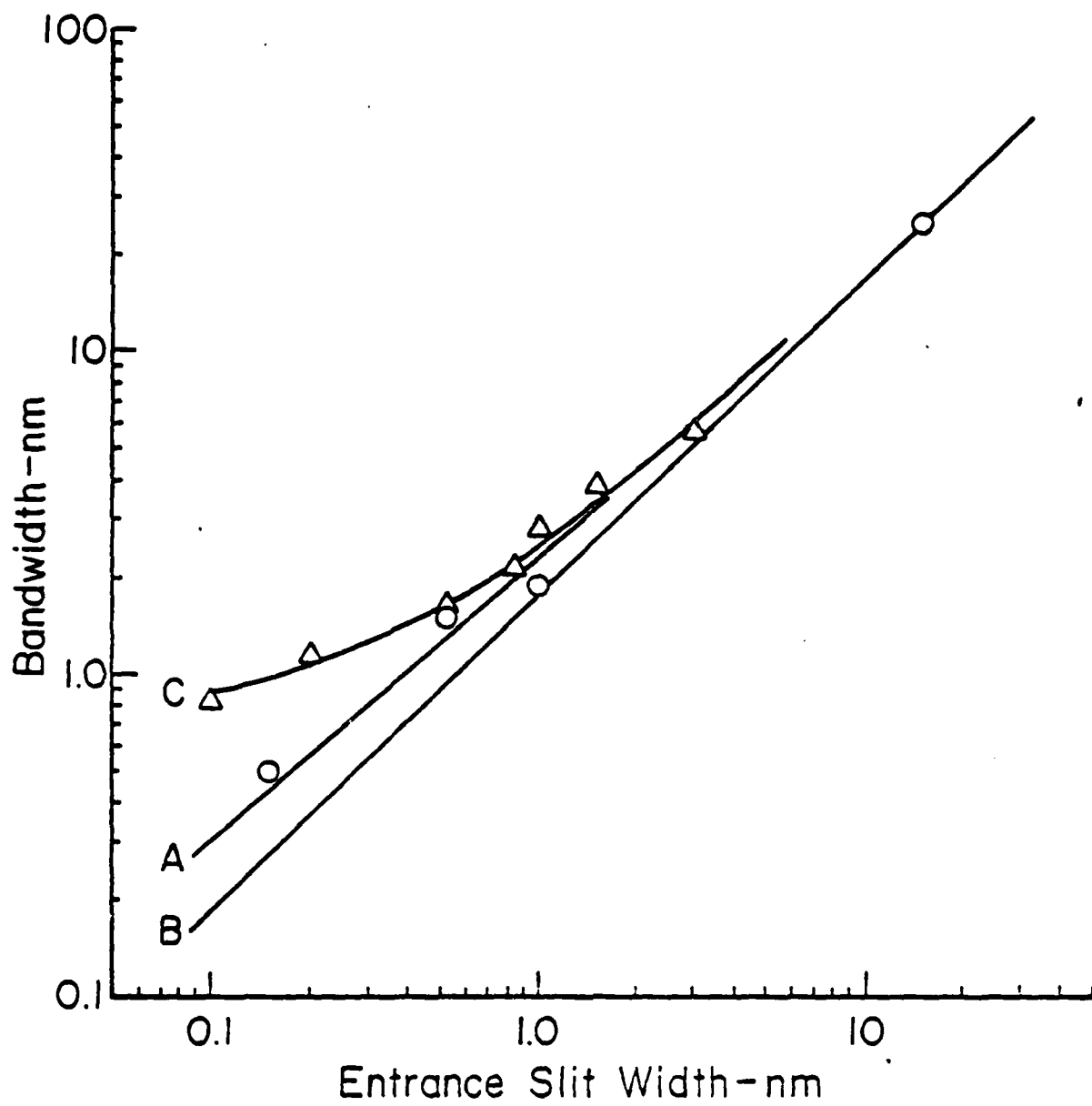
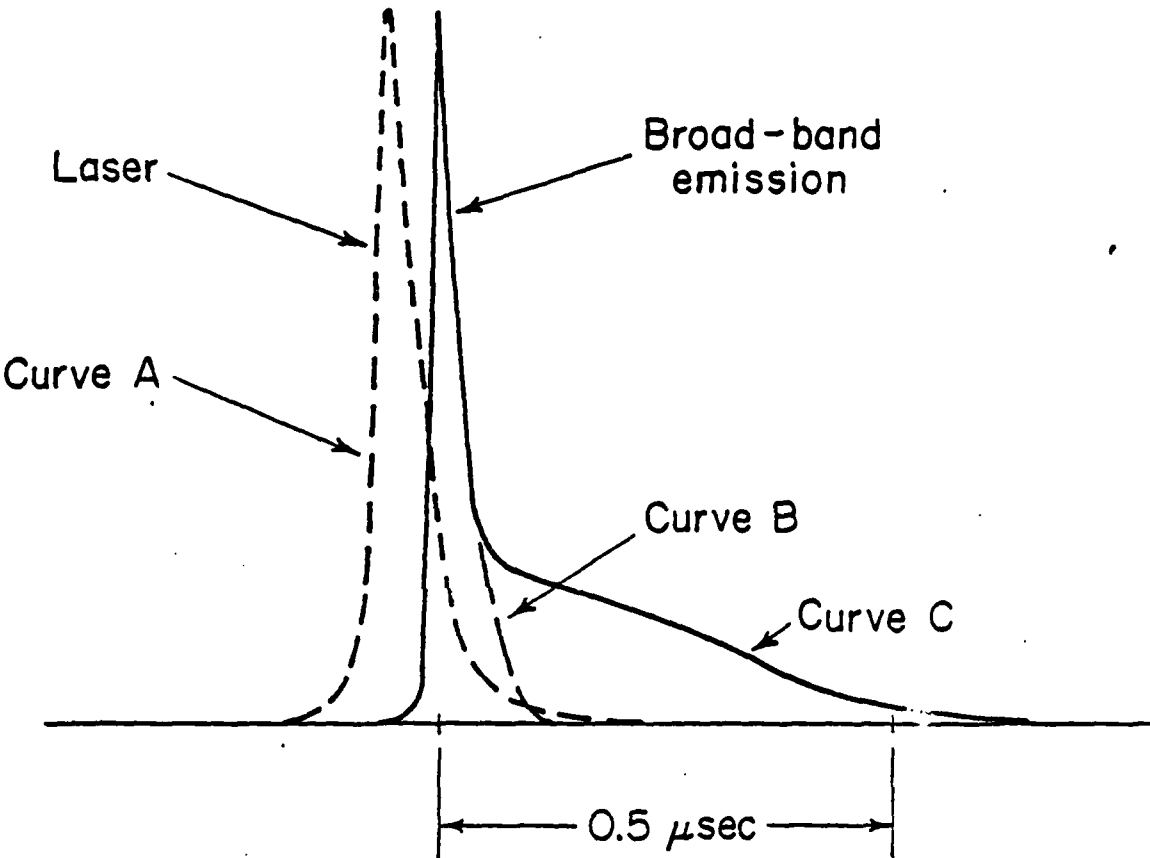


Fig. 4.16

Curve A is the laser pulse versus time. Curve B is a broad band emission pulse observed with low oscilloscope gain (no tail visible). Curve C is a broad band emission pulse from a damaged rabbit lens. Curve C shows a tail. All three curves were normalized to the same amplitude for this figure. Curves B and C were obtained with the monochromator set to 347nm. The delayed peak of curves B and C indicates that these pulses were not due to second-harmonic generation.



## CHAPTER 5

## SECOND-HARMONIC GENERATION FROM COLLAGEN

In chapter 4, second-harmonic generation was reported in cornea, sclera, tendon and skin. The major solid component of these tissues is collagen. It is therefore possible that the principle site for second-harmonic generation in these tissues was collagen. The purpose of the experiments reported in the present chapter is to determine whether second-harmonic generation can be observed in collagen fibers.

## 5.1 Methods and materials

A commercial preparation of collagen fibers from bovine Achilles tendon was obtained for these studies (Sigma Chemical Company number C9879). These collagen fibers were prepared for Sigma Chemical by the method of Einbinder and Schubert (Einbinder and Schubert, 1951). Einbinder and Schubert describe their technique as one in which mucopolysaccharides are removed and purified undegraded collagen is obtained. In their method, fresh bovine Achilles tendon is manually freed of non-collagenous tissue, cut into small pieces and placed in 3 per cent  $\text{Na}_2\text{HPO}_4$  for three days at  $0^\circ\text{C}$ . The residue is then washed with water and dehydrated with absolute alcohol. The alcohol is then allowed to evaporate in air. (We assume that some water re-enters the preparation during handling; although the stiffness of the fibers compared to the flexibility of fresh tissue collagen suggests that this was minimal (Elden, 1968)).

Sigma collagen fibers were packed loosely in a 9mm x 6mm x 1mm rectangular cross-section chamber made from microscope slides and then covered with a glass cover slip. The remaining volume of the chamber was filled with anise oil to reduce light scattering.

Before irradiation, the optical transmission of the chamber was measured at 347nm and 694nm (Beckman Model B spectrophotometer) while containing collagen alone, anise oil alone, and collagen-anise oil mixtures.

The chamber was irradiated using the same experimental set-up as shown in Figure 4.1. In these studies, the monochromator entrance slit was opened wide to 3.5mm in order to collect as much of the weak second-harmonic radiation as possible. Collagen alone, anise oil alone, and collagen-anise oil mixtures were irradiated.

The chamber was examined before and after irradiation with a polarizing microscope.

## 5.2 Results

### 5.2a Sample transmission

Initially the collagen was a white opaque stiff mat of fibers. It retained this appearance when the clear, colorless anise oil was first added. It was easy to observe the clarification of the collagen-anise oil mixture in the sample cell with time. During the first 15 minutes most areas of the collagen fiber mat became less opaque; however, the outline of the fibers remained evident. After approximately 45 minutes, the sample appeared to be only slightly more

transparent than it was after 15 minutes. The polarizing microscope was used during the first 45 minutes to determine the presence of very thin collagen fibers in the chamber in certain places where no material was visible to the unaided eye; the number and size of the collagen fibers appeared to be unchanged.

The progressive clarification of collagen-anise oil samples was also followed spectrophotometrically at 347nm and 694nm. The results are summarized in the following table.

Wavelength	Transmission	
	No oil	30 minutes after adding oil
694nm	0.0%	80%
347nm	0.0%	3.5%

Transmission measurements were also made for anise oil alone. Most of the above attenuation at 347nm after 30 minutes was due to the anise oil itself (The glass slide attenuation was negligible).

#### 5.2b Sample emission

No second-harmonic emission was observed from the Sigma collagen fibers without the anise oil on ruby laser irradiation at 694nm. These samples were easily damaged, and "plume" emission signals were often observed (see chapter 4 for a description of plume emission). No emission was detected from anise oil alone in the sample chamber over the wavelength range 320nm - 400nm.

The sample emission spectrum shown in Figure 5.1 was obtained on irradiation 20 to 30 minutes after the addition of anise oil to the Sigma collagen. There is an evident peak at 347nm. The emission band is slightly assymmetric. No other peaks were observed between 320nm and 400nm.

After 45 minutes in anise oil, the emission pulses at 347nm increased in amplitude by a factor of 1.7 compared to those observed thirty minutes after the addition of anise oil. Measurements also indicated that an additional increase in second-harmonic emission pulse amplitude occurred for samples stored at room temperature overnight in anise oil. Relative to corneas, the collected 347nm emission from Sigma collagen was weaker.

The pulses at 347nm were temporally narrower than the laser pulses at 694nm. The relative pulse widths were like those shown in Figure 4.14. Verification of a quadratic relationship between the 347nm pulse height and the laser pulse height was not performed. The laser power could not be varied over a sufficiently wide range for this test. We were limited on the low side by system noise, and limited on the high side by sample damage. While the addition of anise oil raised the collagen damage threshold, damage still occurred at relatively low laser input levels.

When sample damage occurred, the sample chamber exploded and plume emission signals were observed. No visible signs of damage were present in the samples when a 347nm emission peak was observed.

After removal from the chamber, the collagen fiber mat appeared to have retained its structure and stiffness. The fibers were somewhat more translucent than initially.

### 5.3 Discussion

We believe that the isolated emission peak near 347nm and the temporally narrowed emission pulses near 347nm indicate that second-harmonic generation occurred in these Sigma collagen samples.

Since no second-harmonic emission was observed from anise oil or collagen separately but was observed when anise oil was added to the collagen, it is possible that the oil and collagen interacted to form sites for second-harmonic generation that were not present in collagen or anise oil alone. While this is an interesting possibility, we believe that there is a simpler explanation of the role of anise oil in these experiments.

Immersing the collagen fibers in anise oil apparently reduced light scattering at 694nm and 347nm (Table 1). This may have been due to a better refractive index match between collagen and anise oil compared to collagen and air. For example, Maurice gives a value of approximately 1.5 for the refractive index of collagen at an unspecified visible wavelength (Maurice, 1969). The refractive index of anise oil is 1.54 at 656nm which is near the ruby laser wavelength (American Institute of Physics Handbook, 1957). Reduced 694nm light scattering at the fiber-oil interfaces may have resulted in two effects. First, reduced light scattering at 694nm may have allowed

a forward lobe to develop in the scattering pattern for second-harmonic radiation. This would have increased the fraction of collected second-harmonic radiation using the apparatus in Figure 4.1. Second, the laser peak power at which sample damage occurred may have been raised. By operating at higher fundamental peak power levels, the second-harmonic conversion efficiency of the collagen was probably improved and second-harmonic radiation then became detectable.

The refractive index match at 347nm may have been poorer than it was at 694nm due to an anise oil absorption band near 347nm whereas there are no collagen absorption bands in this region (Gratzer et al, 1963). Nevertheless, the index match at 347nm was probably improved over that which occurred in air. By reducing light scattering at 347nm, a forward lobe in the second-harmonic emission pattern may have been allowed to form.

The importance of anise oil in these studies may, therefore, have been to reduce light scattering at 694nm and 347nm. Higher levels of second-harmonic radiation might be obtained by using an imbedding material with less absorption at 347nm and with a better refractive index match at 694nm and 347nm than was offered by anise oil.

The 347nm emission band was slightly asymmetric (Fig. 5.1). The long wavelength data ( $\sim 355\text{nm}$ ) is of higher amplitude than the short wavelength data ( $\sim 340\text{nm}$ ). The long wavelength data was obtained last. The resulting asymmetry may, therefore, have been caused by the ongoing wetting action of the anise oil. Data near

340nm and 355nm was also of low enough amplitude to have been affected by system noise.

Native collagen in anise oil has been shown to yield weak second-harmonic radiation. Absorption at 347nm in the anise oil may have produced as much as an order of magnitude attenuation of the second-harmonic. When this factor is considered, the second-harmonic generation efficiency of Sigma collagen is comparable to that of the collagenous tissues discussed previously. Native collagen fibers may therefore have been the principal site for second-harmonic generation in the collagenous tissues that we have investigated.

The preparation of the Sigma collagen fibers used in these studies did not involve dissolving the collagen during preparation (Einbinder and Schubert, 1951). Therefore, it is assumed that these fibers retained their native periodic band and interband structure. For comparison, a quantity of purified collagen was obtained that had been dissolved (extracted chemically) from guinea pig skin and then precipitated as so-called "amorphous" fibrils. "Amorphous" collagen fibers show no periodic structure under the electron microscope (Schmitt, 1956); they are, however, optically birefringent. "Amorphous" is therefore used to describe the electron-microscopic appearance of the fibrils and does not refer to the actual material properties of the fibril. Native and "amorphous" fibrils are different aggregation patterns of the same (collagen) molecule. "Amorphous" fibrils are not found in tissue (Glimcher, 1959).

The "amorphous" fibers used in these studies were thinner and less stiff than the Sigma fibers and had the appearance of fine cotton wool. To the unaided eye, this white cotton wool appearance changed to that of a hazy blue cloud when the "amorphous" fibers were immersed in anise oil. In anise oil, the outline of the "amorphous" fibers was indistinct, whereas the outline of most of the Sigma fibers was relatively distinct. The "amorphous" collagen samples were subjectively more transparent in anise oil than were Sigma collagen samples of equal weight. Both the "amorphous" and the Sigma collagen fibers retained their original gross structure when removed from the anise oil. Both fiber types were more translucent after removal from the anise oil.

#### 5.4 Amorphous collagen

No second-harmonic generation was observed from "amorphous" guinea pig skin collagen in air or in anise oil. Whole dry, guinea pig skin did yield narrow band emission at 347nm with temporally narrowed pulses, which we believe to be second-harmonic generation.

These studies indicate that native collagen fibers are capable of second-harmonic generation whereas "amorphous" collagen fibers yielded either much lower second-harmonic radiation levels or none at all. Both the gross appearance and the electron microscope appearances are different for these two fibrous collagen aggregates. There is no evident reason why the gross property differences between the fibers that we described should have produced marked differences

in second-harmonic generation efficiency. Therefore, it appears that the aggregation pattern of collagen fibrils may be an important factor in second-harmonic generation.

Aggregation pattern models of native and "amorphous" collagen fibrils have been presented by Schmitt (Schmitt, 1956). He has suggested that native collagen fibrils are formed by the end-to-end and side-by-side aggregation of collagen molecules with a regular stagger between adjacent end-to-end chains of collagen molecules (Fig. 5.2a). In Schmitt's model, amorphous fibrils differ from native fibrils only in that the stagger between adjacent chains is irregular (Fig. 5.2b). In both models, the asymmetric collagen molecules of a given fibril are "pointed" in the same direction.

We believe that an alternative model of amorphous fibrils is possible. For example, assume, with Schmitt, that all collagen molecules are oriented the same within a given end-to-end chain. Then, unlike Schmitt, assume that adjacent end-to-end chains have approximately equal likelihood of being aligned parallel or antiparallel in addition to being irregularly staggered (Fig. 5.2c). This alternative amorphous fibril model should have the same electron microscopic appearance as Schmitt's amorphous fibril model. Both fibril models can be optically birefringent. On this qualitative basis, these amorphous fibril models are optically and electron-microscopically indistinguishable. However, from the standpoint of optical second-harmonic generation, the amorphous fibril models may be distinguishable.

In the alternative model of an amorphous fibril, the irregular orientation of the collagen molecules within a fibril may lower the measured second-harmonic generation efficiency of the alternative "amorphous" fibril relative to the Schmitt models of the "amorphous" and native fibrils. This may be the reason why no second-harmonic generation was observed from the "amorphous" collagen used in our studies. Consideration of the effect of orientational irregularities within a fibril is given in Appendix A of this chapter.

#### 5.5 Summary and conclusions

1. On irradiation at 694nm with a Q-switched ruby laser, an isolated emission band near 347nm was observed from purified, undegraded collagen (Sigma Chemical Company) in anise oil. No 347nm emission was observed from this collagen or anise oil alone. Emission pulses at 347nm were temporally narrowed with respect to the laser pulse. We believe this to be second-harmonic emission from collagen. It is felt that the role of anise oil in these experiments was to reduce light scattering at 694nm and 347nm.
2. No isolated 347nm emission was observed from "amorphous" collagen fibers that were precipitated from guinea pig skin extracts. These experiments were carried out with and without anise oil. Second-harmonic generation was observed from guinea pig skin which contains native, and not "amorphous", collagen fibers. The lack of 347nm emission from "amorphous" fibrils may have been due to an irregular orientation of collagen molecules within these fibrils.

## APPENDIX A

In this appendix, the effect of molecular orientational irregularities on optical second-harmonic generation is discussed. For this discussion the coupling between induced molecular dipoles is neglected.

To provide simple illustrations, the tensor properties of molecular dipoles will be neglected and a scalar equation will be used to relate the induced dipole moment  $\mu$  to the electric field  $E$ . To second-order terms this equation is:

$$\mu = aE + bE^2 \quad (\text{A1})$$

A graph of Equation (A1) is sketched in Figure 5.3a.

Since molecules described by Equation (A1) are non-centrosymmetric, a direction of molecular orientation can be defined. Assume, therefore, that Figure 5.3a applies when a molecule is aligned with the positive  $E$  direction (arrowhead in Fig. 5.3a). If this molecule is rotated by  $180^\circ$ , so as to be aligned with the negative  $E$  direction, then Figure 5.3b applies (note arrowhead in Fig. 5.3b). In Figure 5.3b, the relationship between  $\mu$  and  $E$  is:

$$\mu = aE - bE^2 \quad (\text{A2})$$

Equations (A1) and (A2) differ by a minus sign in the second-order

term. If  $E$  oscillates at frequency  $\omega$ , then this minus sign difference shows that the phase of the induced dipole moment at frequency  $2\omega$  is shifted by  $\pi$  when the orientation of the molecule is reversed.

When two molecules are oriented in the same direction (parallel) and driven by mutually in-phase electric fields, then they will execute mutually in-phase second-harmonic dipole moment oscillations. If these molecules are oriented in opposite directions (anti-parallel), then their second-harmonic dipole moment oscillations will be  $180^\circ$  out of phase. In the case of parallel molecules, an observer that is equidistant from the two molecules will detect constructive interference between the radiated second-harmonic fields. In the case of anti-parallel molecules this observer will detect no second-harmonic radiation.

Consider a large number of molecules in a volume element whose dimensions are small compared to an optical wavelength. With plane wave illumination, the driving field is then approximately in-phase for each molecule. A distant observer located on an axis defined by the plane wave direction through the volume element will be approximately equidistant from the various molecules in the volume element, the second-harmonic fields will interfere constructively at the observer location. The second-harmonic intensity at the observer location will be proportional to the square of the number of radiating molecules. If there is an equal division between parallel and anti-parallel molecules in the volume element, then the second-harmonic fields will

interfere destructively at the observer location. The second-harmonic intensity will be zero for this observer.

These results can now be applied to the cases of collagen molecules in native or amorphous fibrillar units. To a first approximation, the collagen molecule is a line of molecular dipole oscillators. Actual collagen molecules are  $\sim 300\text{nm}$  in length and  $\sim .4\text{nm}$  in diameter. The dipole oscillators are associated with various amino-acids, side chains, and linkages within the collagen molecule. The individual dipole oscillators with resonances near  $347\text{nm}$  are thought to be in regular positions and orientations (approximately parallel) along the molecule (Gratzer, 1967). In the Schmitt models of native fibrils and amorphous fibrils the collagen molecules are considered to be parallel. In the alternative model of amorphous fibrils, some of the collagen molecules are parallel and others are anti-parallel as shown in Figure 5.2c. In all of these models the molecules are assumed to be closely packed. The Schmitt models of native fibril or amorphous fibrils (Figs. 5.2a and 5.2b) can, therefore, produce appreciable levels of second-harmonic radiation. The alternative model of an amorphous fibril should produce no second-harmonic radiation.

If there is not an equal division between parallel and anti-parallel molecules in volume elements of an amorphous fibril, then some second-harmonic radiation may occur.

Fig. 5.1

Emission spectrum from Sigma collagen in anise oil. Peak emission wavelength is  $\lambda_p = 347.2\text{nm}$  which agrees with the second-harmonic wavelength.

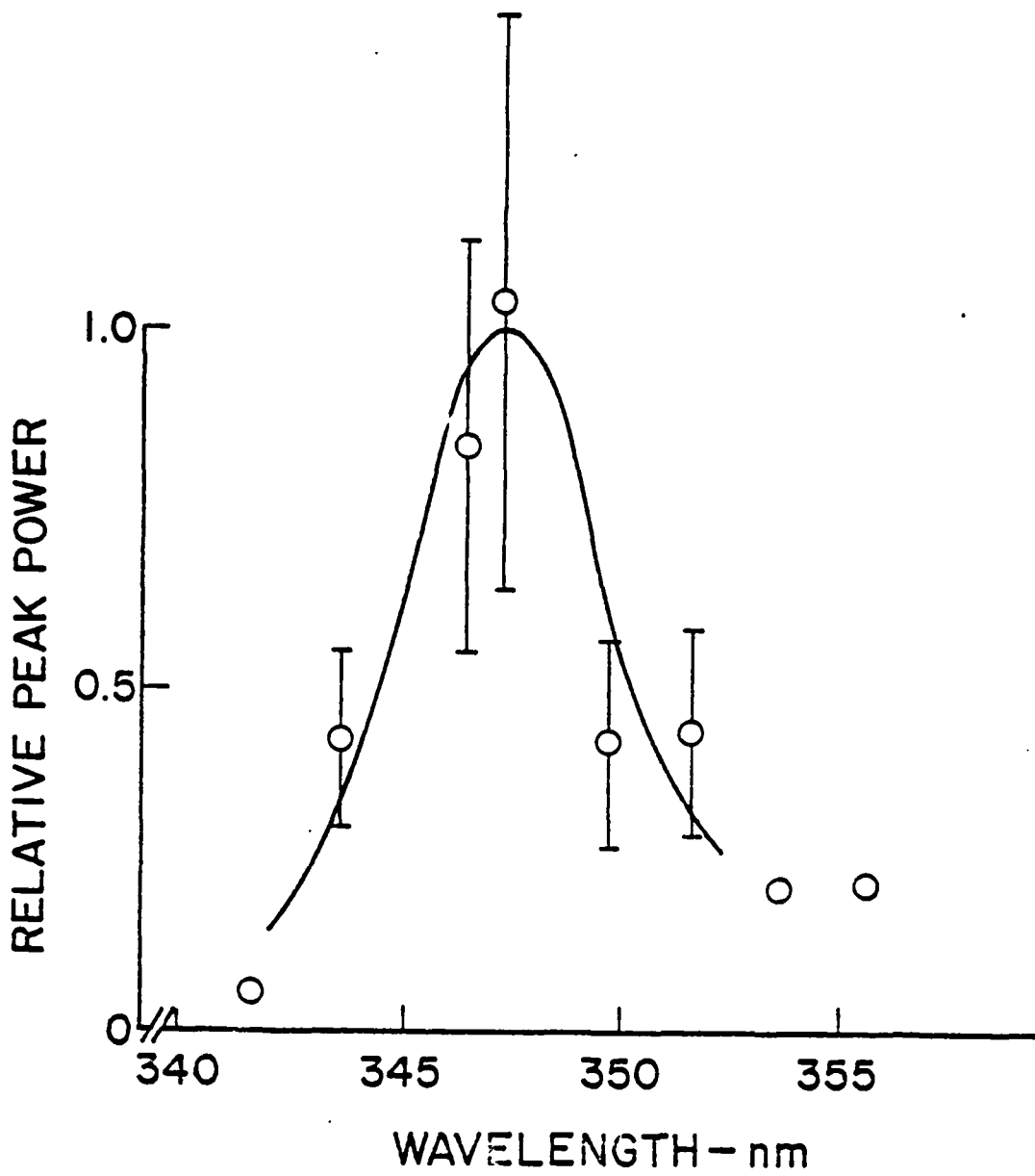


Fig. 5.2a

Native fibril aggregation pattern (after Schmitt)

Fig. 5.2b

"Amorphous" fibril aggregation pattern (after Schmitt)

Fig. 5.2c

Alternative model of "amorphous" fibril aggregation pattern. The conclusions drawn in this chapter regarding this model will also hold for models of amorphous fibrils in which there are equal numbers of collagen molecules oriented in opposing directions.

Collagen molecule

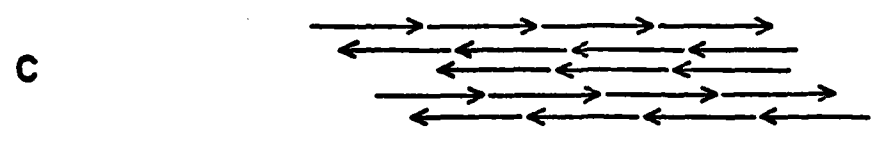
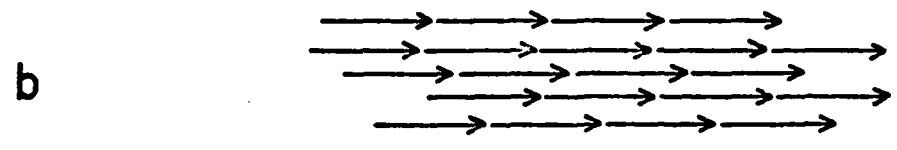
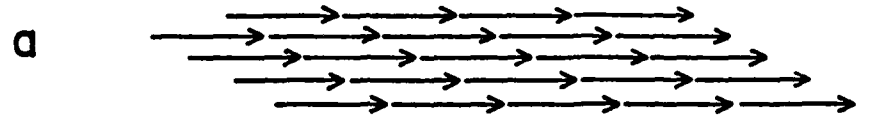
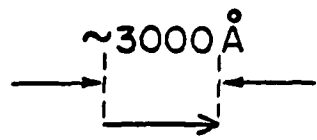
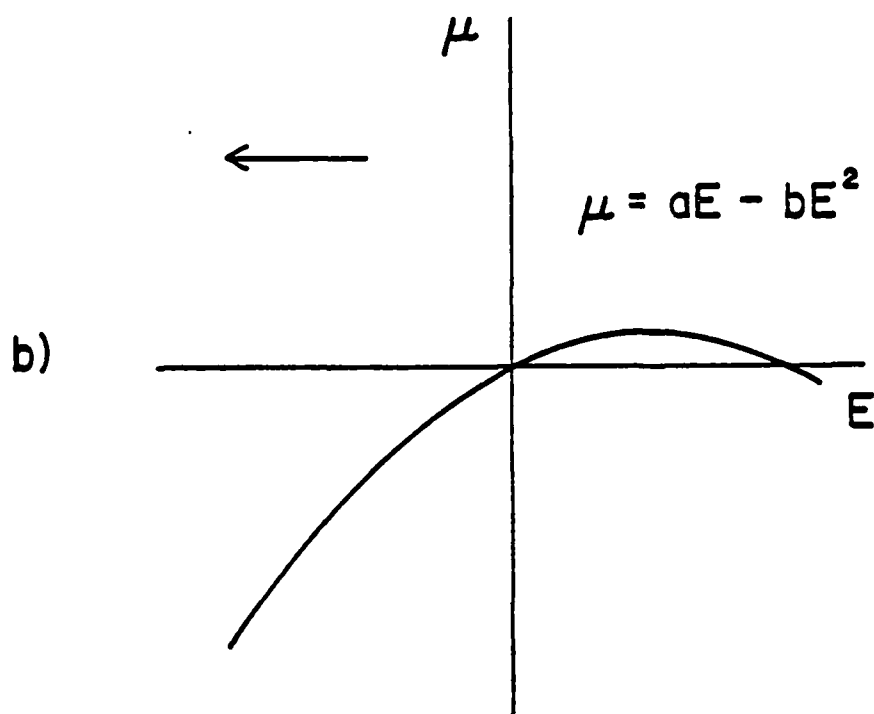
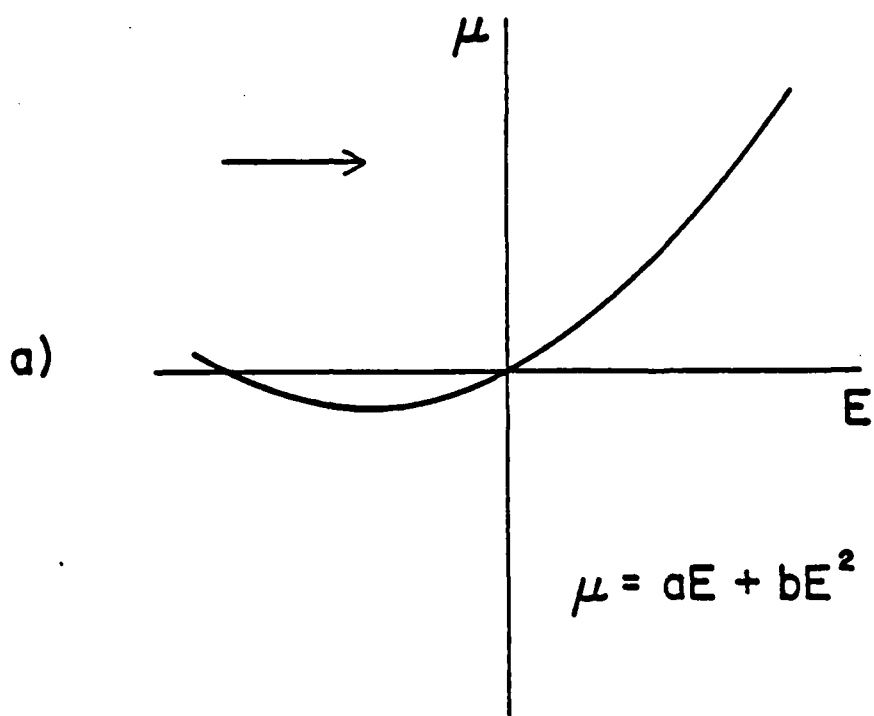


Fig. 5.3

Sketch of the  $\mu$ -E characteristic of a non-linear non-centrosymmetric oscillator. Figs. 5.3a and 5.3b show the characteristic for opposite orientations of the oscillator. The assumed orientation of the oscillator is shown by the arrowheads.



CHAPTER 6  
ANGULAR DISTRIBUTION OF SECOND-HARMONIC RADIATION  
FROM THE RABBIT CORNEA

In this chapter we shall compare the observed angular distribution of second-harmonic radiation from rabbit corneas with that expected theoretically from crystalline media and from amorphous media. Our measurements on corneas were made over a limited angular range in the forward scattering direction. These measurements showed the presence of a narrow lobe of forward-scattered second-harmonic radiation. This lobe may have been slightly broadened by light scattering in the cornea. Minck et al have reviewed analytical and experimental results of second-harmonic generation in crystalline and amorphous media (Minck et al, 1966). They have pointed out that in amorphous media, second-harmonic radiation emerges as weak scattered radiation (Minck et al, 1966, p. 1371) with a broad angular distribution. Ward and New have presented a scalar model for second-harmonic generation in crystalline media and have shown that in this instance second-harmonic radiation emerges as a narrow beam in the forward direction (Ward and New, 1969). The measurements that we have been able to perform show that second-harmonic generation in the rabbit cornea resembles coherent second-harmonic generation in a crystalline medium more closely than it does incoherent second-harmonic generation in an amorphous medium.

### 6.1 Methods and materials

The experimental apparatus for measuring the angular distribution of second-harmonic radiation from corneas is shown in Fig. 6.1. A cornea was placed at point P in the converging part of a focused ruby laser beam. The half-angle of convergence of the beam was about  $2^\circ$ . At the other side of the laser beam focus the half-angle of divergence,  $\theta_1$ , was also  $2^\circ$ . These estimates of convergence and divergence were made three ways. These were: a geometrical optics analysis of the ruby laser, measurements of polaroid film burn patterns produced at various positions in the ruby laser beam, and measurements of a He-Ne laser beam that was used to simulate the ruby laser beam (Fig. 6.1 for position of He-Ne laser). All three estimates were in close agreement.

Radiation from the cornea was collected by lens B (Fig. 6.1). This lens subtended a half-angle  $\theta_B = 8^\circ$  with respect to the sample at point P. Thus,  $\theta_B > \theta_1$ .

Masks with annular apertures concentric with the laser beam axis were sequentially placed against lens B to allow monitoring radiation over different angular ranges in the forward direction (Fig. 6.1). The scattering angle range covered by each mask is listed below.

<u>Mask</u>	<u>Range of <math>\theta</math></u>
1	$0^\circ - 2.1^\circ$
2	$2.1^\circ - 3.2^\circ$
3	$3.2^\circ - 4.2^\circ$
4	$5.3^\circ - 6.3^\circ$

The largest scattering angle that was monitored by these masks was at  $\theta = 6.3^\circ$  whereas lens B subtended a half-angle of  $8^\circ$ . Masks at larger angles were not used so as to avoid possible spherical aberration effects near the edge of lens B. Radiation that passed through lens B was monitored by the same equipment that was discussed in Chapter 4. The monochromator was set to pass 347.2nm radiation and the slits were opened wide. No laser radiation at 694.3nm was detected.

Tests were performed that showed that the amount of light collected by each annular aperture was simply proportional to the open area of the aperture. A Lambertian source of diffuse illumination was simulated at the sample position. To do this, three layers of white paper (paper used for duplicating machines) were placed over the diffusing glass case of a high pressure ultraviolet lamp. The spectral range of the lamp was from about 300nm to about 500nm. The paper was covered in turn by an opaque shield with a 2mm hole in the center. The 2mm hole was located at the sample position (at point P in Fig. 6.1). The illuminated hole satisfied the subjective criterion for a Lambertian source inasmuch as it appeared to have a constant brightness as one moved his eye in an arc from  $0^\circ$  to about  $80^\circ$  from the normal (Charschan, 1972, pp. 586-587). With only one layer of paper the hole appeared brighter when viewed at  $0^\circ$  than it did at about  $80^\circ$ . As a further check, a small selenium visible light detector with about a 5mm area was positioned at  $0^\circ$ , then at  $30^\circ$ , and finally

at  $50^\circ$  to the normal to the illuminated hole. The ratios of the detector readings at these three positions was 1:0.86:0.62. For a Lambertian source the corresponding ratios should be 1:0.87:0.64 (Charschan, 1972, Eq. 10-4). The detector readings were at most 3% lower than the readings expected for a Lambertian source. It was therefore assumed that the 2mm illuminated hole acted as a Lambertian source.

For a Lambertian source, the power per unit area at a fixed distance from the source, and at an angle  $\theta$  to the normal of the surface of the source, is proportional to  $\cos \theta$  (Charschan, 1972, p. 586). The outer edge of the largest annular aperture was at  $\theta = 6.3^\circ$ . At  $\theta = 0^\circ$   $\cos \theta = 1$  and at  $\theta = 6.3^\circ$ ,  $\cos \theta = 0.994$ . Therefore, it was assumed that the power per unit area was constant over the range of areas subtended by the annular apertures. On this basis, the photomultiplier response to illumination from the test Lambertian source should be proportional to the open area of the annular aperture.

The smallest annular aperture area was normalized to unity in the following computations. The relative mask area and the relative response of the photomultiplier when viewing the Lambertian source through the monochromator (set to 350nm), the  $\text{CuSO}_4$  filter, lens B, and the various annular apertures is listed below. The photomultiplier was determined to be linear at these low illumination levels.

<u>Mask</u>	<u>Relative Area</u>	<u>Relative Response</u>
1	1.0	1.0
2	1.25	1.23
3	1.75	1.74
4	1.38	1.36

(The relative area of mask 4 was smaller than the area of the annular aperture due to a shield that was accidentally placed too low behind lens B. The shield was left in position during all of these experiments). There is very close agreement between the relative areas and relative response of the photomultiplier which indicates that the amount of light collected by each aperture and directed to the photomultiplier was proportional to the area of the aperture.

The oscilloscope pulse height was corrected for the photomultiplier nonlinearity (Fig. 4.4). The corrected oscilloscope height,  $H$ , was proportional to the second-harmonic peak power passing through a given mask. This height was divided by the area  $A_a$  of the annular opening of the mask. The average and standard deviation of  $H/A_a$  was obtained for five laser pulses with each mask. The average values of  $H/A_a$  were then normalized to unity for the largest value. This normalized quantity  $W_a$  was, therefore, proportional to the second-harmonic peak power per unit area averaged over the area of the aperture and averaged over five laser pulses. For brevity, we shall call  $W_a$  the relative second-harmonic intensity.

The actual second-harmonic power per unit area may have been

variable from point to point of a given aperture. Our measurement method could not show this, whereas a photographic method could.

Three wide angle positions were monitored by rotating lens B and the rest of the collection and detection system around point P in Fig. 6.1. Since lens B subtended a half-angle of  $8^\circ$ , the scattering angle range  $-20^\circ < \theta_s < +33^\circ$  was monitored by placing the center of lens B at  $-12^\circ$ ,  $+12^\circ$ , and then at  $+25^\circ$ .

The room that was available for these studies was too narrow to allow wider angle measurements in the horizontal plane. It was considered far too time-consuming to construct apparatus that would allow vertical plane measurements. Backscattering measurements were made, however the detector was then so close to the Pockels cell Q-switch that pickup from the Pockels cell became greater than the expected second-harmonic pulse height (Chapter 4 for discussion of pickup).

The corneal samples were prepared as follows (Fig. 6.2). A fresh rabbit cornea was pressed lightly against a clean microscope slide. The central area of the cornea adhered naturally to the slide and the interface between the slide and the cornea appeared smooth. The outer surface of the cornea was covered with a few drops of aqueous from the enucleated eye. A glass cover slip was placed over the aqueous-wetted surface. Both corneal surfaces appeared to be flat and smooth. The angle of the cover slip had to be adjusted in

some cases to prevent the formation of a prismatic wedge that would deviate the direction of the laser beam axis as it passed through the sample. The He-Ne beam was used to monitor this adjustment. Since this adjustment could only be made at the beginning of a run it is possible that the laser beam axis may have moved with respect to the center of the annular apertures during a run. This movement could have occurred if, for example, the cornea dried unevenly during a run. In this case, the corneal sample could have become a prismatic wedge during drying. This source of error could perhaps be eliminated by using antireflecting sample cells with optically plane parallel sides filled with a fluid that matched the refractive index of the cornea.

## 6.2 Results

The relative second-harmonic intensity  $W_a$  is shown below with the corresponding angular range subtended by the annular aperture of the mask.

<u>Mask</u>	<u>Range of <math>\theta_s</math></u>	<u><math>W_a</math></u>
1	0° - 2.1°	0.86
2	2.1° - 3.2°	1.00
3	3.2° - 4.2°	0.77
4	5.3° - 6.3°	0.25

The values of  $W_a$  are averages for five laser pulses. The per-cent

standard deviation was about 30% in each case. The per-cent standard deviation in the laser pulse height was about 8%. The sum of the powers measured separately by the annular apertures was about 10% lower than the power as measured directly with no apertures over lens B. This agreement indicates that the annular apertures introduced no significant losses.

No second-harmonic pulses were detected when lens B was centered at  $\theta_s = +12^\circ$ ,  $+25^\circ$ , and  $-12^\circ$ . As a check, dried corneas were monitored at these wide angle positions. No second-harmonic radiation was detected until the surface of the cornea was roughened with a scalpel or a diffusing glass plate was placed between the cornea and lens B. These last measures apparently caused the second-harmonic radiation from the cornea to be scattered at wider angles.

The results are summarized in Fig. 6.3. A bar graph is used to represent  $W_a$  as a function of  $\theta_s$ . This data is taken from the above table. For simplicity, the plots are made with  $\theta_s$  a positive number. The wider angle data taken at  $\theta_s = +12^\circ$ ,  $+25^\circ$  and  $-12^\circ$  are shown by the circled points at  $\theta_s = +12^\circ$  and  $\theta_s = +25^\circ$ .

By drawing a smooth curve through the bar graph ( $W_a(\theta_s)$  in Fig. 6.3) and measuring the area under this curve from  $\theta_s = 0^\circ$  to another given value of  $\theta_s$  we could estimate the relative second-harmonic power  $W_R$  that was confined within  $\theta_s$  degrees of the laser beam axis. This calculation neglects any second-harmonic radiation that may have been

AD-A106 237

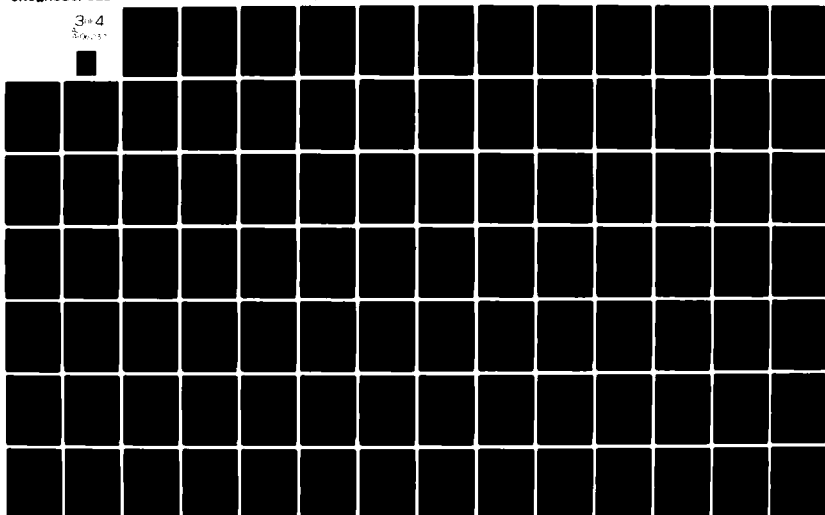
NORTHEASTERN UNIV BOSTON MASS DEPT OF BIOPHYSICS AN--ETC F/6 6/18  
BIOLOGICAL EFFECTS OF LASER RADIATION. VOLUME IV. OPTICAL SECON--ETC(U)  
OCT 78 W P HANSEN, S FINE DA-49-193-MD-2436

UNCLASSIFIED

NL

3-4

3-4



present outside our angular range of measurements.  $W_R$  was normalized to unity for the integration to  $\theta_s = 12^\circ$  in Fig. 6.3. A graph of  $W_R$  versus  $\theta_s$  is shown in the upper right of Fig. 6.3. It can be seen from this graph that 50% of the measured second-harmonic power was within the range  $0^\circ \leq \theta_s \leq 2.4^\circ$  and that 95% of the measured second-harmonic power was within the range  $0^\circ \leq \theta_s \leq 6^\circ$ .

According to geometrical optics calculations and polaroid film burn patterns, virtually all of the laser power at 694.3nm was within the range  $0^\circ \leq \theta_s \leq 2^\circ$ . As a second check, the He-Ne laser was set up as shown in Fig. 6.1 to imitate the ruby laser beam. The  $\text{CuSO}_4$  solution was removed and the He-Ne beam was monitored with masks 1 and 2. A distinct signal was observed with mask 1, but the signal was at least ten times smaller when the He-Ne beam was monitored with mask 2. Visually, the beam was confined within the angular range of mask 1. The ruby laser was not used for these measurements with the mask because of the possibility of damaging the photomultiplier. The above burn pattern and He-Ne simulation measurements indicate that the ruby laser beam was confined within the approximate range  $0 \leq \theta_s \leq 2^\circ$  and that the masks system did not introduce an artificial apparent broadening of the beam near 694.3nm. There is no apparent reason why the mask system would not also properly resolve the second-harmonic scattering pattern at 347.2nm.

It has been shown that 95% of the measured second-harmonic power was within the range  $0^\circ \leq \theta_s \leq 6^\circ$ . The ruby laser beam was confined to the range  $0^\circ \leq \theta_s \leq 2^\circ$ . Therefore, the angular spread of second-

harmonic radiation may have been greater than the angular spread of the laser beam.

### 6.3 Discussion

The results of these measurements indicate that the divergence of the second-harmonic beam was small. However, the divergence of the second-harmonic beam was greater than the divergence of the laser beam. For coherent second-harmonic generation in crystalline media, one would expect that the beam divergence of the second-harmonic would be less than the beam divergence of the laser (Ward and New, 1969). For incoherent second-harmonic generation in amorphous media, one would expect a very broad pattern of second-harmonic radiation (Minck et al, 1966, p. 1371). We shall present background material below that will enable an analytical estimate to be made of the second-harmonic beam divergence from crystalline media and amorphous media. These analytical estimates will be compared with the experimental results that have been given above. We shall then discuss whether the cornea behaves as a crystalline medium or an amorphous medium for second-harmonic generation.

Ward and New have carried out experimental studies of coherent optical third-harmonic generation by a focused laser beam in gases (Ward and New, 1969). Although their experimental work was primarily concerned with third-harmonic generation, they have presented a simple scalar model for coherent generation of the general  $q^{\text{th}}$  harmonic by a focused laser beam (Ward and New, 1969, Sect. III). Their scalar model

of a crystalline medium is the same as that used in Chapter 2 of this thesis. They have presented a detailed analysis of the case where the focused laser beam is a lowest order gaussian mode ( $TEM_{00}$  mode). Less detail is supplied for more complicated beam structures. We shall give a brief review of their results.

Figure 6.4 illustrates the characteristics of a focused  $TEM_{00}$  mode (Siegman, 1971, Chapt. 8). The intensity profile at any beam cross section is a gaussian function of radial position  $r$  from the beam axis. The dashed curves are the loci of the  $e^{-1/2}$  points of the beam profile. The focal region, where these loci are closest, is called the beam waist. The dashed curves approach straight diverging lines at distances from the beam waist that are large compared to the waist diameter. The angle  $\theta_1$  in Fig. 6.4 is called the far-field divergence angle of the beam. Higher order gaussian  $TEM_{mn}$  modes have intensity nulls symmetrically placed with respect to the beam axis. The envelope of these higher order intensity distributions is, however, still gaussian. The  $e^{-1/2}$  points of the gaussian envelopes are used to define the divergence angle,  $\theta_1$ , of these higher order modes.

A discussion of  $TEM_{mn}$  modes found in Siegman (Siegman, 1971, Chapt. 8) states that the wavefronts of these modes are spherical, except at the beam waist, where they are planar. The field strength is highest at the beam axis and decays monotonically along the wavefront away from the beam axis. In the far-field, the center of curvature

of the wavefronts is located at the beam waist.

Ward and New have shown in their analysis that a gaussian  $TEM_{00}$  laser beam mode generates a second-harmonic beam which is also a gaussian  $TEM_{00}$  mode. Both beams share the same waist position. However, the divergence angle of the second-harmonic beam,  $\theta_2$ , is smaller than the divergence angle of the laser beam  $\theta_1$  (Ward and New, 1969, p. 60). This last conclusion is based on their demonstration that the confocal beam parameter  $b = 2\lambda/\pi\theta^2$  (Ward and New, 1969, Eq. III) is the same for both beams. From this, the two divergences are related by

$$\theta_2 = 0.707 \theta_1 \quad (1)$$

They point out, without detailed analysis, that their conclusions for the  $TEM_{00}$  mode are essentially unchanged for higher order modes or mixtures of modes. Presumably, the conclusion regarding  $\theta_2 < \theta_1$  also holds for higher order modes and mode mixtures.

We expect that the divergence of the second-harmonic beam generated by the very complicated (generally non-gaussian) mode structure of a ruby laser beam is also narrower than the divergence of the laser beam. This is based qualitatively on the assumption that the beam intensity profile has an envelope that is a monotonically decreasing, non-rectangular, function of radial position  $r$  with respect

to the beam axis. The second-harmonic power per unit area,  $S_2$ , is proportional to the fundamental intensity,  $S_1$ , squared. The second-harmonic intensity profile envelope must therefore be narrower than the fundamental intensity profile envelope when these are both normalized to unity on the beam axis. On this basis, the divergence of the second-harmonic beam is less than the divergence of the laser beam.

We shall now compare these results with those expected for incoherent second-harmonic generation in an amorphous medium. Minck et al (1966, p. 1371) have stated that second-harmonic radiation from amorphous materials does not appear as a beam, and have suggested that it be thought of as analogous to Rayleigh scattering in linear media. Presumably, this analogy is meant only to indicate the diffuse character of the incoherent second-harmonic radiation pattern. A better quantitative idea of the diffuse character of the incoherent second-harmonic radiation pattern can be obtained from the theoretical work by Bersohn et al (1966). These investigators have derived general theoretical equations for the angular distribution of incoherent second-harmonic radiation from an amorphous medium. In their analysis, the incident laser beam can be plane polarized, unpolarized, or elliptically polarized (Bersohn et al, 1966, Sect. III). The expressions that they have developed are difficult to interpret when presented in general form (See Eqs. 25-27 in Bersohn et al, 1966). Therefore, we shall present a simplified special case as a working example.

Consider a plane polarized fundamental wave propagating in the Z direction with the electric field polarized along the Y direction ( $\psi = 0$  in Eq. 17 of Bersohn et al). Let  $\theta$  be the angle between the Y axis and a radius vector drawn from the origin to a distant observer. Using Eqs. 25-32 in Bersohn et al, one can write the following simplified expressions for the intensity of the second harmonic radiation as a function of  $\theta$ , when the observer is at a fixed distance and is confined to the X-Y, X-Z and Y-Z coordinate planes respectively.

$$I_{X-Y}(\theta) = A(1 + \cos^2\theta) + B \sin^2\theta \quad (2)$$

$$I_{X-Z}(\theta) = A + B \quad (3)$$

$$I_{Y-Z}(\theta) = A(1 + \cos^2\theta) + B \sin^2\theta \quad (4)$$

In Eqs. 2, 3, and 4, A and B are quadratic functions of the tensor components of the second-order nonlinear polarizability of the molecules of the medium (Bersohn et al, 1966, p. 3189; This article uses the notation  $\beta_{XZZ}^2$  and  $\beta_{ZZZ}^2$  for quantities that are proportional to A and B). The quantities A and B are constants for a given medium.

For the remainder of this discussion it will be convenient to express Eqs. 2, 3 and 4 in the form:

$$I_{X-Y}(\theta) = (A + B) + (A - B) \cos^2\theta \quad (5)$$

$$I_{X-Z}(\theta) = A + B \quad (6)$$

$$I_{Y-Z}(\theta) = (A + B) + (A - B) \cos^2 \theta \quad (7)$$

According to Eq. 6, the intensity distribution in the X-Z plane is a constant for all angular positions of the observer. Therefore, the distribution in the X-Z plane has no beam-like properties. According to Eqs. 5 and 7, the distributions in the X-Y and Y-Z planes are identical. When  $A > B$  these distributions can be beam-like in the forward direction. The most forward peaked distribution is obtained when  $B = 0$ . In this instance,

$$I_{X-Y}(\theta) = I_{Y-Z}(\theta) = A(1 + \cos^2 \theta) \quad (8)$$

The  $e^{-1/2}$  points of this distribution occur for  $\theta = 62.5^\circ$  which indicates a very broad beam. This divergence is much greater than the divergence of most laser beams. One should contrast this with the beam divergence for coherent second-harmonic generation which is expected to be less than the beam divergence of the laser. Consequently, with incoherent second-harmonic generation, one would expect a beam width greater than  $63^\circ$  whereas with coherent second-harmonic generation one would expect a beam width that is less than the laser beam width.

The results of our measurements shown in Fig. 6.3 indicate that there was a high concentration of second-harmonic power from the rabbit cornea at low forward angles near the laser beam axis. In other

words, within our range of measurements second-harmonic emission appeared in a well-defined beam. In order to produce detectable amounts of second-harmonic radiation outside this beam it was necessary that scattering media be inserted in the beam path. This was accomplished by roughening the surface of a dried corneal sample or by introducing a diffusing glass plate between the cornea and lens B (See Results section 6.2). When no scattering medium was present, no second-harmonic radiation was detected at  $\theta_s = +12^\circ$ ,  $+25^\circ$  and  $-12^\circ$  (See Results section 6.2). The existence of a beam of forward-directed second-harmonic radiation is in best agreement with the scalar model for coherent second-harmonic generation from a crystalline medium that was outlined above. It is in poor agreement with the broad pattern expected from an amorphous medium.

There is, however, a difference between the theoretical beam for coherent second-harmonic generation and the observed beam. We have indicated in outlining the scalar model that the theoretical second-harmonic beam from a crystalline medium should have a smaller divergence than the fundamental beam. In the measurements, the opposite situation appears to exist for the rabbit cornea.

The simplest explanation for the wider divergence of the observed second-harmonic beam is based on the light scattering properties of the mammalian cornea. Models presented by Hart and Farrell (Hart and Farrell, 1969) and by Benedek (Benedek, 1971) have shown that light scattering in the rabbit cornea is negligible at  $\lambda_1 = 694.3\text{nm}$  (ruby

laser wavelength) but is significant at  $\lambda_2 = 347.2\text{nm}$  (second-harmonic wavelength). Hart and Farrell have also given experimental spectrophotometric light transmission data for the rabbit cornea (Hart and Farrell, 1969, Fig. 4) that is in good agreement with their theoretical model of transmission based on light scattering. They show that transmission is about 95% near  $\lambda_1 = 694.3\text{nm}$  and only about 70% near  $\lambda_2 = 347.2\text{nm}$ . We have obtained transmission values in fresh rabbit corneas that are in good agreement with this data. Based on the above information, it is reasonable to assume that the divergence of a ruby laser beam will not be significantly affected by light scattering in the cornea, while a second-harmonic beam may be markedly broadened. This may, therefore, explain why we have observed a divergence for the second-harmonic beam from rabbit corneas that is greater than the divergence of the laser beam.

The wider beam divergence of the second-harmonic radiation may also indicate that there is only local crystallinity in the rabbit cornea. The analysis of this aspect requires further experimental work and is beyond the scope of this presentation.

The data that has been obtained regarding the divergence and profile of the second-harmonic beam is approximate. Each histogram bar in Fig. 6.3 has a 30% standard deviation in height. Therefore, the smooth curve that has been drawn through the bars in Fig. 6.3 and used to estimate the second-harmonic beam divergence is not precise. It can also be seen in Fig. 6.3 that the bar between  $0^\circ$  and  $2^\circ$  is

about 12% lower than the bar between  $2^\circ$  and  $3^\circ$ . The difference in these two heights is well within the 30% standard deviation in height. Therefore, one cannot conclude that this difference represents an actual feature of the second-harmonic beam profile.

No extensive work was performed to determine the distribution of second-harmonic intensity as a function of the polar angle at a given cross section of the beam. The only investigation of this kind consisted of covering the bottom half of lens B with the top half open and then covering the top half of lens B with the bottom half open. No annular apertures were used in this investigation. No significant difference in second-harmonic power was observed between covering the top half or the bottom half (15% higher power through the top half). Studies of the beam profile and beam divergence could be carried out photographically. In this case, the entire beam cross section would be observed with each exposure if the dynamic range of the film was sufficiently large.

#### 6.4 Summary and conclusions

Our experimental results have indicated the following:

- a. A well-defined beam of ruby laser radiation at 694nm produced a well-defined beam of second-harmonic radiation at 347nm from rabbit cornea.
- b. Virtually all of the laser radiation was within  $2^\circ$  of the beam axis. However, the second-harmonic beam was broader.

Ninety-five per-cent of the measured second-harmonic power in the forward direction was within  $6^\circ$  of the beam axis.

- c. The observed beam of second-harmonic radiation from the cornea is in better agreement with coherent second-harmonic generation from a crystalline medium than it is with incoherent second-harmonic generation from an amorphous medium.
- d. The observed broadening of the second-harmonic beam may be due to light scattering in the cornea at 347nm or due to local rather than overall alignment of the second-harmonic oscillators of the rabbit cornea.

Figure 6.1

Schematic of the apparatus used to monitor the angular distribution of second-harmonic radiation from rabbit cornea. For the most part, the apparatus is the same as that shown in Fig. 4.1. Annular apertures are added at lens B in order to map the distribution of second-harmonic power as a function of the forward scattering angle  $\theta_s$ . The He-Ne laser and beam expander shown within dotted lines were inserted for alignment purposes. They were removed while the ruby laser was operating.

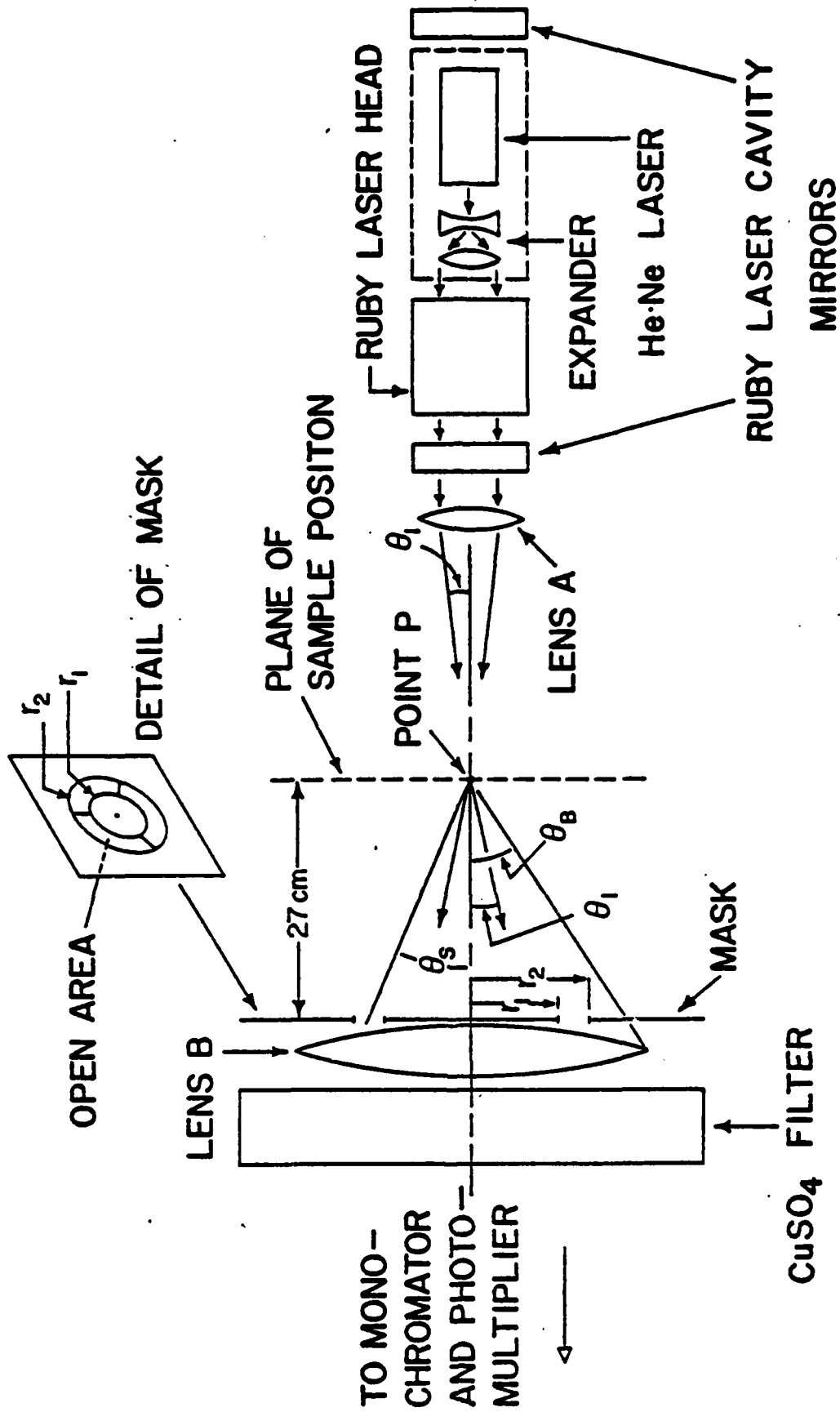


Figure 6.2

Diagram of corneal sample preparation. The center of the cornea was flattened against a glass microscope slide where it adhered naturally. Aqueous from the rabbit eye was spread over the front surface and covered with a glass cover slip. The cover slip was held in place with tape.

**RABBIT CORNEA, FLATTENED AGAINST SLIDE AT CENTER**

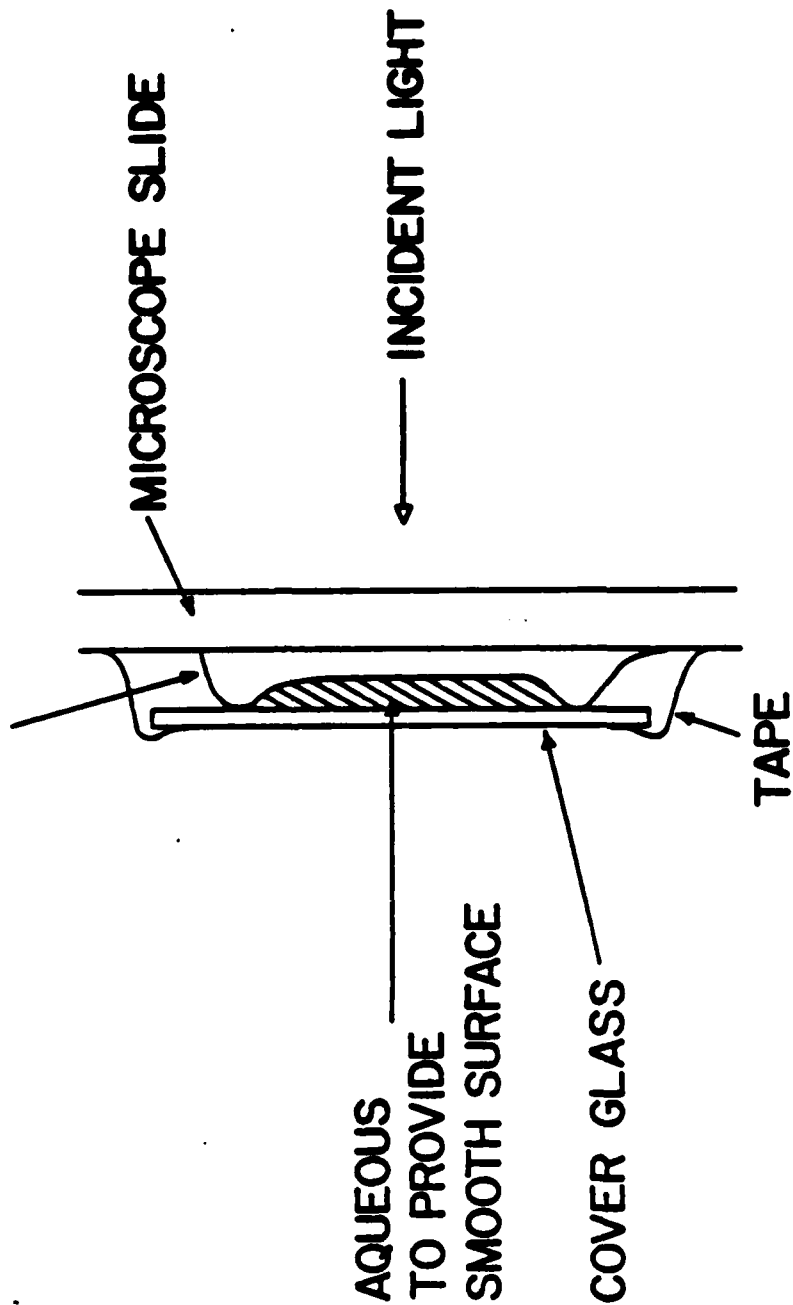


Figure 6.3

The large experimental plot shows the relative second-harmonic peak-power per unit area of the annular apertures,  $W_a$ , versus the forward scattering angle,  $\theta_s$ .  $W_a$  is recorded as a histogram. The variance in the histogram heights is 30%. A smooth curve  $W_a(\theta_s)$  is drawn by eye through the histogram data. The cumulative power  $W_R$  as a function of  $\theta_s$  was obtained by a numerical integration of  $W_a(\theta_s)$  and is shown as a small plot of  $W_R$  versus  $\theta_s$ . This latter plot shows that 95% of the measured forward power was within  $6^\circ$  of the beam axis.

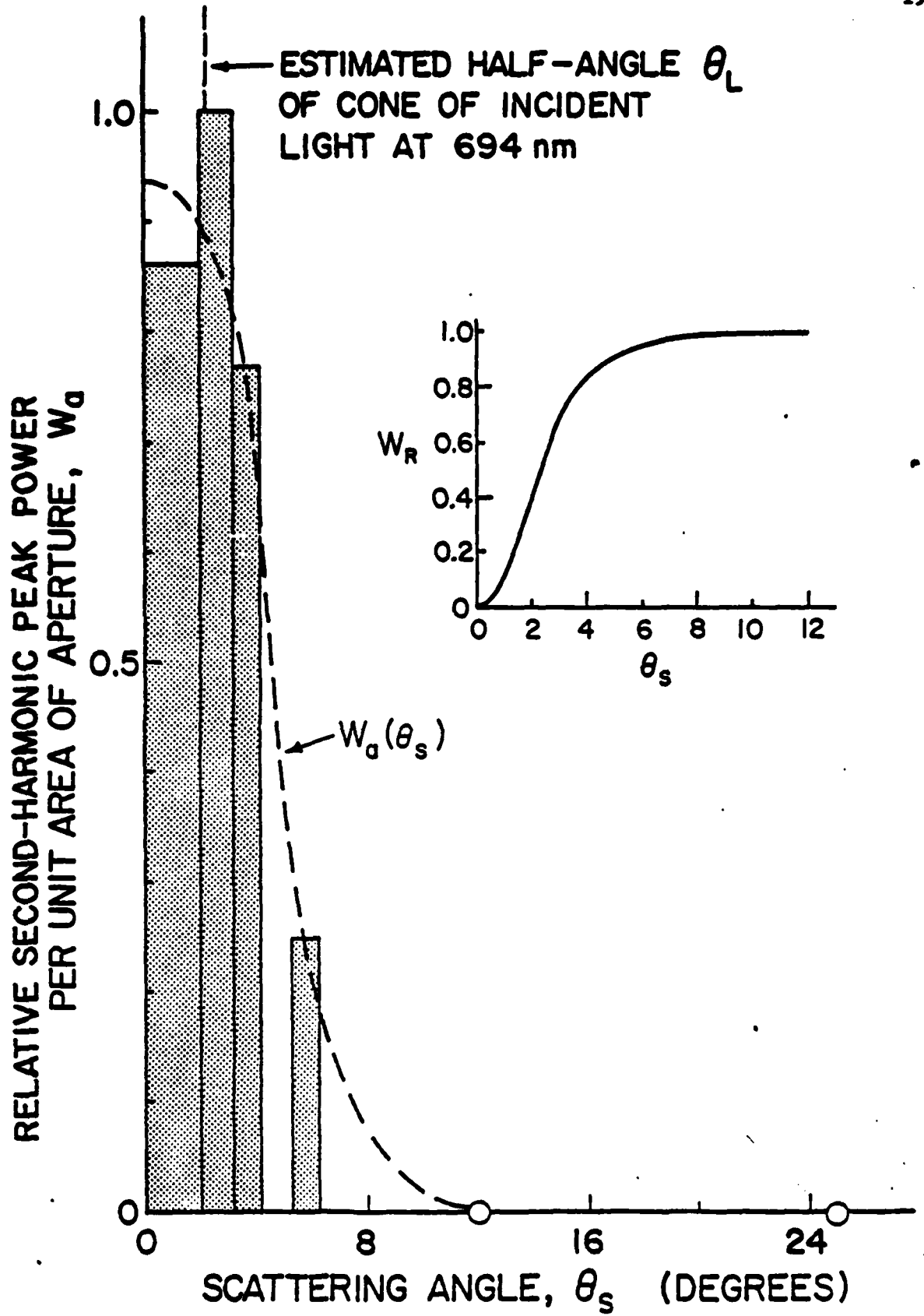
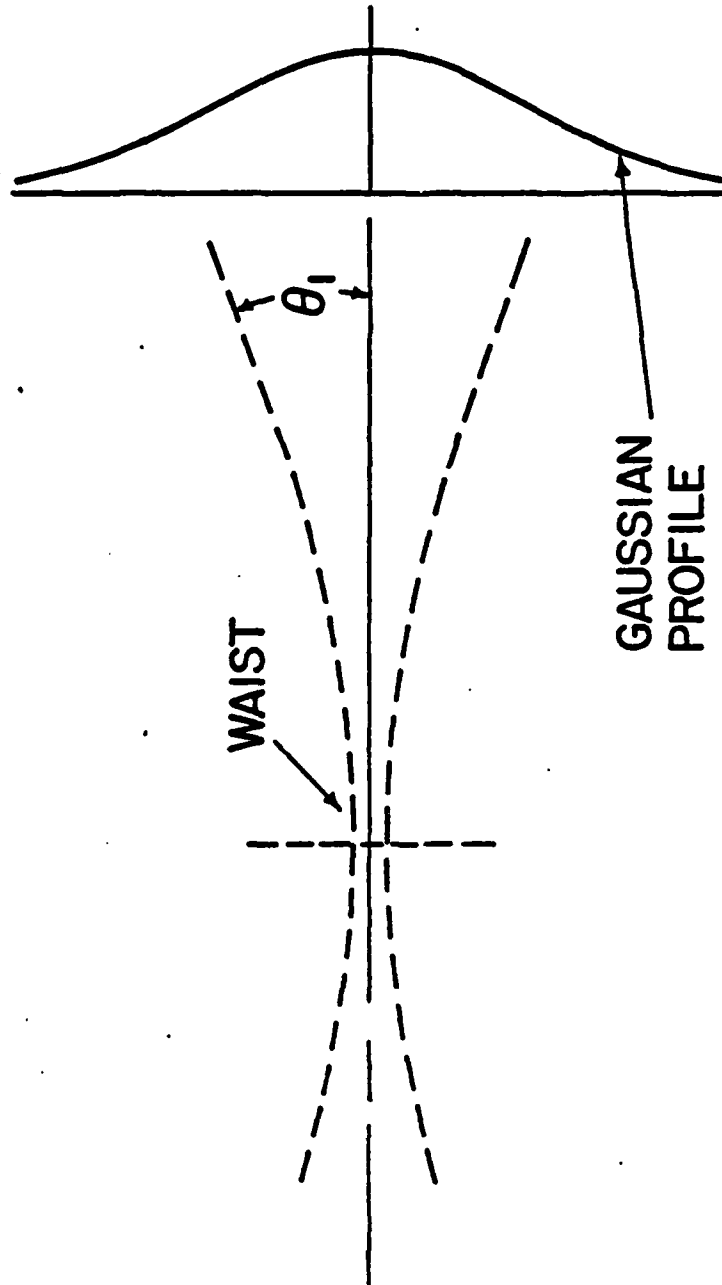


Figure 6.4

Sketch of the salient features of a  $TEM_{00}$  gaussian beam. The broken lines are the loci of the  $e^{-1/2}$  points of the beam intensity. The waist region is where these lines are closest and almost parallel. The gaussian profile is also sketched for convenience. The angle  $\theta_1$  is the beam divergence angle.



## CHAPTER 7

EFFECTS OF COLLAGEN PHASE TRANSFORMATION  
ON SECOND-HARMONIC GENERATION

It has been recognized for about 150 years that connective tissue fibers shorten when they are heated (Bear, 1952). There is strong evidence that this thermal contraction of the tissue is produced by changes in the collagen component of the fibers. Contraction occurs in a narrow temperature range, but the location of this range depends on whether the fibers have been previously heated and on the state of hydration of the fibers. In most cases, with fresh moist tissue, the fiber contraction occurs between 60°C and 67°C (Bear, 1952; Flory, 1965; Banga, 1966). With care, the temperature range over which contraction occurs can be made less than 3°C (Flory and Garrett, 1958).

A number of thermodynamic, X-ray diffraction, light microscope, and electron microscope studies have provided a basis for formulation of current models of the thermal contraction process (Elden, 1968, Sect. VA; Banga, 1966, Chapt. XI; Rice, 1960, Veis and Cohen, 1960; Bear, 1952, Sect. IV.5). Thermodynamic studies of tendon collagen fibers have indicated that thermal contraction approximates a first order phase transformation when care is exercised to maintain thermal equilibrium (Flory and Garrett, 1958; Flory, 1956, p. 57).

The bond energies that appear to be important in this phase

transformation are those associated with the intramolecular hydrogen bonds of the collagen molecules themselves (Flory, 1961). The forces that bind collagen molecules together to form fibrils are very weak and are not significant in the phase transformation (Flory, 1961). The intramolecular hydrogen bonds stabilize the three stranded helical structure of the collagen molecule and produce an overall rigid rodlet molecule (Doty, 1959; Ramachandran and Sasisekharan, 1961). Disintegration of these bonds occurs in a narrow temperature range. When this happens, the three component chains of the collagen molecule also separate and become flexible, non-helical, random coil macromolecules themselves. Local attachments may occur between two of the separated strands (Schmitt, 1959, p. 351). The molecular weights of the individual strands are each about 100,000 (Schmitt, 1959, pp. 351-352). These changes are, of course, not directly visible.

Macroscopically, during the phase transformation the highly anisotropic, relatively inextensible collagen fibers are changed into amorphous, extensible fibers. Flory has observed in tendon that this phase transformation is characterized by a small volume increase, a marked length decrease, and a latent heat that must be supplied to the tendon (Flory, 1956; Flory and Garrett, 1958; Flory and Spurr, 1961). Other changes that accompany the phase transformation in fibers are; increased optical transparency and decreased birefringence (Flory, 1956; Elden, 1968, pp. 333-335). When collagen is heated in solution, the optical rotatory power decreases as the random coil

phase appears (Flory and Garrett, 1958). Only slight changes occur in the 190nm peptide absorption band of collagen during this heating (Wood, 1963).

We expect that the collagen phase transformation described above should affect the second-harmonic conversion efficiency of collagenous tissue. If we consider native collagen fibrils to be non-centrosymmetric "crystallites" then an induced, macroscopic, second-order nonlinear polarization may exist in these fibrils and lead to the growth of a travelling second-harmonic wave by coherent second-harmonic generation in the tissue. When these fibrils are converted to a random coil macromolecular phase, the tissue may become amorphous. Under these conditions, the tissue could no longer support a second-order nonlinear macroscopic polarization and produce coherent growth of second-harmonic wave. In this disordered phase, second-harmonic generation only occur as weak incoherent second-harmonic generation from randomly oriented, individual, independent, microscopic dipoles. Second-harmonic generation has been compared for crystalline and amorphous media in Chapter 2. There it was shown that the conversion efficiency is generally orders of magnitude lower in amorphous media compared to crystalline media. Other changes involving the oscillators themselves may also occur, which could reduce the second-harmonic conversion efficiency.

The purpose of this chapter is to show that the second-harmonic

conversion efficiency of rabbit cornea and rat tail tendon decreases during the collagen phase transformation. A drop in efficiency may be due to decreased order in the collagen component of these tissues.

## 7.1 Methods and materials

### 7.1a Outline of methods and materials

Six groups of rat tail tendons were heated under slight tension for five minutes in separate distilled water baths at six different temperatures between 20°C and 68°C (Figs. 7.1 and 7.4). During heating, dimensional changes of the tendons were estimated using a centimeter scale placed in the bath. After heating, the tendons were mounted on six different glass microscope slides. Each sample was dried in a continuously evacuated vessel at room temperature for one-half hour. After drying, the transmission of the mounted samples was measured at 694nm and 347nm using a Beckman Model B spectrophotometer. Qualitative sample birefringence observations were then made with a polarizing microscope.

The six samples were then irradiated using the set-up shown in Fig. 4.1. The laser pulse duration was  $\sim 100$ nsec and the energy was varied between approximately 5mJ and 50mJ. Scattered second-harmonic radiation was collected in a forward cone of  $\sim 8^\circ$  half-angle by lens B in Fig. 4.1. The collected, relative second-harmonic peak power  $W_{R2}$  was recorded as a function of relative laser peak power  $W_{R1}$  for each

of the six samples.

A single rabbit cornea was cut in half along a diameter and taken through six heating steps in a water bath at temperatures between 20°C and 69°C (Figs. 7.2 and 7.8). The first immersion in the bath was at 20°C for one hour. The other immersions were each for ten minutes in water at higher temperatures.

After each heating step, the sample was mounted on a glass slide and the major and minor chords A and B (Fig. 7.3) were measured in inches to the nearest 1/32 inch and then converted to centimeters. The sample was then dried on the glass slide for a few minutes in partial vacuum until the 347nm optical transmission returned to approximately the same level (17%) observed after the initial 20°C immersion step. Qualitative birefringence changes were observed with a polarizing microscope after completing the transmission check. The sample was then irradiated using the set-up in Fig. 4.1.

Relative second-harmonic versus relative fundamental peak power data was obtained at several power levels for each temperature as described previously for tendons.

While only six tendon samples and one corneal sample, whose optical transmission was adjusted to 17%, (Table 2) will be discussed in detail in this chapter, a number of other tendon and corneal samples were used to explore specific results in specific temperature ranges. These latter results are incorporated into Tables 1 and 2. Preliminary

studies were carried out on a number of corneas and tendons before running the actual experiments.

#### 7.1b Details of methods and materials

Seven or eight tendon fiber bundles from mature Sprague-Dawley rats were used for each of the six tendon samples. When laid side-by-side on a glass slide with no apparent spaces between the bundles, the fresh samples were  $\sim 0.7$ cm wide and  $\sim 2.5$ cm long. The cornea was obtained from a mature albino rabbit. It was cut in half along a diameter so that it would lay flat against the microscope slide. The fresh cornea measured  $\sim 1.4$ cm along the major chord A and  $\sim 0.7$ cm along the minor chord B when flat.

Ordinary 20ml test tubes containing 5ml of distilled water with initial pH of 7.0 at 20°C were used for heating the samples. The test tubes were suspended in a circulating water bath whose temperature could be controlled to  $\pm 1^\circ\text{C}$ . A thermometer was placed in the test tube to show when the desired temperature had been reached. When the samples were immersed in the preheated water, the test tube water temperature remained within  $\pm 1^\circ\text{C}$  of the desired temperature throughout the heating period.

Both the tendons and cornea adhered naturally to the glass microscope slides.

When measuring the optical transmission of the tissue samples (see Chapt. 4), the sample position was varied laterally to allow

the monitoring beam to pass through various zones of the tissue that were near the zone to be irradiated. Transmission was recorded for each position and an average value and standard deviation was computed on the basis of about 5 measurements. At 347nm, the percentage standard deviation for the cornea was approximately 6%, and for the tendons it was approximately 10%. At 694nm the standard deviation for tendons was approximately 4%. Measurements at 694nm were not made for corneas.

The blue color of the hydrated cornea indicated that 347nm radiation was, perhaps, more intensely scattered than 694nm radiation. For the cornea, we wished the ordinary scattering properties to be approximately the same after each heating step, therefore it was decided to maintain a constant transmission at 347nm in one of the corneas. The 347nm transmission was adjusted by partial drying, to 17% after each heating step in this cornea. Since the properties of the moist cornea changed with time when exposed to air, cornea transmission measurements at 694nm were omitted to speed the experimental procedure.

Newton's color scale was used for qualitative assessment of birefringence changes (Lin and Sullivan, 1972, Fig. 5).

Complete results from only six tendon samples and one corneal sample will be reported in this chapter; however approximately a dozen tendons and a slightly greater number of corneas were used to

develop various aspects of the methods described above. For example, three other corneas were heated in air rather than in water, while other corneas were heated in buffer solutions. Second-harmonic generation efficiency changes were also measured for these samples. The six tendon samples described previously in the methods and materials outline were heated with a 0.4gm lead weight attached to supply slight tension. Several other tendons were also heated without a weight. Transmission and birefringence changes were also studied for a number of corneas and tendons; only a few spot checks were made of second-harmonic conversion efficiency in most of these. These ancillary studies did not yield results that were inconsistent with those obtained from the six tendon samples and the one cornea that are described in this chapter.

## 7.2 Results

### 7.2a Brief summary of results

Near 60°C, the tendons and cornea underwent abrupt changes that were characteristic of the collagen phase transformation that has been studied in detail by Flory (Flory and Garrett, 1958; Flory, 1956). These changes were:

- a. Shrinkage along the direction of the collagen fibers (Figs. 7.4, 7.8)
- b. Swelling in the directions perpendicular to the fibers
- c. Decreased birefringence

- d. Increased optical transmission (Figs. 7.6, 7.9)
- e. Increased mechanical compliance
- f. In the case of tendon, creep along the original direction of the fibers following shrinkage (Fig. 7.5).

In addition to these changes, the second-harmonic conversion efficiency in these tissues dropped by more than an order of magnitude near 60°C and remained low at higher temperatures (Figs. 7.7, 7.10).

Reversal of these effects with time was not observed.

#### 7.2b Results from tendons

##### i. Dimensional changes (tendon)

The length of the lead weighted tendon samples was estimated from a centimeter scale placed in the water bath used for heating. Figure 7.4 shows the maximum length changes that occurred at various bath temperatures for each of the six tendon samples that were to be irradiated. No length changes were produced at temperatures below 57°C. At 60°C there was a slight contraction. At 65°C and 68°C the tendons contracted to approximately 25% of their original length within 100sec after immersion, and then were observed to creep to 75% of their original length.

Figure 7.5, curve A, is a sketch showing the approximate alteration in length of a typical, contracting tendon weighted sample as a function of time. The length was estimated periodically using the centimeter

scale in the bath. Contraction began within a few seconds after immersion in the preheated water. Approximately 100 seconds after immersion, the sample reached its minimum length ( $\sim 25\%$  of original length). At this time, marked radial swelling of the tendon was apparent. After 100 seconds, sample creep (re-elongation at constant force) was evident. Creep was rapid at first, but slowed to an imperceptible rate approximately 300 seconds after the time of immersion. At this time the samples were removed from the heating bath, placed on a microscope slide, and kept in air at  $20^{\circ}\text{C}$  while the final sample length was measured. This final length was found to be  $80\%$  of the original length at the time of immersion. No further changes occurred while the samples remained moist in air at  $20^{\circ}\text{C}$  prior to drying in vacuum.

In an ancillary experiment, several tendons were heated above the contraction temperature without a weight. These samples contracted maximally within a few seconds of immersion (Fig. 7.5, curve B). Creep was evident shortly after maximal contraction had occurred. These samples returned to an asymptotic value of  $75\%$  of their original length after 300 seconds of creep.

Each fiber bundle in those tendon samples that had been heated to temperatures below the contraction temperature ( $\sim 60^{\circ}\text{C}$ ) became slightly smaller in cross-section after  $1/2$  hour of drying in vacuum at  $20^{\circ}\text{C}$ . No length changes were observed during drying. The fibers that had been heated to temperatures above the contraction temperature also

did not change in length during 1/2 hour of drying in vacuum at 20°C; that is, they maintained their length of 75% of the original length. However, there were marked radial changes. In these samples, the tendons on the microscope slide became flattened during drying and appeared to "fuse" together so that individual bundles were not easily distinguished. The thickness of these fused fiber bundles (measured as a height above the microscope slide surface) was about 70% of the diameter of the non-contracted fiber bundles; the overall cross-sectional area appeared to be the same for both non-contracted and contracted bundles.

ii. Light transmission changes (tendon)

Light transmission was measured at 694nm and 347nm after heating and vacuum drying. Figure 7.6 shows the light transmission as a function of temperature for the same six tendon samples whose contraction characteristics are shown in Fig. 7.4. There was an increase in transmission at both 694nm and 347nm between 50°C and 57°C. Light transmission continued to improve over a broad range from 50°C to 68°C; which was the highest temperature used.

iii. Birefringence changes (tendon)

Qualitative birefringence changes were noted using a polarizing microscope and Newton's color scale (Lin and Sullivan, 1972). The microscope was necessary in this case since birefringence colors change when the sample thickness changes by very small amounts. There-

fore, only small sample regions possess distinct colors which must be viewed with magnification. Brilliant complementary colors appearing with crossed and then parallel polarizer and analyzer are indicative of high birefringence. A grey or black field of view with crossed polarizer and analyzer is indicative of low birefringence.

When scanned along their length, non-contracted fibers (fibers heated below 60°C) showed a progression of birefringence colors. This was probably related to small thickness changes in the fibers. When the microscope polarizer or analyzer was rotated by 90 degrees, each of these colored regions changed to its complementary hue. For example, the most commonly observed colors in non-contracted fibers were green, yellowish-green, greenish-blue, indigo (reddish-blue) with crossed polarizer and analyzer. When the polarizer and analyzer were rotated so as to be parallel, these colors changed to purplish-red, violet, brownish-orange, and gold-yellow respectively. These are complementary color changes. The complementary color changes and the purity (or saturation (Monk, 1963, p. 331) ) of the colors are a qualitative indication of high birefringence in the non-contracted fibers (Vickers, 1963).

Fibers that had been heated to 65°C or 68°C (and allowed to creep) were uniformly grey with crossed polarizer and analyzer. They were a brilliant white with parallel polarizer and analyzer. This is a qualitative indication of low birefringence. Therefore, in the six

tendon samples that are described in Figures 7.4 and 7.6, birefringence was high after heating and drying below 60°C, but dropped markedly at 65°C to 68°C.

iv. Second-harmonic conversion efficiency changes (tendon)

Low-angle, forward-scattered, second-harmonic peak power and the incident laser peak power could be measured either as oscilloscope pulse heights or as actual peak powers with the apparatus shown in Figure 4.1. Two measures of experimental second-harmonic conversion efficiency were used in these studies. A relative forward conversion efficiency  $C_{MRF}$  was defined from the ratio of the oscilloscope pulse heights

$$C_{MRF} = H_2/H_1$$

where

$H_2$  = Pulse height for second-harmonic oscilloscope channel

$H_1$  = Pulse height for fundamental oscilloscope channel

A measured forward scattered power conversion efficiency  $C_{MPF}$  was defined as the ratio of the second harmonic peak power  $W_{2B}$  collected in the forward direction by lens B (Fig. 4.1) to the laser peak power

incident at the sample  $W_1$

$$C_{MPF} = W_{2B}/W_1$$

Since  $H_1 \propto W_1$  and  $H_2 \propto W_{2B}$  it is clear that  $C_{MRF} \propto C_{MPF}$ .

In most of the studies reported in this chapter we were interested in changes that occurred in the low-angle, forward conversion efficiency of corneas and tendons as these tissues were heated. These changes will generally be reported as the ratio of  $C_{MRF}$  below the collagen phase transformation temperature to  $C_{MRF}$  above the collagen phase transformation temperature.

In some cases it was important to compare theoretical and experimental estimates of the actual low-angle, forward scattered, second-harmonic peak power. These comparisons were made using  $C_{MPF}$ .

Figure 7.7 shows values of  $C_{MRF}$  for various values of  $H_1$  and the sample heating temperatures. The same six tendon samples used in Figures 7.4 and 7.6 are used in Figure 7.7. Each data point is labeled with the sample heating temperature. Values of  $C_{MRF}$  were obtained from samples that were heated at 65°C and 68°C. At 65°C and 68°C the forward conversion efficiency was so low that system noise affected the second-harmonic oscilloscope signals. One laser pulse was fired at  $H_1 = 18$  units using a 65°C sample (Fig. 7.7). This was considered to be a laser level at which sample damage might occur;

however, it was risked in order to try to obtain higher second-harmonic radiation levels from a thermally contracted sample. No gross damage was evident. The conversion efficiency in this case was consistent with that obtained from contracted samples at lower laser power levels.

Samples with the same second-harmonic forward conversion efficiency should yield  $C_{MRF}$  versus  $H_1$  data that is grouped around a straight line of the form:

$$C_{MRF} = AH_1 \quad (1)$$

Where A is a constant that depends upon the sample material properties and the irradiated area of the sample. (See Chapter 2 for a discussion of efficiency fluctuations). When one observes the data in Figs. 7.7 and 7.10, the points appear to lie in two groups. In both figures, one group contains only points obtained from non-contracted samples and the other group contains only points from contracted samples. A regression line was obtained for each group.

The ratio of the slopes of the regression lines in Fig. 7.7 for tendons was 30:1 which is indicative of the fact that two distinct data groups were present. The data group corresponding to thermally contracted tendons had consistently lower values of  $H_2$  over the range of  $H_1$  values employed. The cornea data will be discussed in the next section.

## 7.2c Details of results from corneas

### i. Dimensional changes (cornea)

The length of the heated corneal sample was measured to the nearest 1/32 inch and converted to centimeters after each heating step while the cornea was resting flat on a microscope slide. Figure 7.8 shows the changes that occurred in chords A and B (see Fig. 7.3) as a function of the bath temperature. No significant length changes were produced for temperatures below 57°C. At 64°C both chords A and B contracted to 65% of their original length. Chords A and B remained contracted to this length at 69°C. In this, and other corneas, the contraction process was monotonic - no creep was observed following contraction. When chords A and B shortened, the thickness of the cornea (C in Fig. 7.3) increased. The thickness change was not measured but was clearly visible while the sample was being heated.

### ii. Light transmission changes (cornea)

Light transmission was measured at 347nm after heating, while the cornea was mounted on the glass slide. The sample was slightly dried in vacuum for a few minutes to return the transmission to approximately the same value after each heating. In Fig. 7.9, the data points enclosed in circles show the 347nm transmission after the mild vacuum drying step before irradiation. The transmission was held to between 16% and 18%. (No drying was needed at 69°C). For comparison, the transmission at 347nm is shown for another rabbit cornea (data

points enclosed in squares; Fig. 7.9) that was taken through the same heating procedure except that no vacuum drying was performed. The transmission of this cornea was also relatively constant between 20°C and 51°C. At 57°C the transmission dropped by almost a factor of two. This drop preceded contraction. The transmission remained low at 63°C, where contraction was evident. At 64°C and 69°C the transmission rose markedly. The amount of contraction was approximately constant between 64°C and 69°C.

### iii. Birefringence changes (cornea)

Qualitative birefringence changes were monitored in the same way for corneas as for the tendons. Below the contraction temperature, the cornea was uniformly grey with crossed polarizer and analyzer. With parallel polarizer and analyzer, it was a brilliant white. This is indicative of low birefringence. After contraction, both grey and black areas were visible with crossed polarizer and analyzer. These grey and black areas became a brilliant white with parallel polarizer and analyzer.

These results are indicative of low birefringence for light propagating in the normal direction in the cornea both below and above the contraction temperature. The presence of black areas above the contraction temperature may indicate that some local reduction in birefringence occurred on contraction. The low initial birefringence of the corneas made it more difficult to observe birefringence changes

than had been the case with tendon.

iv. Second-harmonic conversion efficiency changes (cornea)

As was indicated in Section 7.2a.iv, the data for  $H_2$  versus  $H_1$  lies in two groups in Fig. 7.10. One group contains only points obtained from non-contracted corneas while the other group contains only points obtained from contracted corneas. A regression line was obtained for each group. Both groups are for corneas whose transmission had been adjusted to 17% transmission at 347nm.

The ratio of the slopes of the regression lines in Fig. 7.10 for corneas was about 10:1, which is indicative of the fact that two distinct data groups were present. The data group corresponding to thermally contracted cornea had consistently lower values of  $H_2$  over the range of  $H_1$  values employed.

7.2d Ancillary results

In an ancillary experiment, tendons were thermally contracted at 68°C both with and without a weight as described previously. However these tendons were removed from the bath at the time of maximal contraction (100 seconds), placed on microscope slides and dried in vacuum at 20°C. These tendons remained maximally contracted. "Fusion" of the tendon fiber bundles was evident; as was the case with contracted tendons in our principal studies. Several differences between these maximally contracted tendons and the previously described tendons

were noted. These tendons were amber in color rather than clear; their surfaces were badly wrinkled rather than smooth; they showed zones of qualitatively unaltered, high birefringence. The relative second-harmonic conversion efficiency of these maximally contracted tendons was much greater than that observed with the contracted tendons that had been allowed to creep and was slightly less than that for tendons that had not yet contracted. No transmission measurements were made on these samples. The observed changes in  $C_{MRF}$  may have been due to changes in the surface quality of the tissue, therefore these tissues could not be used for comparing  $C_{MRF}$  before and after the collagen phase transformation.

### 7.3 Discussion

When heated in water to a temperature of approximately 60°C, tendons, corneas and other collagenous tissues contract along the collagen fiber direction; become less birefringent; and generally become more transparent. Flory has reviewed evidence that suggests these changes are caused by a rigid-rod to random-coil phase transformation within the collagen molecules, of the tissue fibers (Flory, 1956). The collagen phase transformation temperature is different for different tissues and also depends on a number of experimental conditions such as tissue temperature history and hydration. For convenience in this discussion, we shall use 60°C as an approximation

to the collagen phase transformation temperature.

Below 60°C, the collagen molecule in tissue is a stiff, rope-like structure consisting of three helical polypeptide chains that are wound around each other in a lower pitch helical pattern. In this conformation, the collagen molecule is approximately 3000Å long and its diameter is approximately 14Å. Hydrogen bonds are considered to be responsible for the attachment of the polypeptide chains to each other and are also responsible for the helical structure of the individual chains (Schmitt, 1959, p. 35; Flory, 1956, pp. 56-58). The rigid rodlet collagen molecules are laid down in a regular parallel array and bound together by weak intermolecular bonds to form collagen fibrils (Fig. 7.12) (Flory, 1956, pp. 56-58).

In moist tissue near 60°C, there is a relatively narrow temperature range (less than 3°C) in which the intramolecular hydrogen bonds of the collagen molecules are broken (Flory, 1956, p. 57). When this occurs, the polypeptide chains also separate, lose their own helical structure, and become flexible macromolecules. These flexible chains assume a random-coil configuration (Flory, 1956, p. 58).

The thermal contraction of collagen fibers is generally attributed to the shortening of the distance between the polypeptide chain ends when the random coils are formed (Flory, 1956, pp. 55-56). The reduced birefringence of the tissue and tissue fibers is due to the greater isotropy of the random coil collagen phase (Banga, 1966, pp. 122-125).

The increase in tissue transparency has not been explained quantitatively; however a qualitative explanation can be constructed from current interpretations of light scattering in collagenous tissues.

There are no significant optical absorption bands for the normal cornea in a spectral region ranging from the middle ultraviolet ( $\sim 310\text{nm}$ ) to the very near infrared ( $\sim 900\text{nm}$ ) (Maurice, 1962, p. 316). This may also be true for the tendon. It has been suggested that the opacity or transparency of the cornea (and the sclera) is determined by light scattering (Benedek, 1971). Maurice has performed measurements that show the refractive index of collagen fibrils to be higher than that of the surrounding ground substance (Maurice, 1962, p. 313). Benedek has suggested that spatial variations in the number density and diameter of collagen fibrils produce spatial fluctuations in the refractive index of the tissue, and that, under certain conditions, these fluctuations can cause light scattering (Benedek, 1971). Direct back-scattering at a given wavelength is produced by spatial fluctuations in refractive index with dimensions of the order of one-half the wavelength in the tissue (Benedek, 1971, p. 464). Progressively more forward scattering is produced by spatial fluctuations of the refractive index that occur over dimensions much longer than a wavelength (Benedek, 1971, p. 464, Eq. 18). The tissue is opaque to a given wavelength when backscatter is predominant. The tissue is transparent to a given wavelength when the refractive index is uniform or when fluctuations in refractive index occur over dimensions that

are much smaller than half the wavelength in the tissue (Benedek, 1971, p. 464, Eq. 18).

According to Hart and Farrell, the collagen fibrils of fresh normal rabbit corneas are of small diameter (26nm), closely spaced (50nm) (Hart and Farrell, 1969, p. 766), and have spatial fluctuations in their number density extending over distances that are small compared to half the wavelength of visible radiation (Hart and Farrell, 1969, Fig. 2). Noticeable fluctuations with dimensions less than 150nm are present (Hart and Farrell, 1969, Fig. 2). Consequently, these corneas are relatively transparent to wavelengths longer than about 300nm but shorter than about 900nm (where water bands appear). Hydrated human corneas (corneas containing excess water) have spatial fluctuations in the number density of collagen fibrils with dimensions up to approximately 230nm according to Benedek (Benedek, 1971, p. 470). Benedek's model predicts that these fluctuations cause backscattering of wavelengths up to  $\sim 500$ nm (green light). Hydrated corneas are highly opaque to middle ultraviolet radiation ( $\sim 10\%$  transmission at 347nm) but are less opaque to red light ( $\sim 50\%$  transmission at 694nm) which is consistent with strong backscatter at wavelengths less than 500nm. These corneas are also blue in color under room lights.

Tendons contain irregularly positioned fibrils that range from about 30nm to 200nm in diameter (see Chapter 3). Both small and large fibrils are found together in any given region of the tissue. Spatial fluctuations of refractive index with dimensions ranging up to

200nm or more might be expected in this tissue. This may account for the low optical transmission of these tissues at middle ultraviolet wavelengths ( $\sim 2\%$  transmission at 347nm) and somewhat higher transmission for red light ( $\sim 20\%$  transmission at 694nm). Fresh tendons are white in color under room lights, therefore scattering must be relatively intense over most of the visible spectrum.

When cornea, sclera and tendon are dried, they are all relatively transparent. Maurice, in his studies of cornea and sclera, has suggested that this may be due to a concentration of the ground substance; which raises its refractive index to nearly that of the collagen fibrils (Maurice, 1969, p. 315 and p. 322). With a more uniform refractive index, light scattering should decrease at all wavelengths. This may also be true in tendon.

When tendon and hydrated cornea are heated above the collagen phase transformation temperature they become more transparent; as we have noted previously. Flory has suggested that this is generally observed during crystalline to amorphous polymer phase transformations (Flory, 1956, p. 54). When the phase transformation occurs, the collagen fibrils are converted to a random-coil material that is distributed over a slightly larger volume than the original fibril (Flory and Garrett, 1958, p. 4836). Flory suggests that if a flexible polymer of fully extended length  $r_{\max}$  is released, then the rms separation,  $r$ , between the chain ends in the released random coil configuration is

given by  $r = r_{\max} / \sqrt{n}$  where  $n$  is the number of flexible links in the polymer (Flory, 1956, p. 53). For a single collagen strand,  $n \sim 10^3$  and  $r_{\max} \sim 300\text{nm}$ ; therefore ideally  $r \sim 9.5\text{nm}$  for a collagen strand in a random coil configuration. If  $r$  is assumed to also be the approximate size of the random coil chain, then the size for this chain is about an order of magnitude smaller than the second-harmonic wavelength of the ruby laser in tissue. The spaces around the random coil molecules are presumably filled with water. Therefore, after the collagen phase transformation, the collagen is dispersed as very small particles which means that the refractive index of the tissues may become more uniform. Under conditions of a more uniform refractive index, light scattering should be reduced at all wavelengths, and the tissue should become more transparent.

This discussion has qualitatively related the contraction, loss of birefringence, and increase in transparency that occurs near  $60^\circ\text{C}$  in moist collagenous tissue to changes that are thought to occur in the collagen molecule and collagen fibril at this temperature. In addition to these changes, we have observed a decrease in the conversion of ruby laser radiation to forward scattered second-harmonic radiation after tendons and corneas were heated to  $60^\circ\text{C}$ . Since purified native collagen fibers have been shown to produce second-harmonic radiation (Chapter 5), this decrease in conversion efficiency may also be related to changes that occur in the collagen molecule during its phase transformation near  $60^\circ\text{C}$ .

In a previous section of this chapter, we have adopted the measured relative forward scattered second-harmonic conversion efficiency,  $C_{MRF}$ , as a measure of the ability of a tissue to generate forward scattered second-harmonic radiation.  $C_{MRF}$  was defined as the ratio of the oscilloscope pulse height  $H_2$  (second-harmonic) to the oscilloscope pulse height  $H_1$  (laser), recorded with the apparatus shown in Fig. 4.1.

In this discussion we will consider that there are three possible mechanisms by which the forward conversion efficiency,  $C_{MRF}$ , of tendons and corneas could have been altered when the collagen phase transformation occurred. These three mechanisms are:

1. Light scattering increased in the tissue
2. The nonlinear polarizability,  $\beta$ , of the nonlinear oscillators of collagen decreased
3. The mechanism for second-harmonic generation changed from coherent to incoherent second-harmonic generation (Chapter 2).

Let us consider the first mechanism - the effects of light scattering on the forward conversion efficiency,  $C_{MRF}$ .

If light scattering at the fundamental wavelength were increased, then the average intensity of the fundamental, in the collagenous tissue discussed, would decrease. A reduction in the fundamental intensity would decrease the conversion efficiency for either coherent or incoherent second-harmonic generation. If light scattering at 347nm

increased, then a beam of coherent second-harmonic radiation might be broadened beyond the collection angle of lens B in Fig. 4.1. This would lower the relative conversion efficiency  $C_{MRF}$  which is based on oscilloscope pulse heights. Both of these arguments can be reversed to show that  $C_{MRF}$  could increase if light scattering decreased.

In our experimental work, we used measurements of spectrophotometric transmission and visual examination as a qualitative means of determining when light scattering had increased or decreased in tendons and corneas. In hydrated corneas, our spectrophotometric measurements were limited to 347nm alone. (The time required to readjust the single beam spectrophotometer to monitor other wavelengths and obtain several measurements at each wavelength would have been sufficiently long that undesirable changes in the level of tissue hydration might have occurred). Since short wavelength scattering was predominant in hydrated corneas, a given change in 347nm transmission was expected to be accompanied by a smaller change in 694nm transmission. This supposition was found to be correct in tendon where measurements were carried out at 347nm and 694nm.

Tables 1 and 2 summarize our observations of optical transmission and relative forward conversion efficiency  $C_{MRF}$ . We shall first consider the tendon data in Table 1. Following heating in water below 60°C, it was found that moist tendons had very low 347nm and 694nm transmission. Drying these tendons resulted in an increase in optical

transmission at 347nm and 694nm, and also resulted in a corresponding increase in  $C_{MRF}$ . These increases were completely reversed when the tendons were rehydrated. Following heating in water above 60°C (above the contraction temperature) it was found that the 347nm and 694nm transmission of moist tendon was relatively high. Drying these tendons resulted in a further increase in transmission. Despite these increases in transmission, it was observed the  $C_{MRF}$  decreased above 60°C.

Now consider Table 2 which summarizes the data for corneas. When corneas were hydrated in a water bath below the contraction temperature, the 347nm transmission and  $C_{MRF}$  decreased. Drying these corneas reversed the above changes. When corneas were heated in a water bath above the contraction temperature, both the 347nm transmission and  $C_{MRF}$  decreased relative to fresh non-hydrated corneas at 20°C. When these corneas were dried, the above changes were not reversed.

A second set of cornea experiments were also carried out. In these studies, the 347nm transmission was "adjusted" to 17% following each water bath heating step. In this case, the value of  $C_{MRF}$  was constant below the contraction temperature but decreased by about an order of magnitude above the contraction temperature.

We believe that, below 60°C,  $C_{MRF}$  was affected mainly by changes in light transmission in both tendons and corneas. Decreases in light transmission were probably the result of increases in light scattering

and vice versa. On this basis, increased light scattering reduced  $C_{MRF}$  and decreased light scattering raised  $C_{MRF}$ . These results are consistent with our previous interpretation of the effect of light scattering changes, per se, on the forward conversion efficiency.

The decrease in  $C_{MRF}$  that accompanied the collagen phase transformation (Tables 1 and 2) was not due to an increase in light scattering. For example, tendon that had been dried after heating above the collagen phase transformation temperature had the highest optical transmission and also appeared to have the most regular surfaces and the clearest interior on visual examination (Table 1). Therefore, if light scattering alone affected  $C_{MRF}$ , it would have been expected to have the lowest light scattering and the highest conversion efficiency; however,  $C_{MRF}$  actually decreased markedly in comparison to tendon that had been dried after heating below the collagen phase transformation temperature (Table 1). We believe that this decrease in  $C_{MRF}$  that was observed above the collagen phase transformation temperature was not related to (increased) light scattering, but may have been related to changes in certain nonlinear properties of the tissue (mechanisms 2 and 3).

The conclusion that the decrease in  $C_{MRF}$  was not associated with increased light scattering was supported by our results from the cornea. In our corneal studies it was found necessary to adjust the hydration of the tissue after each heating step in order to maintain a constant

347nm transmission (17%) at each irradiation step (Table 2). With the 347nm transmission constant, the forward conversion efficiency decreased markedly after heating the cornea above the collagen phase transformation temperature (Table 2). If the 347nm transmission was, indeed, a measure of light scattering changes, and if light scattering changes alone affected  $C_{MRF}$ , then we would have expected  $C_{MRF}$  to be constant when the 347nm transmission was constant. The fact that  $C_{MRF}$  decreased after the cornea had been heated above the collagen phase transformation temperature (while light scattering was expected to be constant as measured by the 347nm transmission) indicated that  $C_{MRF}$  was affected by a mechanism other than light scattering changes. The decrease in  $C_{MRF}$  may have been caused by changes in certain nonlinear properties of the cornea (mechanisms 2 and 3).

There were a number of other combinations of hydration and temperature history for which changes in  $C_{MRF}$  were observed in both tendons and corneas. In these cases one could not separate the effects of light scattering on  $C_{MRF}$  from the possible effects of changes in the nonlinear properties of the tissue (Tables 1 and 2).

In summary, then, we have presented evidence that a mechanism other than changes in the light scattering properties of tendons and corneas could be responsible for the observed decrease in  $C_{MRF}$  near the collagen phase transformation temperature. While there are a number of tissue optical properties that may change near this

temperature, we believe that it is important that we examine two specific nonlinear optical properties for changes that could lower  $C_{MRF}$ . These changes were stated previously as mechanisms 2 and 3. For convenience they are restated again below.

mechanism 2. The nonlinear polarizability,  $\beta$ , of the microscopic subunits of the collagen molecule might have been reduced by the collagen phase transformation.

mechanism 3. The mechanism for second-harmonic generation changed from coherent to incoherent second-harmonic generation (Chapter 2).

We shall begin our discussion of mechanism 2 by identifying the microscopic subunits of the collagen molecule that may be important for second-harmonic generation at 347nm. An important subunit will be one that has a relatively large (second-order) nonlinear polarizability,  $\beta(\omega, 2\omega)$ , where  $\omega$  corresponds to the ruby laser frequency ( $\omega = 2.7 \times 10^{15}$  rad/sec).

A large molecule, like collagen, contains many subunits. Each subunit in turn may behave like a quantum mechanical system with several electronic energy transitions corresponding to optical photon energies  $h\omega_j$ . In a linear classical model of a dipole oscillator, each of these transitions is analyzed as an independent damped harmonic oscillator with resonant frequency  $\omega_j$ , oscillator strength  $f_j$ , and bandwidth  $\Gamma_j$ .

In the case of a nonlinear noncentrosymmetric restoring force, the damped anharmonic oscillator with quadratic restoring force  $m\Omega_j X^2$  is often used to model the corresponding quantum mechanical transition. In the anharmonic restoring force,  $m$  is the electron mass,  $\Omega_j$  is the anharmonic coefficient and  $X$  is the oscillator displacement. This nonlinear oscillator model can be used to describe second-harmonic generation (Chapter 2).

Each anharmonic oscillator contributes an amount  $\beta_j(\omega_j, \Gamma_j, f_j, \Omega_j; \omega, 2\omega)$  to the overall second-order nonlinear polarizability,  $\beta(\omega, 2\omega)$ , of the subunit (Chapter 2, Section 2.4). Thus:

$$\beta(\omega, 2\omega) = \sum_{j=1}^N \beta_j(\omega_j, \Gamma_j, f_j, \Omega_j; \omega, 2\omega) \quad (2)$$

where

$$\beta_j = \frac{f_j^2 \Omega_j e^3}{m^2} \frac{1}{(\omega_j^2 - \omega^2 - j\Gamma_j \omega)^2 (\omega_j^2 - 4\omega^2 - 2j\Gamma_j \omega)} \quad (3)$$

( $e$  is the charge of the electron and  $m$  is the mass of the electron.

The equations are in terms of Gaussian cgs units (Chapter 2, Appendix A).

From Eqs. 2 and 3, it can be seen that strong oscillator resonances near  $\omega$  or  $2\omega$  make the greatest contribution to  $\beta(\omega, 2\omega)$ . For the ruby laser,  $\omega$  is the frequency of "deep red" radiation ( $\lambda = 694.3\text{nm}$ ,

$\omega = 2.7 \times 10^{15}$  rad/sec) and  $2\omega$  is a "middle ultraviolet" frequency ( $\lambda/2 = 347.2\text{nm}$ ,  $2\omega = 5.4 \times 10^{15}$  rad/sec). Therefore, one would expect that strong ultraviolet absorption bands and strong visible and near infrared absorption bands could have the greatest effect on  $\beta$ . This, of course, presupposes that these bands correspond to non-centrosymmetric anharmonic oscillator resonances.

For collagen, most of the readily available spectroscopy literature deals with ultraviolet spectra between 180nm and 320nm. For example, a standard handbook of visible and ultraviolet spectra of proteins gives the optical density of corneal collagen solutions only up to 320nm of wavelength in the ultraviolet, and does not show a near ultraviolet or visible spectrum (Kirschenbaum, 1972, p. 59). Based on other entries in this handbook, this is indicative of there being no known absorption bands in these latter regions. We have found no absorption bands in concentrated solutions of rat-tail tendon collagen in HCl over the wavelength range 400nm-700nm. While very thick and viscous, these solutions are extremely clear to the unaided eye. According to measurements made by Langham, the rabbit cornea, which contains 13% collagen by weight, is quite transparent from 350nm to 900nm with no evidence of absorption bands in this region (Hart and Farrell, 1968, Fig. 4). The transparency of the cornea decreases sharply at wavelengths between 350nm and 300nm, but this is mainly due to scattering (Hart and Farrell, 1969). There are absorption bands for the cornea between 900nm and  $1.4\mu$ , however, these are similar to those

for water (Ham et al, 1966, p. 518) and may not be associated with collagen per se. Based on the above information, it appears that there are no oscillator resonances in collagen near the fundamental frequency of the ruby laser.

There are oscillator resonances in collagen that are relatively near the second-harmonic frequency of the ruby laser. For example, the strongest absorption peak that has been identified with collagen lies at 190nm (Gratzer et al, 1963). Some references show a much weaker absorption peak between 280nm and 290nm (Kirschenbaum, 1972, p. 59). The height of this peak depends upon the history of the collagen, and the peak has been shown to virtually disappear when the collagen preparation has been carefully purified (VanWinkle, 1954). We shall neglect this peak in our analysis of collagen.

The 190nm peak in collagen is associated with the peptide subunit (Gratzer et al, 1963). The peptide subunit is a link appearing between each amino acid subunit on a given protein polypeptide chain. In proteins that form  $\alpha$ -helices, there are other observable peaks associated with the peptide subunit. In these instances the peptide band is split into a 190nm peak (strong), a 150nm (slightly weaker), 200nm (very weak), and 165nm (weak) (Wetlaufer, 1962, p. 329). This band splitting has not been observed in the poly-L-proline II helix which is not an  $\alpha$ -helical polypeptide (Gratzer et al, 1963 p. 325). The collagen helix is thought to be similar to that of poly-L-proline

II (Gratzer et al, 1963, p. 320). Gratzer does not show any band splitting of the 190nm peak in his collagen spectra (Gratzer et al, 1963, Fig. 5). If there was any band-splitting it may not have been resolved in Gratzer's experiments. We shall assume that the 190nm peak is the only resonance for the peptide link in collagen.

There does not appear to have been any reported studies of collagen absorption spectra at wavelengths shorter than about 185nm. This is not surprising in view of the difficulties encountered in obtaining transparent diluents for proteins at these short wavelengths. Some studies have been performed at short wavelengths on the amino acids that can be found in collagen. In a review article by Yannas, he stated that while there are possibly as many as 18 different amino acids in human tendon collagen (Yannas, 1972, p. 46) only a few are present in significant amounts. In terms of the approximate number of residues per 1000 total residues, there are 111 alanine residues, 324 glycine residues, 126 proline residues, 92 hydroxyproline residues, 72 glutamic acid residues, and 275 miscellaneous residues in human tendon collagen (Yannas, 1972, p. 46). The absorption peaks of the amino acids that appear in significant numbers in collagen appear to lie at wavelengths shorter than 185nm in the spectra shown by Wetlaufer (Wetlaufer, 1962). The exact location of all these peaks may be as yet unknown. While absorption by these amino acids seems to be strong, Gratzer et al have calculated that, at 190nm, only 17% of the observed absorption is due to amino acids, while 83% of the absorption is due

to the peptide bond (Gratzer et al, 1963, p. 326). This may indicate that the significant collagen amino acid peaks lie at wavelengths that are much shorter than 190nm and therefore may not be significant to second-harmonic generation at 347nm.

A number of amino acid crystals including alanine, proline, hydroxyproline, and glutamic acid have been shown to generate the second-harmonic of ruby laser radiation (Reickoff and Peticolas, 1965). Glycine is an exception that will be discussed later. Second-harmonic generation by peptide links has not yet been definitively demonstrated although poly-glycine may be useful for this purpose. We shall show evidence that the peptide link oscillator in collagen is bound by a non-centrosymmetric restoring force. According to the scalar model of Chapter 2, second-harmonic dipole moments can occur in non-centrosymmetrically bound oscillators.

The evidence for the non-centrosymmetry of the collagen peptide link is contained in studies of the optical activity of collagen solutions. In optically active media, one can consider that a plane polarized incident wave is decomposed into right-handed and left-handed circularly polarized waves in the medium. The right-handed wave travels with a phase velocity  $c/n_R$  and the left-handed wave travels with a phase velocity  $c/n_L$  in the medium, where  $n_R$  and  $n_L$  are the refractive indices of right-handed and left-handed waves respectively. The medium can be isotropic (eg. liquid); in which case these phase

velocities are independent of the original incident wave polarization direction and propagation direction. In anisotropic media the incident wave is decomposed into elliptically polarized waves, where the ellipticity is direction sensitive. We shall only consider isotropic liquid media. The rotation of the incident wave polarization is a result of the difference in phase velocities of the circularly polarized waves. The specific rotatory power of the liquid  $[\alpha]$  is defined by  $[\alpha] = \alpha/Lc'$ ; where  $\alpha$  is the net angular rotation of the plane of polarization in degrees,  $L$  is the distance travelled in the liquid in decimeters, and  $c'$  is the concentration of optically active solute in gms per ml (Urnes and Doty, 1961, p. 405). The specific rotatory power is wavelength dependent. This dependency is called optical rotatory dispersion.

For a molecule to produce optical activity in liquid solution, it is necessary that it be both non-centrosymmetric and lacking in a plane of symmetry (Sommerfeld, 1964, p. 164). Condon, Altar, and Eyring have shown that optical activity can be modeled by assuming a single dipole oscillator moving in a force field having these same unsymmetrical characteristics (Condon et al, 1937; Glasstone, 1946, p. 608). Some previous models had been based on coupled dipole oscillators (Glasstone, 1946, pp. 607-608). In Chapter 2, it was shown that when a dipole oscillator moves under the influence of a non-centrosymmetric restoring force, then it is possible to produce a second-harmonic dipole moment in that oscillator. Since the

oscillators responsible for optical activity move under the influence of non-centrosymmetric restoring forces, then it should be possible for these oscillators to have second-harmonic dipole moments and produce second-harmonic radiation.

In optically active media, the specific rotatory power  $[\alpha]$  increases markedly when the wavelength of the incident radiation approaches the absorption band of an oscillator that participates in optical activity. In some materials, where absorption is weak enough, one can explore optical activity within an absorption band. Sometimes, when this is done, one observes a maximum in rotation near the band, then a decrease to zero rotation within the band, and finally an increase to a second maximum of rotation in the opposite sense on the other side of the band. The general name of Cotton effect is applied to these observations (Glasstone, 1946, p. 605). According to Glasstone, the angle of rotation becomes zero and is reversed in sign in an absorption band only when the oscillator producing that band is the sole, or by far the most important, contributor to the total observed optical activity (Glasstone, 1946, p. 606). When this is not the case, the dispersion curve does not pass through a zero of rotation but does show an inflection point. This is due to a steadily increasing or decreasing contribution from another oscillator added to that of the absorption band under consideration (Glasstone, 1946, p. 606).

Collagen solutions have been shown to be optically active (Blout et al, 1963). A large Cotton effect has been observed at 195nm (Blout et al, 1963, p. 645), which is within the 190nm absorption band of the collagen peptide link (Gratzer et al, 1963, Fig. 5). According to the above discussion, this indicates that the 190nm peptide band is the sole, or by far the most important, contributor to optical activity that has been observed in collagen. The amino acid oscillators, which have shorter wavelength absorption bands, do not significantly contribute to the observed optical activity of collagen according to the interpretation that we have adopted from Glasstone. Furthermore, according to the previous discussion of optical activity, the peptide link oscillator in collagen is bound by a restoring force that is non-centrosymmetric for most directions of oscillation. This discussion indicates that the collagen peptide link oscillator is capable of optical second-harmonic generation. Conformational changes in collagen may affect the second-harmonic generation properties of the peptide link.

With present day information it is not possible to determine whether all of the amino acid oscillators of collagen have larger or smaller values of  $\beta$  than the peptide link for second-harmonic oscillations induced by a ruby laser. The missing values of  $f_j$ ,  $\Gamma_j$ ,  $\omega_j$ , and  $\Omega_j$  for the amino acids would be required for this determination (some of these values are available for the peptide link).

For the purposes of the remainder of this discussion we will assume that the amino acid oscillators of collagen have much smaller polarizabilities,  $\beta$ , than the peptide link at the second-harmonic frequency of the ruby laser. This assumption is loosely based first on the observation that the 190nm peptide link absorption band is closer to the ruby laser second-harmonic wavelength than the amino acid absorption bands. A second basis is that glycine, which is a centrosymmetric molecule, constitutes approximately 33% of the amino acid content of the collagen macromolecule (Yannas, 1972, p. 46). Being centrosymmetric, the glycine  $\beta$  should be zero. This has been partially confirmed by Reickhoff and Peticolas (Reickhoff and Peticolas, 1965), who observed very low levels of second-harmonic radiation from crystalline glycine compared to other crystalline amino acid preparations. We have performed similar experiments with glycine and have observed no detectable second-harmonic radiation (see Chapter 4). Peptide links should therefore outnumber the amino acid subunits that can yield second-harmonic radiation in a given collagen molecule.

In summary, then, there are several optical frequency resonances in the far ultraviolet and vacuum ultraviolet that are associated with the peptide links and amino acids of collagen. Some of these resonances appear to be relatively far removed from the ruby laser second-harmonic frequency. One resonance, the 190nm absorption band of the peptide link, appears to be both sufficiently strong and

sufficiently close to the ruby laser second-harmonic to make a major contribution to the second-order polarizability  $\beta(\omega, 2\omega)$ .

For the remainder of this discussion, we will assume that the peptide link is the only subunit and that the 190nm transition represents the only oscillator that contributes to  $\beta(\omega, 2\omega)$  in collagen where  $\omega$  is the ruby laser frequency. Equation 2, in this case, is reduced to one term:

$$\beta(\omega, 2\omega) = \beta_p(\omega_p, \Gamma_p, f_p, \Omega_p; \omega, 2\omega) \quad (4)$$

where the subscript "P" stands for the 190nm peptide resonance and  $\omega$  is the ruby laser frequency.

We now wish to determine whether  $\beta_p(\omega, 2\omega)$  given by Eq. 4 changes during the collagen phase transformation. We note that  $\beta_p$  depends on a number of properties such as  $\omega_p$ ,  $f_p$ , and  $\Gamma_p$  that affect linear as well as nonlinear interactions. Therefore, changes in  $\omega_p$ ,  $f_p$ , and  $\Gamma_p$  that occur during the collagen phase transformation should be evident from the ordinary linear spectroscopy of the peptide link. Such spectroscopy has been performed by Wood (Wood, 1963) in the range 185nm to 230nm for collagen molecule solutions at temperatures that ranged from below to above the collagen phase transformation temperature. He observed a slight temperature broadening of the 190nm band, a slight ( $\sim 3\%$ ) increase in the extinction at 190nm, no apparent shift in the

wavelength position of the peak and a slight distortion of the shape of the absorption band. Wood believes that these changes in the 190nm band were produced by the rigid-rod to random-coil conformational change in the collagen polypeptides during the phase transformation. He notes that these spectral changes are small compared to those that occur in  $\alpha$ -helical proteins during thermal denaturation (collagen is not an  $\alpha$ -helical protein). It seems reasonable to assume that  $\omega_p$ ,  $f_p$  and  $\Gamma_p$  are invariant during the collagen phase transformation in solution. We will extend this assumption to collagen in tissue as well.

We have no way of directly ascertaining whether the anharmonic coefficient  $\Omega_p$  for the peptide oscillator in Eq. 4 changes during the collagen phase transformation. There is, however, some indirect evidence that  $\Omega_p$  may change. Blout et al have observed a significant reduction in the optical rotatory power of collagen solutions near 190nm during the collagen phase transformation (Blout et al, 1963, p. 646). Since optical activity requires a lack of inversion center and a lack of any mirror planes, it is conceivable that the observed changes in optical activity are related to possible changes in the symmetry properties of the individual peptide link or the inter-relationships between the peptide links of the molecule. Changes related to inversion symmetry could in turn affect  $\Omega_p$ , which exists only when there is a lack of inversion symmetry. There is no clear evidence that the specific rotatory power  $[\alpha]$  in collagen is related

to  $\Omega_p$ , however, there is a possibility of such a relationship occurring. The exploration of this relationship is beyond the scope of this dissertation.

In summary, then, using spectroscopic evidence by Gratzer et al and Wood,  $\omega_p$ ,  $f_p$  and  $\Gamma_p$  do not appear to be significantly changed during the collagen phase transformation (Gratzer et al, 1963; Wood, 1963). Insofar as these affect  $\beta(\omega, 2\omega)$  for collagen we would expect second-harmonic generation to also be unchanged by the collagen phase transformation. However, we have indicated that it is difficult to assess changes in  $\Omega_p$  and, indeed, there are some reasons, based on a decreased Cotton effect in collagen during denaturation (Blout et al, 1963) to consider possible changes in  $\Omega_p$  during the collagen phase transformation. A reduction in  $\Omega_p$  would reduce the second-harmonic conversion efficiency of the peptide bond by reducing  $\beta_p(\omega, 2\omega)$  (Eq. 3).

So far we have considered two mechanisms for the observed reduction in the second-harmonic conversion efficiency of cornea and tendon after the collagen phase transformation. Evidence was presented to show that mechanism 1 (an increase in light scattering) was not a reasonable explanation for the reduction in  $C_{MRF}$ . We have seen that there is some possibility that  $\beta$  for collagen may be reduced during the phase transformation (mechanism 2) as a result of a reduction in  $\Omega_p$  as discussed above.

We shall now consider mechanism 3 which involves changes from coherent to incoherent second-harmonic generation. With regard to mechanism 3, if coherent second-harmonic generation occurs in the fibers of tendons and corneas, then a change in the second-order dielectric susceptibility  $\chi_2$  (Eq.35, Chapter 2) for these fibers will change  $C_{MRF}$ . If the fibers are changed to an amorphous material then  $\chi_2$  will become very small ( $\chi_2 = 0$  in an ideal amorphous material) without any necessary change in  $\beta(\omega, 2\omega)$ .

In the tendon, the fibril sizes cover a broad range and the spatial distribution of these fibrils is not known. Since there is not enough information on the optical properties of tendon, calculation of second-harmonic conversion efficiency in this tissue is difficult. Therefore, calculations will be limited to the cornea where optical properties information is available.

As a specific example, let us consider second-harmonic generation in a single corneal lamella from a normal rabbit eye. This lamella will typically have the appearance of a thin slab with length  $\sim 1\text{cm}$ ; width  $\sim 200\text{microns}$ ; and thickness  $\sim 2\text{microns}$  (Chapter 3). In the cornea, light propagates along the direction of the lamella thickness. To simplify our calculations, we will model this lamella as follows (Fig. 7.11):

1. The model lamella will be an infinite slab (length =  $\infty$ , width =  $\infty$ ) with thickness =  $2\text{microns}$ .

2. The model lamella has a constant second-order dielectric susceptibility  $\chi_2$  (Chapter 2).
3.  $\chi_2$  is derived from the spatial average number density of collagen peptide bonds in the model lamella (See Appendix A for details regarding this assumption).
4. Incident radiations at  $\omega$  and second-harmonic radiation at  $2\omega$  propagate as uniform plane waves along the direction of the model lamella thickness.
5. At  $\omega$  and  $2\omega$ , the refractive index and the optical dispersion of the model lamella is equal to that of water, and is constant throughout the medium.
6. There is no light scattering at  $\omega$  and  $2\omega$ ; and the medium is considered to be lossless.
7. Since the second-harmonic conversion efficiency has been experimentally determined to be low, we shall assume no attenuation of the incident beam at  $\omega$  due to harmonic generation.

In Chapter 2 we have reviewed the results of a coherent second-harmonic conversion efficiency analysis in nonlinear slabs with properties similar to those assumed above. There, it was shown that a second-harmonic wave will grow monotonically from relatively in-phase contributions from the oscillating second-harmonic polarization

over distances less than:

$$L_{\text{coh}} = \lambda/4\Delta n \quad (5)$$

where  $\lambda$  is the vacuum wavelength of the ruby laser (694.3nm) and  $\Delta n$  is the dispersion of the medium between  $\omega$  and  $2\omega$ . Using assumption 5, that the refractive index of the slab is that of water, we have  $\Delta n = 0.18$  (ICT, Vol. 7, p. 14). Therefore,  $L_{\text{coh}} = 9.6$ microns in the model lamella. On this basis we expect that a second-harmonic wave will grow monotonically in a 2micron thickness model lamella.

This monotonic growth of a second-harmonic travelling wave will not occur in the model lamella if we alter the model to represent the lamella after the collagen phase transformation. To alter the model we need only change assumptions 2 and 3 above. Assumption 2 is replaced by:

- 2a. The thermally transformed model lamella is amorphous and therefore, macroscopically centrosymmetric. Consequently, the second order dielectric susceptibility,  $\chi_2$ , is zero everywhere.

This accounts for the fact that, under ideal conditions, the lamella is converted to an isotropic random coil material after the collagen phase transformation. This also accounts for the fact that both the

tensor and scalar second-order nonlinear susceptibilities become zero in a centrosymmetric medium (Franken and Ward, 1963). In assumption 3, the spatial averaging over the peptide bonds yields  $\chi_2 = 0$  in the amorphous lamella. Thus, assumption 3 is replaced by:

3a.  $\chi_2 = 0$  in the thermally transformed model lamella.

With  $\chi_2 = 0$ , the transformed model lamella cannot support a macroscopic second-harmonic polarization that could act as a source for coherent second-harmonic generation. Therefore, assuming this polarization to be a necessary condition, coherent second-harmonic generation will not occur in the thermally transformed model lamella. (This does not preclude the possibility of the occurrence of incoherent second-harmonic generation).

The above changes in  $\chi_2$  occur because the peptide link oscillators are assumed to be randomly oriented in the thermally transformed lamella. The value of  $\beta_p(\omega, 2\omega)$  can remain unchanged during the collagen phase transformation. After the collagen phase transformation, incoherent second-harmonic generation by the individual peptide links may still occur. In Chapters 2 and 6, it was shown that incoherent second-harmonic generation from amorphous media is an inherently weak process with low forward conversion efficiency.

If a complete transformation to an amorphous state occurred in a corneal lamella, then we would expect the forward conversion efficiency

of the transformed lamella to be very low compared to that for our model of a normal lamella. In order to make this comparison on an analytical basis we will need models for both the normal and thermally transformed whole cornea. Simple models can be constructed for normal and completely thermally transformed corneas from our models for single lamellae; where transformation is not complete, analysis becomes difficult.

We shall assume that coherent second-harmonic generation occurs independently in each model lamella before the collagen phase transformation. Therefore, the total second-harmonic energy generated by the cornea will be assumed to be the sum of the energies generated by each model lamella. The spacing between lamellae in real corneas may be partially determined by the presence of large flat cells, called fibroblasts, between the lamellae. This spacing is irregular; therefore there may be only a very low correlation in phase between second-harmonic travelling waves generated in separate lamellae (Fig. 7.11). In our model we will assume that this correlation is zero, which leads to the assumption of additive energies.

In Appendix A of this chapter we have calculated the coherent forward power conversion efficiency  $C_{CP}$  for a model cornea consisting of 200 model lamella. This number of lamellae is based on estimates by Maurice in the human eye (Maurice, 1969, p. 297) (and estimates of the thickness of a particular moist rabbit stroma that was used

in one of our studies), a 2micron model lamella thickness, and a 15% allowance for the space occupied by cells between lamellae in the stroma. The laser pulse was assumed to be a plane wave field confined to a uniformly illuminated circular area 2mm in diameter. A 75nsec, 20mJ pulse was assumed. The calculated value of  $C_{CP}$  for the whole model cornea is (Appendix A):

$$(C_{CP})_{\text{cornea}} = 9.8 \times 10^{-10}$$

with an estimated peak error range of plus or minus a factor of 30.

In Appendix B we have used a simple model for a whole cornea, after a complete collagen phase transformation, to estimate the incoherent conversion efficiency. In this model, we have assumed that the peptide link concentration after the phase transformation is the same as the spatial average concentration of peptide links in a lamella before the phase transformation. The other assumptions regarding scattering and uniformity remain the same. We have used the model presented in Chapter 2 to calculate  $C_{IP}$  for incoherent second-harmonic generation from independent, randomly oriented peptide oscillators in the transformed stroma. The laser pulse was again assumed to be 20mJ, 75nsec, and confined to a 2mm diameter beam. The collecting lens was assumed to be as shown in Fig. 4.1. Based on this lens, our calculated value of the forward, incoherent, power conversion efficiency,  $C_{IPF}$ , for a completely thermally transformed

cornea is (Appendix B):

$$(C_{IPF})_{\text{cornea}} = 6.9 \times 10^{-16}$$

with an estimated peak error range of plus or minus a factor of 600.

Let us summarize the model cornea calculations. The coherent conversion efficiency  $(C_{CP})_{\text{cornea}}$  has been calculated as  $(C_{CP})_{\text{cornea}} = 9.8 \times 10^{-10}$ . This conversion efficiency is assumed to hold for a normal, non-hydrated cornea that is completely transparent. The incoherent conversion efficiency for radiation collected by lens B in the forward direction has been calculated as  $(C_{IPF})_{\text{cornea}} = 6.9 \times 10^{-16}$ . This conversion efficiency is assumed to hold for a completely transparent, completely thermally transformed cornea. The forward conversion efficiency is, therefore, predicted to decrease by a factor of from  $10^2$  to  $10^8$  when the corneal collagen is transformed to a completely random coil state. These calculations assume no change in the second-harmonic oscillators (peptide bonds), other than a change from perfect mutual alignment to a condition of randomly oriented independent oscillators. This is the underlying assumption on which mechanism 3 is based.

The above calculations could not be completely checked experimentally because  $(C_{IPF})_{\text{cornea}} = 6.9 \times 10^{-16}$  was too small to be measured with available instrumentation. The computed value of

$(C_{CP})_{\text{cornea}} = 9.8 \times 10^{-10}$  was checked experimentally. A fresh non-hydrated normal rabbit cornea at 20°C was used to obtain a value of  $C_{MPF}$ , which is the measured forward peak-power conversion efficiency.  $C_{MPF}$  should agree with the calculation of  $(C_{CP})_{\text{cornea}}$  given above. Details of the methods used to measure  $C_{MPF}$  are given in Appendix C. The results of these measurements gave the following range for  $(C_{MPF})_{\text{cornea}}$ :

$$1.2 \times 10^{-11} \leq (C_{MPF})_{\text{cornea}} \leq 1.7 \times 10^{-10}$$

This range is based on estimates of peak measurement errors.

The accompanying table shows the computed values of  $(C_{IPF})_{\text{cornea}}$ ,  $(C_{CP})_{\text{cornea}}$  and the measured range for  $(C_{MPF})_{\text{cornea}}$ . The estimated ranges of error are also given.

	<u>Upper bound</u> <u>estimate</u>	<u>Estimated</u> <u>mean</u>	<u>Lower bound</u> <u>estimate</u>
$C_{IPF}$	$4.1 \times 10^{-13}$	$6.9 \times 10^{-16}$	$1.2 \times 10^{-18}$
$C_{CP}$	$2.9 \times 10^{-8}$	$9.8 \times 10^{-10}$	$3.3 \times 10^{-11}$
$C_{MPF}$	$1.7 \times 10^{-10}$	$9.1 \times 10^{-11}$	$1.2 \times 10^{-11}$

The estimated range of measured conversion efficiency of a normal rabbit cornea partly overlaps the estimates range of calculated conversion efficiency based on coherent second-harmonic generation in independent lamellae. The lower limit of the measured conversion

efficiency ( $1.2 \times 10^{-11}$ ) is about 30 times lower than the highest estimate of the calculated conversion efficiency ( $4.1 \times 10^{-13}$ ) based on incoherent second-harmonic generation from randomly oriented independent peptide bonds in the cornea. In Chapter 6, it was shown that a distinct forward lobe was present in the forward emission pattern of second-harmonic radiation from the rabbit cornea. This was shown to be consistent with coherent second-harmonic generation from a crystalline medium. The conversion efficiency measurements and the emission pattern measurements are not inconsistent with the hypothesis that optical second-harmonic generation at 347nm in freshly excised rabbit corneas occurs much like coherent second-harmonic generation in crystalline materials. Peptide bonds in collagen may be the principal second-harmonic oscillators, and coherent second-harmonic generation may occur within individual lamellae. It will require a substantial program of future investigation to verify these preliminary hypotheses.

The results of our calculations in Appendix B for incoherent second-harmonic generation do not agree with our experimental observations. From Appendix B we calculated that if a complete transformation to a random coil phase occurred in collagen, then the forward conversion efficiency of the rabbit cornea should be from  $10^2$  to  $10^8$  times lower than it was before the phase transformation. We have found in practice that  $C_{MRF}$  was only about a factor of 50 times lower in hydrated corneas that had been heated above the collagen phase

transformation when compared to  $C_{MRF}$  from fresh normal corneas (Table 2). The thermally transformed corneas in this comparison were turgid whereas the fresh corneas were not. Therefore, light scattering differences could account for some of the observed decrease in  $C_{MRF}$ . When corneas with approximately the same transmission were compared (Table 2) it was found that  $C_{MRF}$  decreased by about a factor of 10 after the collagen phase transformation. Therefore, our experimental results indicate that  $C_{MRF}$  decreased by between one and two orders of magnitude rather than by from 2 to 8 orders of magnitude during the collagen phase transformation in corneas.

The theoretical estimate of  $C_{IPF}$  after the collagen phase transformation was based partially on the assumption that all of the collagen molecules had been converted to a random coil form and that incoherent second-harmonic generation predominated. Our experimental results may indicate that only part of the corneal collagen was converted to a random-coil form and that the remaining collagen still produced significant levels of coherent second-harmonic generation.

It is possible that not all of the collagen was converted to a random coil form. Let us assume that  $C_{CP}$  for coherent second-harmonic generation was affected only by a decrease in the number of aligned peptide bonds after the collagen phase transformation. Since  $C_{CP}$  is proportional to  $(N_{vpa})^2$ , where  $N_{vpa}$  is taken to be the number of aligned peptide oscillators, we can estimate for the cornea that a

factor of 10 decrease in  $C_{CP}$  could be caused by about a factor of 3 decrease in  $N_{vpa}$  and a factor of 100 decrease in  $C_{CP}$  could be caused by a factor of 10 decrease in  $N_{vpa}$ . Therefore, the observed decrease in  $C_{MRF}$  may have been produced by a conversion of from 70% to 90% of the collagen molecules in the cornea to a random coil form. The unaltered fraction of the collagen may have been in the form of fibril regions that still contained intact, aligned collagen molecules, or contained unravelled collagen polypeptide chains that, due to possible cross-linking hinderances, had not assumed a random coil conformation but rather remained extended and parallel to intact collagen molecules. The above calculation is not exact and neglects the contribution from incoherent second-harmonic generation.

Flory has pointed out that to completely convert the collagen molecules of tissue fibers to a random coil form it is necessary to raise the temperature of the fiber very slowly (Flory and Garrett, 1956). In his studies, fiber temperatures were raised at the rate of approximately 2°C per day. In these lengthy experiments it was necessary to heat the fibers in ethylene glycol rather than in water to prevent fiber decomposition. We considered a replication of Flory's procedures, but it would have been too time-consuming and required temperature control equipment that was not at our disposal. As a result, the tissues used in our studies were heated quickly in water at rates of about 10°C per minute. Although we observed tissue contraction at the temperature generally associated with the collagen

phase transformation, it was probably true that we did not achieve a complete transformation of the collagen to a random coil phase as indicated by Flory.

According to a recent review (Elden, 1968), Puette has suggested that a complete transformation of collagen to a random coil phase is best detected by a complete loss of fiber birefringence. Our observation of a residual birefringence in both corneas and tendon may also have provided evidence that the collagen phase transformation was not complete.

Calculations for tendon have not been presented; partly because of the inherent difficulties associated with second-harmonic generation calculations for a medium with significant light scattering and irregular surfaces. Qualitatively, it is reasonable to conclude that coherent second-harmonic generation could occur in local sites such as the fibers and fibrils of dried tendon that had not undergone a collagen phase transformation. After the phase transformation, the conversion efficiency of these fibers and fibrils could be reduced by mechanism 3. An improved method for preparing tendons for optical studies must be developed before quantitative analyses are possible. For example, immersing the tendon in an oil of matching refractive index may improve the optical quality at the interface.

To summarize our investigation of mechanism 3; it appears that coherent second-harmonic generation may occur in corneas (and possibly

in tendons) below the collagen phase transformation temperature, but that above this temperature a partial replacement of native collagen by a random coil phase of collagen can reduce the second-harmonic conversion efficiency of the tissue fibers. It is difficult to say whether the reduction in the measured forward conversion efficiency,  $C_{MRF}$ , occurs as a result of a uniform decrease in the spatial average number density of the peptide bonds in a lamella or fiber, or whether macroscopic regions of the lamella or fiber remained intact while other distinct regions became "100%" random coil.

#### 7.4 Summary and conclusions

After heating tendon and cornea in water at approximately 60°C (plus or minus about 3°C), we observed a tissue contraction; a decrease in tissue birefringence; and a decrease in light scattering. With respect to the last observation, it was noted that tendons became transparent relative to their normal state and corneas became transparent relative to their hydrated state. These changes can be related to a rigid-rod to random-coil phase transformation in the tissue collagen which has been described by other investigators. After the collagen phase transformation in these tissues, we also observed a marked decrease in the second-harmonic conversion efficiency,  $C_{MRF}$ , for forward scattered second-harmonic radiation.

Three possible mechanisms for the observed decrease in the measured relative forward conversion efficiency,  $C_{MRF}$ , were considered.

The first, that this was due to increased light scattering, was shown to not be a reasonable explanation. We obtained a marked decrease in  $C_{MRF}$  even when light scattering decreased after the collagen phase transformation.

The second possible mechanism was related to changes in the nonlinear polarizability,  $\beta$ , of each of the nonlinear oscillators of tendon and cornea. A literature review of the linear optical properties of collagen indicated to us that these oscillators may be associated with the 190nm absorption band for the collagen peptide link. According to a simple scalar model for the peptide link second-order nonlinear polarizability,  $\beta_p$ , there are four explicit factors, which, if changed during the collagen phase transformation, would produce a change in  $\beta_p$ . The literature review indicated that three factors; the oscillator strength, linewidth and center frequency are essentially unchanged by the collagen phase transformation. It was not possible to determine if there are changes in the fourth factor, the peptide oscillator anharmonic coefficient,  $\Omega_p$ . There is reason to consider a possible reduction in  $\Omega_p$  based on a known decrease in the Cotton effect that occurs near 190nm when collagen solutions are thermally transformed. Some of the oscillator properties that are required for a Cotton effect, such as a lack of an inversion center, are also required for the anharmonic coefficient to exist and second-harmonic generation to occur. Therefore, a change in the Cotton effect

may be accompanied by a change in the requisite properties for second-harmonic generation.

The third mechanism was related to a decrease in  $\chi_2$  for collagen fibrils by virtue of a decrease in the number of aligned peptide oscillators after the collagen phase transformation. In rabbit corneas that had not been thermally transformed, the observed second-harmonic generation more closely resembled the calculated characteristics of coherent second-harmonic generation from crystalline media than it did the calculated characteristics of second-harmonic generation from amorphous media. Coherent second-harmonic generation should be reduced when the mutual alignment of the collagen second-harmonic oscillators is reduced during the creation of the collagen random coil phase. This would seem to most easily explain the experimental result that second-harmonic generation decreased when the collagen of cornea and tendon was thermally transformed.

In summary then, three mechanisms have been considered for the observed decrease in the forward second-harmonic conversion efficiency after the collagen phase transformation in cornea and tendon. The observed decrease in conversion efficiency was probably not due to increased light scattering, which was mechanism one. Mechanism two, that changes occurred in the individual peptide oscillators, could not be excluded. The third mechanism, that coherent second-harmonic generation was partly changed to incoherent second-harmonic generation

due to decreased mutual alignment of the peptide oscillators, was the most ready explanation of the experimental results of this chapter.

## APPENDIX A

In this appendix, we shall perform an analytical estimate of the second-harmonic conversion efficiency,  $C_{CP}$ , of a normal, fresh, rabbit cornea. These computations are based on the scalar model for coherent second-harmonic generation in a crystalline medium discussed in Chapter 2.

We shall begin by computing the conversion efficiency of a single model lamella. The following assumptions are also given in Section 7.4. We assume that:

1. The model lamella is an infinite slab (length =  $\infty$ , width =  $\infty$ ) with thickness = 2microns.
2. The model lamella has a constant second-order dielectric susceptibility,  $\chi_2$  (see Chapter 2 for definition).
3.  $\chi_2$  is derived from the spatial average number density of collagen peptide bonds in the lamella.
4. Radiation at  $\omega$  and  $2\omega$  propagates as plane waves in the direction of the lamella thickness.
5. At  $\omega$  and  $2\omega$ , the refractive index and the optical dispersion of the model lamella is equal to that of water and is constant throughout the medium.
6. There is no light scattering at  $\omega$  and  $2\omega$ ; and the medium is considered to be lossless.

7. Since the second-harmonic conversion efficiency has been experimentally determined to be low, we shall assume no attenuation of the incident beam at  $\omega$  due to harmonic generation.

We will first compute the spatial average number density of peptide bonds,  $N_v$ , in a typical lamella. We will then obtain a scalar estimate of  $\beta_p$  (see Eq. 10 for definition) for the collagen peptide bond. Using an approximate Lorentz correction factor we shall then evaluate  $\chi_2$  for the model lamella. With this value of  $\chi_2$  we shall go on to find the coherent forward conversion efficiency of a single lamella.

To find the coherent forward conversion efficiency of whole cornea we shall use the following model.

8. The model lamellae are arranged in a stacked series with irregular spacing.
9. Each lamella in the stroma is identical.
10. Only the stroma contributes to second-harmonic generation.
11. Each lamella acts as an independent source of second-harmonic radiation.

We shall assume that the total second-harmonic energy from the cornea is the sum of the energies from the individual lamellae. The energy from a single lamella will be computed from the scalar model given in Chapter 2.

a. Number density of peptide oscillators (Fig. 7.12)

The fundamental screw translation period along the long axis of the collagen molecule is  $2.8\text{\AA}$  (Rich, 1959, p. 59). Within this period there are three amino acid residues on separate collagen chains and three peptide bonds. The dimensions of this cylindrical subunit are: diameter =  $14\text{\AA}$  (diameter of collagen molecule) and height =  $2.8\text{\AA}$  (one screw translational period). Consider an average corneal collagen fibril in man with diameter with  $260\text{\AA}$  (Maurice, 1969, p. 299). Assume that the collagen molecules are arranged as a hexagonal close-packed bundle of cylinders within this fibril (Fig. 7.12).

There are then approximately 250 collagen molecules and hence about 250 cylindrical subunits in a given cross-section of the fibril. The number of cylindrical subunits per unit volume of a typical fibril,  $N_{vc}$ , is then:

$$N_{vc} = \frac{250}{A_F L_C}$$

where  $A_F$  = cross-sectional area of fibril ( $\frac{\pi}{4} \times [260 \times 10^{-8} \text{ cm}]^2$ ) and  $L_C$  = the length of the cylindrical unit ( $2.8\text{\AA}$ ). We can then compute

$$N_{vc} = 1.68 \times 10^{21} \text{ cylindrical units/cm}^3$$

There are three peptide bonds per cylindrical unit, therefore  $N_{VPF}$ , the number of peptide bonds per unit volume of the fibril is:

$$N_{VPF} = 5.05 \times 10^{21} \text{ peptide bonds/cm}^3$$

Collagen fibrils occupy approximately 20% of the total volume of a lamella (Maurice, 1969, p. 316). Therefore we shall assume that the average density of peptide bonds per unit volume of a lamella is,

$$N_{VPL} = 0.20 N_{VPE}, \text{ or:}$$

$$N_{VPL} = 10^{21} \text{ peptide bonds/cm}^3$$

b. Lorentz correction factors

We will assume that the refractive index of a fibril is 1.5 (Maurice, 1969) at both the fundamental second-harmonic frequencies for the purposes of computing the Lorentz correction factors (Chapter 2). Then both  $L(2\omega)$  and  $L(\omega)$  can be approximated by

$$L = \frac{n^2 + 2}{3} = 1.42$$

and:

$$L^3 = 2.84$$

c. Peptide link polarizability

The scalar polarizability of the peptide link  $\beta_p$  will be calculated from Eqs. (26), (31) and (34) of Chapter 2:

$$\beta_p = \frac{f_p^2 e^3 \Omega_p}{m^2} \frac{1}{D_p^2(\omega) D_p(2\omega)}$$

$$D_p(\omega) = \omega_p^2 - \omega^2 - j\Gamma_p \omega$$

$$D_p(2\omega) = \omega_p^2 - 4\omega^2 - 2j\Gamma_p \omega$$

The factors  $D_p(\omega)$  and  $D_p(2\omega)$  are complex numbers. The following table compares the real and imaginary parts of these factors when  $\omega_p = 9.9 \times 10^{15}$  rad/sec which is the center frequency of 190nm peptide band;  $\omega$  is the ruby laser frequency which is  $\omega = 2.7 \times 10^{15}$  rad/sec; and  $\Gamma_p$  is the bandwidth of the 190nm peptide resonance which is  $\Gamma_p \approx 1.6 \times 10^{15}$  rad/sec (estimated bandwidth of 30nm from Gratzner et al, 1963, Fig. 5). The entries in the third column show that the imaginary part of the  $D_p$  factors is small compared to the real part. We shall therefore retain only the real part as an approximation to the  $D_p$  factors when computing  $\beta_p$ .

$D_p$ Factor	$\text{Re}\{D_p\} + j I_m\{D_p\}$	$(I_m\{D_p\}/\text{Re}\{D_p\})\%$
$D_p(\omega)$	$9.1 \times 10^{31} - j4.3 \times 10^{30}$	4%
$D_p(2\omega)$	$6.9 \times 10^{31} - j8.6 \times 10^{30}$	13%

The anharmonic coefficient  $\Omega_p$  will be obtained from the following approximation developed in Chapter 2

$$\omega_p = \left( \frac{\omega_p^8 m}{e^2} \right)^{1/3}$$

The resonant frequency,  $\omega_p$ , for the peptide link is  $9.9 \times 10^{15}$  rad/sec ( $\lambda_p = 190\text{nm}$ ). With the electron mass  $m = 9.1 \times 10^{-28}$  gm and the electron charge of  $e = 4.8 \times 10^{-10}$  esu we obtain:

$$\Omega_p = 7.14 \times 10^{39} \text{ sec}^{-8/3} \text{ gm}^{1/3} \text{ esu}^{-2/3}$$

The oscillator strength of the peptide bond is  $\sim 0.3$  (Ham and Platt, 1952; Gratzer et al, 1963, Fig. 5; these authors use  $f_p = 0.27$ , we shall use 0.3). Using these additional parameters, we obtain

$$\beta_p = 1.50 \times 10^{-31} \text{ cm}^{9/2} / \text{erg}^{1/2}$$

#### d. Susceptibility of single model lamella

We shall compute  $\chi_2$  for a single model lamella from Eq. (36)

of Chapter 2:

$$\chi_2 = N_{\text{VPL}} L^2(\omega) L(2\omega) \beta_p$$

This equation is only an approximation. The limitations of its use are discussed in Chapter 2, Section 1.7. From our prior results for  $N_{\text{VPL}}$ ,  $L(\omega)$ ,  $L(2\omega)$  and  $\beta_p$  we obtain

$$\chi_2 = 4.26 \times 10^{-10} \text{ cm}^{3/2} \text{ erg}^{-1/2}$$

e.  $C_{\text{CP}}$  for a single model lamella

In Chapter 2, Section 1.7 we obtained the following expression for the coherent second-harmonic power conversion efficiency for a uniform nonlinear slab of thickness  $L$ :

$$C_{\text{CP}} = W_1 \left( \frac{64\pi^3 k_2^2 \chi_2^2 A_2}{A_1^2 c n_2^4} \right) \left( \frac{\sin^2 \Delta k L/2}{\Delta k^2} \right)$$

where  $W_1$  is the laser peak power,  $k_2$  is the second-harmonic wave vector in air,  $\chi_2$  is the second-order susceptibility,  $A_2$  is the cross-sectional area of the second-harmonic beam,  $A_1$  is the cross-sectional area of the laser beam,  $c$  is the speed of light in vacuum,  $n_2$  is the refractive index at the second-harmonic wavelength,  $\Delta k = 2k_1 - k_2$  (where  $k_1$  and  $k_2$  are the laser wave vector and second-harmonic

wave vector in the medium), and L is the thickness of a lamella.

In our experiments

$$W_1 = 2.66 \times 10^{12} \text{ erg/sec (2.66} \times 10^5 \text{ Watts, measured)}$$

$$k_2 = 2\pi/\lambda_2 = 3.31 \times 10^5 \text{ cm}^{-1} \text{ (calculated)}$$

$$\chi_2 = 4.26 \times 10^{-10} \text{ cm}^{3/2} \text{ erg}^{-1/2} \text{ (calculated)}$$

$$A_1 = 3 \times 10^{-2} \text{ cm}^2 \text{ (measured)}$$

$$A_2 \approx A_1 \text{ (approximation for these calculations)}$$

$$c = 2.99 \times 10^{10} \text{ cm/sec}$$

$$n_2 = 1.35 \quad (\text{ICT Vol. 7, p. 14})$$

$$\Delta k = (2\omega/c)(n_2 - n_1) = (2\omega/c)(0.018) = 5.96 \times 10^3 \text{ cm}^{-1}$$

(ICT, Vol. 7, p. 14)

$$L = 2 \times 10^{-4} \text{ cm (assumption based on Maurice, 1969, pp. 295-300).}$$

With these parameters we obtain

$$C_{CP} = 4.9 \times 10^{-12}$$

for a single model lamella

f.  $C_{CP}$  for the whole corneal stroma

We shall assume that second-harmonic generation occurs independently in each lamella and that the relative phase of the radiation from the various lamellae is random. Based on this, we shall assume that the second-harmonic power from each lamella is additive to yield the total radiated power from the cornea. Maurice has stated that the human cornea is at least 200 lamellae thick (Maurice, 1969, p. 297). We have estimated the number of lamellae in thickness of the rabbit cornea to be between 150 and 200. We shall assume 200 lamellae for the thickness of the rabbit cornea. The calculated forward peak power conversion efficiency of the rabbit cornea is then:

$$\begin{aligned} (C_{CP})_{\text{stroma}} &= (C_{CP})_{\text{lamella}} \times 200 \\ &= 4.9 \times 10^{-12} \times 200 \\ &= 9.8 \times 10^{-10} \end{aligned}$$

g. Uncertainties in the calculations

In these calculations we do not have the same difficulties in computing  $A_1$  and  $A_2$  that we encountered in Chapter 2 when analyzing Terhune's focused beam experiments. In our focused beam experiments, the beam radius was about 1mm at the cornea and the beam was very

slowly divergent over the corneal thickness. Thus we could more easily estimate the volume over which second-harmonic generation occurred.

The serious uncertainties in the present calculation concern: the degree to which corneal lamellae can actually be considered uniform non-linear crystals; the assumption of independent harmonic generation with random phase in each lamella; the assumption of the dispersion of water for the cornea; and the assumption that all lamellae are the same in thickness. Some of these assumptions could be checked in further experiments. For example, if the cornea were sectioned in layers of known thicknesses, containing many lamella, then the conversion efficiency should be proportional to the thickness if second-harmonic generation occurs independently in each lamella. Of course the same would be true for second-harmonic generation from amorphous media, but a second check involving the angular distribution of second-harmonic radiation could be used in this case (see Chapter 6).

The calculated value of  $C_{CP}$  is apparently dependent upon the assumed dispersion. The dispersion  $(n_2 - n_1)$  enters in the factor

$$\frac{\sin^2(\omega(n_2 - n_1)L/c)}{(n_2 - n_1)^2}$$

where we have assumed  $(n_2 - n_1) = 0.018$ ,  $L = 2 \times 10^{-4}$  cm,

$\omega = 2.7 \times 10^{15}$  rad/sec and  $c = 2.99 \times 10^{10}$  cm/sec. The factor  $\omega(n_2 - n_1)L/c$  is of the order of 0.3 with these parameters. Therefore let us approximate the above expression by

$$\frac{(\omega[n_2 - n_1] L/c)^2}{[n_2 - n_1]^2} = \frac{\omega^2 L^2}{c^2}$$

(Using this approximation results in about a 3.5% error). We see, therefore, that because the assumed value of  $L$  is small, the assumed value of  $n_2 - n_1$  does not critically affect the calculated value of  $(C_{CP})_{\text{lamella}}$ .

The assumed value of  $L = 2 \times 10^{-4}$  cm may not be correct. If it were in error by a factor of two, then assuming  $L = 4 \times 10^{-4}$  cm yields a factor of 3.6 change in the calculated value of  $(C_{CP})_{\text{lamella}}$  and  $(C_{CP})_{\text{stroma}}$ .

As we noted in our calculations in Chapter 2, there may be significant uncertainties in using the equation

$$\chi_2 = N_V \beta L^2(\omega) L(2\omega)$$

in calculating  $\chi_2$ . Unfortunately, there is not enough information to estimate the error involved in using this equation.

The most serious source of error in our calculations is probably the uncertainty in the oscillator strength for the peptide bond. In

Chapter 2 we showed that the conversion efficiency is proportional to  $f^4$ . In the case of the peptide bond, only a little more than half of the absorption band has been measured (Gratzer et al, 1963, Fig. 5). Oscillator strengths have been estimated by assuming that the absorption band is symmetric (Ham and Platt, 1952). If the value of  $f_p = 0.3$  were in error by as much as plus or minus a factor of 2, then the calculated value of  $(C_{CP})$  could be in error by as much as plus or minus a factor of 8 as a result of this.

Combining the important calculated uncertainties in  $C_{CP}$  which are a factor of 3.6 due to  $L$  and a factor of 8 due to  $f$  we obtain a peak error of as much as plus or minus a factor of 30 in  $(C_{CP})_{stroma}$ . Assuming  $(C_{CP})_{stroma}$  to account for all the conversion efficiency of the cornea may be in error since we do not know the contributions from Bowman's zone or Descemet's zone. We feel that these contributions are small due to the thinness of these layers. We therefore shall use  $(C_{CP})_{stroma}$  as the value for  $(C_{CP})_{cornea}$  when the cornea has not been thermally transformed.

## APPENDIX B

In this appendix, we shall perform an analytical estimate of the forward conversion efficiency of rabbit cornea after the collagen phase transformation.

We shall assume that the collagen of the stroma has been completely converted to a random coil macromolecular material that is uniformly dispersed throughout the tissue. The peptide bonds of the random coil chains will be taken to be the microscopic nonlinear oscillators of the tissue. We shall utilize the simple scalar model discussed in Chapter 2 for incoherent second-harmonic generation from a collection of independent randomly oriented dipoles and assume that this radiation is distributed uniformly over  $4\pi$  steradians of solid angle.

In Chapter 2 we obtained the following expression (Eq. 57) for the total incoherent second-harmonic conversion efficiency of a collection of independent randomly oriented second-harmonic oscillators:

$$C_{IP} = \frac{1024\pi^2 \omega^4}{3c^5 A_1} L_t N_{VP} \beta_P^2 L^4(\omega) L^2(2\omega) W_1 \quad (B.1)$$

In Eq. (B.1),  $\omega$  is the laser frequency;  $L_t$  is the thickness of the thermally transformed cornea;  $c$  is the speed of light in vacuum;  $A_1$  is the laser beam area in the sample (assumed to be constant);

$N_{VP}$  is the average number density of peptide bonds;  $\beta_p$  is the second-order nonlinear polarizability of these bonds;  $L(\omega)$  and  $L(2\omega)$  are Lorentz correction factors for the local field; and  $W_1$  is the laser peak power in the sample.

To obtain the forward conversion efficiency (i.e. as would be measured using lens B, Fig. 4.1),  $C_{IPF}$ , we multiply  $C_{IP}$  by the ratio of the solid angle,  $\Omega$ , subtended by lens B with respect to the sample (Fig. 4.1) to  $4\pi$  steradians:

$$C_{IPF} = C_{IP} \frac{\Omega}{4\pi} \quad (B.2)$$

where

$$\Omega = 2\pi (1 - \cos \theta) \quad (B.3)$$

and

$\theta$  = half-angle of cone subtended by lens B. Since  $\theta = 8^\circ$ , we obtain:

$$\frac{\Omega}{4\pi} = 5.7 \times 10^{-2} \quad (B.4)$$

In Eq. (B.1) the parameters  $\omega$ ,  $c$ ,  $A_1$ ,  $\beta_p$ , and  $W_1$  will be assumed to be the same as calculated in Appendix A for travelling wave second-

harmonic generation. Due to increased light scattering, the beam area,  $A_1$ , may be somewhat larger in real corneas after the phase transformation when compared to the beam area in real, freshly excised corneas. We shall neglect this difference in this appendix. The thickness,  $L_t$ , of the contracted corneas was  $\sim 10^{-1}$  cm. We will assume that  $N_{VP}$  was approximately the same as the average number density of peptide bonds that was computed for normal corneas in Appendix A. We base this assumption on the fact that when the corneal thickness increased on contraction (tending to lower  $N_V$ ), the lateral dimensions, A and B (Fig. 7.3) decreased (tending to raise  $N_V$ ). Insofar as an order of magnitude estimate is concerned, we will assume that the volume average concentration of peptide bonds in the stroma was unchanged by the collagen phase transformation.

Thus the parameters we shall use in our calculations are:

$$\omega = 2.7 \times 10^{15} \text{ rad/sec}$$

$$L_t = 10^{-1} \text{ cm}$$

$$N_{VP} = 10^{21} \text{ peptide bonds/cm}^3$$

$$\beta_p = 1.5 \times 10^{-31} \text{ cm}^{9/2}/\text{erg}^{1/2}$$

$$L(\omega) = L(2\omega) = 1.42$$

$$c = 2.99 \times 10^{10} \text{ cm/sec}$$

$$A_1 = 3 \times 10^{-2} \text{ cm}^2$$

$$W_1 = 2.66 \times 10^{12} \text{ erg/sec}$$

With these parameters and assumptions, we then obtain as an order of magnitude estimate of  $C_{IP}$ :

$$C_{IP} = 1.2 \times 10^{-14}$$

Using Eq. (B.2) and Eq. (B.4) we can then compute  $C_{IPF}$  for an  $8^\circ$  half-angle for collection which is:

$$C_{IPF} = 6.9 \times 10^{-16}$$

The following factors may contribute the largest errors in the above estimate of  $C_{IPF}$ . First, we may not be correct in assuming  $L_c = 10^{-1}$  cm is the correct thickness of a completely transformed cornea.  $L_c = 10^{-1}$  cm is probably too small, however it is probably within a factor of 2 of the correct value. Second, in Appendix A we have assumed that there are lamella. We calculated a spatial average number density of peptide bonds  $N_{VP}$  partly on the basis of the dimensions of these lamellae. After the thermal phase transformation, the thickness of the cornea increases and the lateral dimensions decrease, which may mean that the overall volume of the

cornea is not appreciably changed. On this basis we therefore assume that  $N_{VP}$  in the transformed cornea is the same as  $N_{VP}$  in the normal cornea. We estimate that the assumed value of  $N_{VP}$  for the thermally transformed cornea is probably within plus or minus a factor of 5 of the correct value. Third, as discussed in Appendix A, the assumed value of  $\beta_p^2$  may be in error by as much as plus or minus a factor of 8 in normal cornea. We are assuming that  $\beta_p^2$  is unchanged during the collagen phase transformation in the present calculation. Therefore, we shall retain the factor of 8 error estimate. Fourth, the assumed Lorentz correction factors may contribute a smaller error in an amorphous medium, such as thermally transformed cornea, than in normal cornea. This judgment is based on suggestions by Bloembergen that the local field correction represented by these factors may be correct only for certain cubic crystals and amorphous media (Bloembergen, 1965, Eq. 3.18). Fifth, the error in the assumption that incoherent second-harmonic generation occurs uniformly over  $4\pi$  steradians may be significant. There could be a lobed structure to the second-harmonic emission pattern of random coil collagen chains. Some of this lobed structure would become diffuse as a result of light scattering in the tissue. Therefore, there is no satisfactory way to estimate the error in the ratio of collected second-harmonic radiation. It seems reasonable to assume no more than plus or minus an order of magnitude error in the assumed value of  $\Omega/4\pi = 5.7 \times 10^{-2}$  in Eq. (B.4).

Flory has shown that it is necessary to heat tendon very slowly for a complete transformation to the random coil phase to occur. In our studies, heating was rapid, therefore a complete transformation may not have occurred. In this instance, some coherent second-harmonic generation may still be present with our thermally transformed corneas.

Combining these factors yields a final peak error range of plus a factor of 800 and minus a factor of 400. We shall simplify this result and for convenience call the peak estimated error range plus or minus a factor of 600.

## APPENDIX C

This appendix contains the results of measurements of the second-harmonic conversion efficiency,  $C_{\text{MPF}}$ , for the moist, fresh, normal rabbit cornea. The conversion efficiency  $C_{\text{MPF}}$  is defined as the ratio of the peak power  $W_{2B}$  at  $2\omega$  collected in the forward scattering direction by lens B (Fig. 4.1) to the incident peak power  $W_1$  at the cornea. Using the results in this appendix for  $C_{\text{MPF}}$  in fresh, moist, normal rabbit cornea one can compute  $C_{\text{MPF}}$  for corneas under other conditions of hydration and temperature history by consulting Table 2 of Chapter 7.

## a. Apparatus

A freshly excised rabbit cornea was mounted on a glass slide and moistened with aqueous humor as shown in Fig. 2 of Chapter 6. The monitoring apparatus and the laser were arranged as shown in Fig. 1 of Chapter 4.

## b. Procedure

Five laser pulses were used to obtain an average value and standard deviation of the oscilloscope heights  $H_1$  and  $H_2$  for the laser and second-harmonic pulses respectively. The average laser pulse height was converted to the peak power  $W_1$  from a prior calibration of the KD1 photodiode against a TRG ballistic thermopile and a measurement of the oscilloscope pulse width (Methods and materials,



Chapter 4). The average second-harmonic pulse height was converted to peak power  $W_{2B}$  by using the manufacturer's value of responsivity at 347nm for the 1P28 photomultiplier with a correction for the non-linearity of the photomultiplier (Methods and materials, Chapter 4 and RCA Tube Manual for 1P28 photomultiplier) and by correcting for transmission losses between lens B and the photomultiplier. The manufacturer's nominal responsivity value of  $6.18 \times 10^4$  amp/watt at 1 KV bias and 347nm wavelength may be incorrect by as much as a factor of 2 for a given photomultiplier. We had no facility by which one could accurately calibrate the photomultiplier used in these studies.

#### c. Transmission losses

In order to obtain the second-harmonic peak power collected by lens B,  $W_{2B}$ , one must take into account the 347nm transmission of lens B, lens C, the copper sulfate filter, and the monochromator (Fig. 4.1). These transmissions are denoted by  $T_L = T_B T_C$ ;  $T_{CU}$ ; and  $T_M$  respectively. The system transmission at 347nm will be  $T_L T_{CU} T_M$ .

The combined 347nm transmission of lenses B and C is  $T_L = 0.14$  with an estimated peak percent error of measurement of  $\pm 5\%$  (see Methods and materials, Chapter 4).

Estimating the 347nm transmission of the monochromator was difficult. Measurement of  $T_M$  will be considered in three parts. These

are: the transmission of the entrance slit, the transmission of the exit slit, and the transmission of the internal mirror and grating of the monochromator.

The approximate transmission of the entrance slit was determined as follows. A He-Ne laser was placed inside the ruby laser cavity and its beam was expanded to simulate the ruby laser beam. It was assumed that the second-harmonic forward lobe described in Chapter 5 propagated as a beam with slightly larger divergence than the He-Ne beam. Lens B imaged the He-Ne beam onto the entrance slit of the monochromator. It was estimated by visual observation that the image was slightly smaller than the slit opening (6mm slit used). The estimate may be too large by about 50%. This large uncertainty arises because the second-harmonic forward lobe has a larger divergence than the ruby laser (Chapter 5) and the He-Ne beam divergence is not the same as the ruby laser beam divergence. Imaging differences due to chromatic aberration were calculated to be only about 10% for 347nm and He-Ne laser radiation. These effects of image aberration were small and were neglected.

The approximate transmission of the exit slit was estimated as follows. A blue spectroscopic line (near 400nm) was selected from a low pressure Hg-Cd lamp spectrum using glass filters. This radiation was imaged at the entrance slit of the monochromator. The bandwidth of this line was about 0.2nm (see Chapter 4 Methods and materials for manufacturer's specifications on lamp). The 400nm

radiation leaving the exit slit was monitored with the 1P28 photomultiplier while the entrance and exit slits were set to the openings used to monitor second-harmonic generation. The exit slit alone was then widened. The power at the photomultiplier was observed to increase to a final level that was 25% higher than the initial level. Visual examination showed the image of the entrance slit to be tilted with respect to the exit slit. No means were available on the monochromator to correct this. On this basis, the transmission of the exit slit was taken to be 0.75 for second-harmonic generation. The error in this estimate is probably small, and will be assumed as zero.

The internal components of the monochromator consisted of a mirror imaging the entrance slit onto the exit slit, and a reflection grating. We shall assume the mirror reflectance to be unity. The grating was blazed at 400nm. This means that at 400nm there is very nearly 100% reflection into a single spectral order. The reflected energy at a wavelength  $\lambda$  relative to the reflected energy at the blaze wavelength is given by Klein (Klein, 1970, p. 346)

$$\frac{\sin^2 \pi \left( \frac{\lambda_b}{\lambda} - 1 \right)}{\left[ \pi \left( \frac{\lambda_b}{\lambda} - 1 \right) \right]^2}$$

which is 0.92 for  $\lambda_b = 400\text{nm}$  and  $\lambda = 347\text{nm}$ . Therefore we shall

assume that approximately 0.9 of the energy at 347nm inside the monochromator was transmitted to the exit slit.

The net transmission of the monochromator will be taken to be the product of the entrance slit transmission, the internal transmission and the exit slit transmission which is  $T_M = 0.68$ . The error in  $T_M$  cannot be exactly determined from our measurements. If anything, the above value of  $T_M$  is too large. We shall assume that  $T_M$  could be as much as a factor of 2 smaller.

The system transmission is  $T_L T_{CU} T_M = T$ . Based on the above analysis, one obtains an estimated range for T of  $5.5 \times 10^{-3} \leq T \leq 3.4 \times 10^{-2}$ .

d. Measurement of  $W_{2B}$  and  $W_1$

Five second-harmonic pulses gave an average peak current of 12ma from the photomultiplier with a standard deviation of 4ma. Using the manufacturer's 347nm nominal current responsivity value of  $6.18 \times 10^4$  amp/Watt yields a peak radiant power at 347nm at the photomultiplier of  $1.9 \times 10^{-7}$  Watts with a standard deviation of  $6.5 \times 10^{-8}$  Watts. The second-harmonic power incident at lens B will be estimated as being in a range

$$\frac{1.25 \times 10^{-7}}{T_{\max}} \leq W_{2B} \leq \frac{2.55 \times 10^{-7}}{T_{\min}}$$

which is based on the relation

$$W_{2B} = \frac{\text{Peak power at photomultiplier}}{T}$$

Thus

$$3.7 \times 10^{-6} \text{ Watts} \leq W_{2B} \leq 4.6 \times 10^{-5} \text{ Watts}$$

The laser peak power was determined from photodiode and thermopile measurements that were taken before and after the measurements of second-harmonic peak power. The average of these measurements was  $W_1 = 2.9 \times 10^5$  Watts with a standard deviation of  $2.3 \times 10^4$  Watts.

e. Measured peak power conversion efficiency in the forward direction,  $C_{MPF}$

The measured conversion efficiency for second-harmonic radiation collected by lens B is defined as

$$C_{MPF} = \frac{W_{2B}}{W_1}$$

We estimate  $C_{MPF}$  as being in the range

$$1.2 \times 10^{-11} \leq C_{MPF} \leq 1.7 \times 10^{-10}$$

The final value of  $C_{MPF}$  spans a range of about an order of magnitude.

Figure 7.1

The general set-up for heating tendons. The lead weight was used to promote creep after contraction of the tendon.

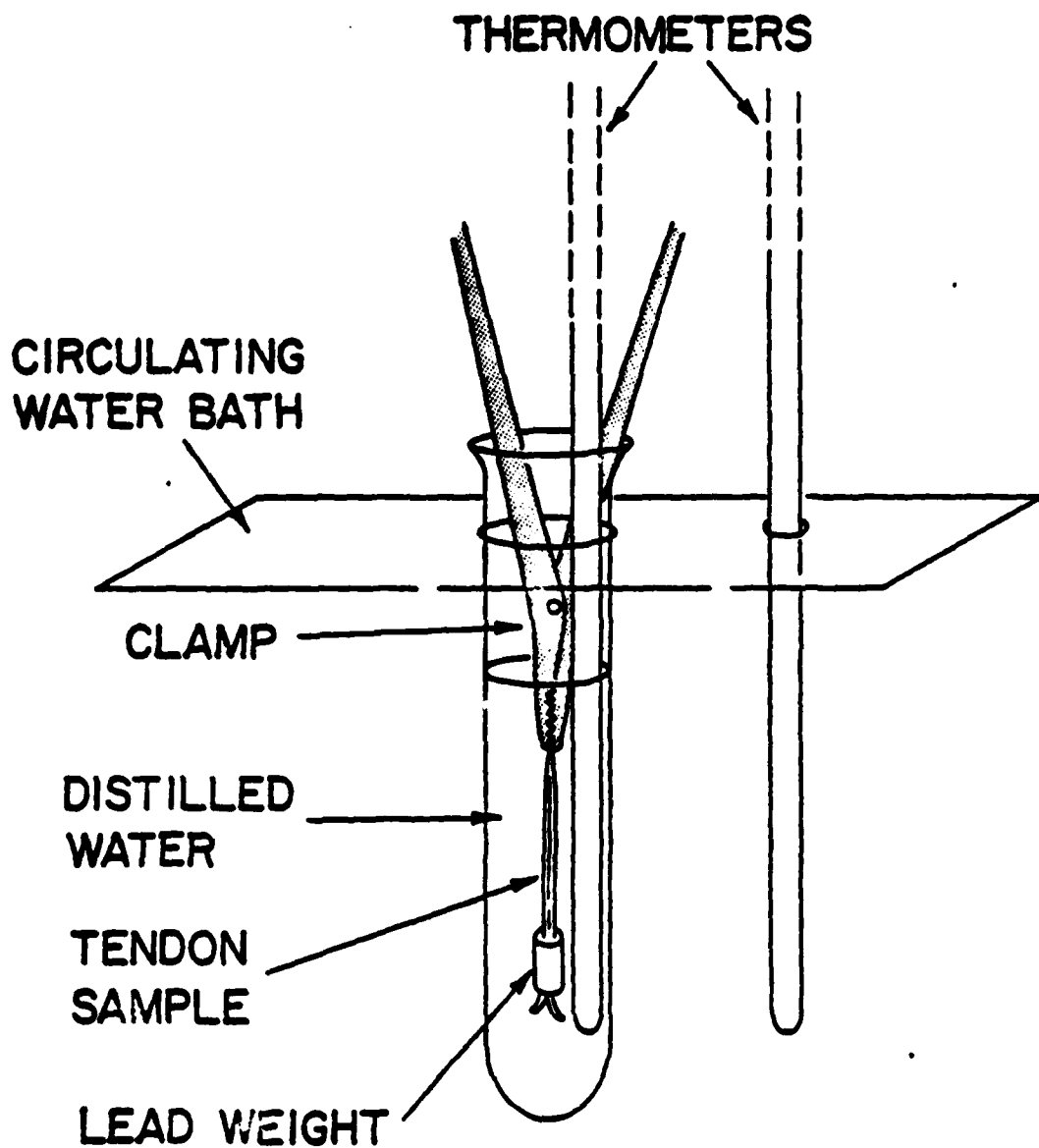


Figure 7.2

The general set-up used for heating corneas.

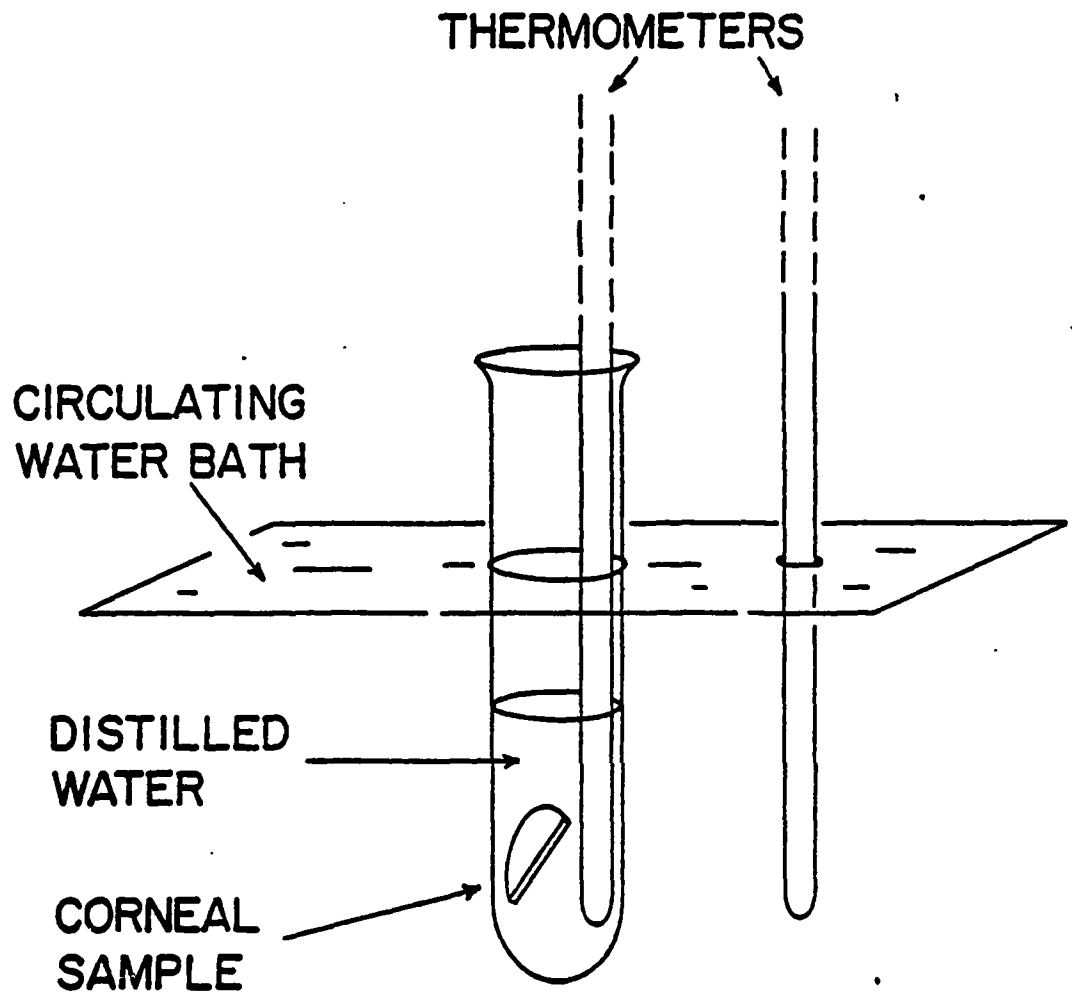


Figure 7.3

The dimensions A, B, and C defined in the main  
text for a half-cornea.

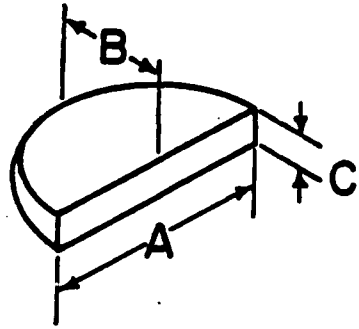


Figure 7.4

The normalized length of tendon samples measured at the time of greatest contraction and then plotted as a function of water bath temperature. No contraction occurred at 20°C, 50°C, and 54°C. Slight contraction at 60°C. At 65°C and 68°C the samples contracted to 25% of their original length. Creep followed contraction. The six samples used for this graph were heated with a lead weight attached. Curve was drawn free-hand.

Contraction near 60°C is indicative of the collagen phase transformation.

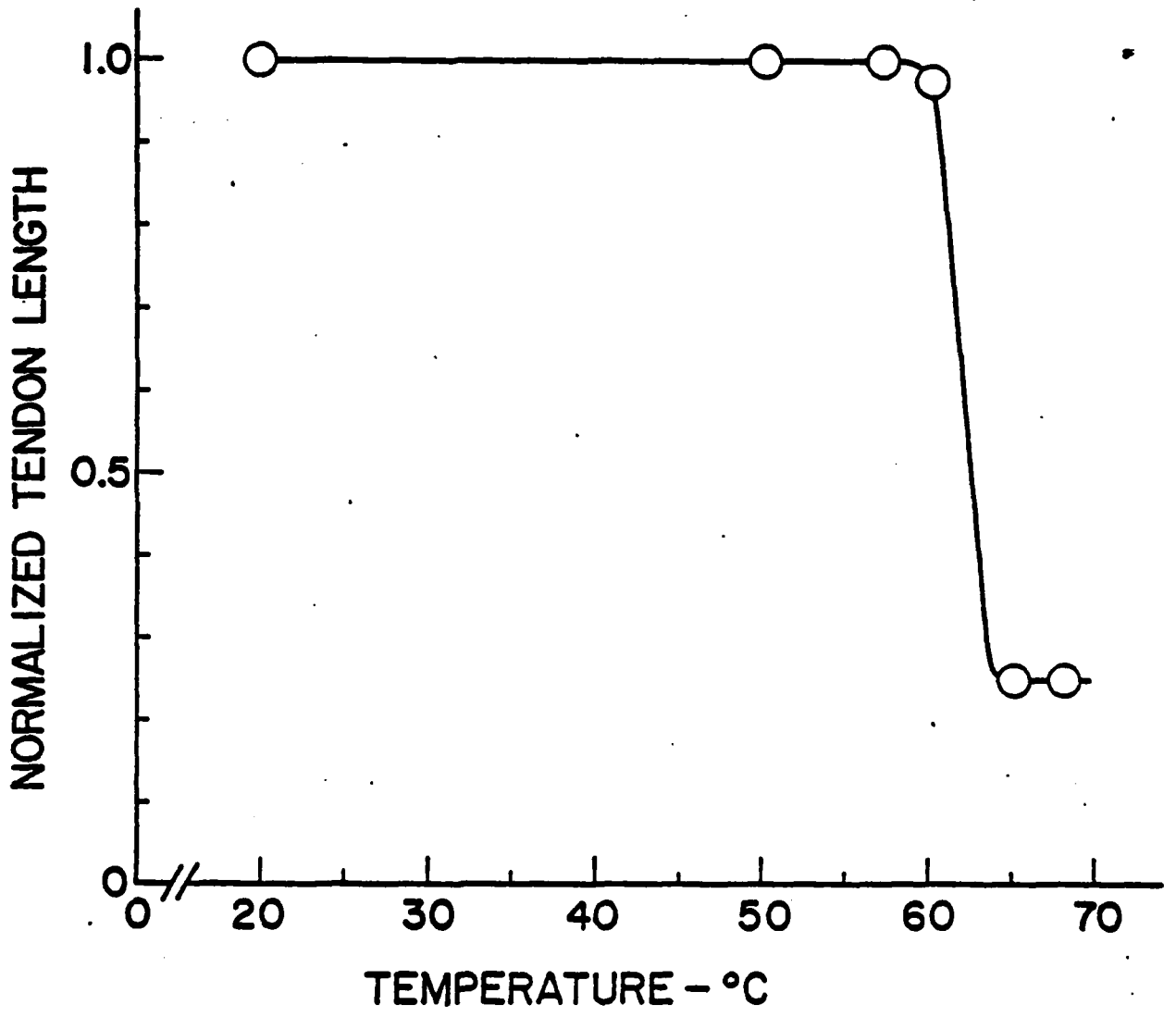


Figure 7.5

Normalized tendon length versus time during the heating of tendons above 60°C. Tendons heated with the lead weight attached contracted to a minimum length in 100 seconds. Tendons heated without the weight attached contracted to a minimum length in less than 10 seconds. Creep followed contraction in both cases.

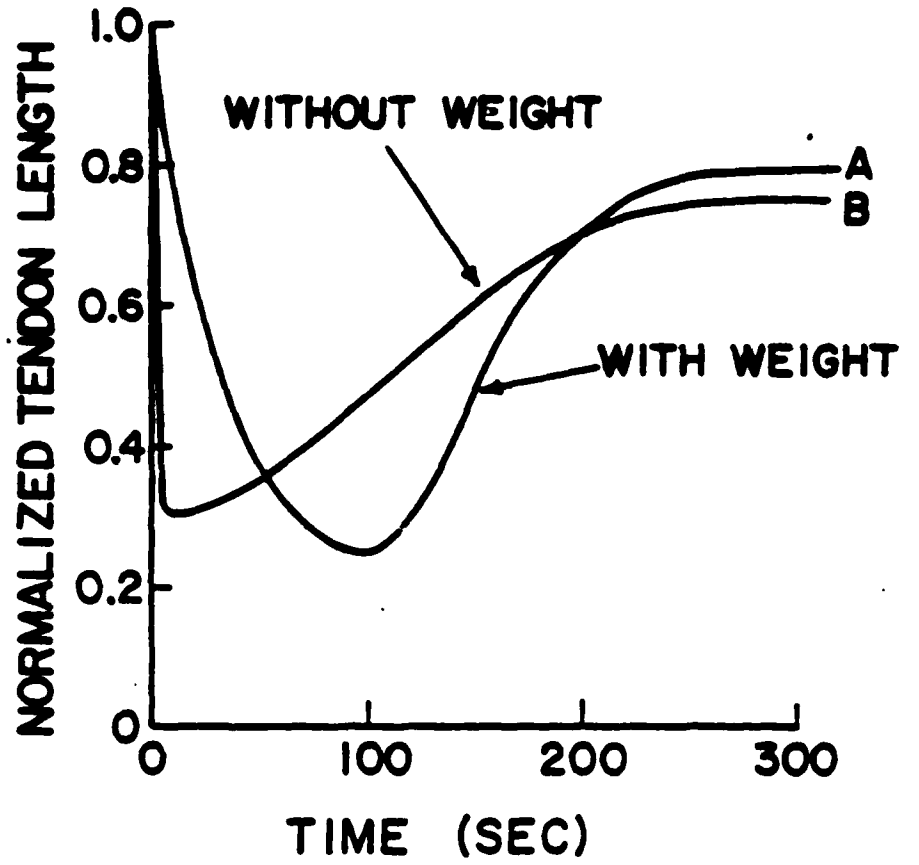


Figure 7.6

Spectrophotometric transmission of the tendon samples used for Fig. 7.4 versus water bath temperature. Transmission was measured after heating and 1/2 hour of vacuum drying at room temperature. Transmission was higher at 694nm than it was at 347nm. Transmission at both wavelengths increased after heating to 60°C or above. Increased transmission is indicative of the collagen phase transformation.

Curves were drawn free-hand. Shapes were chosen partially on the basis of visual examination of the samples.

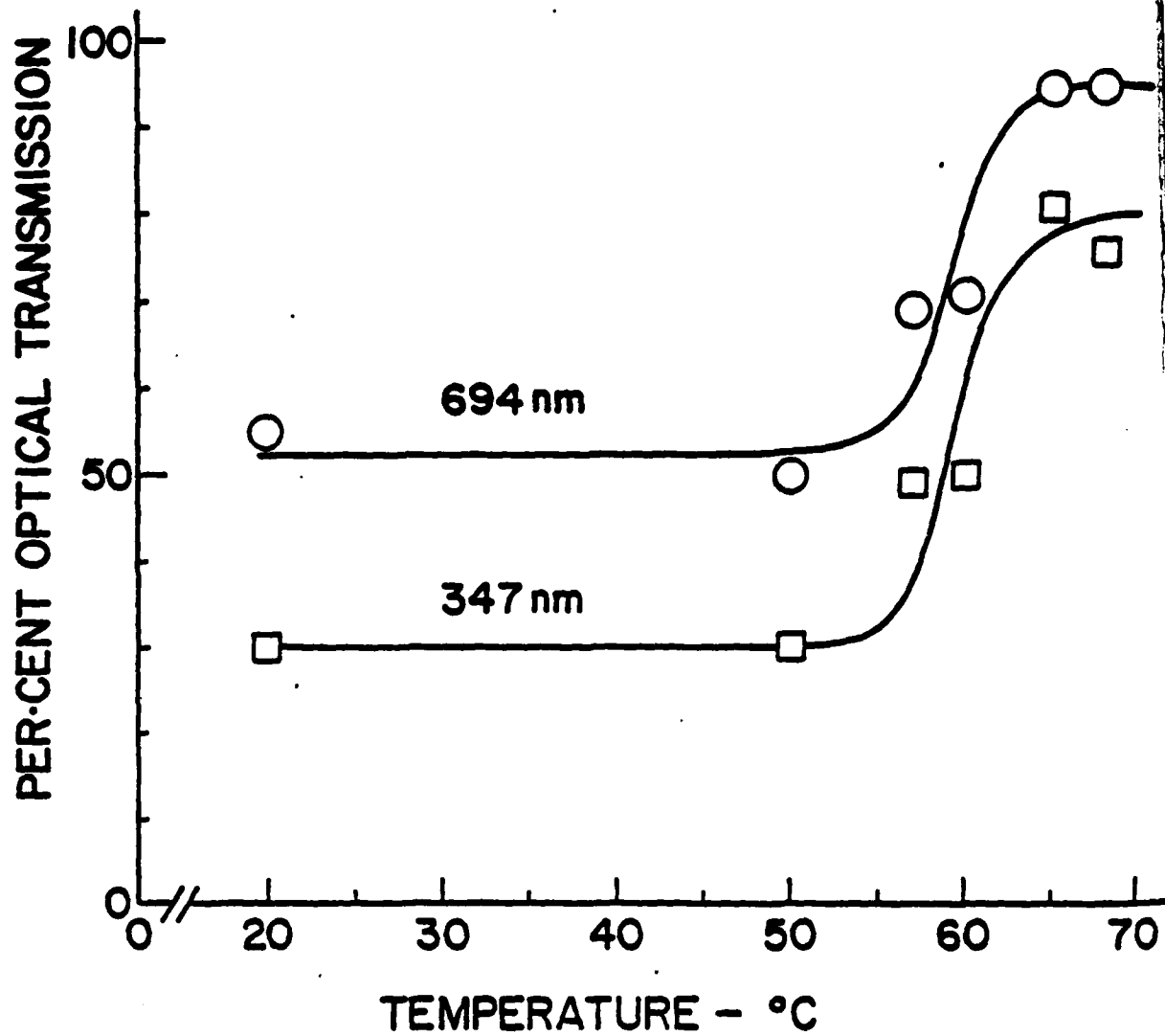


Figure 7.7

Relative forward scattered second-harmonic conversion efficiency  $C_{MRF}$  versus relative laser peak power  $H_1$ , for the tendon samples used for Figs. 5.4 and 5.6.  $C_{MRF}$  is defined as the ratio of oscilloscope pulse heights  $H_2/H_1$  obtained with the apparatus used in Fig. 4.1.  $H_2$  is the second-harmonic pulse height and  $H_1$  is the laser pulse height in arbitrary units.

Each data point is labelled with the temperature to which the tendon has been heated.  $C_{MRF}$  was evidently lower for tendons heated above  $60^\circ\text{C}$ . The straight lines A and B are regression lines fitted to the data for  $T \leq 60^\circ\text{C}$  and  $T > 60^\circ\text{C}$  respectively. The slope of line A is 0.95 and the slope of line B is 0.029. This difference in slope is taken to indicate that a decrease in  $C_{MRF}$  occurred when tendons were heated above the collagen phase transformation temperature ( $T = 60^\circ\text{C}$ ).

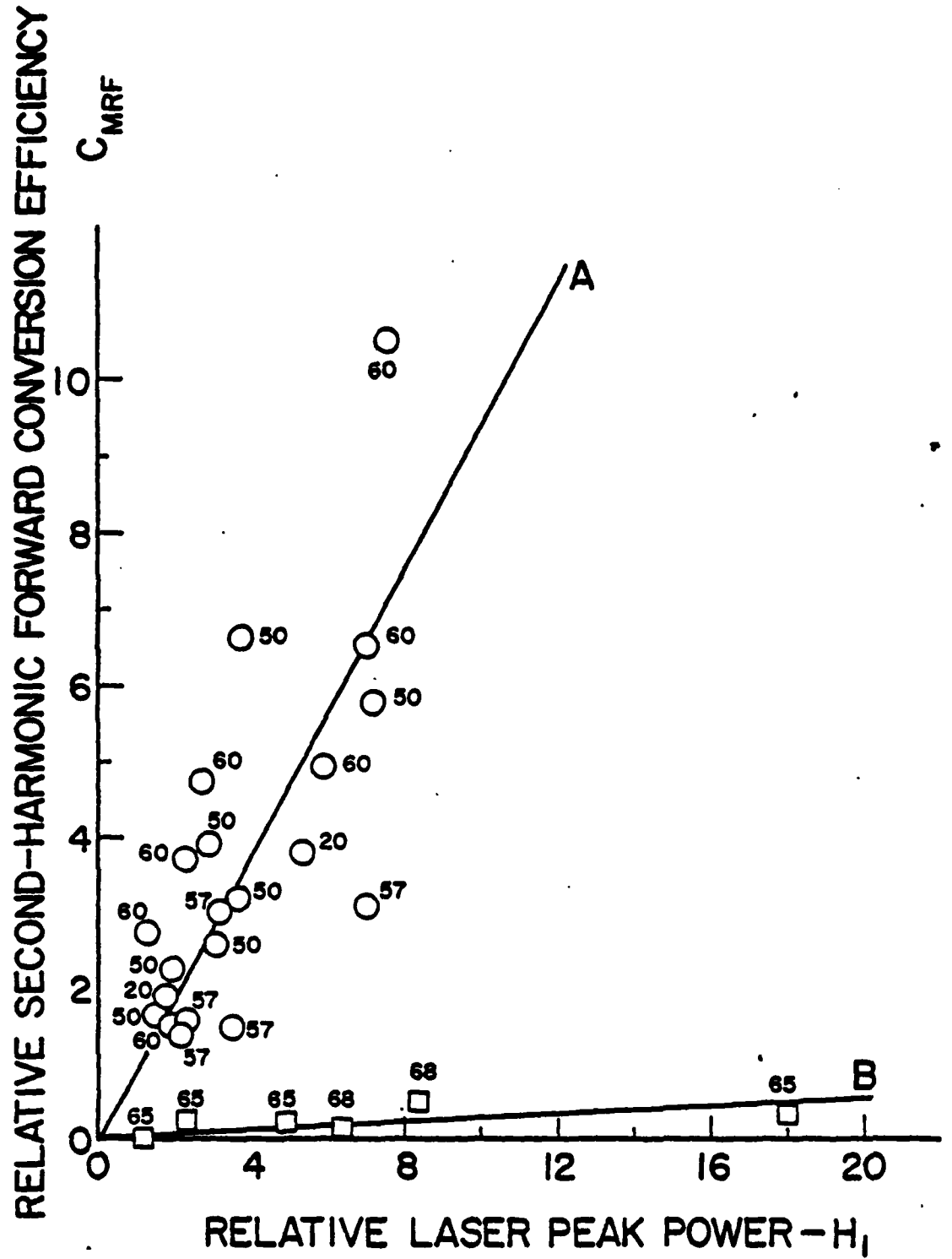


Figure 7.8

Length of chords A and B (Fig. 7.3) of corneal sample after heating to indicated temperatures. No contraction occurred below 57°C. Contraction was evident at 64°C and 69°C. Contraction near 60°C is indicative of the collagen phase transformation.

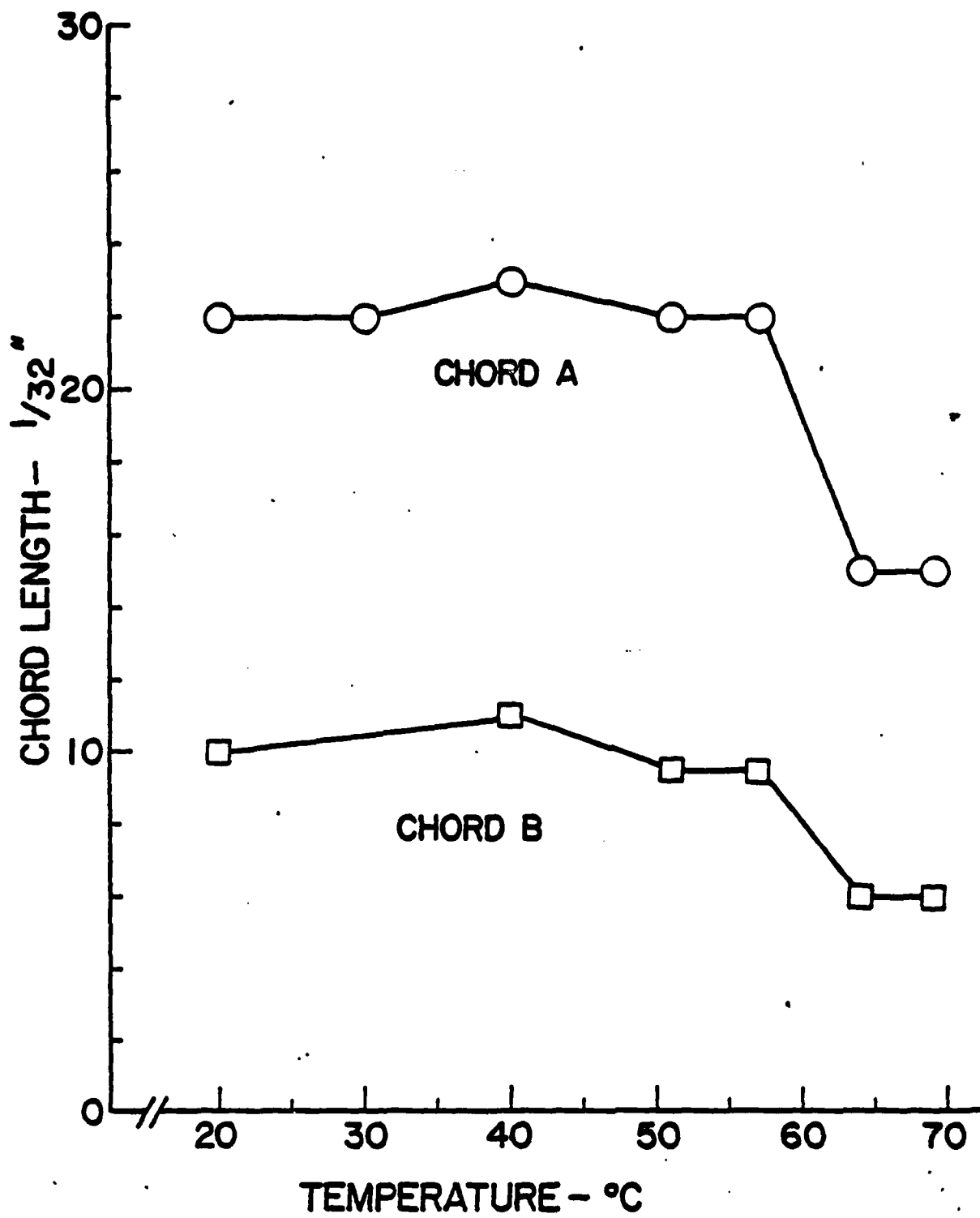


Figure 7.9

Spectrophotometric transmission of corneal sample used for Fig. 7.8 versus water bath temperature. Only 347nm transmission was monitored.

Data enclosed in squares represents transmission "immediately" after sample was withdrawn from bath. Data enclosed by circles is transmission after vacuum drying at room temperature to adjust the transmission to  $\sim 17\%$ .

Decrease in transmission between  $50^{\circ}\text{C}$  and  $60^{\circ}\text{C}$  may be due to denaturation of non-collagen protein. Increase in transmission above  $60^{\circ}\text{C}$  may be due to the collagen phase transformation.

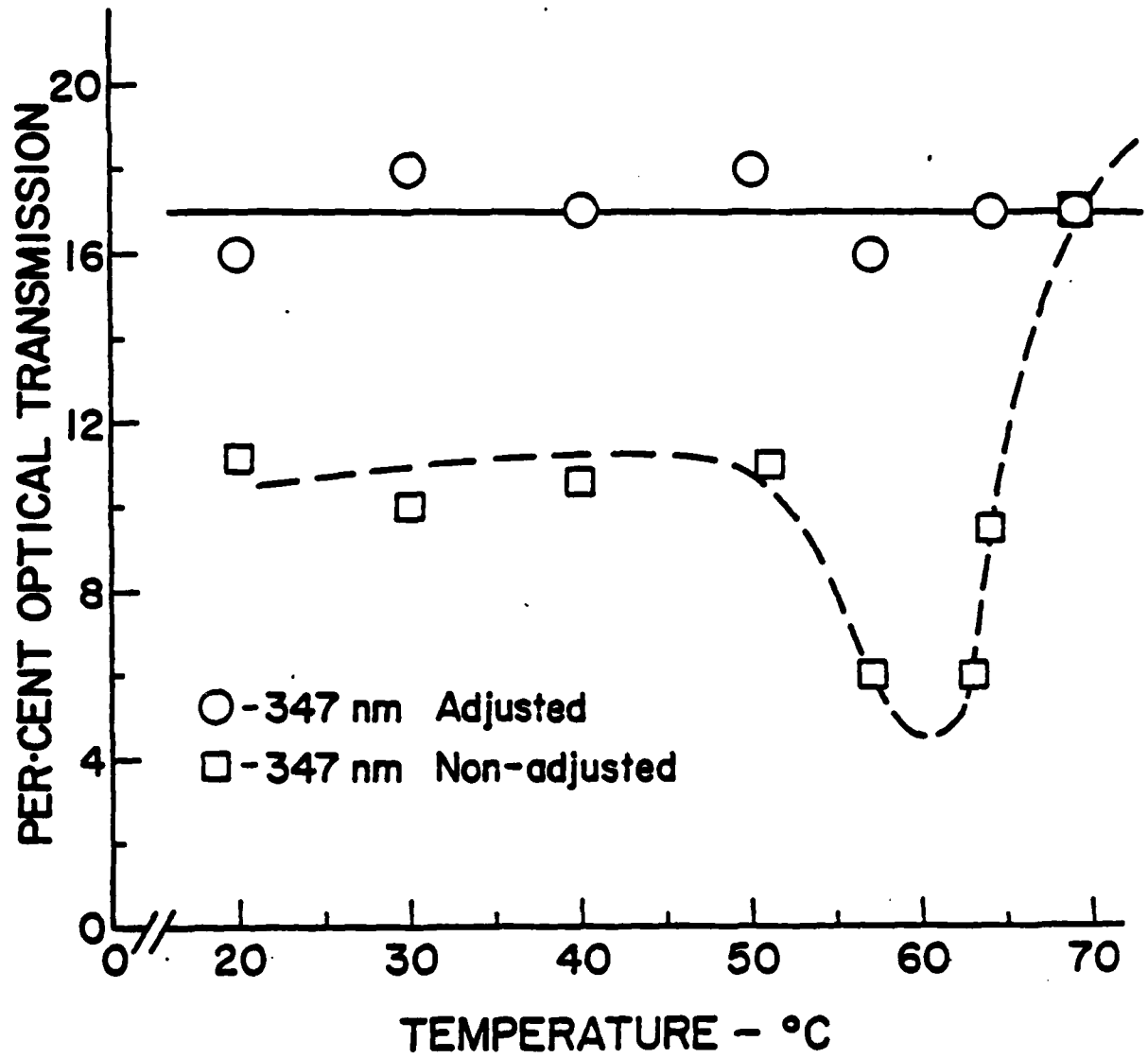


Figure 7.10

Relative forward scattered second-harmonic conversion efficiency  $C_{MRF}$  versus relative laser peak power,  $H_1$  for the corneal sample used in Figs. 7.8 and 7.9.

Each data point is labelled with the temperature to which the cornea had been heated.  $C_{MRF}$  was evidently lower after heating the cornea above  $60^\circ\text{C}$ . The straight lines C and D are regression lines fitted to the data for  $T \leq 57^\circ\text{C}$  and  $T > 57^\circ\text{C}$  respectively. The slope of line C is 1.04 and the slope of line D is 0.092. (These slopes should not be directly compared with those in Fig. 7.7 as different scales were used). The difference in slope between lines C and D is taken to indicate that a decrease in  $C_{MRF}$  occurred when the cornea was heated above the collagen phase transformation temperature ( $T = 60^\circ\text{C}$ ).

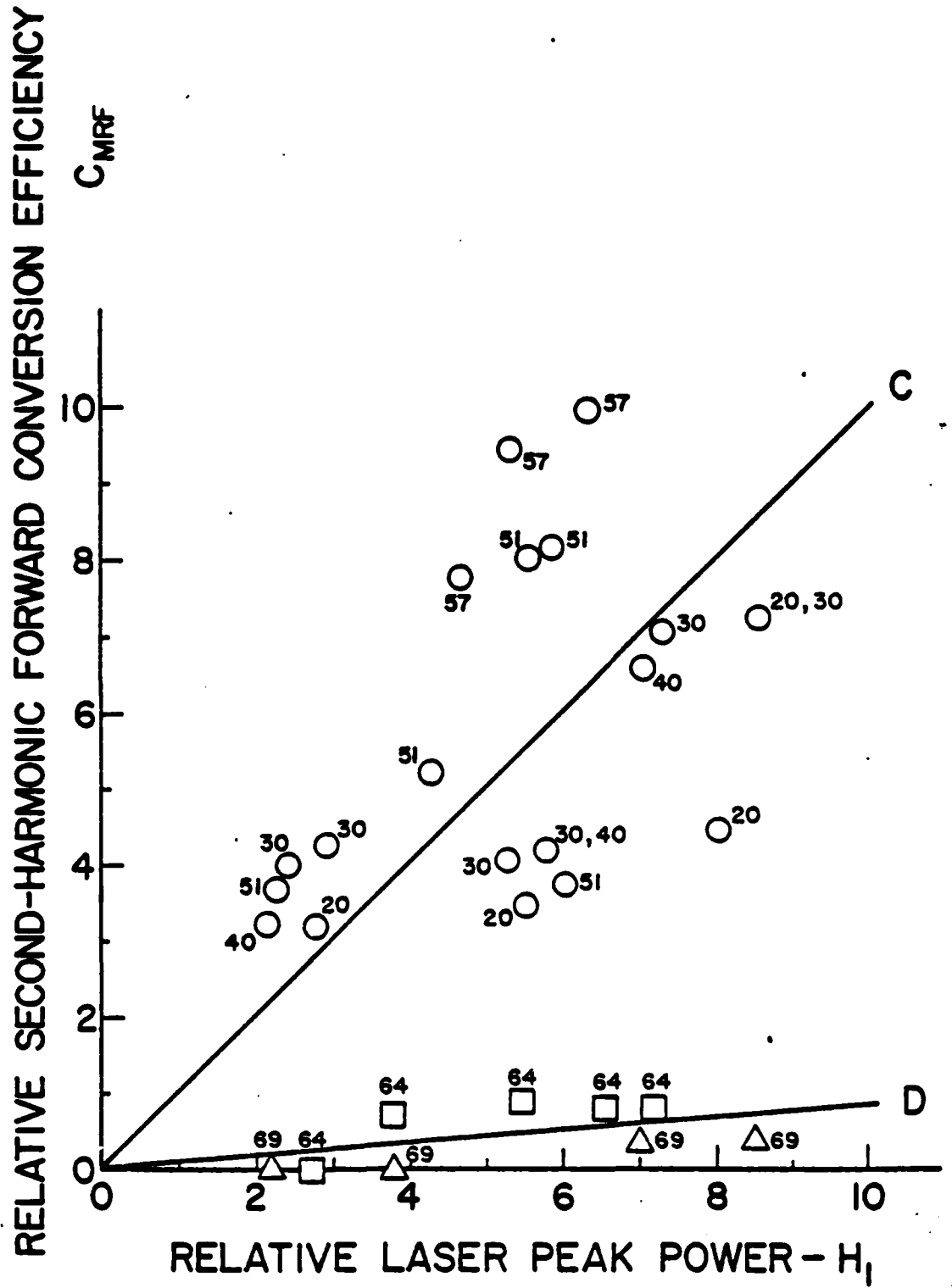


Figure 7.11

Schematic of model lamellae and model cornea. Each lamella is an infinite plane slab,  $2u$  in thickness. Separation between lamella is irregular. Total number of model lamella in model rabbit cornea is 200.

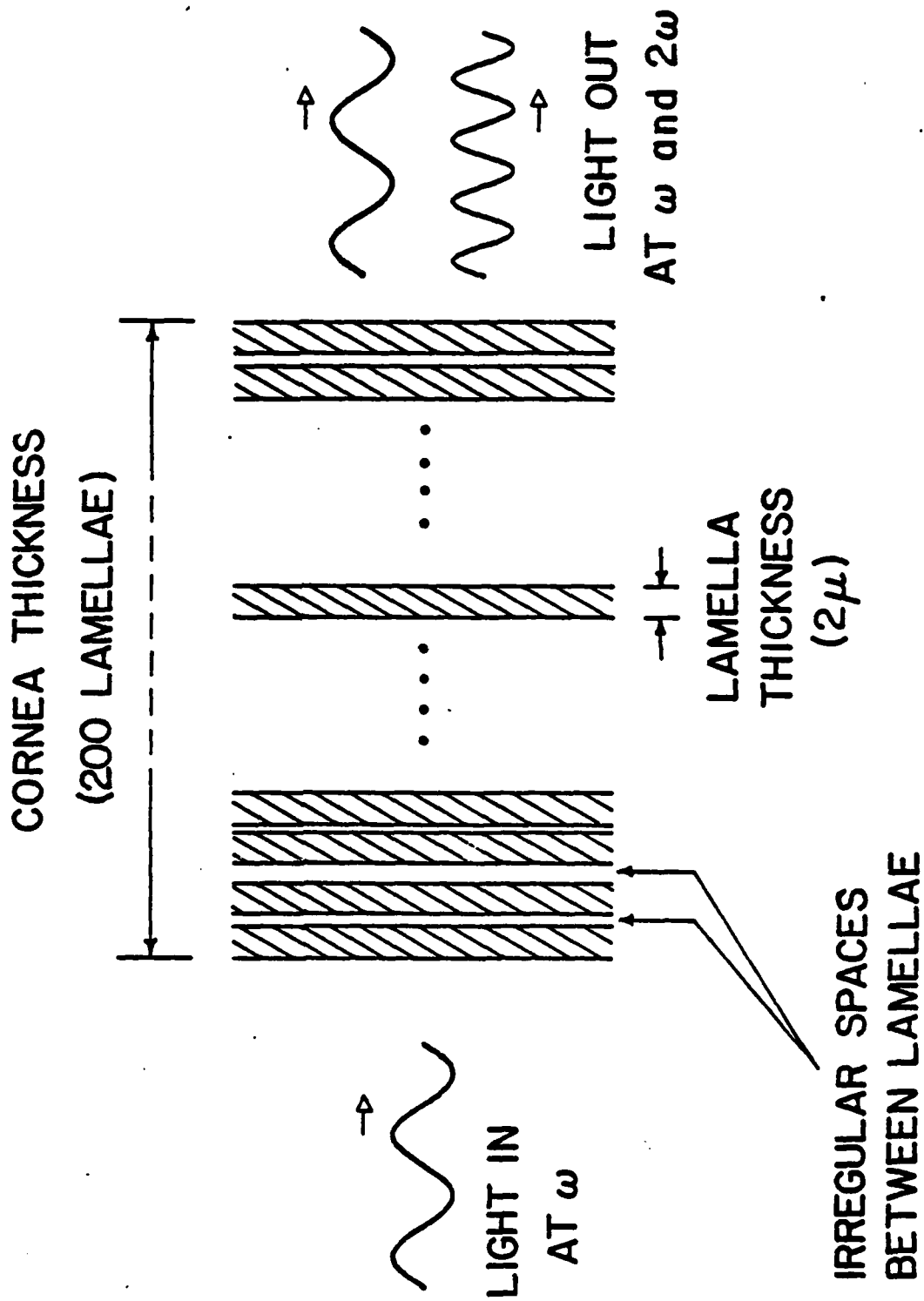


Figure 7.12

- (a) Schematic of a single strand of the collagen molecule showing the coiled helix conformation. The circles denote the amino acid positions. There is a peptide link between each amino acid.
- (b) Schematic of a segment of the three-stranded collagen molecule. Only the backbones of the separate strands are depicted. Three peptide link locations ( $P_1$ ,  $P_2$  and  $P_3$ ) are shown within a  $2.8\text{\AA}$  segment of the molecule.
- (c) A single rigid-rod collagen molecule is shown to the upper left. Such molecules are bundled together to form fibrils as indicated to the lower right. The fibril diameter shown is for corneas. The insert to the lower left shows an end view of the assumed packing of molecules in the fibril.

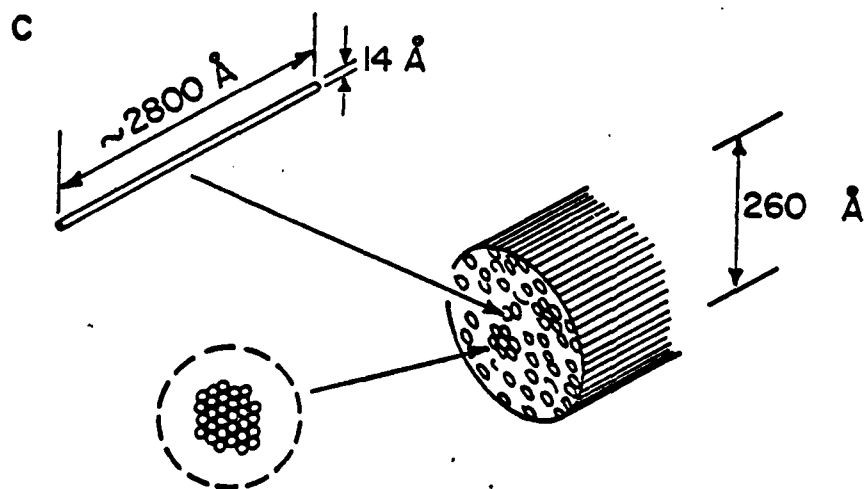
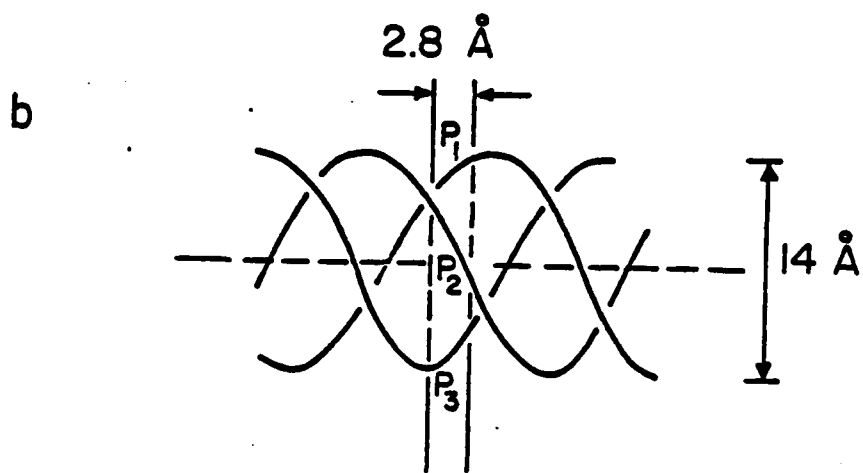
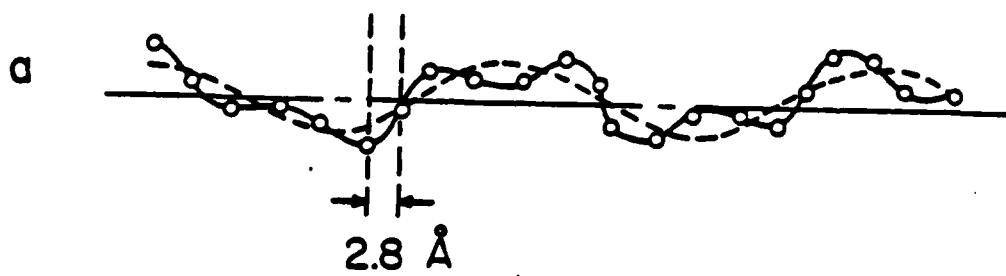


Table 1 --- Tendons

Temperature History*	Hydration during irrad.	Optical Trans. during irrad.		$C_{MRF}$ (normalized**)
		347nm	694nm	
Below 60°C	Moist (fresh)	2%	20%	0.01 - 0.05
Below 60°C†	Dry	30%	50%	1.0
Above 60°C	Moist	35%	80%	0.01 - 0.05
Above 60°C†	Dry	85%	95%	0.03

\* The collagen phase transformation occurred between 60°C and 65°C as evidenced by the contraction of the tissue (Fig. 4. ).

\*\*  $C_{MRF}$  in this column has been normalized to a magnitude of unity for dry tendon below 60°C.

† These are the six tendons discussed in detail in the main text.

Table 2 --- Corneas

Temperature History*	Hydration during irradiation.	Optical Trans. during irradiation. 347nm	C <sub>MRF</sub> (Normalized**)
20°C†	Moist (fresh)	60%	5
20°C - 50°C	Hydrated (excess H <sub>2</sub> O)	11%	0.1
20°C - 50°C	Dried after heating	70%	5
Above 63°C	Dried after heating	10%	0.1
20°C - 50°C	Adjusted***	17%	1.0
50°C - 63°C	Adjusted	17%	1.0
Above 63°C	Adjusted	17%	0.1

\* The collagen phase transformation occurred between 60°C and 63°C as evidenced by the contraction of the tissue.

\*\* C<sub>MRF</sub> in this column has been normalized to unity for corneas with 17% transmission at 347nm (partially hydrated) that had been "heated" at 20°C

† The first four rows are data summaries for a number of different corneas.

\*\*\* "Adjusted" hydration means that a fully hydrated cornea was partially dried in vacuum at 20°C following heating until the 347nm transmission rose to 17%. This cornea is discussed in detail in the main text.

## REFERENCES

1. Abella, I. D., and H. Z. Cummins, "Thermal Tuning of Ruby Optical Maser," Journ. Appl. Phys., 32, 1177, 1961.
2. Adolf Meller Company, Synthetic Sapphire Properties, Providence, R. I.
3. (AIP) American Institute of Physics Handbook, 1957.
4. Adelmanov, S. A., and R. V. Khoklov, Problems of Nonlinear Optics, (Gordon and Breach Science Publ., N. Y.), 1972.
5. Armstrong, J. A., N. Bloembergen, J. Ducuing, and P. S. Pershan, "Interactions Between Light Waves in a Nonlinear Dielectric", Phys. Rev., 127, pp. 1918ff, 1962.
6. Baldwin, G. C., An Introduction to Nonlinear Optics, (Plenum Press, N. Y.), 1969.
7. Baldwin, W. R., "Observations of Laser Standing Wave Patterns to Determine Refractive Status", Am. J. Optom. and Arch. Ac. Optom., 45, p. 143ff, 1968.
8. Banga, I. D., Structure and Function of Elastin and Collagen, Akademiai Kiado, Budapest, 1966.
9. Barnes, F. S., Chia-hun Hu, J. R. Lauridson and A. L. McGibbon, Characteristics of Biological Damage by Lasers", NEREM Record, Vol. VIII, IEEE Boston, pp. 164f, 1966.
10. Bear, R. S., The Structure of Collagen Fibrils in Advances in Protein Chemistry, Vol. 7, M. L. Anson, K. Baily, and J. T. Edsall editors (Academic Press, Inc., N. Y.), 1952.

11. Benedek, G. B., "Theory of the Transparency of the Eye", Appl. Optics, 10, 459, 1971.
12. Berns, M. W., D. E. Rounds, and R. S. Olson, "Effects of Laser Microirradiation on Chromosomes", Exptl. Cell. Res., 56, p. 292ff, 1969.
13. Bersohn, R., Y. Pao, and H. L. Frisch, "Double Quantum Light Scattering by Molecules", J. Chem. Phys., 45, pp. 3184ff, 1966.
14. Bloembergen, N., Nonlinear Optics, p. 131 (Benjamin, N. Y.), 1965.
15. Bloom, W. and D. W. Fawcett, Histology, (W. B. Saunders Company, Philadelphia), 1968.
16. Blout, E. R., J. P. Carver and J. Gross, "Intrinsic Cotton Effects in Collagen and Poly-L-Proline", Am. Chem. Soc. J., 85, pp. 644-646, 1963.
17. Bolduan, O. E. A. and R. S. Bear, J. Appl. Physiol., 20, 267, 1949.
18. Braun-Falco, O. and M. Rupec, "Some Observations on Dermal Collagen Fibrils in Ultra-thin Sections", Journ. Invest. Derm., 42, 15, 1964.
19. Campbell, J., S. Fine, "Heat Sensation Thresholds for CO<sub>2</sub> Laser Radiation", Radiation Res., 43, 1970.
20. Carslaw, H. S., and J. C. Jaeger, Conduction of Heat in Solids, 2nd ed., p. 199 (Oxford, London), 1959.
21. Charschan, S. S., Lasers in Industry, (Van Nostrand Reinhold Company, New York, N. Y.), 1972.
22. Clarke, A. M., W. J. Geeraets, and W. T. Ham, Jr., "An Equilibrium Thermal Model for Retinal Injury From Optical Sources", Appl. Optics,

- 8, p. 1051ff, 1969.
23. Condon, Altar and Eyring, J. Chem. Phys., 5, p. 763, 1937.
  24. Derr, V. E., E. Klein, and S. Fine, "Free Radical Occurrence in Some Laser-Irradiated Biologic Materials", Fed. Proc., Suppl. 14, Jan.-Feb., pp. S-99-S-103, 1965.
  25. Dische, Z., "Biochemistry of Connective Tissue of the Vertebrate Eye," pp. 247-271, in Int. Revs. of Conn. Tissue Res., Vol. 5, D. A. Hall and D. S. Jackson editors (Academic Press, N. Y.), 1970.
  26. Ditchburn, R. W., Light, Second Edition (Interscience Publishers), 1963.
  27. Doty, P., Biophysical Science, J. L. Oncley editor, Chap. 6 (John Wiley and Sons, Inc., N. Y.), 1959.
  28. Dubin, S. B., J. H. Lunacek and G. B. Benedek, "Observation of the Spectrum of Light Scattered by Solutions of Biological Molecules", Proc. Nat. Acad. Sci., 57, p. 1164ff, 1967.
  29. Ducuing, J., and N. Bloembergen, "Statistical Fluctuations in Nonlinear Optical Processes," Phys. Rev., 133, 1493, 1964.
  30. Elden, H. R., "The Physical Properties of Collagen", in Int. Revs. of Conn. Tissue Res., Vol. 4 (Academic Press, Inc., N. Y.), 1968.
  31. Einbiner, J., and M. J. Schubert, "Binding of Mucopolysaccharides and Dyes by Collagen," Journ. Biol. Chem., 188, 335, 1951.
  32. Fine, B. S., S. Fine, G. R. Peacock, W. J. Geeraets, and E. Klein, "Preliminary Observations on Ocular Effects of High-Power Continuous

- CO<sub>2</sub> Laser Irradiation", Amer. J. Ophthalmol., 64, pp. 209ff, 1967.
33. Fine, S., Fed. Proc. 24, Suppl. 14, p. S-47, 1965.
  34. Fine, S., W. Bushor, and M. Cox, Proceedings of the Laser Industry Association Convention, 1968.
  35. Fine, S., J. Edlow, D. MacKeen, L. Feigen, E. Ostrea, and E. Klein, "Focal Hepatic Injury and Repair Produced by Laser Radiation", Amer. J. Pathol., 52, pp. 155-176, 1968.
  36. Fine, S., and W. P. Hansen, "Optical Second Harmonic Generation in Biological Systems", Appl. Opt., 10, 2350, 1971.
  37. Fine, S., W. P. Hansen, G. R. Peacock, E. Klein, F. Hust and Y. Laor, "Biophysical Studies with the CO<sub>2</sub> Laser", NEREM Record, Vol. VIII, IEEE Boston, pp. 166ff, 1966.
  38. Fine, S., and E. Klein, "Biological Effects of Laser Radiation", in Advances in Biological and Medical Physics, Vol. 10 (Academic Press, N. Y.), p. 149ff, 1965.
  39. Fine, S. and E. Klein, Biological Effects of Laser Radiation Management Study Part I - Survey of the Literature, pp. 1-467, Final Report Contract No. Af-29(600)-5136, Air Force Missile Development Command, Air Force Systems Command, U. S. Air Force, 1966.
  40. Fine, S., and E. Klein, "Lasers in Biology and Medicine", Laser Focus, pp. 28-36, July 1969a.
  41. Fine, S., and E. Klein, "Ultraviolet Lasers" in Biologic Effects of Ultraviolet Radiation, ed. F. Urbach M.D. (Pergamon Press, N. Y.), pp. 115-123, 1969b.

42. Fine, S., and E. Klein, "Lasers in Biology and Medicine", in Proc. of Seminar on Developments in Laser Technology, Society of Photo-Optical Instrumentation Engineers, pp. 129ff, 1970.
43. Fine, S., E. Klein, W. Nowak, R. E. Scott, Y. Laor, L. Simpson, J. Crissey, J. Donoghue and V. E. Derr, "Interaction of Laser Radiation with Biologic Systems. I", Proc. First Ann. Conf. Biol. Eff. Laser Radiation, Fed. Am. Soc. for Exptl. Biol., Washington, D.C., p. S-35ff, 1965.
44. Fine, S., E. Klein, and R. E. Scott, "Biological Effects of Laser Radiation", IEEE Spectrum, p. 81ff, April 1964.
45. Flory, P. J., "Role of Crystallization in Polymers and Proteins", Science, 124, July 13, p. 53, 1956.
46. Flory, P. J., and R. R. Garrett, "Phase Transitions in Collagen and Gelatin Systems", Am. Chem. Soc. Journ., 80, p. 4836, 1958.
47. Franken, P. A., A. E. Hill, C. W. Peters, and G. Weinrich, "Generation of Optical Harmonics", Phys. Rev. Lett., 7, pp. 118ff, 1961.
48. Franken, P. A., and J. F. Ward, "Optical Harmonics and Nonlinear Phenomena", Revs. Mod. Phys., 35, p. 23, 1963.
49. Garrett, C. G. B., and F. N. H. Robinson, "Miller's Phenomenological Rule for Computing Nonlinear Susceptibilities", IEEE J. Quantum Elec., Aug., pp. 328-329, 1966.
50. Geeraets, W. J., W. T. Ham, Jr., R. C. Williams, H. A. Mueller, J. Barkhart, Guerry, DuPont, and J. J. Vos, "Laser versus Light Coagulator", in Proc. First Ann. Conf. Biol. Eff. Laser Radiation,

- Fed. of Am. Soc. for Exptl. Biol., Washington, D.C., p. S-48ff, 1965.
51. Glasstone, S., Textbook of Physical Chemistry (D. Van Nostrand Company, N. Y.), pp. 605-608, 1946.
  52. Glimcher, M. J., "Molecular Biology of Mineralized Tissues", pp. 368-370, in Biophysical Science, J. L. Oncley editor, (John Wiley and Sons, Inc., N. Y.), 1959.
  53. Goldman, L., Biomedical Aspects of the Laser (Springer, N. Y.), 1967.
  54. Goldman, L., and J. R. Rockwell, Jr., Lasers in Biomedicine, (Gordon and Breach, Science Publishers, Inc., N. Y.), 1971.
  55. Gratzer, W. B., Poly-A-Amino Acids, G. D. Fasman editor, p. 177 (Marcel Dekker, Inc., N. Y.), 1967.
  56. Gratzer, W. B., W. Rhodes, and G. D. Fasman, "Optical Properties of the Poly-L-Proline and Collagen Helices," Biopolymers, 1, 319, 1963.
  57. Gross, J., "Collagen," Sci. Am., 204, 120, May 1961.
  58. Gross, J., and F. O. Schmitt, Journ. Exp. Med., 88, 555, 1948.
  59. Ham, J. S. and J. R. Platt, J. Chem. Physiol., 20, 335, 1952.
  60. Ham, W. T., Jr., R. C. Williams, H. A. Mueller, DuPont Guerry, III, A. M. Clarke, and W. J. Geeraets, "Effects of Laser Radiation on the Mammalian Eye," Trans. N. Y. Acad. Sci., Ser. II, 28, p. 517-526, 1966.
  61. Handbook of Chemistry and Physics, 46th Edition, R. C. Weast editor,

- (a) p. E-143 (Chemical Rubber Company, Cleveland), 1965.
62. Hansen, W. P., T. A. Balasubramaniam, R. J. Greenwald, and H. F. Bowman, "A System Design for Noninvasive Thermal Conductivity Measurements in Biomaterials", to be published in Advances in Thermal Conductivity, Univ. of Missouri at Rolla, 1973b.
63. Hansen, W. P., L. Feigen, and S. Fine, "A Worst-Case Analysis of Continuous Wave He-Ne Laser Hazards to the Eye", Appl. Optics, 6, p. 1973ff, 1967 (Erratum, 7, p. 1860, 1968).
64. Hansen, W. P., and S. Fine, "Melanin Granule Models for Pulsed Laser Induced Retinal Injury", Appl. Opt., 6, pp. 155-159, 1968.
65. Hansen, W. P., and S. Fine, "Application of Thermal Models to Retinal Threshold Injury", Proc. Laser Industry Association Convention, pp. 95-108, 1968b.
66. Hansen, W. P., S. Fine, G. R. Peacock, and E. Klein, "Focusing of Laser Light by Target Surfaces and Effects on Initial Temperature Conditions", WEREM Record (IEEE Cat. No. F-60), pp. 156-157, 1965.
67. Hansen, W. P., R. J. Greenwald, and H. F. Bowman, "Application of the CO<sub>2</sub> Laser to Thermal Properties Measurements in Biomaterials", Trans. ASME J. Eng. Matis. and Technology.
68. Hart, R. W., and R. A. Farrell, "Light Scattering in the Cornea", Journ. Opt. Soc. Am., 39, p. 766, 1969.
69. Hayes, J. R., and M. L. Wolbarsht, "Thermal Model for Retinal Damage Induced by Pulsed Laser", Aerospace Med., 39, pp. 474ff, 1968.
70. Herzberg, G., Molecular Spectra and Molecular Structure III.

Electronic Spectra and Electronic Structure of Polyatomic Molecules,

(D. Van Nostrand Company, Inc., Princeton, N. J.), 1966.

71. (ICT) International Critical Tables
72. Jackson, J. D., Classical Electrodynamics (John Wiley and Sons, Inc., N. Y.), 1962.
73. Jakus, M. A., J. Biophys. Biochem. Cytol. Suppl. 2, 241, 1956.
74. Kielich, S., "Nonlinear Light Scattering by Molecules Without a Centre of Inversion", Bulletin de L'Academie Polonaise des Sciences, Ser. des sciences math., astr., et phys. - Vol. XI, No. 1, pp. 53ff, 1964.
75. Kirschenbaum, D. M., Atlas of Protein Spectra in the Ultraviolet and Visible Regions, (Plenum Press, N. Y.), p. 59, 1972.
76. Kittel, C., Introduction to Solid State Physics, Second Edition, (John Wiley and Sons, Inc., N. Y.), 1956.
77. Klein, E., Laor, Y., Fine, S., Simpson, L. C., Edlow, J., Litwin, M. "Threshold Studies and Reversible Depigmentation in Rodent Skin," NEREM Record (IEEE Cat. No. F-60), Vol. 7, pp. 108-109, 1965.
78. Klein, M. V., Optics, (John Wiley and Sons, Inc., N. Y.), 1970.
79. Kleinman, D. A., "Theory of Second-Harmonic Generation of Light", Phys. Rev., 128, pp. 1761ff, 1962.
80. Kohn, R. R., Principles of Mammalian Aging, p. 33 (Prentice-Hall, Englewood Cliffs, N. J.), 1971.
81. Langham, M. E., R. W. Hart, J. Cox, "The Interaction of Collagen and Mucopolysaccharides" in The Cornea, M. Langham editor, p. 157,

- (Johns Hopkins Press, Baltimore), 1969.
82. L'Esperance, F. A., "Reconstituted Collagen Tape in Retinal Detachment Surgery," Arch. of Ophthal., 73, p. 472, 1965.
  83. Lin, C., and R. F. Sullivan, "An Application of White Light Interferometry in Thin Film Measurements," IBM Journ. Res. and Devel., 16, p. 269, 1972.
  84. Litwin, M. S., and K. M. Earle, Proceedings of the First Annual Conference on the Biologic Effects of Laser Radiation, (Federation of American Societies for Experimental Biology, Washington, D.C.), 1964.
  85. Maker, P. D., R. W. Terhune, M. Nisenoff, and C. M. Savage, "Effects of Dispersion and Focusing on the Production of Optical Harmonics", Phys. Rev. Lett., 8, pp. 21-22, 1962.
  86. Mathews, M. B., in The Cornea, M. Langham editor (Johns Hopkins Press, Baltimore), 1969.
  87. Maurice, D. M., The Cornea and Sclera, p. 289, in The Eye, Vol. 1, H. Davson editor (2nd edition, Academic Press, N. Y.), 1969.
  88. Maurice, D. M., and M. V. Riley, "The Cornea", in Biochemistry of the Eye, C. N. Graymore editor, (Academic Press, London), 1970.
  89. Meyer, P. L., Introductory Probability and Statistical Applications, p. 126 (Addison-Wesley Publ. Co., Reading, Mass.), 1965.
  90. Minck, R. W., R. W. Terhune, and C. C. Wang, "Nonlinear Optics", Proc. IEEE, 54, pp. 1357-1374, 1966.
  91. Monk, G. S., Light, Principles and Experiments, 2nd Edition, (Dover

- Publications, Inc., N. Y.), 1963.
92. Nye, J. F., Physical Properties of Crystals, (Oxford, Clarendon Press), 1967.
  93. Parratt, L. G., Probability and Experimental Errors in Science, pp. 126-129, (Dover Publications, Inc., N. Y.), 1961.
  94. Peppers, N. A., A. Vassiliadas, K. G. Dedrick, H. Chang, R. R. Peabody, H. Rose, and H. C. Zweng, "Corneal Damage Thresholds for CO<sub>2</sub> Laser Radiation", Appl. Optics, 8, p. 377ff, 1969.
  95. Pershan, P. S., "Optical Second-Harmonic Generation", in Progress in Optics, Vol. V, E. Wolf editor, p. 133, (North-Holland Publishing Co., Amsterdam), 1966.
  96. Pressley, R. J., Handbook of Lasers, (The Chemical Rubber Company, Cleveland, Ohio), 1971.
  97. Ramachandran, G. N., and V. Sasisekharan, Nature, 190, p. 1004, 1961.
  98. Ready, J. F., Effects of High-Power Laser Radiation, (Academic Press, N. Y.), 1971.
  99. Reickhoff, K. E., and W. J. Peticolas, "Second-Harmonic Generation From Amino Acids", Science, 147, p. 610, 1965.
  100. Rich, A., "Molecular Configuration of Synthetic and Biological Polymers", in Biophysical Science, A Study Program, pp. 50-60, J. L. Oncley editor, (John Wiley and Sons, Inc., N. Y.), 1959.
  101. Rounds, D. E., R. S. Olson, and F. M. Johnson, "The Effect of the Laser on Cellular Respiration", NEREM Record (IEEE Cat. No. F-60),

- pp. 106-107, 1965.
102. Saks, N. M., "Cell Biology by Laser Light", in Laser Applications in Medicine and Biology, ed. by M. H. Wolbarsht, (Plenum Press, N. Y.), pp. 67-86, 1971.
  103. Schmitt, F. O., "Macromolecular Interaction Patterns," Proc. Am. Phil. Soc., 100, p. 476, 1956.
  104. Schmitt, F. O., "Interaction Properties of Elongate Protein Molecules with Particular Reference to Collagen," in Biophysical Science - A Study Program, J. L. Oncley, ed. in chief, (Wiley and Sons, N. Y.), 1959.
  105. Schmitt, F. O., C. E. Hall, M. A. Jakus, "Electron Microscope Investigation of the Structure of Collagen," J. Cell. and Comp. Physiol., 20, p. 11, 1942.
  106. Schwarz, W., in Connective Tissue, R. E. Tunbridge editor, (Blackwell Scientific Publ., Oxford), p. 149ff, 1957.
  107. Schwarz, W., and D. Graf Keyserlingk, in The Cornea, M. Langham editor, (Johns Hopkins Press, Baltimore), p. 158ff, 1969.
  108. Setlow, R. B., and E. C. Pollard, Molecular Biophysics, (Addison-Wesley Publ. Co., Reading, Mass.), 1962.
  109. Siegman, A. E., An Introduction to Lasers and Masers, (McGraw Hill, N. Y.), 1971.
  110. Sommerfeld, A., Optics (Lectures on Theoretical Physics Vol. IV), Translated by O. Laporte and P. A. Moldauer (Academic Press, N. Y.), 1964.

111. Stratton, K., M. A. Pathak, and S. Fine, "ESR Studies of Melanin Containing Tissues after Laser Irradiation", NEREM Record (IEEE Cat. No. F-60), pp. 150-151, 1965.
112. Taylor, H. L., and R. W. Ebbers, "Effect of Pulsed Laser Radiation on Discriminative Avoidance Behavior", NEREM Record, Vol. VIII, IEEE Boston, pp. 162ff, 1966.
113. Terhune, R. W., P. D. Maker, and C. M. Savage, "Measurements of Nonlinear Light Scattering", Phys. Rev. Lett., 14, pp. 681-684, 1965.
114. Tregear, R. T., Physical Functions of Skin, pp. 81-88, (Academic Press, N. Y.), 1966.
115. Urnes, P., and P. Doty, "Optical Rotation and the Conformation of Polypeptides and Proteins" in Advances in Protein Chemistry, Vol. 16, (Academic Press, N. Y.), pp. 402-563, 1961.
116. Vanamee, P., and K. R. Porter, "Observation With the Electron Microscope on the Solvation and Reconstitution of Collagen" Journ. Exp. Med., 94, p. 255, 1957.
117. Van Winkle, W., Jr., Collagen Purity in Catgut, (Ethicon, Inc.), 1954.
118. Vasilenko, L. S., V. P. Chebotaev, and Yu. V. Triotskii, "Visual Observation of Infrared Laser Emission" Zh. Exsp. Teor. Fiz., 48, p. 777, 1965 (Sov. Phys. JETP, 21, 513, 1965).
119. Vassiliadas, A., "Ocular Damage from Laser Radiation", in Laser Applications in Medicine and Biology, ed. M. Wolbarsht, (Plenum Press, N. Y.), pp. 125-162, 1971.
120. Verzar, F., "The Aging of Collagen" Sci., Am., 208, p. 104, April 1963.

121. Vickers, A. E. J., in Polarized Light, American Institute of Physics, N. Y., 1963.
122. Ward, J. F., and G. H. C. New, "Optical Third-Harmonic Generation in Gases", Phys. Rev. Lett., 19, pp. 556-559, 1967.
123. Watanabe, K., and M. Zelikoff, "Absorption Coefficients of Water Vapor in the Vacuum Ultraviolet", J. Opt. Soc. Amer., 43, p. 753, 1953.
124. Wetlaufer, D. B., "Ultraviolet Spectra of Proteins and Amino Acids", in Advances in Protein Chemistry, Vol. 17, ed. by Anfinsen, C. B., M. L. Anson, K. Bailey, and J. T. Edsall, (Academic Press, N. Y.), pp. 304-405, 1962.
125. Wolbarsht, M. L., Laser Applications in Medicine and Biology, (Plenum Press, N. Y.), 1971.
126. Wood, G. C., "Spectral Changes Accompanying the Thermal Denaturation of Collagen," Biochem. and Biophys. Res. Comm., 13, 1963.
127. Wood, G. C., "The Precipitation of Collagen Fibers from Solution", in Int. Revs. of Conn. Tissue Res., Vol. 2, D. A. Hall and D. S. Jackson editors, (Academic Press, N. Y.), pp. 8ff, 1970.
128. Yannas, I. V., "Physical Chemistry of Collagen in the Solid State", in Biomedical Physics and Biomaterials Science, ed. by H. E. Stanley, (The M.I.T. Press, Cambridge, Mass.), p. 41ff, 1972.
129. Yariv, A., Quantum Electronics (John Wiley and Sons, N. Y.), 1968.
130. Yariv, A., Introduction to Optical Electronics, (Holt, Rinehart and Winston, Inc., N. Y.), 1971.

131. Zaret, M. M., "Analysis of Factors of Laser Radiation Producing Retinal Damage"; Fed. Proc., Suppl. 14, pp. S-62-S-64, 1965.
132. Zobel, R. C., and A. B. F. Duncan, "Vacuum Ultraviolet Absorption Spectra of Some Halogen Derivatives of Methane. Correlation of the Spectra", J. Chem. Phys., 77, pp. 2611ff, 1955.

PERSONNEL RECEIVING CONTRACT SUPPORT AND GRADUATE DEGREES OBTAINED

Arnold Aaron	Ph.D. in Engineering
Charles Aaronson	M.S. in Engineering
John Campbell	M.A. in Psychology
John Caron	M.S. in Engineering
Joel Cohen	M.S. in Biology
John Donoghue	M.S. in Engineering
Larry Feigen	M.S. in Physics
James Forman	M.S. in Engineering
Peter Hansen	Ph.D. in Engineering
Karl Hergenrother	Ph.D. in Engineering
Donald MacKeen	Ph.D. in Biology

Note: The above individuals were supported in full or in part for contract related work while carrying out graduate work. In some cases, the support was minimal.

OTHER NON-GRADUATE DEGREE PERSONNEL RECEIVING SUPPORT INCLUDE:

James Blout  
Francis Daniels  
Evelina Gorman  
Mary Laananen  
Audrey Marino  
Angela Reed  
Grace Woods

## PUBLICATIONS

### A. Laser-Related

1. Fine, S., Klein, E., Scott, R.E., Aaronson, C. and Donoghue, J. "Biological Effects of Laser Radiation," Second Boston Laser Conference, August 1, 1963.
2. Fine, S., Maiman, T.H., Klein, W. and Scott, R.E. "Biological Effects of High Peak Power Radiation," Life Sciences, 3:309-322, March, 1964.
3. Fine, S. and Klein, E. "Effects of Pulsed Laser Irradiation of the Forehead in Mice," Life Sciences, 3:199-207, March, 1964.
4. Fine, S., Klein, E. and Scott, R.E. "Studies on Interaction of Laser Radiation with Biological Systems," IEEE Spectrum, March, 1964.
5. Fine, S., Klein, E., Derr, V.E. and Nowak, W.B. "Hazards and Biological Effects of Laser Radiation," Proceedings of the Martin Interdivisional Solid State Symposium, March 1964.
6. Edlow, J., Farber, S., Fine, S. and Klein, E. "Prenatal and Neonatal Effects of Laser Radiation," Biological Abstracts of Boston Laser Conference, 1964.
7. Klein, E., Fine, S., Cohen, E., Ambrus, J., Meter, E., Lyman, R. and Scott, R.E. "Effects of Laser Radiation on Biological Systems," American College of Physicians (Atlantic City, N.J.), April 10, 1964.
8. Klein, E. and Fine, S. "Effects of Laser Radiation on Animal Tissues," presented at Conference on Lasers, New York Academy of Sciences, May 4, 1964.
9. Klein, E., Fine, S. and Laor, Y. "Modification of Effects of Laser Radiation by Light Absorbing Chemicals," Biological Abstracts of Boston Laser Conference, August, 1964.
10. Klein, E., Fine, S., Scott, R.E. and Farber, S. "Observations of Laser Irradiation of Experimental Tumors," Proceedings, American Association for Cancer Research, 1964.
11. Derr, V., Klein, E. and Fine, S. "Electron Spin Resonance Tests of Laser Irradiated Biological Systems," Applied Optics, 3:786, 1964.
12. Fine, S., Klein, E., Aaronson, C., Hardway, G., King, W. and Scott, R.E. "Closed Circuit Television in Laser Investigations," Journal of Invest. Derm., 4:289-91, 1964.
13. Klein, E., Fine, S., Laor, Y., Litwin, M., Donoghue, J. and Englander, L. "Laser Irradiation of the Skin," Journal of Invest. Derm., 43:565, 1964.

14. Fine, S., Klein, E., Ambrus, J., Cohen, E., Derr, V. and Ambrus, C. "Interaction of Relatively Coherent Laser Radiation and Biological Systems," Federation Proceedings, 23, 1964.
15. Fine, S., Klein, E., Nowak, W.B., Hansen, W.P., Hergenrother, K., Scott, R.E. and Donoghue, J. "Measurements and Hazards on Interaction of Laser Radiation and Biological Systems," NEREM Record, 1958, 1964.
16. Nowak, W.B., Fine, S., Klein, E., Hergenrother, D., Hansen, W.P. "On the Use of Thermocouples for Temperature Measurement During Laser Irradiation," Life Sciences, 3:1495-1581, 1964.
17. Derr, V., Klein, E. and Fine, S. "Free Radical Occurrence in Some Laser Irradiated Biological Materials," Federation Proceedings, 24 (1), Suppl. 14, Part III, January-February, 1965.
18. Fine, S., Klein, E., Nowak, W.B., Scott, R.E., Simpson, L., Crissey, J. and Donoghue, J. "Interaction of Laser Radiation with Biological Systems. I. Studies on Interaction with Tissues," Federation Proceedings, 24 (1), Suppl. 14, Part III, January-February, 1965.
19. Klein, E., Fine, S., Laor, Y., Simpson, L., Ambrus, J., Richter, W., Smith, G.K. and Aaronson, C. "Interaction of Laser Radiation with Biological Systems. II. Experimental Tumors," Federation Proceedings, 24 (1), Suppl. 14, Part III, January-February, 1965.
20. Klein, E., Fine, S., Ambrus, J., Cohen, E., Ambrus, C., Neter, I., Bardos, T. and Lyman, R. "Interaction of Laser Radiation with Biological Systems. III. Studies on In Vitro Preparations," Federation Proceedings, 24 (1), Suppl. 14, Part III, January-February, 1965.
21. Edlow, J., Fine, S. and Vawter, G.F. Federation Proceedings, 24:556, April, 1965.
22. Litwin, M., Fine, S., McCombs, H.E. and Klein, E. "Effects of Laser Radiation on the Surgically Exposed Canine Liver," Federation Proceedings, 24 (1), Suppl. 14, Part III, 566, March-April, 1965.
23. Fine, S., Klein, E., Fine, B.S., Litwin, M., Nowak, W.B., Hansen, W.P., Caron, J. and Forman, J. "Mechanisms and Control of Laser Hazards and Management of Accidents," Laser Technology Conference, April, 1965.
24. Laor, Y., Simpson, L.C., Klein, E. and Fine, S. "The Pathology of Laser Irradiation on the Skin and Body Wall of the Mouse," The American Journal of Pathology, Vol. 47, No. 4, October, 1965, pp. 643-63.
25. Hansen, W.P., Fine, S., Peacock, G.R. and Klein, E. "Focusing of Laser Light by Target Surfaces and Effects on Initial Temperature Conditions," NEREM Record, Vol. 7, 156-157, 1965.

26. Stratton, K., Pathak, M.A. and Fine, S. "ESR Studies of Melanin Containing Tissues After Laser Irradiation," NEREM Record, p. 150, 1965.
27. Klein, E., Laor, Y., Fine, S., Simpson, L.C., Edlow, J., Litwin, M. "Threshold Studies and Reversible Depigmentation in Rodent Skin," NEREM Record, Vol. 7, pp. 108-109, 1965.
28. Edlow, J., Fine, S., Vawter, G.F., Jockin, H. and Klein, E. "Laser Irradiation Effect on Rat Embryo and Fetus in Utero," Life Sciences, 4:615-23, 1965.
29. Klein, E. and Fine, S. "Biological Aspects of Laser Radiation." Abstract presented at the 149th National Meeting of the American Chemical Society, Detroit, Michigan, 1965.
30. Fine, S. and Klein, E. "Biological Effects of Laser Irradiation," in Advances in Biological and Medical Physics, Academic Press, 10:149-225, 1965.
31. Fine, S., Klein, E., Litwin, M., Peacock, G., Hamar, M. and Hansen, W.P. "Biological Effects of High Power Continuous N<sub>2</sub>-CO<sub>2</sub> Laser Radiation at 10.6 Microns," Federation Proceedings, Vol. 25, No. 2, Part I, March-April, 1966.
32. Laor, Y., Hust, F., Fine, S. and Klein, E. "Studies on Biological Effects of Laser Radiation," Symposium on Biomedical Engineering, Marquette University, Milwaukee, Wisconsin, Vol. 1, pp. 316-318, June, 1966.
33. Lobene, R. and Fine, S. "Interaction of Laser Radiation with Oral Hard Tissues," Journal of Prosthetic Dentistry, 16:3, 589-597, May-June, 1966.
34. Fine, S., Klein, E., Litwin, M. "Laser Radiation and Therapy of Malignant Melanomas," New Views of Skin Diseases, Boston: Little, Brown & Co., 1966.
35. Fine, S., Klein, E., Fine, B.S., Hansen, W.P., Peacock, G.R. and Litwin, M. "Implementation of Procedures and Techniques for Safe Operation of Lasers," Proceedings of the First Conference on Laser Safety, November, 1966.
36. Klein, E., Fine, S., Laor, Y., Hust, F. and MacKeen, D. "Injurious Effects of Laser Radiation on Mammals," published in Proceedings of the First Conference on Laser Safety, November, 1966.
37. Fine, S. and Klein, E. "Ultraviolet Lasers," presented at the First Conference of the Biologic Effects of Ultraviolet Radiation, published in The Biologic Effects of Ultraviolet Radiation, F. Urbach, editor, Pergamon Press, 1969.

38. Fine, S., Hansen, W.P., Peacock, G.R., Klein, E., Hust, F. and Laor, Y. "Bio-physical Studies with the CO<sub>2</sub> Laser," NEREM Record, 8:166-167, November, 1966.
39. Fine, B.S., Fine, S. and Zimmerman, L.E. "CO<sub>2</sub> Lasers Irradiation on the Rabbit Eye, Clinical and Histopathologic Observations," NEREM Record, 8:160-161, November 1966.
40. Fine, S., Klein, E. "Biological Effects of Laser Radiation," in McGraw-Hill Yearbook of Science and Technology, 1966.
41. Klein, E., Fine, S., Laor, Y. and Hust, F. "Biological Effects of Laser Radiation," Proceedings American Society for Cancer Research, 1966.
42. Fine, S., Klein, E., Hansen, W.P. and Litwin, M. "Biological Effects of Laser Radiation," Digest of Technical Papers, International Quantum Electronics Conference, 1966.
43. Fine, S., Klein, E., Haynie, W.H., Litwin, M., Laor, Y. and Hust, F.S. "Biological Effects and Hazards of Laser Radiation," presented at American College of Physicians Conference, 1966.
44. Fine, S., Klein, E., et al. "Management Study on Biological Effects of Laser Radiation Program" for U.S. Air Force, Parts I, II, and III, 1000 pages, 1966.
45. Klein, E., Fine, S., Laor, Y., Hust, F., Litwin, M. and Knubbe, K. "Interaction of Laser Radiation with Experimental Melanoma," Proc. Am. Assoc. Cancer Res., 7:36, 1966.
46. Litwin, M.S., Fine, S., Klein, E., Fine, B.S. and Raemer, H. "Hazards of Laser Radiation Mechanisms, Control and Management," American Industrial Hygiene Assoc. Journal, 28:68-75, January-February, 1967.
47. Fine, S., Klein, E., Parr, W.H., Fine, B., Fisher, R.S., Peacock, G.R., MacKeen, D., Hansen, W.P. and Feigen, L. "Hazard Studies with Laser Radiation," Conference on Laser Technology, April, 1967.
48. Hardy, L.B., Hardy, F.S., Fine, S. and Sokal, J. "Effect of Ruby Laser on Mouse Fibroblast Culture," Federation Proceedings, 26:688, April, 1967.
49. Fine, B.S., Fine, S., Peacock, G.R., Geeraets, W. and Klein, E. "Preliminary Observations on Ocular Effects of High-Power, Continuous CO<sub>2</sub> Laser Irradiation," American Journal of Ophthalmology, Vol. 64, No. 2, pp. 209-222, August, 1967.
50. Peacock, G.R., Hansen, W.P. and Fine, S. "Increasing the Power Output from Inexpensive CO<sub>2</sub> Lasers," American Journal of Physics, Vol. 35, No. 8, 776-777, August, 1967.

51. Fine, S., Feigen, L., MacKeen, D. and Klein, E. "Hazards and Protective Devices Associated with 10.6  $\mu$  Radiation," presented at Conference on Engineering in Medicine and Biology, 1967. Published in Proceedings, November, 1967.
52. Hansen, W.P., Feigen, L. and Fine, S. "A 'Worst Case' Analysis of Continuous Wave He-Ne Laser Hazards to the Eye," Applied Optics, Vol. 6, No. 11, pp. 1973-1975, November, 1967.
53. Laor, Y., Simpson, L., Klein, E., Fine, S. and Hust, F. "Effects of Laser Radiation on the Skin and Underlying Tissue of Mice during Controlled Hair Growth Cycle," Journal of Invest. Derm., 48:297-298, 1967.
54. Fine, S., Edlow, J., MacKeen, D., Feigen, L., Ostrea, E. and Klein, E. "Focal Hepatic Injury and Repair Produced by Laser Radiation: Pathologic and Biophysical Studies," American Journal of Pathology, Vol. 52, No. 1, pp. 155-176, January, 1968.
55. Hansen, W.P. and Fine, S. "Melanin Granule Models for Laser Induced Retinal Injury," Applied Optics, Vol. 7, No. 1, pp. 155-159, January, 1968.
56. Aaron, A., Fine, S. and Schetzen, M. "Safety Improvement for Unattended Lasers," Laser Focus, February, 1968.
57. Lobene, R.R., Raj Bhussry, B. and Fine, S. "The Interaction of Carbon Dioxide Laser Radiation with Enamel and Dentin," Journal of Dental Research, Vol. 47, No. 2, pp. 311-317, March-April, 1968.
58. Cohen, E. and Fine, S. "In Vitro Effects of Laser Irradiation on Human Gamma Globulin," Federation Proceedings, 27:1, 473, March-April, 1968.
59. Parker, G.S., Bavley, H.A. and Fine, S. "Report on Massachusetts Laser Survey," Laser Focus, 11:30-32, May, 1968.
60. Parker, G.S., Bavley, H., Fine, S., Powell, C. and Keene, B. "Laser Survey in Massachusetts," Health Physics Society Annual Meeting, Denver, Colorado, June 16-20, 1968. (Abstract.)
61. Fine, B.S., Fine, S., Feigen, L. and MacKeen, D. "Corneal Injury Threshold to Carbon Dioxide Laser Irradiation," Vol. 66, No. 1, pp. 1-15, July, 1968, American Journal of Ophthalmology.
62. Cohen, E., Klein, E. and Fine, S. "Effects of Laser Irradiation on Some Serologic Properties of Human Gamma Globulin," accepted for publication.
63. MacKeen, D., Fine, S. and Klein, E. "Toxic and Explosive Hazards Associated with Lasers," Laser Focus, pp. 47-49, October, 1968.
64. Fine, B.S., Berkow, J.W., Fine, S. "Corneal Calcification," Science, Vol. 162, pp. 129-130, October 4, 1968.

65. Hansen, W.P. and Fine, S. "Application of Thermal Models to Retinal Threshold Injury," presented at Laser Industry Association meeting, October 24-26, 1968, published in Proceedings of the Laser Industry Association Convention, 1968.
66. Bock, F., Laor, Y., Fine, S. and Klein, E. "Exploration of Potential Carcinogenic Effects of Pulsed Laser Radiation," presented at Laser Industry Association meeting, October 24-26, 1968, published in Proceedings of the Laser Industry Association Convention, 1968.
67. Fine, S., MacKeen, D., Feigen, L. and Fine, B. "Anterior Chamber Measurements on CO<sub>2</sub> Laser Corneal Irradiation," Proceedings of the Annual Conference on Engineering in Medicine and Biology, Vol. 10, p. 6, November 4, 1968.
68. Feigen, L., MacKeen, D. and Fine, S. "A Method for Detecting and Measuring Frequency of Surface Vibrations Using a Helium-Neon Laser," Review of Scientific Instruments, Vol. 40, pp. 381-382, February 2, 1969.
69. Geeraets, W., Fine, B.S. and Fine, S. "Ophthalmic Studies on CO<sub>2</sub> Laser Irradiation," Acta Ophthalmologica, (Kobenhavn), Vol. 47, pp. 80-92, 1969.
70. Laor, Y., Simpson, C.L. Klein, E. and Fine, S. "Pathology of Internal Viscera Following Laser Radiation," American Journal of Medical Sciences, Vol. 257, pp. 242-252, April, 1969.
71. Litwin, M.S., Fine, S., Klein, E. and Fine, B.S. "Burn Injury After Carbon Dioxide Laser Irradiation," Arch. Surg., Vol. 98, pp. 219-222, February, 1969.
72. Fine, S. and Klein, E. "Lasers in Biology and Medicine," Laser Focus, pp. 28-36, July, 1969.
73. Fine, S., Bushor, W. and Cos, M. editors. Proceedings of the Laser Industry Association Meeting, October 24-26, 1968.
74. Fine, S. and Klein, E. "Lasers in Biology and Medicine" published in Development in Laser Technology, Society of Photo-Optical Instrumentation Engineers.
75. MacKeen, D., Fine, S., Feigen, L. and Fine, B.S. "Anterior Chamber Measurements on CO<sub>2</sub> Laser Radiation," Investigative Ophthalmology, Vol. 9, No. 5, pp. 366-371, May, 1970.
76. MacKeen, D., Edlow, J., Fine, S., Kopito, L. and Klein, E. "Calcium and Magnesium in Focal Hepatic Lesions," Federation Proceedings, Vol. 29, No. 2, March-April, 1970.
77. Klein, E., Laor, Y. and Fine, S. "Interaction of Laser Radiation with the Skin," Abstract-Laser Journal, Vol. 2, No. 1, January-February, 1970.

78. Fine, S., MacKeen, D., Berkow, J. and Fine, B.S. "Biological Studies with Laser Protective Materials," American Journal of Ophthalmology, Vol. 71, No. 4, April, 1971.
79. Campbell, J. and Fine, S. "Heat Sensation Thresholds for CO<sub>2</sub> Laser Radiation," Radiation Research, 43 (1), 1970.
80. MacKeen, D., Fine, S., Aaron, A. and Fine, B.S. "Cataract Production in Rabbits with an Ultraviolet Laser," Laser Focus, April, 1971.
81. Fine, S. and Hansen, W.P. "Optical Second Harmonic Generation in Biological Systems," Applied Optics, October, 1971.
82. MacKeen, D.L., and Fine, S. "Effect of Suprathreshold CO<sub>2</sub> Laser Irradiation of the Weanling Rabbit Eye on Lenticular Ascorbic Acid and Reduced Glutathione," Federation Proceedings, Vol. 32, No. 3, Pt. 1, 1973.
83. MacKeen, D., Fine, S. and Fine, B.S. "Production of Cataracts in Rabbits with an Ultraviolet Laser" - Ophthalmic Research, 5:317-324, 1973.
84. MacKeen, D., Cohen, J., and Fine, S. "Simultaneous Corneal Surface and Anterior Chamber Temperature Measurements on CO<sub>2</sub> Laser Irradiation," Federation Proceedings, Vol. 33, No. 3, Pt. 1, March, 1974. (Abstract.)
85. MacKeen, D.L., Szabo, G., and Fine, S. "The Effects of UV Laser Radiation at 325 nm on the Skin," The Yale Journal of Medicine, 1973 (Abstract).

B. Non-Laser Related

In addition, credit was given to non-laser related studies, in which the principal investigator and his associate were involved. A number of these were listed in the annual progress reports; several are listed below.

86. Fine, S., Klein, E., R.E., Hainish, H. and Aaronson, C. "Bio-Engineering in the Biological Sciences," IEEE Student Journal, January, 1964, 1:33-39.
87. Litwin, S.B., Cohen, J., Fine, S. and Aaron, A. "Rupture and Tensile Strength Measurements of Fresh and Teated Canine Aortic Tissue," Proceedings of the Annual Conference on Engineering in Medicine and Biology, Vol. 10, p. 44, November 4, 1968.
88. Aaron, A., Litwin, S.B., Fine, S. and Sillin, L. "Pressure and Flow Relations in Canine Aortic-Pulmonary Shunts," presented at Second International Conference on Medical Physics, Boston, Massachusetts, August, 1969, published in Abstracts of Conference.
89. Aaron, A., Litwin, S.B., Fine, S. and Rosenthal, A. "Determination of Cardiac Output by Dye Dilution," in Proceedings of the 23rd Annual Conference on Engineering in Medicine and Biology, Vol. 12, 1970.

90. Cohen, J., Litwin, S.B., Aaron, A. and Fine, S. "The Rupture Force and Tensile Strength of Canine Aortic Tissue," J. Surg. Research, December, 1972.
91. Litwin, S.B., Cohen, J. and Fine, S. "Effects of Sterilization and Preservation on the Rupture Force and Tensile Strength of Canine Aortic Tissue," J. Surg. Research, 1973.

C. Laser-Related Presentations as Invited Lecturer, Pertinent to Contract to Which Credit Was Given

1. Conference on Biological Effects of Laser Radiation, Washington, D.C. - Sponsored by U.S. Army Medical Research and Development Command, 1964
2. Conference on Lasers, New York Academy of Sciences, 1964
3. Gordon Research Conference on Biological Effects of Laser Radiation, 1965
4. Conference on the Biological Effects of Lasers, National Institutes of Health, Bethesda, Maryland, October 4-5, 1965
5. Gordon Research Conference on Biological Effects of Laser Radiation, 1966
6. Bell Telephone Laboratories - invited lecturer, 1966
7. The Martin Company - symposium on Biological Effects of Laser Radiation, 1966
8. Boston Medical Physics Society - Lecturer on Biophysical Studies with Laser Radiation, 1966
9. Seminar on Biological Effects of Laser Radiation, University of Texas, Austin, 1966
10. Conference on Development of Lasers in the Biological Sciences, Veterans Administration, Department of Medicine and Surgery, Washington, D.C., August 5, 1966
11. Presentation before the Physicians of the Association of American Railroads, Montreal, June 4, 1967
12. Gordon Research Conference on Biological Effects of Laser Radiation, 1967 (Session Chairman)
13. American College of Obstetrics - District I Meeting - Invited Participant - Biological Studies on Laser Radiation, October 1967
14. Invited Lecturer on Lasers - P.R. Mallory & Co. - Laboratory for Physical Sciences - Biological Effects of Laser Radiation, February, 1968
15. Brookhaven National Laboratory, Upton, New York "Biophysical Effects of Laser Radiation", May, 1968
16. New England Chapter Health Physics Society, "Biological Effects and Hazards of Laser Radiation", May, 1968
17. Case Western Reserve University, Cleveland, Ohio, Summer course on Laser Technology and Applications, presented lecture "Lasers in Biology and Medicine," July, 1968
18. G-APURSI Symposium (International Antenna and Propagation Symposium) "Electromagnetic Waves (Lasers) for Biological and Medical Applications", September, 1968

19. Rutgers University, New Brunswick, New Jersey, Participant in "Evaluation of Laser Hazards Course", October, 1968
20. S. Fine - "Biological Studies Relating to Laser Irradiation, Particulary with Respect to the Eye", Howe Laboratories, Massachusetts Eye and Ear Infirmary, Harvard Medical School, December, 1968
21. S. Fine - "Control of Laser Hazards and Management of Accidents", National Center for Radiological Health, U.S. Department of Health, Education and Welfare, Rockville, Maryland, February, 1969
22. S. Fine - "The Application of Lasers to Biology and Medicine," Conference on Trends and Directions in Biological Sciences of the Thirteen Colleges Curriculum Program Biology Teachers, Clark College, Atlanta, Georgia, March, 1969
23. S. Fine, Participation in Skin Laser Workshop, Second International Laser Safety Conference, Cincinnati, Ohio, March, 1969
24. S. Fine, Lasers--Characteristics, Use, Hazards and Biological Effects, Seminar Series, Environmental Health Engineering and Science, Graduate School of Engineering, Northeastern University, March, 1969
25. S. Fine, Lasers--Characteristics and Uses in Biology and Medicine, Surgical Seminar Series, Boston University School of Medicine, March, 1969
26. S. Fine, Use of Lasers in Biology and Medicine, Laser Applications Course, Washington University, St. Louis, Missouri, May, 1969
27. E. Klein, and S. Fine, Tissue and Cell Effects of Laser Radiation--Gordon Research Conference on Lasers in Medicine and Biology, June, 1969
28. S. Fine, "Lasers in Biomedicine," I.E.E.E. Student Branch, Northeastern University, July, 1969
29. S. Fine, "Biological Hazards and Effects of Laser Radiation," in course on Fundamentals of Non-Ionizing Radiation Protection, Northeastern Radiological Health Laboratory, August, 1969
30. S. Fine, Lasers in Industry, Associated Hazards and Protection, National Safety Congress, Chicago, Illinois, October 28, 1970
31. S. Fine, Non-invasive Testing in Medicine, I.E.E.E. group on Engineering in Biology and Medicine, Boston, Massachusetts, November, 1970
32. S. Fine, Uses and Hazards of Laser Radiation in Industry and in Atmospheric Pollution Studies, 24th AMA Clinical Convention, Boston, Massachusetts, November 30, 1970
33. S. Fine, "Bioengineering", Massachusetts Epsilon Chapter, Tau Beta Pi (Northeastern University), September, 1969

34. S. Fine, "Laser Biology", in Laser Fundamentals and Applications course, Polytechnic Institute of Brooklyn Graduate Center, September, 1969
35. S. Fine and E. Klein, "Biological Effects of Laser Radiation," the Theobald Smith Society, New Jersey, October, 1969
36. S. Fine, "Lasers--Biological Effects and Medical Applications," Society of Photo-optical Instrumentation Engineers Meeting, co-sponsored by the University of Rochester Institute of Optics, Rochester, New York, November, 1969
37. S. Fine, Session Chairman, Laser and Ultraviolet Contributed Papers, Fourth Annual Midyear Topical Symposium, Health Physics Society Meeting, Louisville, Kentucky, January 28-30, 1970
38. S. Fine, Lasers in Industry, Associated Hazards and Protection, National Safety Congress, Chicago, Illinois, October 28, 1970
39. S. Fine, Non-invasive Testing in Medicine, I.E.E.E. group on Engineering in Biology and Medicine, Boston, Massachusetts, November, 1970
40. S. Fine, Uses and Hazards of Laser Radiation in Industry and in Atmospheric Pollution Studies, 24th AMA Clinical Convention, Boston, Massachusetts, November 30, 1970
41. S. Fine, "Lasers in Biology and Medicine," in course on Lasers and Optics for Applications, Massachusetts Institute of Technology, Cambridge, Massachusetts, July 30, 1971
42. S. Fine, Guest Lecturer in Graduate Course 2.77, "Biological Effects and Medical Applications on Non-Ionizing Radiation," Fall, 1971, Massachusetts Institute of Technology
43. S. Fine, "Medical Applications, Research and Safety," Boston Section I.E.E.E. 1972 Lecture Series, February, 1972
44. S. Fine, "Lasers in Biology and Medicine," a course on lasers and optics for application, M.I.T., July, 1972
45. S. Fine, "Biological Effects and Medical Applications on Non-Ionizing Radiation," guest lecturer for several sessions in graduate course 2.77, M.I.T., 1972-1973
46. S. Fine, "Biological Effects and Medical Applications of Non-Ionizing Radiation," guest lecturer in graduate course at M.I.T., 1973-1974
47. S. Fine, lectured at Raytheon Research Laboratory on Electrical Hazards and Emergency Management of Accidents, 1974
48. S. Fine, "Biological Effects and Medical Applications of Non-Ionizing Radiation", guest lecturer in summer session course, M.I.T., July, 1975

Most other conferences in which abstracts or papers were published are included in the preceding bibliography.

- D. Laser-Related Conference Organization and Planning; Pertinent to Contract
1. Boston Laser Conference, 1963
  2. Boston Laser Conference, 1964
  3. Institute of Electrical and Electronics Engineers - Member, NEREM Program Committee, 1965
  4. Institute of Electrical and Electronics Engineers - Member, NEREM Program Committee, 1966
  5. American Association for the Advancement of Science - Session Organizer and Chairman of Session on Biological Effects of Laser Radiation, 1966
  6. Laser Industry Association Convention, October 24-26, 1968
  7. Course on "Fundamentals of Laser Radiation Protection" given to personnel of U.S. Department of Health, Education and Welfare, 1968
  8. Member, program planning committee on seminar series in applications of physical chemical techniques in Biology and Medicine, EMB, IEEE, Boston Section, 1969
  9. Laser Industry Association Meeting - Los Angeles, California, October 20-22, 1969
  10. Electro-Optical System Design Conference, September 22-24, 1970, New York Coliseum. Planning of sessions, session organization and chairman.
  11. Major participant in the organization, planning, and instruction of personnel, and field work related to the first major survey on lasers and laser devices in the United States which was carried out by the State of Massachusetts and Occupational Health and Radiological Health, H.E.W., 1968.

DISTRIBUTION LIST

USAMRDC (SGRD-RMS)  
Fort Detrick  
Frederick, MD 21701

Defense Technical Information Center (DTIC)  
ATTN: DTIC-DDA  
Cameron Station  
Alexandria, VA 22314

